LBL-7574
UC-34c
CONF-780345

Proceedings of the Workshop on Producing High Luminosity High Energy Proton-Antiproton Collisions

March 27-31, 1978
Berkeley, California

LAWRENCE BERKELEY LABORATORY
FERMI NATIONAL ACCELERATOR LABORATORY

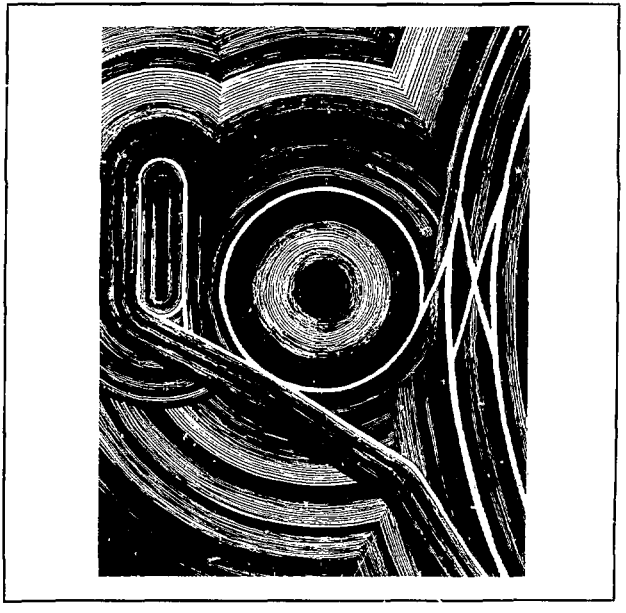

Sponsored by the U.S. Department of Energy, National Science Foundation, and American Physical Society

Prepared for the U.S. Department of Energy under Contract W-7405-ENG-48

Proceedings of the Workshop on Producing High Luminosity High Energy Proton-Antiproton Collisions

March 27-31, 1978

Lawrence Berkeley Laboratory
Fermi National Accelerator Laboratory

Sponsored by the
Department of Energy
National Science Foundation
American Physical Society

CONTENTS

WORKSHOP PROGRAM

March 27, 1978

PHYSICS WITH $p\bar{p}$ INTERACTIONS — Morning Chairman: H. Grunder

9:00 a.m.	Welcome	A. M. Sessler
9:05 a.m.	Colliding Beams and Beam Cooling at Fermilab	R. R. Wilson
9:20 a.m.	Use of $p\bar{p}$ Machines to Explore Very High Energy Interactions	C. Rubbia
10:20 a.m.	Coffee Break	
10:40 a.m.	Expectations for Ultrahigh Energy Interactions	R. Feynman
11:40 a.m.	Study of Weak Interaction and Electromagnetic Processes with High Luminosity $p\bar{p}$ Machines	D. Cline
12:30 p.m.	Lunch	

BEAM COOLING "PLANNED" $P\bar{P}$ MACHINES — Afternoon Chairman: D. Cline

1:45 p.m.	The Effects of Beam Cooling on Accelerator-Storage Ring Developments	A. Sessler
2:00 p.m.	Electron Cooling Theory and Devices	F. Mills
3:00 p.m.	Coffee Break	
3:20 p.m.	Stochastic Cooling Theory and Devices	S. Van der Meer
4:15 p.m.	CERN SPS Used as $p\bar{p}$ Collider	R. Billinge
4:45 p.m.	TEVATRON Used as $p\bar{p}$ Collider	L. Teng
5:15 p.m.	ISABELLE as a $p\bar{p}$ Collider	B. Palmer
5:45 p.m.	Wine Tasting, LBL Cafeteria	

March 28-30, 1978 - WORKING SESSIONS

March 31, 1978 - SUMMARY SESSION

9:00 a.m.	Large Acceptance Cooling Rings	F. Mills
9:30 a.m.	$\bar{p}$ Production Characteristics and Collection Systems	D. Cline

ELECTRON BEAM COOLING

9:50 a.m.	Status of Theory	E. Courant
10:10 a.m.	Prospects of Ribbon-Type e-Beams	F. Krienen

March 31, 1978 - SUMMARY SESSION (continued)

STOCHASTIC COOLING

10:30 a.m.	Theory of dc and Bunched Beams.....	F. Sacherer
10:50 a.m.	Hardware/Diagnostics/Amplifiers.....	G. R. Lambertson
11:10 a.m.	Discussion	
11:30 a.m.	Detectors; Relation of Detectors to $p\bar{p}$ Machines.....	G. Salvini
11:50 a.m.	Luminosity Limitations and Instabilities in Storage Rings.....	L. Teng
12:15 p.m.	Cooling of High Energy Beams with Electrons.....	P. McIntyre
12:45 p.m.	Discussion	
1:00 p.m.	Lunch	

INTRODUCTION

SCOPE OF THE WORKSHOP

D. Cline
Fermi National Accelerator Laboratory
and
University of Wisconsin at Madison

A Workshop was held during the week of March 27-31 at the Lawrence Berkeley Laboratory in Berkeley, California. The purpose of the Workshop was to discuss various beam-cooling techniques and to investigate the possibility of constructing high luminosity proton-antiproton storage rings. Herman Grunder and other members of the LBL staff were largely responsible for the efficient operation of the Workshop and the success. The Workshop was jointly sponsored by Fermilab and LBL.

That this was the first workshop totally devoted to beam cooling and to high luminosity $\bar{p}p$ storage rings indicates the close coupling between the two subjects. The construction of $\bar{p}p$ storage rings is an old dream of accelerator physicists, the practical realization of these machines certainly relies on beam-cooling techniques. The late G. Budker often discussed the possibility of $\bar{p}p$ storage rings and realized that beam cooling would be crucial to such schemes. The first realistic schemes for such machines using existing accelerators were outlined in 1976 (Appendix VIIa). Subsequently, both CERN and Fermilab have made detailed plans for such machines (IIIc,d). There are also discussions of a $\bar{p}p$ option at ISABELLE (IIIe). The reports in which the CERN and Fermilab machines are described in some detail are reproduced in Appendices VII b and c of these proceedings for completeness.

The first day of the Workshop was devoted to the physics motivation for high luminosity $\bar{p}p$ machines (Section II) and the general concepts of beam-cooling techniques as well as the most up-to-date plans for $\bar{p}p$ machines at CERN, Fermilab, and BNL (Section III).

The reports of the working groups are given in Section IV. It is with deep regret that we note that Frank Sacherer was killed in Switzerland after the Workshop was finished. He made a brilliant contribution to the theoretical understanding of stochastic cooling (IVa).

The highlights of the Workshop in my biased opinion were:

1. The very interesting talk of R. Feynman on ultra high energy interactions (IIa) and the historical surveys of beam cooling by A. Sessler and R. R. Wilson.

2. The general conviction that $\bar{p}p$ machines proposed in the present CERN and Fermilab schemes are sound (IIIc,d; IVc; Vb).

3. The discussion of the cooling of high energy proton-antiproton beams by electrons (Rubbia, Month, Ruggiero) or by synchrotron radiation (Wilson). The report of Ruggiero, Vh, was completed after the Workshop and is reproduced here for completeness.

4. The understanding of improvements in target efficiency that can raise the $\bar{p}$ yield by a considerable factor (IVd).

5. The possibility of high luminosity $\bar{p}p$ machines with $\mathcal{L} \geq 10^{31} cm^{-2} sec^{-1}$ either at CERN, Fermilab, or BNL now seems very likely. There are no fundamental obstacles to such machines (IVc).

6. Looking to the future there was a lively debate about the relative merits of high energy - high luminosity $\bar{p}p$ machines and e^+e^- machines. The maximum useful luminosity to these machines given present detector capabilities was also debated (IVe).

All in all, the Workshop was a good start towards the future of $\bar{p}p$ storage rings and refined beam-cooling techniques. We can now probably look forward to the day when a multi-TeV $\bar{p}p$ storage ring with $\mathcal{L} > 10^{31}$ $cm^{-2}sec^{-1}$ will exist somewhere in the world soon after the machines at CERN and Fermilab are operational.

I would like to thank our hosts and the participants for a very interesting Workshop.

WELCOMING REMARKS

Andrew M. Sessler
Lawrence Berkeley Laboratory

It is a pleasure to welcome you to this Workshop on beam cooling and, I must say, that I am particularly pleased that LBL is co-hosting this conference on such a significant advance in the science of beam-handling devices. I like to believe that this Workshop is consonant with the more than 45 year history of this Laboratory, which stretches back to E. O. Lawrence's invention of the cyclotron and includes such notable advances as Luis Alvarez's linear accelerator and Ed McMillan's concept of phase focusing with his subsequent development of the FM cyclotron and the electron synchrotron. In recent years we have tried to maintain this tradition through the activities of our Advanced Accelerator Research and Development Group and it is that very group which is sponsoring -- with Fermilab -- this meeting.

In my opinion, and I will learn more as the week goes on, beam cooling is one of the two most important advances in beam-handling techniques to have reached the point of practical, engineered availability within the last 5 years. The other is, of course, hard superconducting bending and focusing magnets which are being incorporated most notably, in the Fermilab Energy Doubler/Saver and in Brookhaven's Isabelle.

Beam cooling should make possible tremendous gains in $\bar{p}p$ colliding-beam devices, and this week's Workshop will be devoted to this topic. It is interesting to compare Kjell Johnsen's estimate, in 1962, of the luminosity which might be achieved in the ISR as a $\bar{p}p$ device; namely $L \approx 10^{24}\text{cm}^{-2}\text{sec}$ or the optimistic estimates of Paul Csonka and myself in 1967; namely $L = 5\times10^{26}\text{cm}^{-2}\text{sec}^{-1}$, with the Fermilab goal of L up to $10^{32}\text{cm}^{-2}\text{sec}^{-1}$ or the current CERN estimate of the luminosity in the SPS for $\bar{p}p$ collisions, namely $L = 10^{30}\text{cm}^{-2}\text{sec}^{-1}$. (Of course I am comparing different devices, but the major import of beam cooling is, nevertheless, evident.)

Now it is interesting to go beyond this Workshop to explore how widely beam cooling can be used with advantage. For example, is it of value in pp colliding beam devices? I can recall studying just this question for the ISR in 1966, immediately after learning of Budker's invention of electron cooling. Hugh Hereward did a rather complete study of the subject, which he reported on at the Orsay Conference on Storage Rings (1966), and he concluded that electron cooling wouldn't improve the ISR very much. Now that result was very sensitive to the boundary conditions; namely the given ISR, and it was prior to the invention by Simon van der Meer of stochastic cooling. It is important to my mind, to explore both in $\bar{p}p$ rings, and beyond $\bar{p}p$ rings, what can be achieved with beam cooling both in existing machines and in machines designed to exploit beam cooling.

Perhaps I could make some comments addressed to why beam cooling isn't obviously a good thing in all devices. Consider, for a moment, electron storage rings. Here we have strong cooling and certainly we take advantage of it in injection: The filling time decreases rapidly as the injection energy is increased and the radiation damping, or beam cooling, is increased.

On the other hand, we know that at high energies the naturally occurring strong beam cooling imposes a severe limit on ring luminosity. Consequently, a number of measures have been developed to heat beams so as to increase the incoherent stochasticity limit due to a highly-cooled, compact intense beam. In this example an incoherent single particle phenomenon limits performance rather than phase space density.

Generally, then, *particle handling devices* have their performance limited by (1) single particle external field effect by (2) incoherent collective phenomena, by (3) coherent collective phenomena, or (4) by phase space density. Cooling only helps to remove the last-mentioned limit. Thus in many devices, cooling won't help and in those in which it does help, it is necessary to ascertain how much improvement is actually possible before one hits one of the other limits to performance.

Well, enough for these sobering remarks. I felt they were necessary because so often at a meeting on some particular subject one gets carried away and forgets about other relevant subjects. Despite the limits on what can be achieved with cooling, it is clear that cooling is a very significant new technique which has become available to the designer and builder of particle handling devices.

Now, let us turn to hearing what can be achieved with cooling and, also, the important aspects of how, in fact, one designs, builds, and operates $\bar{p}p$ cooling devices. I wish you, on behalf of the sponsors, an interesting and productive Workshop.

COLLIDING BEAMS AT FERMILAB

R. R. Wilson
Fermi National Accelerator Laboratory

Batavia, IL

It is a pleasure to participate in this timely workshop at the Lawrence Berkeley Laboratory on cooling antiprotons. In discussing "Colliding Beams at Fermilab," I will take a glance backwards and then a glance forward, trying to avoid our present work for that is to be discussed by my colleagues in following talks.

It is interesting that even in the Berkeley 200 BeV Design Study of 1965 it was envisaged that antiprotons could be produced in nucleonic collisions, stored in the Booster, injected into the Main Ring, and then accelerated simultaneously with protons in a manner surprisingly similar to our presently planned method. Storage rings were also envisaged in the Berkeley report and this led to a criterion that the site of the accelerator should be large enough to contain such rings in addition to the accelerator.

During the Summer Study of 1967 at Oak Brook, Illinois, when the National Accelerator Laboratory synchrotron was being designed, various possibilities for storage rings at NAL were also discussed as options for the future. Ernest Courant was especially interested in "By-Passes," both inside the Main Ring and outside, and considerations of this, as well as of more conventional storage rings, appear in the NAL Design Report of 1967 that resulted from the Summer Study.

In 1968, the question of storage rings at NAL was raised by the Atomic Energy Commission. The Board of Trustees of the Universities Research Association asked us at NAL to design a specific set of storage rings. Although our all-too-small group had quite enough to do at that time, Lee Teng took on the assignment and a number of physicists, including the present LBL Director, came from other laboratories to help. They designed a set of conventional rings that would provide 100-GeV protons in collision with 100-GeV protons at good luminosity (see their design report of 1968). They also worked out an alternative design using superconducting magnets which would reach 200 GeV on 200 GeV.

It seemed that in 1968, just as in 1967 when we had considered the practicality of using superconducting magnets for the Main Ring, the art of superconductivity had not advanced to a stage where one could responsibly risk large sums of money on it. The "*frozen-in*" *fields were much too large, almost of* the order of kilogauss, and did not repeat in strength from pulse to pulse or magnet to magnet.

Our next formal involvement with colliding rings resulted from my request in the Spring of 1973 that a representative group of physicists serve as a NAL Long Range Physics Advisory Committee At that time we were about to proceed to build an "Electron Target" under the direction of Tom Collins.[1] This had been invented during the Summer Study at Aspen, Colorado in 1973 and was to use the old Cambridge Electron Accelerator as an electron storage ring to be built tangent to the Main Ring so that collisions between circulating 3 to 4 GeV electrons against countercirculating 100 to 400 GeV protons in the Main Ring could be made to occur at luminosities up to about 10^{32} cm^{-2} sec^{-1}. Although we had acquired the electron linac injector and magnets of the CEA, the Long Range Physics Advisory Committee advised against this project because the energy available in the collisions seemed to them to be too low. They recommended instead, on the basis of the Summer Study of 1973, that we design POPAE (acronym for Protons On Protons And Electrons), a project to build two 1000 GeV storage rings to make 1000 GeV/1000 GeV colliding proton beams possible, and also to build a third electron storage ring so as to make 20 GeV/1000 GeV electron-proton collisions possible. We followed that advice; first in a preliminary study by Collins and Edwards,[2] and then later on in a collaboration between physicists at Fermilab and Argonne National Laboratory led by R. Diebold.[3]

In retrospect, I am not altogether sure that the committee's advice against building the "Electron Target" was sound. The electron target could well have led to an unfolding program of beautiful colliding-beam physics. The POPAE project, although valid scientifically, turned out to be a political fiasco. In several HEPAP "Woods Hole Panel" meetings, it lost out to the ISABELLE project despite what seemed to me (very objectively, no doubt!) to be the technological and economic superiority of POPAE. In any case, the maintenance of three strong centers of high energy physics became national policy, and the construction of the ISABELLE colliding beam project at the Brookhaven National Laboratory became of overwhelming importance in the realization of that goal.

Let me back up a bit to 1971, at which time the so-called Energy Doubler project to build a second ring of superconducting magnets within the Main Ring tunnel was first put forward at Fermilab.[4] We had then essentially built the 200 GeV accelerator and experimental areas, and still had a surplus of funds left over from the initial $250 million for that construction. A ring of superconducting magnets in which 1000 GeV protons could be accelerated seemed to be one way to use up that surplus and to respond to the original challenge of the Joint Committee on Atomic *Energy to produce the highest energy possible.* Indeed such a possibility had been allowed for in the original design, for space had been kept free both above and below the conventional magnets of the Main Ring for the placement of such superconducting magnets. Those early plans were seriously set back by the crisis in 1972 of bringing the accelerator and the experimental areas into reliable operation. The project was further set back in 1976 when much of the remaining surplus construction funds identified for the Energy Doubler were preemptively withdrawn by the AEC

Nevertheless the project has persevered and by now reliable, precise, economical, high-field magnets have been successfully developed. Indeed these superconducting magnets are now being installed in the Main Ring tunnel below the conventional magnets as rapidly as the funding of the project allows. If adequate funds are forthcoming, the installation of a full ring of about a thousand superconducting magnets can be anticipated in 1981.

Given the two congruent rings in the Main Ring tunnel, the idea of bringing beams in each of them into collision surfaced frequently. Dick Carrigan (NAL, FN-238) was the first to put something in writing by his suggestions in 1971 to build two superconducting rings in the tunnel. In 1975 the aperture of the superconducting magnets was increased from an elliptical opening 1-3/4 in. high by 2-1/2 in. wide to a circular opening 3 in. in diameter specifically after a study had been made by Teng which indicated that such an aperture would be adequate for the use of the superconducting magnet ring as a storage ring as well as an accelerator, and hence could be used with the Main Ring as a colliding beam facility. Of course, that decision also increased the cost of the magnets.

The next development was the revival of an old scheme to have a low energy ring in the Main Ring tunnel, the Accumulator,[5] and then to bring the beam of low energy protons stored within it into collision with high energy protons stored in the Main Ring. This eventually developed into a more refined proposal[6] to build an independent small 25 GeV Accelerator/Storage Ring, the SSR (Small Storage Ring) at straight Section E of the Main Ring. By bringing the 25 GeV protons into collision with the 400 protons of the Main Ring, a c. m. energy of about 200 GeV could have been obtained with a luminosity of about 10^{31} cm^{-2}sec^{-1}.

A little later, a number of suggestions came in from outside the laboratory for various forms of clashing beams. For example, in July, 1975, Carlo Rubbia suggested in a letter that good luminosity might be obtained by colliding the proton beam in the Doubler against the proton beam in the Main Ring, and in August of that year B. Richter and D. Cline made a similar suggestion.

The subject of colliding beams was in the air, so a Fermilab Workshop,[7] under the direction of Alvin Tollestrup, was called at Fermilab for January, 1976. The results of a "stochastic cooling" experiment in the ISR at CERN as well as Budker's results on "electron cooling" were also reported at the Workshop, and the implication of cooling on the production of circulating beams of antiprotons intense enough for studying $\bar{p}p$ collisions was briefly discussed. The Workshop had one immediate effect; it eventually led a group of physicists formally to propose an experiment in which 1000 GeV protons in the Energy Doubler were to be brought into collision with protons in the Main Ring.[8]

Shortly after the Workshop, C. Rubbia and D. Cline[9] came up with an enthusiastically worked out *ingenious proposal for studying colliding beams* of antiprotons against protons in one ring. They proposed to utilize both "electron cooling" and "stochastic cooling" of antiprotons using a complicated combination of the Main Ring, the Booster and a separate cooling ring. Anticipating luminosities of about 10^{28} cm^{-2} sec^{-1}, they pushed the idea with typical elan. It too was put forward in the form of a formal experimental proposal.

Competition between the proponents of the three approaches to modest colliding beams became rather intense, and the air was cleared only when the PAC, during their meeting of June, 1976, recommended rejection of all colliding beam proposals.[10] At the same time, the PAC recommended that the laboratory continue the development of facilities which would provide for either high energy p-p or $\bar{p}p$ collisions, or for both. We have been proceeding along those lines, and this Workshop is expected to be an important step along that path.

My colleagues will soon discuss the work currently underway, so now let me turn to some future possibilities for colliding beams at Fermilab.

A principal difficulty with the Main Ring and the Doubler for colliding beam experiments is the interference that would be caused with the regular fixed target experiments. Building "Bypasses" could be useful in decoupling colliding beam facilities from the accelerator and would considerably extend the experimental space available for such facilities. I will not dwell here on the many possibilities for Bypasses, or on the construction of a separate Inner Ring which would almost completely separate the colliding beam experiments from the Tevatron fixed-target experiments as well as to allow for higher luminosities, higher energy (up to 3 GeV c. m.), and for extensive experimental space - all at modest cost.[11, 12]

Instead let me look at a grander possibility for future colliding beams at Fermilab, the Pentevac. One of my first efforts on becoming Director of NAL was to have the form of the Site changed from an elongated rectangle to its present shape so that a larger ring might eventually be inscribed within its boundaries. This ring, shown in the diagram, has an average radius of 2.5 km. Installing our presently developed supermagnets to make a magnet ring in that tunnel would allow for the production of about 2.5 TeV, or, if the ring were used as a storage ring for proton and countercirculating antiprotons, then a c. m. energy of about 5 TeV might be reached in $\bar{p}p$ collisions.

However, we do not anticipate that such a large ring will be constructed in the immediate future, so we must ask what magnetic fields might be attainable at the time, say five or ten years from now, that such a ring might conceivably be started. Although by the use of new materials there is no obvious reason not eventually to reach fields of the order of hundreds of kilogauss, I suggest that a factor of two, i. e., 85 kilogauss, is nearly within the state of the art right now. In that case 5 TeV protons could be produced, hence the name Pentevac, and 10 TeV c. m. might be attained in $\bar{p}p$ collisions!

The present limitation of the field in the Energy Doubler magnets is imposed by three factors: (a) the

current density that can be reached using the present superconductor, NbTi; (b) the mechanical distortion caused by the tremendous magnetic force on the conductors; and (c) the benign disposition after a quench of the large amount of magnetic energy intrinsically stored in each magnet in a manner such that the conductor is not melted. The forces and the stored energy would quadruple in present Doubler magnets, of course, were the magnetic field to be doubled by simply doubling the current density, if that were possible.

The second diagram shows in cross section a possible design of a supermagnet for the Pentevac which might reach 85 kg and which is based on the present Doubler magnet design. Instead of NbTi, Nb_3Sn would be used as the superconductor, for it will reach the required current density at the required field. It has the advantage of reaching these specifications at a somewhat higher temperature (10-15°K) than the temperature (4-5°K) characteristic of NbTi. The present difficulty with Nb_3Sn is that practical conductors made of it are not ductile enough so that sharp bends in the coils can be made without destroying the superconducting property of the wire. Perhaps by making the filaments of superconductor even finer than at present, this problem can be solved. However, even at present, a technique exists for producing strands of wire made of bronze in which fine filaments of Nb have been imbedded. This material is ductile, so that the coils can be prewound in the appropriate shape. Then if the temperature of the material is raised to about 750° C, the tin component of the bronze will migrate and interact with the Nb to form Nb_3Sn. The coils could then be insulated and installed within the restraining stainless steel collars. The present coil structure of NbTi and insulator tends to be somewhat "squishy"; indeed it might not take a four-fold increase in the forces without collapsing. However, loading the epoxy heavily with alumina powder makes a much stiffer material than the present "B-stage" glass fiber now in use. Magnets made using this material have given some indication of being successful. Sprayed-on glass might also be a good insulator for use with Nb_3Sn and one which might withstand the heat conditioning.

The aperture of the magnet shown in the diagram has been made in an elliptical shape 2-1/2" wide by 1-3/4" high instead of the 3 in. OD circular shape in order to reduce the total force on the conductors and to reduce the stored energy. The reduction in the aperture should be possible because the injected beam of, say, 300-1000 GeV protons, would be considerably smaller and stiffer than the beam of about 100 GeV protons which are to be injected into the Tevatron.

The 3 in. ID circular aperture of the Doubler magnets was chosen partly for the practical reason that a lathe could be used in the fabrication of the precision tooling, and partly to allow for vertical as well as horizontal injection and ejection of the beam. A new technique has been developed for making very accurate laminated tooling out of punchings, hence any shape should be feasible. The reduction of vertical height to 1-3/4 in. need not be crucial for beam transfer.

The energy stored in the magnetic field must be rapidly disposed in the event of an accidental quench. There is great danger that the superconducting cable will melt at the point where it becomes a normal conductor. The stored energy in the present Doubler magnets, 0.5 megajoule per magnet, is absorbed in the coil of the magnet in the event that it goes normal. It is important that the whole coil be driven normal by means of a heater wire once a quench is detected. This can still be expected to work even for the higher field design, partly because the stored energy has been reduced by a factor of nearly two by just making the aperture smaller, and partly because the coil is inherently capable of absorbing more energy. A second design using a "pancake" coil winding is also indicated. The cable and hence the current, is four times larger than in the previous example. The distribution of the conductor is a closer approximation to that desired for a uniform field, hence the accuracy of the field should be better. R. Edwards and J. Walton have successfully built a NiTi super magnet of similar geometry but in which the cable is smaller rather than larger than the Doubler cable.

An extremely serious problem has to do with the inherent kinetic energy of the 5 TeV protons - 8 ergs apiece! If the magnets are similar to Doubler magnets in quenching because of being struck by protons, then about 10^8 protons might cause a quench. The magnitude of this problem, as well as the usefulness of the Pentevac, will depend then on the magnitude of the proton current that is to be stored in the ring. A typical cycle of the Pentevac might consist of a 10 second dwell-time at a field of about 5 kG during which three pulses of 300 GeV protons could be injected to fill the Pentevac; then the magnetic field might be ramped up to 85 kG in an appropriate time. The ramping time might be a few minutes, if the Pentevac were to be used as a storage ring, or it might be as short as 10 or 20 seconds, were the Pentevac to be used as a fixed target accelerator. Any length of flat-top could be used, and then the magnet could be ramped down in about 20 seconds.

Even with our present intensity of about 3×10^{13} protons per pulse, an intensity of as much as 10^{14} protons per pulse might be possible in principle, but in that case the total kinetic energy of the protons would be about 100 megajoules. Such a beam would evaporate anything solid with which it came into contact. Even a small fraction, say 10^{-6}, of that beam would drive any superconductor into normalcy. This doesn't mean that the problem of containing such a beam and of benignly aborting it in an emergency is impossible, but it does indicate the seriousness of the problem.

This is not the place to remark about the use of the Tevatron for fixed-target experiments. As the figure shows, if the beam could be extracted, it could be transported to experimental areas as much as 4 km in length, if the transporting magnets were to have a 10-20% greater magnetic field. The Pentevac should make an ideal colliding beam facility if the energy deposition problem can be solved. If beams of antiprotons can be stored in the Tevatron with adequate

intensity for $\bar{p}p$ colliding beam experiments at 2 TeV c. m., then those beams could be easily transferred to the Pertevac with the same peripheral density and then accelerated to 5 TeV each. The beams will be automatically narrowed during the acceleration so the luminosity should increase by about an order of magnitude. It is interesting that at this energy, synchrotron radiation emitted by the protons is significant, and will "cool" the size of the beam down by another order of magnitude.

I will leave it as an exercise for the student to work out how to make pp collisions, how to get dyspepsia with a 100 GeV electron storage ring in the same tunnel, and then how to collide 100-GeV electrons with 5-TeV protons. The future for Fermilab is frighteningly fantastic!

References

[1] T. L. Collins et al., An Electron Target for NAL, NAL 1973 Summer Study Report SS-73, p. 21.

[2] T. L. Collins et al., Summary Report on Phase I of the POPAE Design Study NAL, TM-547, 1973.

[3] R. Diebold et al., POPAE Design Report for a 1000 GeV Proton-Proton Colliding Beam Facility, Fermilab and Argonne, May, 1976). Also see NALREP, page 3, June 1976.

[4] "Proceedings" of the Joint Committee on Atomic Energy, March 9, 1971.

[5] R. R. Wilson, Injection Accumulator, Report NAL-11, May 13, 1968.

[6] J. Walker, 1973 Summer Study Report SS-73, p. 260 Fermilab Report, April (1976), Fermilab Proposal P-478.

[7] R. Johnson and P. Limon, Modest Colliding Beam Meeting, NALREP, (1976).

[8] R. Johnson et al., Fermilab Proposal P-478.

[9] C. Rubbia et al., Fermilab Proposals P-494 and P-493.

[10] E. L. Goldwasser, Highlights of Summer PAC Meeting, NALREP, 9, July 1976.

[11] R. R. Wilson, A Bypass and Inner Ring at Fermilab, 1977 Fermilab Summer Study report, Vol. 2, p. 379.

[12] R. Huson, Colliding Beam Bypass, Fermilab TM-753, Nov. 1, 1977.

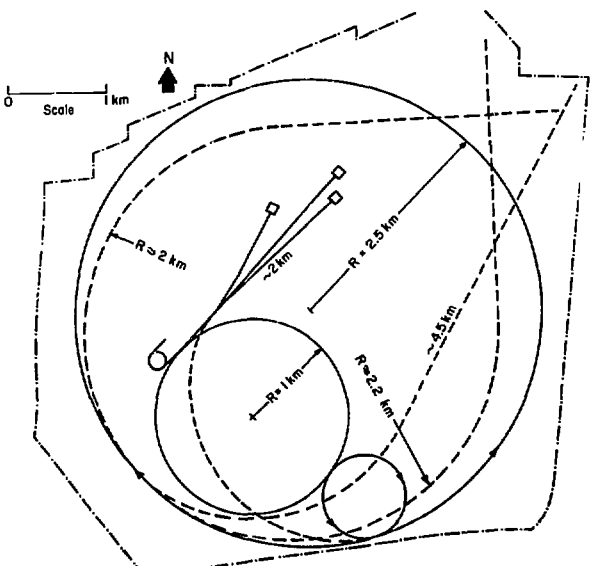

Fig. 1. The Fermilab site with a ring 2.5 Km in radius inscribed and with possible external beam lines indicated.

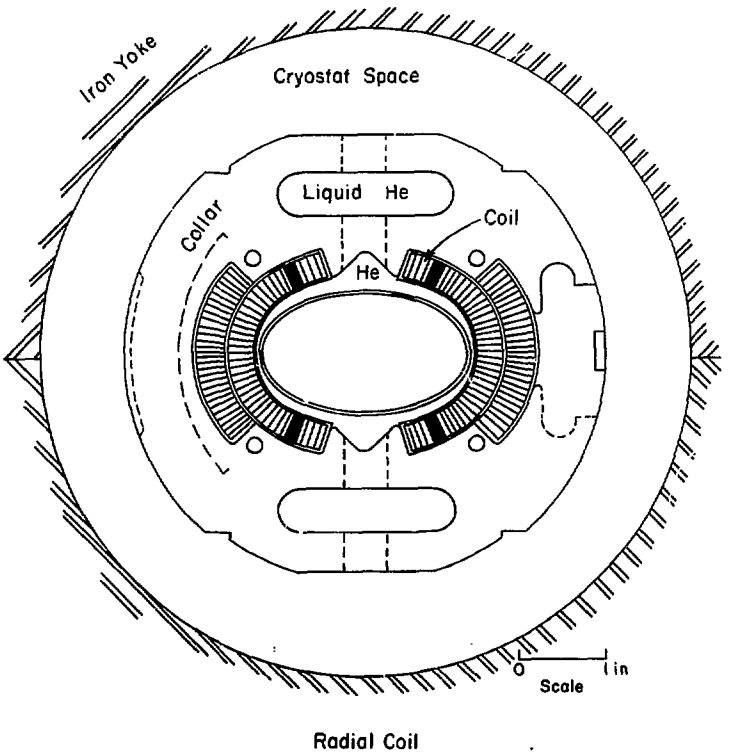

Radial Coil

Fig. 2a. A possible design of an 85 KG Doubler-like super magnet with an elliptical magnet opening of 2 1/2" × 1 3/4". It would fit with a standard doubler cryostat. The conductor cable would be made of Nb, Sn cable 0.050" × 0.300".

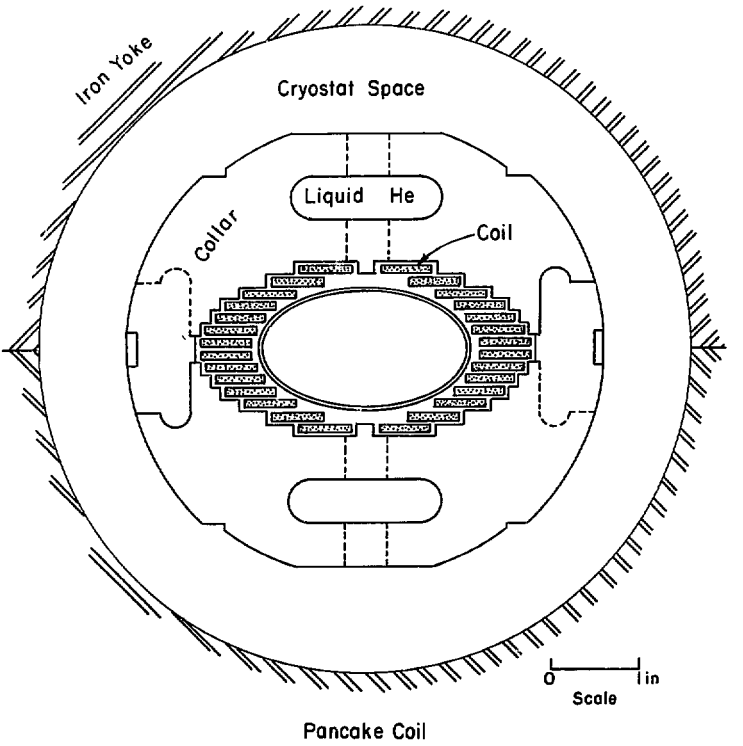

Fig. 2b. A possible design of a high-current "pancake" coil winding for a 85 KG super magnet made 14 turns of Nb_3Sn cable 0.100 × 0.600. The magnet would fit within a standard doubler cryostat.

PHYSICS GOALS OF PROTON-ANTIPROTON STORAGE RINGS

EXPECTATIONS FOR ULTRA-HIGH ENERGY INTERACTIONS

R. P. Feynman
California Institute of Technology

I. Introduction

I will talk about expectations for strong interactions and leave to others the discussion of weak interactions. I will concentrate on the hadrons produced in high-energy collisions.

We have a theory called quantum chromodynamics (QCD) that most people think might be right. This theory has a property called asymptotic freedom which means that at very high energies particles appear to be free. That is, the coupling constants in effect go down as the energy or momentum transfers go up. At high energy, we ought to be able to analyze the physics because we think we know how to analyze small-coupling systems.

But in any real experiment, if, for example, you observe a pion, it involves both high and low energies. By the time the quarks and gluons have cascaded down to become real hadrons, the energy of interaction of the parts in the hadron become important, so that the question of how to separate the high and the low energies is one that has not been completely analyzed. My opinion (to summarize my talk) is that in a rather short time, perhaps even before the machines are completed, we will have developed a theory by which we are able to calculate quite accurately the behavior of the high-energy end and will have some way of translating that information into real experimental facts, either by telling what will happen if you sum the momenta of some particles together or hold certain angles fixed or something. How we will separate the low-energy part, which is involved in every experiment, from the high-energy end is not yet known.

II. Quantum Chromodynamics

I would like to discuss first the evidence that QCD might be the right theory and also some estimates of what will happen from the QCD asymptotic-freedom theory. The work I shall discuss was done in collaboration with Field and Fox.[1] All this work is very preliminary. We do not have anything derived correctly from the LaGrangian, or whatever, of the field theory. This is a qualitative discussion and rough estimate of what might happen if QCD is right. A good deal of my talk will be spent in showing that what we have observed so far is not inconsistent with the possibility that QCD is right, but shows no direct evidence that it is right, only that it isn't necessarily wrong.

The idea is that the partons inside nucleons are gluons and quarks. The hard collisions between two quarks, for example, as in Fig. 1(a), can be analyzed in terms of the exchange of a gluon. Or a gluon in one proton and a quark in another interact, as in Fig. 1(b), making a gluon and a quark. Other combinations are possible. All these are to be analyzed by perturbation theory, both in first approximation and with corrections. The coupling constant is given by

$$g^2 = \frac{12\pi}{25\,\ln\left(\frac{Q^2}{\Lambda^2}\right)},$$

where Q is some momentum transfer in the collision and Λ is a parameter that has been evaluated by Politzer from e-p scattering to be in the neighborhood of 0.5 GeV. If that is true, then

$$g^2 = \frac{1}{\log_2 (2Q)},$$

a simple formula. In a collision at 90° in which there has been a perpendicular momentum transfer $P_\perp$, then

$$g^2 = \frac{1}{1.5 + \log_2 P_\perp}.$$

Thus at $P_\perp = 4$, $g^2 = 0.3$ and at $P_\perp = 32$, $g^2 = 0.15$. We expect to be able to do perturbation theory in the $g^2 = 0.15$ case, but maybe not at $g^2 = 0.3$.

We must add to the first-order approximation the effects of higher collisions. Examples of collisions adding to the lowest order of Fig. 1(a) are shown in Figs. 2(a) and 2(b). The first is an analogue of bremsstrahlung. The second is a virtual-gluon correction to the first order. The result of these higher collisions is to yield an effective non-scaling, that is, that the incoming particles appear to have differing momenta depending on Q^2, a non-scaling effect of the parton distribution. I believe these non-scaling effects are caused by trying to combine the effects of higher collisions with those of the first order. The net result is that the parton distributions do not scale perfectly if you use the elementary theory. The fragmentation functions, the distributions of mesons that come out when a quark comes out, also depend on Q^2.

I will give an example of the physics by discussing e-p scattering. This was analyzed by Politzer.[2] Figure 3(a) is a diagram of the elementary process. The incoming proton contains a quark and perhaps another parton or several. The proton is hit by a virtual γ from the electron and knocks the quark off toward the upper right. It was in these terms that the scaling behavior was first understood, by supposing the distribution of the partons in the hadron scaled. But now we realize that there are higher collisions in QCD and that the proton can emit a gluon ahead of the collision, as in Fig. 3(b), or afterward, as in Fig. 3(c), or have a correction to the original diagram from a virtual gluon, as in Fig. 3(d). If the gluon and the quark come out almost in the same direction, we cannot distinguish Figs 3(b) and 3(c) from Fig. 3(a), because the only thing we can use to distinguish them is kinematics. When the momentum difference is wide enough, the kinematic relations between the momentum of the quark and the energy and momentum of the transfer do not work out because effectively this quark does not have zero mass, but turns into a quark and a gluon which have a relative

mass. If this effective mass $m^2 < \Delta^2$, a constant of the order of 1 GeV, one cannot distinguish 3(b) and 3(c) from 3(a). Therefore we integrate the contributions from 3(b) and 3(c) only over those $m^2 > \Delta^2$. Then it turns out, surprisingly (but interesting, that you understand it) that the relative contributions from 3(b) and 3(c) vary as the square of the coupling constant (because there is one extra coupling) and as the square of the logarithm of (Q^2/Δ^2). They go in the typical bremsstrahlung way as dm^2/m^2, with two logarithms, one for the angle and one for the momenta. Thus the relative contributions increase with Q^2, even though g^2 varies inversely with log Q^2. For corrections at transverse momenta that are more than some finite amount, the higher-order corrections rise with Q^2, rather a surprise in view of the dependence of g^2 on Q^2.

Diagram 3(d) has corrections that affect the total cross section σ (more properly σ multiplied by the momentum p of the observed hadron) that also depend on a cutoff in the integration, and the product σp is roughly the same whether or not these effects are included. But the distribution of outgoing momenta, or the apparent parton distribution, appears to change with Q^2. In the diagram of 3(b), the hard quark leaves only a fraction of its momentum to be hit by the electron. The rest coasts out as the gluon and the electron in effect sees a softer quark. Of course, in diagram 3(c) it sees it at full steam, but 3(c) is decreasing, so the hard quarks are decreased in number because the total momentum of the quarks is conserved, but the low end is increased. So as we make corrections and relate them to the elementary theory, we find that we can represent all the effects by the elementary diagram of 3(a), except that the distribution of momentum of the quarks in the proton varies with Q^2. One can transform this idea into a differential equation and find a simple equation for the moments of the distribution and find how the distributions change. So those for any Q^2 can be gotten if they are known for just one "reference momentum."

The same idea works for the disintegration functions, as we can see in production of hadrons by e^+e^-. In Fig. 4(a), we have the simple diagram of two quarks coming out from e^+e^-. In a higher approximation, there can be a correction that cuts it down, as in Fig. 4(b). There can also be the emission of a gluon in addition to the two quarks. If the gluon angle is large enough to give it a finite momentum, this makes the same kind of logarithmic correction as in the total cross section I discussed above. The net result is that the momentum in the hadrons has been split, so that high momenta are cut down and low momenta are enhanced.

I will now present some experimental evidence on apparent scale breaking at larger x in ep and μp scattering. At larger x, the curves of Fig. 5 fall as Q^2 is increased and at smaller x, they appear to rise. There are still questions as to whether various effects have been properly treated and these results should be regarded as preliminary. They do allow us to determine the Λ that appears in g^2 and it is in the neighborhood of 0.4-0.6 GeV. The net result is that the distribution functions for νW_2 varies with Q^2 in a manner predicted by theory, as shown in Fig. 6(a). We must also guess at the gluon distribution at some given reference momentum inside the proton and we have made a reasonable assumption, given the total momentum of the gluons. We show it in Fig. 6(b). It also varies with Q^2 in an analogous way.

Just as the distribution functions of partons vary with Q^2, so do the disintegration functions. Figure 7 (a) is the disintegration function of π^0's produced from quarks. In the same way as above, we must guess the gluon disintegration function. Here we have no information and have explicitly proposed a definite guess for this distribution, shown in Fig. 7(b). In order to agree with experiment, we propose that when gluons turn into hadrons, they turn into generally softer hadrons - higher multiplicity, but lower momentum each - than do quarks.

III. Comparison with Experiment

I will now discuss fitting of the high $P_\perp$ hadron data by QCD. I am trying to show you that it is not impossible that QCD is right. If it is not wrong, it is the most reasonable theory. It has many qualitative features that seem to be right. It is always true in these kinds of talks when a new machine is being built that you can say that anything will happen and you should go ahead and find the marvelous new things that are bound to happen at high energy. But I would like instead to make a conservative best guess as to what is most likely to happen.

We had done some previous work in which we supposed that the major thing that was happening was collisions between quarks. We had to assume that the cross section varied as $1/E^8$, where E is the energy, because experimentally the cross sections varied as $1/E^8$ if momentum ratios and angles were left fixed and a scaling argument indicated that meant the internal cross section for quarks had to vary the same way. This is not the way that quantum field theory is expected to go. It should give $1/E^4$ with some logarithms. But that was so obviously in disagreement with experiment that we took this ad hoc form, $1/E^8$. We also had to use a $P_\perp$ of 500 MeV for the quarks inside the proton. This model gave good success but with some difficulties. The first was that we needed an arbitrary cross section to fit the data. More important was that the P_{out} that we chose turned out to be too small. Here P_{out} is the transverse momentum of quarks inside, which is easily measured by the outgoing momentum out of the plane of a collision. In addition, if you measured with a target on one side and looked at the particles on the other side, which we supposed were coming from a quark jet, we obtained too large a momentum for these "away" particles. Furthermore, the number of u quarks in the hadron is greater than the number of d quarks and the ratio of π^+/π^- should therefore be greater than unity. We obtained too large a +/- ratio for the away particles.

Our new attempt is based on QCD. It is preliminary in that it uses nonscaling distributions instead of correctly calculating the effects of the higher collisions. It is also necessary to guess the gluon distribution, as I have discussed above. We must also guess how the gluon fragments into hadrons and we have supposed that it fragments into softer hadrons than do quarks.

We chose $\langle P_\perp \rangle$ = 849 to fit the μ^+ and μ^- P_{out} distributions. This is very poor, because these distributions are almost certainly affected strongly by the higher collisions, which we have not treated fairly in our preliminary nonscaling distribution theory. When a quark and an antiquark annihilate to make a μ pair, a gluon is sometimes omitted and therefore the μ pair is moving with a transverse momentum larger than that which comes from the initial transverse momentum of the quarks inside the proton. All this has been summarized in one number in our theory. At any rate, a fit to the data is shown in Fig. 9. The hope is that the effects will be similar in hadron collisions to what they are in the μ collisions, so we can use the transverse momenta we got from the μ experiments.

I should also point out that, since the μ^+ and μ^- are produced in pp collisions, they can also be produced by quark-quark collisions or by quark-gluon collisions. Figure 8(a) is a diagram in which a virtual photon is knocked out and produces a $\mu^+\mu^-$ pair. Figure 8(b) is a diagram in a quark-gluon collision. This second diagram of higher order in g^2 but is not infinitesimal compared with the first [8(a)] in pp collisions because it is more difficult to find an antiquark than to find a gluon. In proton-antiproton, Fig. 8(a) would dominate.

We got as much of our information as we could from non-hadron experiments in trying to compare this QCD model to hadron experiments. First, it turns out that it can be made to fit the cross section, in spite of the $P_\perp^{-8}$. Thus QCD may be all right. If it may be all right, it probably is. In Fig. 10 I show data of cross sections multiplied by $P_\perp^8$. The solid line is QCD theory and we see that we have a not-impossible situation, even though there is some uncertainty (and some skill) in this graph. I emphasize that the absolute cross sections are completely determined by Politzer's coupling constants and that we have no parameters to make a fit. The gluons make relatively important contributions to the cross section and there is some adjustment in that. Second, the transverse-momentum effect that we put in has a large effect. The dotted curves are QCD without the 849 MeV, which is called "smearing" in our work. It is not that with smearing we can predict the result, but that we cannot prove that it is wrong.

The next curve, with a scale with a wider range of $P_\perp$, Fig. 11, is an experiment at very low $x_\perp$ and 90°. The old $P_\perp^{-8}$ extrapolation and the new QCD predict completely different curves by a factor 100. In the next graph, Fig. 12, instead of multiplying by $P_\perp^8$, which we now appreciate is artificial, incidental, and an artifact of the short range of energies covered, we plot it multiplied by $P_\perp^4$, which should give the right behavior at infinity (to within some logarithmic factor) showing how it extrapolates with and without smear up to $P_\perp$ = 20. Note that both curves are getting flatter; the rise at the beginning is caused by other effects, which are not fundamental, we think.

Compared with our earlier attempts, the large P_{out} that we got from the μ experiments shows up in hadron experiments. The solid curve in Fig. 13 is the new prediction of QCD compared with the data of a P_{out} experiment with "away" particles whose momentum is about 65% of the trigger momentum. The old theory is shown as a dashed line. Everyone will appreciate that none of this evidence is very positive or direct, but only shows that nothing is in disagreement.

Some charge ratios are decreased because gluons come out often and gluon jets make as many negatives as positives. But the gluon jets are softer and in a one-particle, one-arm experiment, you are more sensitive to higher momenta and thus to quarks. Because of this bias, the effect is not as large as might be expected, but is still substantial. Figure 14 is a graph of experimental points of the π^+/π^- ratio from pp collisions, with the dashed curve giving our former results and the solid curve our QCD results. The QCD curve is still a little low, so something may still be a little wrong, but at least it is not impossible.

On the other hand, a more dramatic example is the away-side particles with a large fraction Z_D of the trigger momentum. There are many fewer of these particles because the softer gluons are produced most of the time. When you trigger on one side, there is no bias against the gluons on the other side. Because the gluons are assumed to be softer, we get fewer particles of high momentum. Figure 15 shows several examples of data with the old and new predictions.

Finally, I will talk about the charge ratios on the away side. Now, because of the gluons, we should get much closer to equal numbers of positives and negatives, whereas previously we would have predicted more positives than negatives. Figure 16 shows the previous predictions for positives and negatives, both too high compared with the data, shown as circles. The QCD predictions are shown as squares. There is a problem here with the K^-'s, which I will not discuss.

Another change that the new theory makes is that the ratio of jet cross section to single-particle cross section is closer to 1000, instead of the 100 of the previous theory. For the single-particle cross section the new theory is in good agreement with observed data at 53 GeV, but gives a very different prediction from the old theory at 500 GeV, where there are no data as yet (see Fig. 17).

A very serious effect for experiments which are looking for W mesons is illustrated in Fig. 18. Here we have plotted the W meson production expected as analyzed by Quigg[3] (we shall have to reanalyze it in our new model, but it may not be vastly different, although the transverse momenta will be generally higher). These are compared to our old predictions for the number of hadron jets expected as background. You see, as Quigg remarked, they might be observable, but now our hadron predictions are two orders of magnitude higher so the problem of seeing W's in such a background is very severe. (The $\bar{p}p$ production rate for W's is about a factor of 10 greater than the pp rate at this energy which is still significantly below the expected QCD hadronic background.) It is not at all clear how reliable these predictions are, but the orders of magnitude may not be too far off and the new theory has much more physical content than the old phenomenological one.

Thus, in the QCD theory (still to be regarded as preliminary), we find the following new things:

(i) Much larger cross sections at high $P_\perp$.

(ii) Larger values of P_{out}.

(iii) There should occasionally be three-prong jets from two quarks and a gluon, or some other combination. They should be rare, but there is ample phase space available. If you integrate over the momentum of the other jet, then you can get more three-jet than two-jet cases.

(iv) One should be able to see some charm and anticharm particles coming out from gluon-gluon making a quark-antiquark pair, for example. There could also be other kinds of quark-antiquark pairs (t or b). A very crude estimate might show the probability of a charm quark initiated jet to be of the general order of 1.5 to 2% in pp and 4 to 5% in $\bar{p}p$. This does not mean that one will see a few per cent as many charmed as normal hadrons, because in the lower part of the cascade we expect only normal hadrons.

(v) All the effects we expect are nearly the same for pp and $\bar{p}p$, except for the W production and $\mu^+\mu^-$ pairs from a quark-antiquark annihilation, because there are somewhat more $q\bar{q}$ in $\bar{p}p$ than in pp. There is a background effect, a possibility of producing W's from quark-gluon collisions. These contributions, which have not been evaluated, will be the same for pp and $\bar{p}p$. The W will have higher transverse momenta than previously expected. Because of (i) they will have to be observed behind a very large background of hadrons.

IV. A Look into the Future

I would like to illustrate in a qualitative way what will be seen in the future. Instead of the complicated case of two protons making a quark-antiquark pair at high transverse momentum, I'll take the simpler but similar case of e^+e^- making hadrons as a function of energy. I draw in Fig. 19 momentum-space diagrams of where you will find the hadrons. The absolute scale is the beam energy. At a reasonable known energy, say $E \approx 8$, the particles will lie in opposite jets as shown in the first sketch. A finite transverse momentum is possible for the hadrons, of order 0.5 GeV or less.

When we go to higher energy (second sketch), we will expect roughly the same thing, stretched out along the jet by our scaling. The transverse momentum will therefore look smaller. But there is the possibility of a small knob sticking out. We have to go to still higher energy to see what it is (third sketch). It is another jet, perhaps another gluon, coming out. As you increase the energy, you get a more structured picture. At "ultra-high" energy (fourth sketch), there are many prongs. It is like looking at a tree in more and more detail and seeing more and more prongs. Such a "tree" is called a "fractal," known from the mathematical problem of subdividing the sides of a triangle into smaller triangles.[4] We may have to deal with fractals at ultra-high energy.

There is a problem of perturbation theory. We should be able to calculate by small-coupling theory, but it isn't low order, because it has so many prongs. If one wants to calculate down to a cutoff of smaller transverse momentum, then the higher-order diagrams become more important. But they ought to be summable or analyzable. If one looks at moments, one gets simple differential equations. But if one wants to discuss more detail, it is necessary to discuss such a "fractal."

I believe that it is quite possible that by the time the machine is built, the theory will be worked out and under control. The difficulty is to formulate in more technical detail what part you can calculate and what part you cannot. We know generally that we can calculate the high-momentum part and cannot calculate the low-momentum part. Calculation of moments will not give enough detail of the fractal and we need to be able to calculate more detail of each prong. When we can do these calculations, we will be able to prove all the relationships and theorems and have that end of hadron physics worked out.

References

1. R. D. Field, Phys. Rev. Lett. 40, 997 (1978); R. P. Feynman, R. D. Field, and G. C. Fox, "A Quantum Chromodynamic Approach for the Large Transverse Momentum Production of Particles and Jets," CALT-68-651 (submitted to Phys. Rev.).
2. H. D. Politzer, Phys. Reports 14C, 129 (1974); H. Georgi and H. D. Politzer, Phys. Rev. D14, 1829 (1976).
3. C. Quigg, Rev. Mod. Phys. 49, 297 (1977).
4. B. Mandelbrot, Fractals (W. H. Freeman and Co., 1977). He says "The nature of self similarity seems tantalizingly close to the physicists' much more recent and still unsystematic nature of scaling and of renormalization groups."

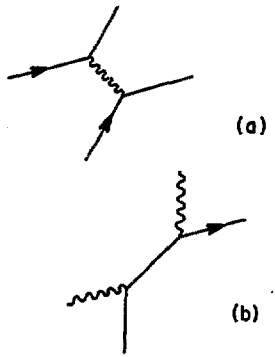

Figure 1

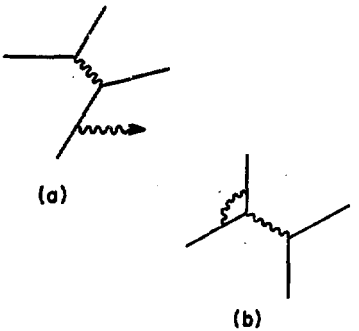

Figure 2

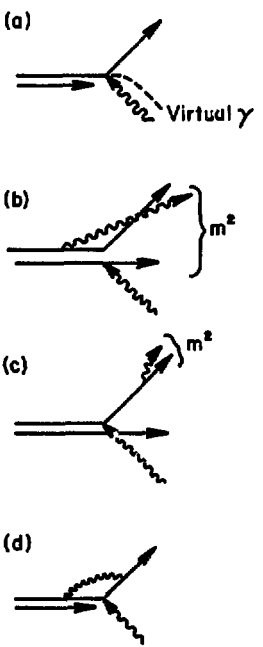

Figure 3

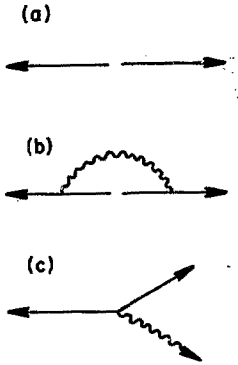

Figure 4

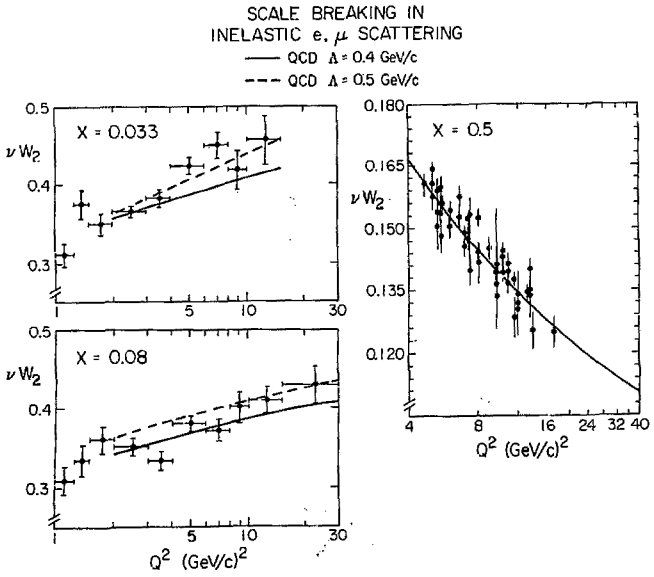

Figure 5

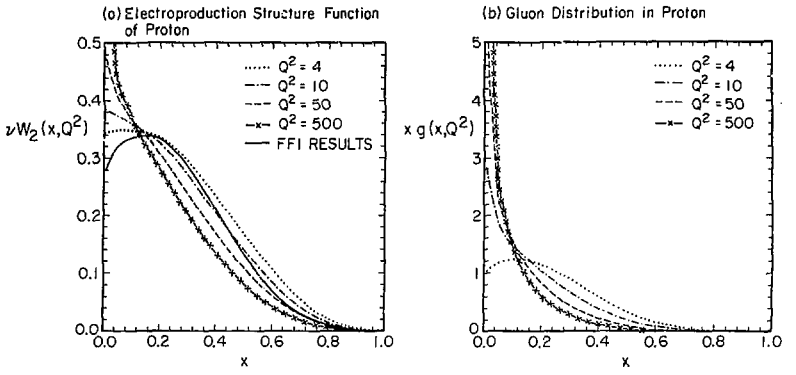

Figure 6

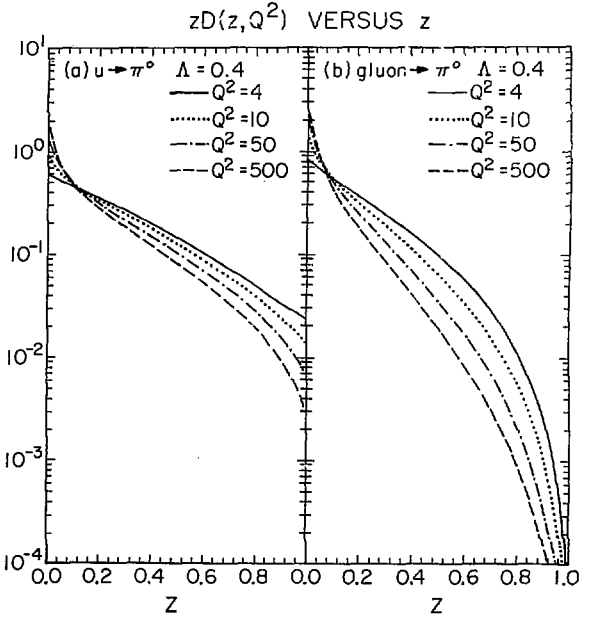

Figure 7

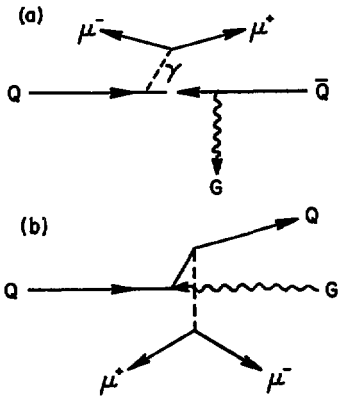

Figure 8

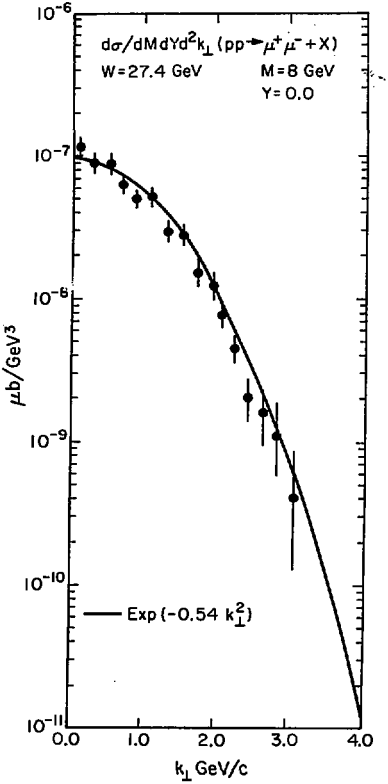

Figure 9

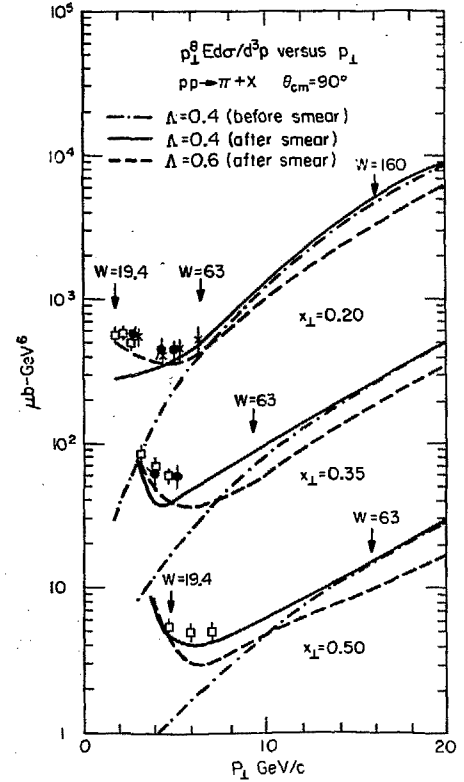

Figure 10

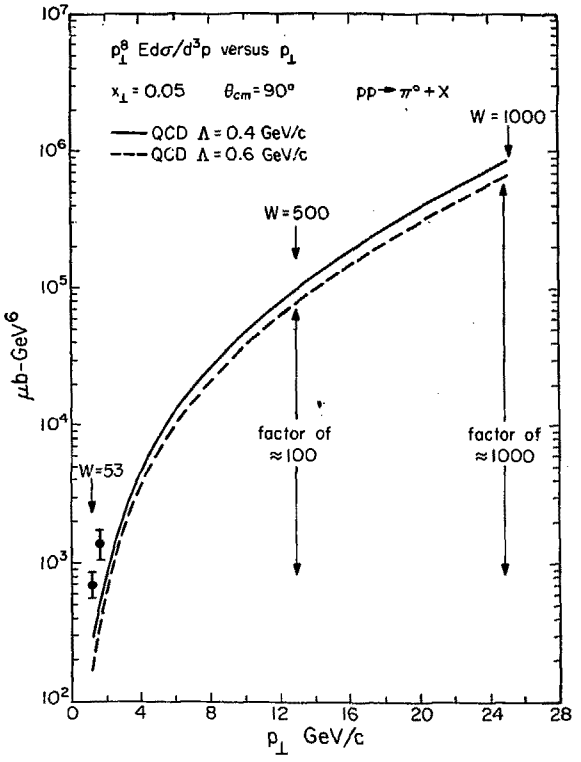

Figure 11

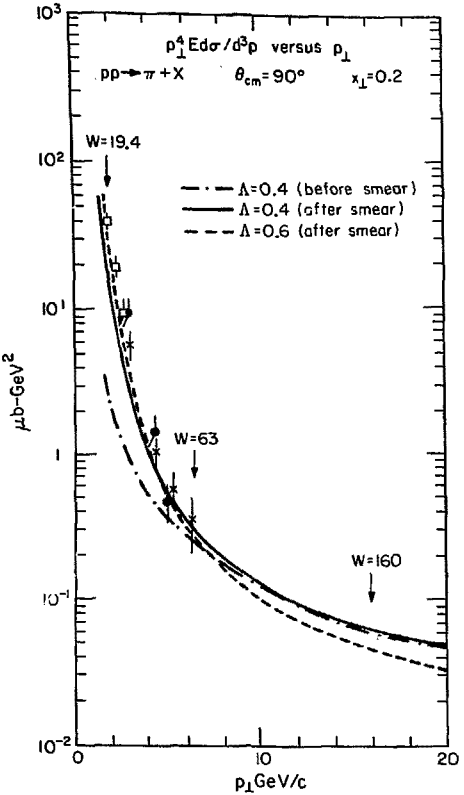

Figure 12

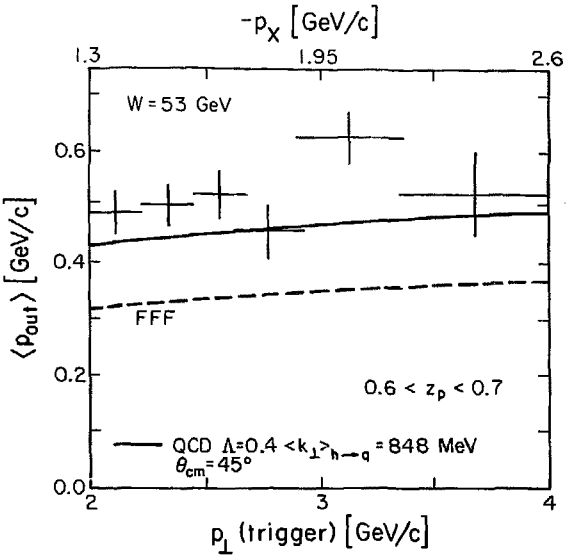

Figure 13

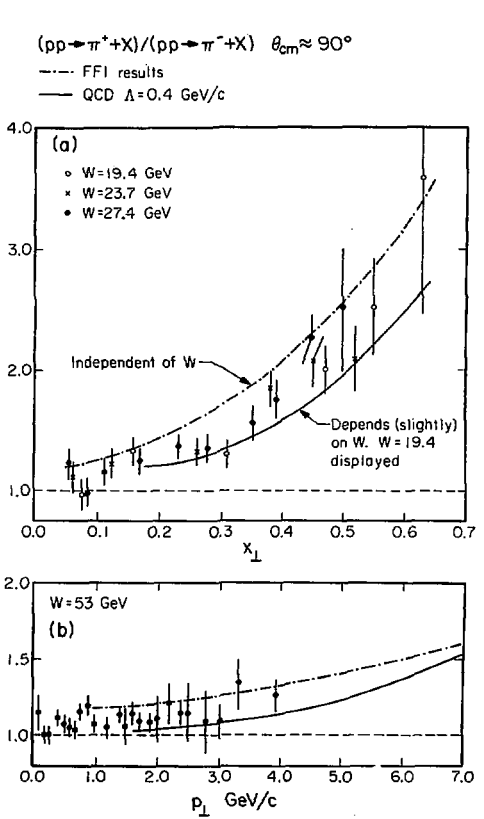
(pp→π⁺+X)/(pp→π⁻+X) θcm≈ 90°
FFI results
QCD Λ=0.4 GeV/c
(a)
W=19.4 GeV
W=23.7 GeV
W=27.4 GeV
Independent of W
Depends (slightly) on W. W=19.4 displayed
X⊥
W=53 GeV
(b)
p⊥ GeV/c

Figure 14

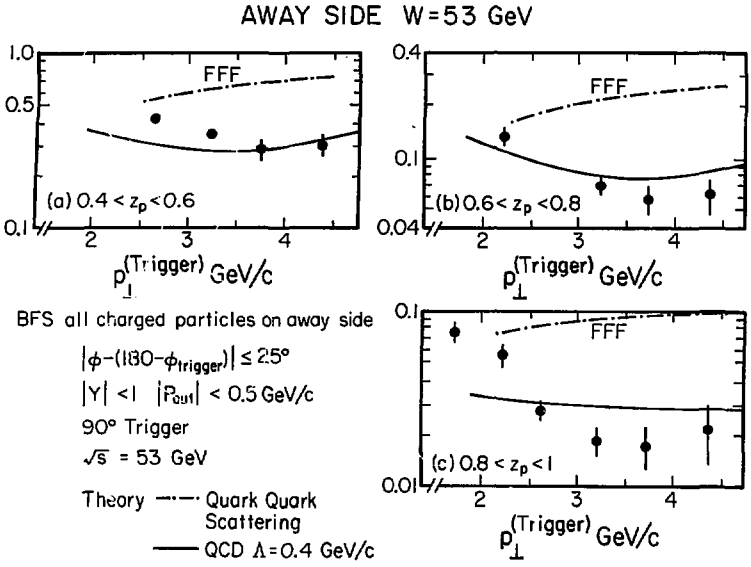
AWAY SIDE W=53 GeV
FFF
(a) 0.4 < z_p < 0.6
(b) 0.6 < z_p < 0.8
(c) 0.8 < z_p < 1
$p_\perp^{(Trigger)}$ GeV/c
BFS all charged particles on away side
$|\phi-(180-\phi_{trigger})| \leq 25°$
$|Y| < 1$ $|P_{out}| < 0.5$ GeV/c
90° Trigger
$\sqrt{s}$ = 53 GeV
Theory Quark Quark Scattering
QCD Λ=0.4 GeV/c

Figure 15

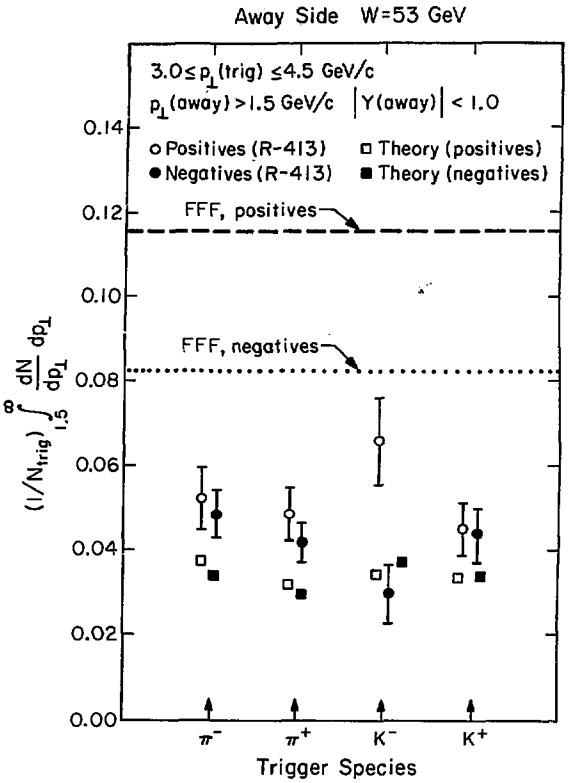
Away Side W=53 GeV
3.0≤ p⊥(trig) ≤4.5 GeV/c
p⊥(away) >1.5 GeV/c |Y(away)| < 1.0
o Positives (R-413)
● Negatives (R-413)
□ Theory (positives)
■ Theory (negatives)
FFF, positives
FFF, negatives
0.14
0.12
0.10
0.08
0.06
0.04
0.02
0.00
$(1/N_{trig}) \int_{1.5}^{8} \frac{dN}{dp_\perp} dp_\perp$
π^-
π^+
K^-
K^+
Trigger Species

Figure 16

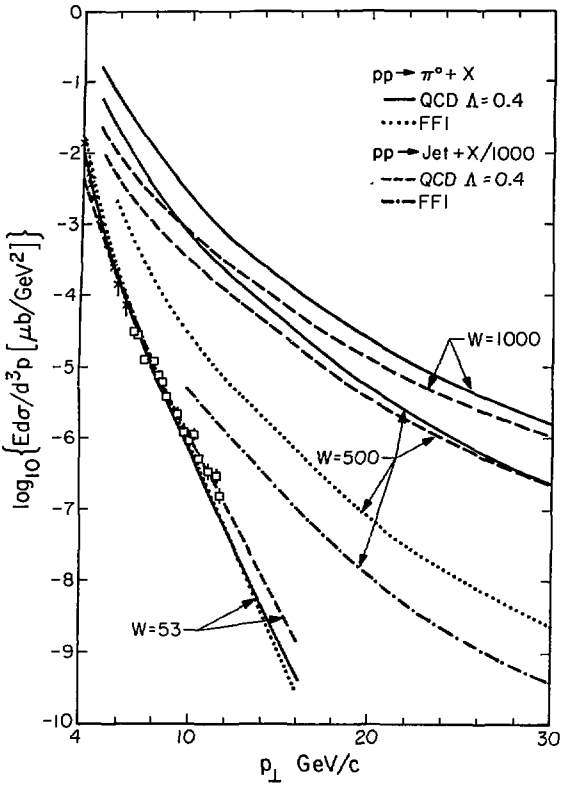
pp → π° + X
QCD Λ = 0.4
FFI
pp → Jet + X/1000
QCD Λ = 0.4
FFI
W=1000
W=500
W=53
log10{Edσ/d³p [μb/GeV²]}
p⊥ GeV/c
0
-1
-2
-3
-4
-5
-6
-7
-8
-9
-10
4
10
20
30

Figure 17

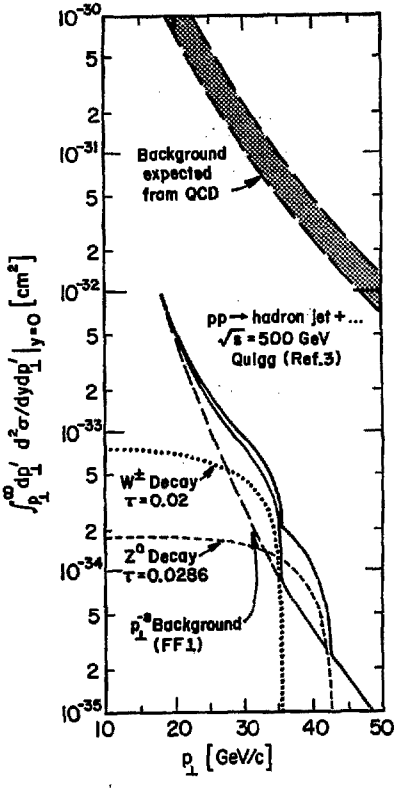
Background
expected
from QCD
pp → hadron jet + ...
√s = 500 GeV
Quigg (Ref.3)
W± Decay
τ=0.02
Z⁰ Decay
τ=0.0286
p_T^-8 Background
(FF1)
∫_{p_T}^{8} dp_T' d²σ/dydp_T'|_{y=0} [cm²]
p_T [GeV/c]

Figure 18

e^+e^- → HADRONS VS. ENERGY

(Drawings Scaled to Beam Energy - Momentum Space, Final Hadrons)

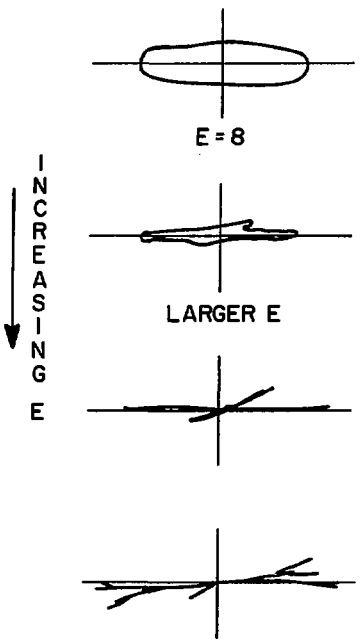

Calculations via "Pert." Theory (Trees)

Figure 19

HIGH LUMINOSITY $\bar{p}p$ MACHINES: THE PHYSICS GOALS

David B. Cline
Fermi National Accelerator Laboratory, Batavia, Illinois 60510
and
University of Wisconsin, Madison, Wisconsin 53706

Abstract

High energy $\bar{p}p$ collisions will provide a laboratory to observe the interactions of point-like constituents. With machines of luminosity $> 10^{31} cm^{-2} sec^{-1}$ the production rate of the intermediate vector bosons and possibly of Higgs bosons will be adequate. The production of massive vector particles that decay electromagnetically as well as the direct production of dileptons will extend knowledge of the electromagnetic interactions. Several schemes to increase the luminosity of $\bar{p}p$ storage rings are discussed.

I. Introduction

The scheme for adding an antiproton source to the Fermilab machines which uses the Booster to decelerate the $\bar{p}$'s and a new electron cooling ring to damp the three dimensional $\bar{p}$ phase space has been described by Cline, McIntyre, Mills, and Rubbia previously. [1] This scheme should provide a luminosity of $\sim 10^{30} cm^{-2} sec^{-1}$ in the energy doubler (Tevatron) ring. At this luminosity many exciting experiments can be carried out including the search for the intermediate vector boson. A lower luminosity is expected in the Main Ring at Fermilab. [1]

Future applications of colliding $\bar{p}p$ machines at Fermilab should likely concentrate on the use of the doubler because:

1. The regular 400-GeV machine program can continue unabated to the experimental areas.

2. Antiproton production can continue simultaneously, thus allowing for a constant luminosity operation.

3. The vacuum in the doubler is expected to give lifetimes in excess of 24 hours.

However, an increased luminosity by a factor of 10-100 would be of extreme interest in order to study exotic weak and strong-interaction processes. As a comparison we may cite e^+e^- machines; very roughly a 2-TeV $\bar{p}p$ machine with a luminosity of $10^{32} cm^{-2} sec^{-1}$ would be equivalent in some sense to an e^+e^- machine (quark-antiquark machine) with a center-of-mass energy of $\sim$ 200 GeV. Thus for purely weak and electromagnetic interactions a high luminosity $\bar{p}p$ machine is in many ways comparable to an e^+e^- machine. However, for strong interactions, especially vector gluon exchange, there is no corresponding e^+e^- process and the $\bar{p}p$ machine has a unique physics capability.

Since this is a workshop, I'd like to discuss two subjects: one is the subject of the Workshop "Can we design high luminosity $\bar{p}p$ machines?" Of course, there is always the question "Should we design high luminosity $\bar{p}p$ machines?" It's a little harder to justify perhaps. For the second part of my talk I will discuss a few points where high luminosity $\bar{p}p$ interactions may give physics an interesting reaction that might be hard to get otherwise.

Let me first start out by reviewing what was said previously. The two machines that are being designed at this moment and are in some stage of being constructed are the $\bar{p}p$ machines at Fermilab which ultimately will have 2 TeV in the center of mass and a luminosity of about $10^{30} cm^{-2} sec^{-1}$ and the machine at CERN using the SPS will have an energy of 0.54 TeV and again a luminosity of $10^{30} cm^{-2} sec^{-1}$. [4] The most important question is "Can one achieve a higher luminosity in these machines?" Some of us have gone through the small exercise to start off the Workshop of discussing how you go about making a higher luminosity machine, let's say at Fermilab. [3] Let me first review the existing scheme which will be discussed in more detail this afternoon.

Figure 1 shows the schematics of the machine at Fermilab. Antiprotons are made by extracting the proton beam at 80 GeV/c and the antiprotons will travel cross country through a FODO channel into the Booster, will then be decelerated to 200 MeV (644 MeV/c) and then transferred to a small cooling ring. Electron cooling will be used to collapse the phase space. This will be done repetitively for a large number of cycles until approximately 5×10^{11} antiprotons are collected in a day. So we start on the assumption that there will be an electron cooling device which is already under construction at Fermilab and that 5×10^{11} antiprotons per day will give a luminosity of $10^{30} cm^{-2} sec^{-1}$.

Now the question is "What is a mechanism whereby the number of antiprotons can be increased by at least a factor of 10?" At the Workshop we will have to discuss this extensively. The existing techniques using electron cooling seem to be limited to a few $\times 10^{11}$ antiprotons per day, and in order to collect larger number of antiprotons, it will probably be necessary to build a new large-aperture device to collect a larger phase space of antiprotons. One possible scheme would be to add a precooler as shown in Fig. 1. The Booster in principle could be accepting antiprotons back into the cooling ring during its idle time, so if a new ring were added, let's say a precooling ring with a very large acceptance, it would be available for cooling the phase space of that beam in approximately 2 to 3 seconds. So, for example, if betatron stochastic cooling is used in this ring, there there would be 2 to 3 seconds to do stochastic cooling, so that the antiprotons from that ring could be put through the Booster, transferred to the electron cooling ring, and then phase space completely collapsed. The scheme is outlined in Fig. 2. The precooler would be collecting antiprotons and the electron cooler would be the storage device for keeping antiprotons

cool for a very long period of time. Using this technique, provided all the problems can be solved, collecting large phase space antiprotons, target heating, and a large list of these which we'll go into in the Workshop, then it seems possible to get 3×10^{12} antiprotons. This scheme depends critically on fast betatron stochastic cooling.

The second scheme is to add a new supercooler ring which would be an enlarged version of the AA ring being constructed at CERN. In this case all the cooling would be done in this ring and the cycling time of the Booster would not set the cooling time required as in the case of the precooler. This scheme has very serious problems because the very large circumference of the Main Ring is not ideally matched to a supercooler. Furthermore, there will be serious target heating problems and finally the large acceptance - large circumference super cooler ring is likely to be extremely expensive if we scale from the expected cost of the CERN AA ring.[2]

II. Increasing the Luminosity of $\bar{p}p$ Machines

In order to improve the luminosity above $10^{30}cm^{-2}sec^{-1}$, there are four possibilities: Increase the number of protons or antiprotons; decrease the beta function at the collision point; decrease the number of bunches; or cool the high-energy beams to decrease the size to the point where the beam-beam tune limits the luminosity.

Let us take a specific example. In order to obtain a $\bar{p}p$ luminosity in excess of $10^{31}cm^{-2}sec^{-1}$ in the energy doubler it will be necessary to collect more then 10^{12} $\bar{p}$ per machine filling cycle. Depending on the actual gas pressure in the doubler and the other sources of beam blowup the filling time may be as short as every 5 hours. This will set as a goal the collection of 10^{12} $\bar{p}$'s in five hours for the design of the large acceptance ring. As discussed before there are several schemes to improve the $\bar{p}$ collection:

1. Construction of a large aperture "super cooler" ring.

2. Addition of a large aperture pre-cooling storage ring.

In the first case a dc ring is constructed with a large enough aperture to allow space for collection and accumulation of intense $\bar{p}$ beams. In the second case the ring is used primarily for collection and the accumulation is carried out on the electron cooling ring.

Let us first review in detail the steps in obtaining the expected yield of $\bar{p}$'s in the present scheme. Secondary particles at ~ 6.5 GeV/c are produced by 80 GeV/c protons from the Main Ring impinging on a small tungsten target. Particles are injected into the Booster ring and decelerated to 200 MeV. Only $\bar{p}$'s survive at the end of the process. The beam is transferred to the storage ring where it is cooled and added to the stack of previous accumulations. One expects to accumulate $\frac{1}{2} \times 10^7$ $\bar{p}$/pulse leading to ~ 10^{11} particles in 2×10^3 pulses (3 hours).

The collected ratio of antiprotons of momentum $\bar{p}$ to protons on target is given by

$$\frac{N\bar{p}}{N} = \frac{1}{\sigma_a}\left(E\frac{d^3\sigma}{dp^3}\right)(\delta p_\perp{}^2)\left(\frac{dp_{\parallel}}{E}\right)\epsilon_T,$$

where σ_a is the absorption cross section, ϵ_T the target efficiency and

$$\frac{dp_{\parallel}}{E} = \delta P_{\bar{p}}/P_{\bar{p}}$$

$$dp_\perp{}^2 = \frac{4p_{\bar{p}}^2\sqrt{\bar{\epsilon}_x\bar{\epsilon}_y}}{\pi\bar{\eta}\beta^*},$$

where $\bar{\epsilon}_x$, $\bar{\epsilon}_y$ are the Booster x, y acceptance for 644 MeV/c antiprotons, $\bar{\eta}$ and β^* have the normal meaning for a synchrotron machine. The invariant production cross section $Ed^3\sigma/dp^3$ is not yet well measured to better than a factor of two at 6.5 GeV/c. Figures 3 and 4 show the available data on $\bar{p}$ production in the relevant proton energy range as a function of production angle.

Figure 5 shows the cross section of 6 GeV/c $\bar{p}$ production in the forward direction as a function of incident proton energy. There is apparently little gain in increasing the incident proton energy. The present extraction scheme is limited to about 100 GeV/c protons. The best present estimate for the invariant cross section is ~ 1 mb/GeV/c^2. The measured acceptance of the Booster is

$$\bar{\epsilon}_x = 2.6\pi\text{mm mrad}$$

$$\bar{\epsilon}_y = 1.3\pi\text{mm mrad}$$

$$\delta P/p = \pm 0.15\%$$

and the estimated target efficiency ϵ_T is 0.15.

Using these values we obtain

$$N\bar{p}/Np = 2 \times 10^{-7}.$$

For 5×10^{13} protons on target (the machine intensity expected in 1979-1980) the yield of $\bar{p}$ for every 3 sec cycle of the Main Ring is 10^7 $\bar{p}$/mrad pulse giving ~ 10^{10} $\bar{p}$/hour. Collecting $\bar{p}$ for 10-20 hours gives ~ 10^{11} $\bar{p}$. There are other possible improvements that might increase the yield by a factor of about 5. Clearly in order to further improve the yield the acceptance of the $\bar{p}$ collection ring must be increased.

Let us first turn to the target and collection system requirements. Antiproton emittance matched to the Booster acceptance is given by

$$\bar{\epsilon}_x = \pi\theta_x a_x$$

$$\bar{\epsilon}_y = \pi\theta_y a_y,$$

where θ_x, θ_y are the maximum production angles accepted and a_x, a_y the spot size of the protons on the target. For the case of $a_x = 0.2$ mm = a_y and realistic Booster acceptance we obtain

$$\theta_x^{max} = 13 \text{ mrad}$$

$$\theta_y^{max} = 6 \text{ mrad.}$$

On the other hand, there are various schemes for increasing the Booster acceptance for the special case of deceleration of $\bar{p}$'s (where space charge effects are probably not too important) and the angular acceptance of the present scheme could well extend to 15-20 mrad. Note that the production angular distribution is relatively flat over a much broader angular range (Fig. 4). Thus we conclude that a sizable gain in antiproduction yield can be obtained by accepting a larger transverse phase space. In the longitudinal phase space the yield is directly proportional to the $dp_{\parallel}/E \sim \delta P_{\bar{p}}/P_{\bar{p}}$. Thus increasing $\delta P/P$ will increase the $\bar{p}$ yield.

In order to increase the yield by at least a factor of 10 consider a collection ring with the following properties

$$\epsilon_x = 20\pi \text{ mm mrad}$$

$$\epsilon_y = 20\pi \text{ mm mrad}$$

$$\delta P_{\bar{p}}/P_{\bar{p}} = \pm 1\%.$$

If a collection system could be constructed to collect a full 20 from the target θ_x, θ_y would increase to

$$\theta_x^{max} = 100 \text{ mrad}$$

$$\theta_y^{max} = 100 \text{ mrad}$$

and give an increase of about a factor of 5 and 7 each plane yielding a factor of 35. It is very unlikely that an adequate collection system could be constructed to realize the full yield. However, a factor of $3 \times 4 = 12$ may be realized (i.e., $\theta_x^{max} \sim 50 \text{ mrad} \sim \theta_y$).

In the longitudinal direction the gain will be a factor

$$[\delta P_{\bar{p}}/P_{\bar{p}}]\text{new} \;/\; [\delta P_{\bar{p}}/P_{\bar{p}}]\text{ old} = \frac{2.0\%}{0.15\%} = 7$$

for each Booster batch. However, it is necessary to collect all 13 Booster batches every Main-Ring cycle (~ 3 sec). In order to accomplish this it will be necessary to work near transition and to rotate the bunches in phase space. It should then be possible to stack all 13 batches with a total $\delta p/p$ in the ring of $\pm 1\%$.

A realistic gain of 7×12 in $\bar{p}$ yield can be anticipated giving

$$N_{\bar{p}}/N_p = 1.7 \times 10^{-5}$$

and 10^{12} $\bar{p}$ per hour. Improved target efficiency could give a factor or two larger yields.

One scheme for using a precooler is as follows: Antiprotons are injected into the precooler ring and the longitudinal and transverse phase space is damped down by stochastic cooling to the values of the acceptance of the Booster, namely $\delta P_{\bar{p}}/P_{\bar{p}} = \pm 0.15\%$; $\bar{\epsilon}_x = 2.6\pi$mm mrad/Booster batch; $\bar{\epsilon}_y = 1.6\pi$mm mrad/Booster batch. A cooling time of 2-3 sec is available for this phase-space damping. Assuming an effective phase space of $\bar{\epsilon}_x = 8\pi$mm mrad and $\bar{\epsilon}_y = 5\pi$mm mrad for the 13 Booster batches the transverse beam damping required is about a factor of 3 in each dimension. The longitudinal phase space must be cooled by a factor of 7 in 2-3 sec. These values of the stochastic cooling time are not out of bounds with the present state of the art in stochastic cooling.

After the beam is stochastically cooled it is injected into the Booster, decelerated and transferred to the electron cooling ring for final cooling.

We have obtained a rough estimate of the parameters of the precooler ring from the above requirements.[3] The machine should be strong focussing with $\gamma_t \sim 9$, $\beta \sim 8\text{M}$ and $\langle X_p \rangle = 1\text{M}$. The transverse space occupied by the beam is

$$\delta P/P_p \langle X_p \rangle = 2 \times 10^{-2} \times 1 = 2 \text{ cm.}$$

At the injection point $\langle X_p \rangle \sim 3\text{-}5$ and a free aperture of 10-20 cm is required in the machine, for injection and stacking.

The parameters of a supercooler could be scaled from the design of a similar ring at CERN.[2] Although the $\bar{p}$ momentum is 3.5 GeV/c in the CERN design it would likely be better to collect at 6.5 GeV/c at Fermilab because of the need to transfer the beam back into the Booster and electron cooling ring.

The luminosity for a head-on collection of N_B bunches is given by

$$\mathcal{L} = \frac{3 N_p N_{\bar{p}} f}{\sqrt{\beta_x^* \beta_y^*}\; \sqrt{\epsilon_{x_1}^o + \epsilon_{x_2}^o}\; \sqrt{\epsilon_{y_1}^o + \epsilon_{y_2}^o}} \frac{1}{N_B} \left(\frac{P_f}{P_i}\right),$$

where P_f is the final $\bar{p}$, p momentum, P_i is the momentum in the cooling ring, f is the revolution frequency, N_p, $N_{\bar{p}}$, are the total number of protons and antiprotons, respectively. β_x^*, β_y^* are the beta function values at the collision point and ϵ_x^*, ϵ_y^* are the emittance of the Booster for p and $\bar{p}$.

In order to increase the luminosity there are several possibilities:

1. Increase N_p, $N_{\bar{p}}$
2. Decrease β_x^*, β_y^*
3. Decrease N_B
4. Increase P_f

For the scheme advocated here $N_{\bar{p}}$ is approximately 6×10^{12}. Clearly β_x^*, β_y^* should be made as small as possible, consistent with the available space in the collision straight section. A further increase in luminosity occurs if N_B, the number of bunches is decreased. Thus it is necessary to increase N_p/N_B. This possibility will be discussed in the next section. In order to obtain a luminosity of $10^{31}\text{cm}^{-2}\text{sec}^{-1}$ with $N_{\bar{p}} = 6 \times 10^{12}$ we take the following parameters

$$(p_f = 1\ \text{TeV/c})$$
$$N_{\bar{p}} = 6 \times 10^{12}$$
$$N_p = 6 \times 10^{12}$$
$$\beta_x^*, \beta_y^* = 1.5\ \text{M}$$
$$N_B = 6.$$

These parameters require stacking in the doubler and superconducting quadrupoles for the low-β section. For these parameters we find 10^{12} protons per bunch and 10^{12} antiprotons per bunch. The luminosity and vertical tune shift are closely related. We use a simple calculation for the SPS but including the factor of P_f/P_i increase for the L TeV/c proton and antiprotons in the Tevatron. For 10^{12} $p/\bar{p}$ in each bunch the expected luminosity is $8 \times 10^{31}\text{cm}^{-2}\text{sec}^{-1}$. However, the tune shift is 3×10^{-2} which may be too large. Thus it will be necessary to separate the $p/\bar{p}$ at every point except the low β region. Again the large tune shift indicates a limitation of the practical luminosity for $\bar{p}p$ machines of $\sim 10^{31}$-$10^{32}\text{cm}^{-2}\text{sec}^{-1}$.

III. Physics Goals of High Luminosity Machines

(i) Point Like Collisions in Hadron-Hadron Interactions. A very large body of evidence now exists in support of the hypothesis that hadrons contain point-like constituents -- so much so that these concepts will play an important role in the future development of particle accelerators. At the same time there is a strong theoretical belief that a field theory of these constitutents is within our grasp (i.e., the QCD theory). This evidence largely comes from the scattering of leptons on hadrons or from e^+e^- scattering with the production of hadrons or from the production of lepton pairs in hadron-hadron collisions. Recently the evidence for point-like constitutents in hadron-hadron collisions has sharpened. Unfortunately, the present generation of machines are at too low an energy to allow completely convincing tests of these concepts for hadron-hadron collisions.

There are five fundamental types of reactions that have been studied:

$$\nu_\mu + \text{hadron} \rightarrow \left[\nu \begin{matrix}\text{charged}\\ \text{lepton}\end{matrix}\right] + (\text{hadrons}) \qquad (1)$$

$$\text{charged lepton} + \text{hadrons} \rightarrow \text{charged lepton} + \begin{matrix}\text{charged}\\ (\text{hadrons})\end{matrix} \qquad (2)$$

$$\text{hadron} + \text{hadron} \rightarrow \begin{matrix}\text{charged}\\ \text{lepton pair}\end{matrix} + (\text{hadrons}) \qquad (3)$$

$$\text{electron} + \text{positron} \rightarrow (\text{hadrons}) \qquad (4)$$

$$\text{hadron} + \text{hadron} \rightarrow \left(\begin{matrix}\text{large p}\\ \text{hadrons}\end{matrix}\right) + \text{hadrons} \qquad (5)$$

The symbol (hadrons) denotes the inclusive production of many hadron states; in the quark model they are thought to be the "spectators" in the hard collision in each case considered.

It is interesting to ask what limits on the "size" of the fundamental constituents come from. The measurement of the limit of the size of the constituents comes from the study of the momentum-transfer distribution in the collisions, much the same as Rutherford measured the "size" of the inside of the atom 60 years ago. Figure 1 shows a typical momentum transfer distribution for high-energy neutrino collisions. Recently there has been some evidence that the constituents carry a "fermi" momentum inside the proton of ~ 800 MeV/c. This possibily has to do with the fact that the constituents are confined (i.e., no free quarks have been seen).

In order to study weak and electromagnetic interactions it seems necessary that an annihilation process occur. For example, the weak neutral vector boson occurs as an annihilation process for

$$e^+e^- \rightarrow Z^0 \rightarrow \mu^+ + \mu^-.$$

Other attempts to observe weak processes, say in the scattering of e^+e^- by the exchange of weak hoson appear to be hopelessly swamped by the background from ordinary processes (i.e., the exchange of photons). Similarly the detection of weak or electromagnetic processes in hadron + hadron collisions requires the observation of quark-antiquark annihilation, i.e.,

$$q + \bar{q} \rightarrow Z^0 \rightarrow \mu^+ + \mu^-.$$

At this point a considerable difference between proton-proton and proton-antiproton collisions becomes apparent -- antiprotons are filled with antiquarks but protons have only a small amount of antiquarks. The evidence for a small component of antiquarks in the proton comes from two sources:

1. Comparison of neutrino and antineutrino collisions with hadrons.

2. The overall rate for the production of lepton pairs by hadron collisions.

Both experiments give information about the momentum spectrum of the antiquarks in the proton as well. Figure 2 illustrates the level and momentum spectrum of the antiquarks as obtained from detailed analyses of neutrino-antineutrino interactions.

For the purpose of the calculations and comparisons in this report we assume that the constituents are truly point like - just like electrons and that the antiquark distribution in the nucleus follows the results of neutrino experiments. Of course the antiproton is considered to be filled mostly with antiquarks and the proton with quarks. The "momentum" spectrum of the quarks (antiquarks) are taken from neutrino experiments. Once these assumptions are made, the resulting calculations are trivial and follow directly from similar calculations for e^+e^- interactions.

(ii) Production of Intermediate Bosons. I will try to go through some graphs to show you what the effect of the different parton-antiparton distribution is on pp or $p\bar{p}$ production cross sections. It's true now, in contrast to a few years ago, the q and $\bar{q}$ distributions have been uniquely extracted from the data so that reliable predictions can be made. The direct evidence for the $\bar{q}q$ interaction now exists, and I believe this gives confidence in the use of $\bar{p}p$ machines. It's almost model-independent. I think the calculations for pp machines are still somewhat model-dependent.

So let me start out first by just showing (this is from the calculation of Quigg) the relative cross sections (Figs 6 and 7). Now what I am going to discuss is the event rates and cross sections for a machine

with the luminosity of 10^{31} giving integrated luminosities of 10^{36} or 10^{37}. That's the kind of experiments I would hope to do in these machines in five years or so. So, we show a comparison of $\bar{p}p$ and pp, that shows what high luminosity buys. In other words, the $\bar{p}p$ machine gives much higher efficiency at the high energy, high mass particles.

Now what about backgrounds? For example, I've shown the Z^0 sitting on top of the background in Fig. 8. Even in the most pessimistic analysis, as far as I can tell, the Z^0 should still stand well above background, provided the Z^0 has an appreciable decay rate into charged lepton pairs. However, it's also, I think, interesting that in a high-luminosity machine one can explore lepton-antilepton production, e^+e^-, e^+e^-, out to about 50 to 100 GeV, which is not so far from the energies that people talk about. Perhaps if the luminosity can be improved, then one can go a little bit higher. So this already indicates that a high luminosity $\bar{p}p$ machine can explore very high mass lepton-antilepton production.

Let me briefly discuss charged W production. There are really two ways of estimating the W cross section. One is to use the Drell-Yan calculation. There it seems that you know that only antipartons can be made. Neutrino experiments give you the contribution. However, using dilepton data and CVC and neglecting the isoscalar component, a lower bound on the W cross section can be obtained. Of course, this is equally true for pp or $\bar{p}p$. I was surprised that using the most recent data, as reviewed by Cronin, this cross section is actually greater than $2 \times 10^{-32}\text{cm}^{-2}$, whereas, the straight-forward Drell-Yan cross section gives 6×10^{-33}, so this indicates the cross section for W production could be larger than we think and this is very interesting, especially for high-luminosity machines. In this case you would get 1/5 of an event per second with a luminosity of 10^{31} or 10^{32} would give you between 0.2 and 0.06 W's per second. This would be a W factory.

One of the strongest items for a $\bar{p}p$ machine, I think, in contrast to a pp machine is shown in Figs. 6 and 7. If you imagine that Nature holds some very high-mass W's as well as some very low-mass W's, then in $\bar{p}p$ one can go to a very high mass. For example, using the integrated luminosity discussed before, a very high mass W can be observed. There's one extremely interesting thing about the W of such high mass, it will decay into two jets of 300 GeV each. I doubt even in Feynman's model if there would be a large background at this p$_\perp$. In other words, the W's out in this region may have much less background than we have discussed before. Anyway, one point is that the W can be searched for up to a mass of about 1.2 TeV with a high-luminosity machine of about 2 TeV center-of mass-energy. The cross section for W or $l\bar{l}$ grows like τ^{-1} to some power so it goes like s^α where α varies from 10 to 0 depending on the machine and so forth. It's clear that the most important parameter is energy in these machines. The second important thing is luminosity in order to get the count rate and probably the third important thing is the machines. So the ideal machine, I believe, would be given by this: 2-10 TeV, luminosity of 10^{31} to 10^{32} and $\bar{p}p$ versus pp. Now, there are one or two more interesting aspects of W production which I'd like to discuss which are a little different than what Feynman mentioned.[4] In the first place, in $\bar{p}p$ collisions the W's are strongly polarized, strongly aligned. This already gives an effect, which has been mentioned by many authors, that when the W decays, it tends to make $\bar{l}$'s go the direction of the incident proton rather than the direction of incident antiprotons (Fig. 9). It gives an asymmetry in the wrong direction. Most background effects will not give an effect in $\bar{p}p$ collisions. This has not been looked at in detail, but I think it should be. If, when the W decays into its various hadronic decay modes, for example, I am assuming that there is a hypothetical new quark called a t quark, which may exist, then again similar kinds of effects exist; there will be a polarization. For example, when the W decays into $\bar{c}s$ then the $\bar{c}$ will want to go along the direction of the proton, and also in the case of the $\bar{t}b$, probably. Now I don't know how to calculate the mass effects in here so it has to be carried out in the future. There may be a signature for the W production mainly coming from its alignment and the flavor cascade effectively goes into multi-flavored final states. One aspect of the asymmetry, which we like to call charge conjugation violation because if we were dealing with simply a proton we wouldn't see this, is shown from a graph in proposal P92 at CERN showing the production of l^+'s, in this case versus l^+'s, the angular distribution (Fig. 10). It is shown that by just sitting at one angle, a lot more e^-'s than e^+'s are produced and that would already, I think, be extremely difficult to explain by any conventional background. That could be another argument in favor of the $\bar{p}p$.

Finally let me list the decay modes of the W. In each case in order to design a detector to see these individual modes one has yet to find the unique characteristics. Probably for the leptonic decays it will be necessary to see missing neutrinos, although on the other hand, there's a large asymmetry which may help. For the hadron decays, there will be effects having to do with a net flavor in the final state in the flavor cascade. For the Z^0's it is much more problematic because we don't know the number of neutrinos in nature. If the number of neutrinos happens to be extremely large, then the leptonic channels will go way down. There will always be a lot of hadronic channels, but the hadronic channels don't have net flavor because of the flavor conservation of the weak neutral current.

(iii) Search for the Higgs Boson. Another process which looks extremely interesting for high-luminosity $\bar{p}p$ machines is the search for the Higgs boson. This is a mythical, hypothetical best and the mass is not predicted nor is the best experimental signature known. In fact, the signature for the object depends critically on its mass. $\bar{p}p$ or pp production could give a signature for the Higgs boson (Fig. 11). Let us consider $\bar{p}p$. In $\bar{p}p$ the fundamental process would be $\bar{q}q$ goes to the W pole which then radiates a Higgs meson. This has been calculated in proposal 92 at CERN (Fig. 12). (The fundamental cross section was calculated by Gaillard and Ellis.) Another process, which has recently been suggested by Glashow and Nanopoulas, uses two gluons making a Higgs meson (Fig. 13). As an estimate to detect 10-100 events

with a high luminosity $\bar{p}p$ machine, you would be sensitive to Higgs boson mass of about 50 GeV. The signature for looking for the Higgs boson would have to be observation of the W, followed by some aspect of the Higgs decay. For example, if it became the two b quarks that became the two heavy leptons, there would be a W plus additional leptons in the final state, which would give a clue that something other than just W production is going on. Clearly the search for Higgs bosons would benefit from a high luminosity $\bar{p}p$ machine.

(iv) Production of New Hadronic Flavors. Finally, let us end up with some speculations on the cross section for producing very high mass new flavors. So far, there is no reliable evidence yet for charm production in pp or $\bar{p}p$ collisions although there are lots of hints, which I'll come to in a moment. Nevertheless one can imagine new flavors, like charm, what have you, could be produced in pp or $\bar{p}p$ collisions and other sorts of things like if color were to become unconfined at extremely high energy could also be produced. We should keep our eye open for that sort of thing. What I've done is to simply illustrate a point. I've taken the best guesses for the cross section for charm production. I've taken the scaling prediction of Halzen and Gaiser to show what the cross section for charm production could look like as a function of energy (Fig. 14). However, there is evidence now from CERN for prompt neutrino production which suggests that the cross section for charm is much higher. So maybe this is even too pessimistic. I've tried to scale for other kinds of objects like b quarks and t quarks. These cross sections are always larger than the W cross section (probably) which means additional backgrounds which we haven't started to think about yet for W search in pp, or $\bar{p}p$ collisions.

IV. Conclusion

In summary, $\bar{p}p$ interactions will provide strong weak and electromagnetic $\bar{p}p$ interactions. That seems to be well established from existing data. $\bar{p}p$ machines that have been designed to achieve a luminosity of $10^{30}cm^{-2}sec^{-1}$ are in progress. The question is, "Is there a good reason to go to higher luminosity?" My conclusion is that there will be very interesting things to do at higher luminosity. In the first place, there will be large rates for very massive W's if W's exist at much higher masses than the Weinberg-Salam model predicts. On the other hand, the Weinberg-Salam particles seem to exist in relatively low mass regions so they have very large backgrounds. We may have some problems to pull these events out of the background whether we have pp or $\bar{p}p$ collisions. It appears because of the behavior of the lepton pair production at low τ that these machines can reach lepton-antilepton invariant masses up to about 0.05 of the center-of-mass energy. There is a strong argument I believe for the production of exotic states like the Higgs boson where undoubtedly c. m. energy and luminosity will be important. Here is an example in which increased luminosity is extremely important. There probably will be exotic $\bar{p}p$ interactions giving new quark flavors or new massive vector mesons where again high luminosity will be crucial. In comparison to e^+e^- machines, the rates are very favorable, but the backgrounds are very unfavorable (Fig. 15). In pp the backgrounds are 10^7 or 10^8 of the signal whereas in e^+e^- machines in some cases the signal-to-noise is extremely large. I think that on the basis of backgrounds e^+e^- machines look very good; on the basis of rates the $\bar{p}p$ machines certainly can hold their own.

It appears that there are very strong reasons to design high luminosity $\bar{p}p$ machines and I hope this workshop will be the first step in that design study.

References

[1] D. Cline, P. McIntyre, F. Mills, and C. Rubbia, Collecting Antiprotons in the Fermilab Booster and Very High Energy $\bar{p}p$ Collisions, Fermi National Accelerator Laboratory Internal Report TM-689, 1976; D. Cline, Possibility for Antiproton-Proton Colliding Beams at Fermilab, CERN $\bar{p}p$ Note 08, May, 1977. E. Gray et al., IEEE Trans. Nucl. Sci. NS-24, 1954(1977).

[2] CERN $\bar{p}p$ Machine Design Report.

[3] F. Mills, P. McIntyre, C. Rubbia, and D. Cline have had several discussions on the subject at different times.

[4] See Feynman's talk at this Workshop.

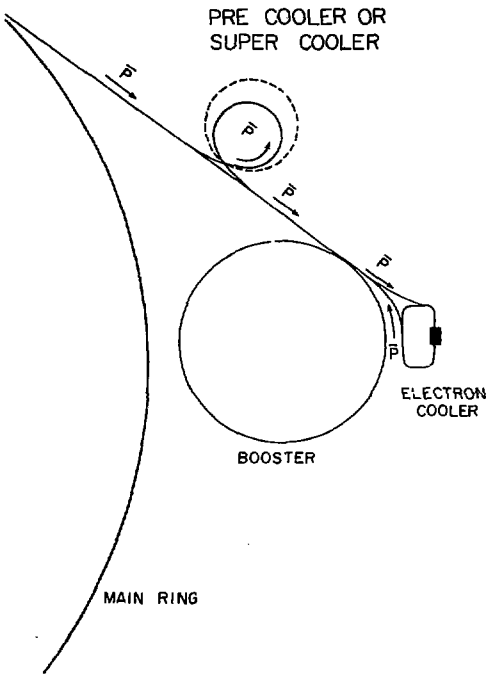

Fig. 1. Fermilab cooling schematic

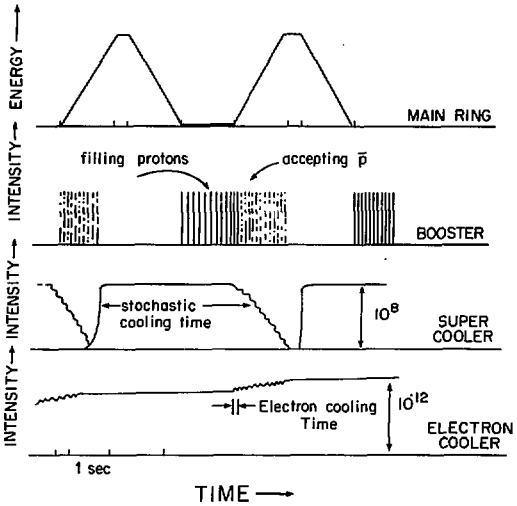

Fig. 2. Basic cooling cycles.

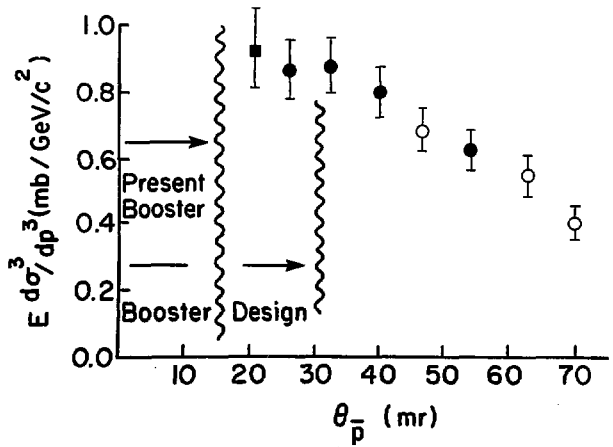

Fig. 3. Production of 6 GeV/c antiprotons.

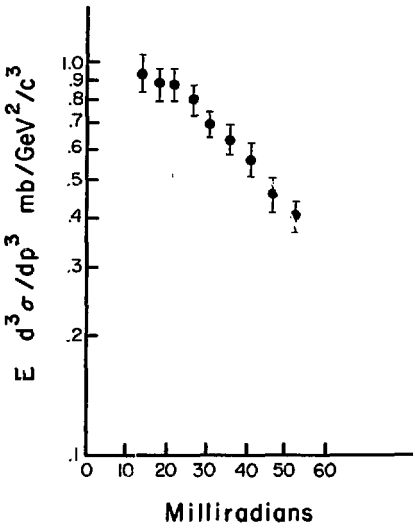

Fig. 4. Production of 9 GeV/c antiprotons from protons on protons at 200 GeV.

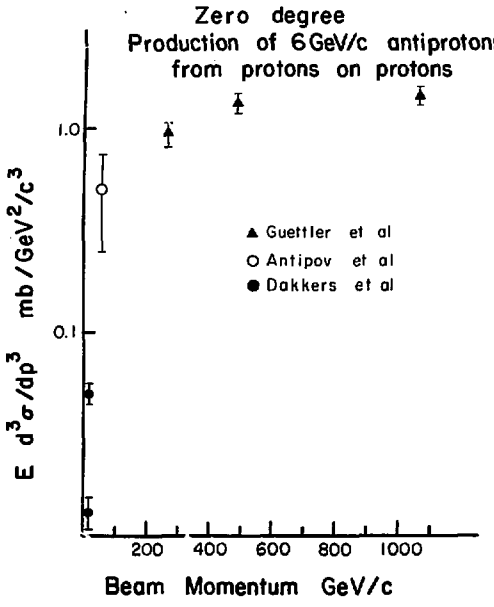

Fig. 5. The production of antiprotons.

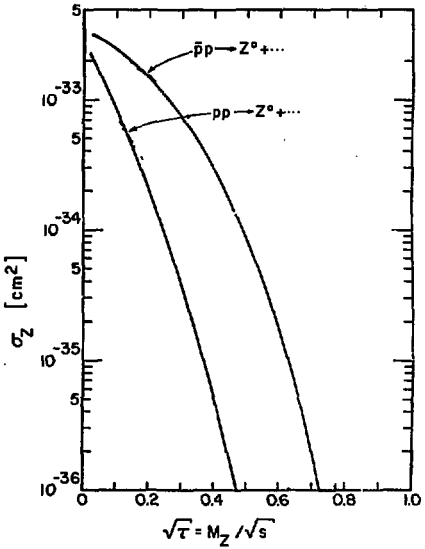

Fig. 6. Z^0 production cross sections.

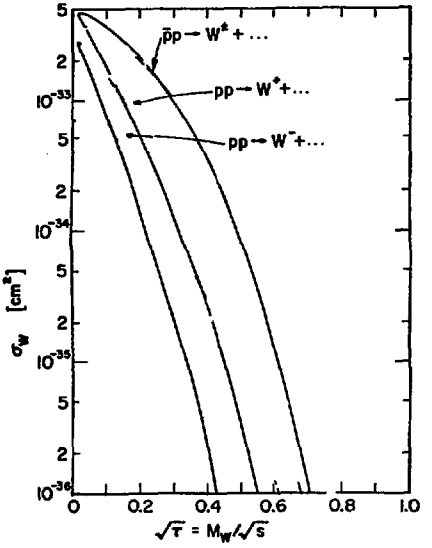

Fig. 7. W± production cross section.

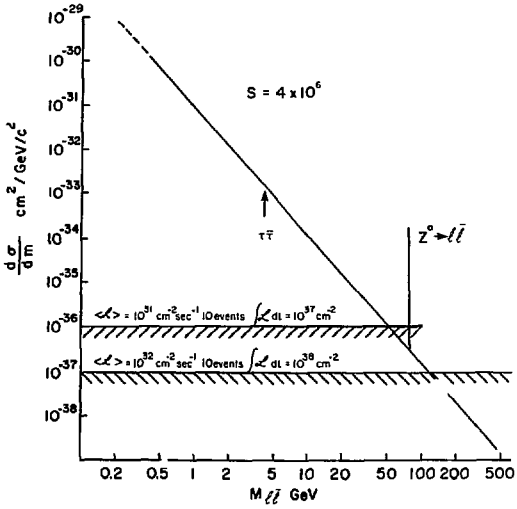

Fig. 8. Lepton pair production cross section.

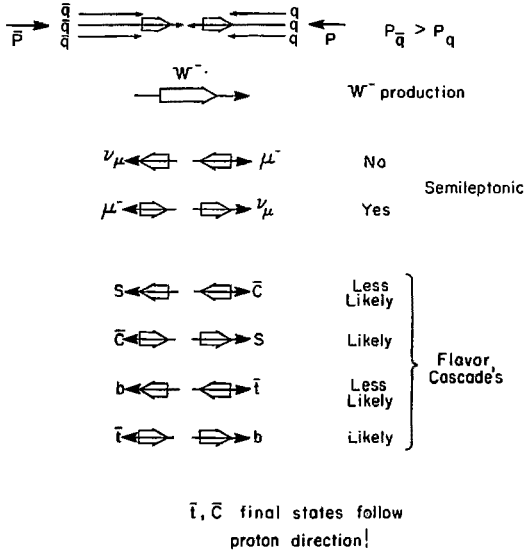

Fig. 9. W± polarization effects in $\bar{p}p$ collisions.

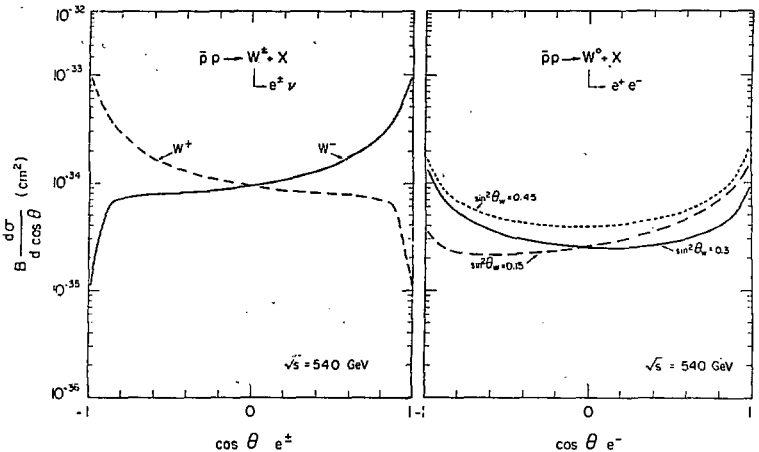

Fig. 10. Charge asymmetries in leptonic decay of intermediate bosons.

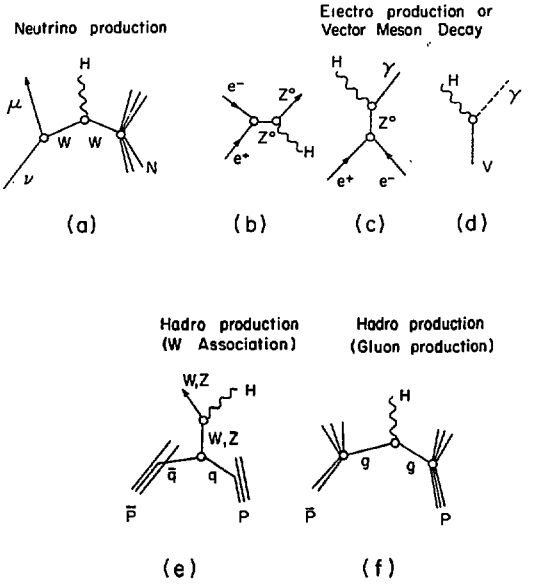

Fig. 11. Mechanisms for Higgs boson production

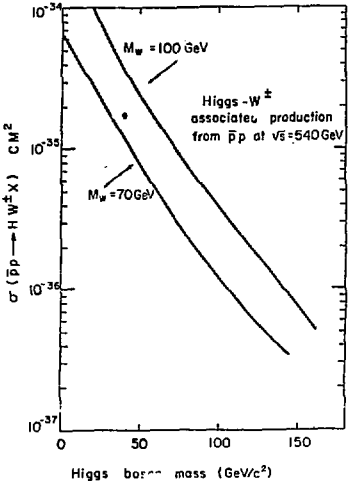

Fig. 12. Associated Higgs-W production according to the quark-parton model and Weinberg Salam couplings

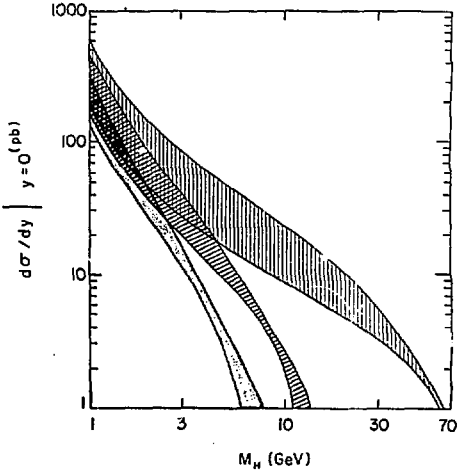

Fig. 13. $d\sigma_H dy^{-1}|_{y=0}$ as a function of H mass Each shaded band represents a different center-of-mass energy ($\sqrt{s}$ = 27.4, 60, 400 GeV).

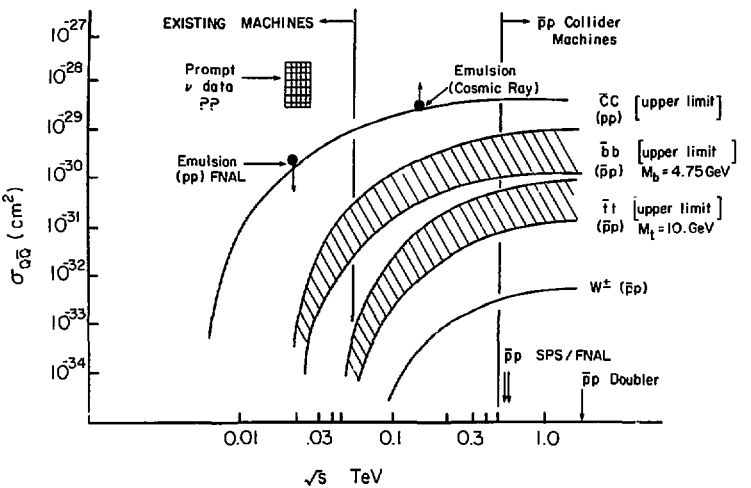

Fig. 14. Production of heavy quarks by $\bar{p}p$ interactions.

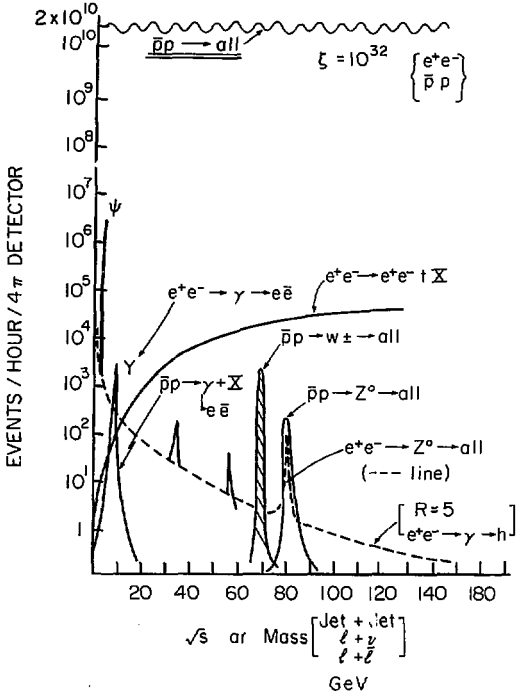

Fig. 15. Comparison of $\bar{p}p/e^+e^-$ rates.

BEAM COOLING TECHNIQUES

AN OVERVIEW OF BEAM COOLING

Andrew M. Sessler
Lawrence Berkeley Laboratory

I. Introduction

In this brief presentation I thought it would be of value to do two things: first, give some history of the efforts to develop beam-cooling ideas and, second, present elementary and simplified descriptions of the two successful methods of cooling.

It is my hope that you will find the history of interest, for through it one can see the development of the realization of the limits on devices in the absence of cooling and, then, the various unsuccessful attempts to develop cooling which, in due course, culminated in the effective proposals of electron cooling and stochastic cooling.

It is my further hope that some of you, at least, will find useful an over-simplified description of the two cooling techniques. In particular, I think that two simple formulas, summarizing the primary dependence upon parameters, are quite useful in delineating the conditions required for cooling.

II. History

With the development of fixed-field alternating-gradient accelerators and the concept of rf stacking it became possible,[1] for the first time, to seriously consider colliding-beam devices.[2] (The idea goes back to Wideroe, but earlier there was no means proposed to achieve an interesting luminosity.) It was immediately pointed out by E. Wigner that Liouville's theorem imposed a limit upon performance, but the MURA Group concluded that other limits were, in practice, more severe.

In the very first paper proposing a storage ring, by G. K. O'Neill, a crucial part of the proposal was the use of tapered foils to provide a non-Liouvillian injection mechanism.[3] (As a historical footnote, the storage ring idea--without the use of foils--was independently conceived by W. Brobeck and by D. Lichtenberg, R. Newton, and M. Ross.)

Immediately, the MURA Group set to work to study the effect of foils.[4-6] They were able to show that the non-Liouvillian character of even an "ideal" foil is small; that is, the relative reduction in phase volume is just twice the relative reduction in longitudinal momentum.[6] Thus a foil which would significantly reduce phase volume must significantly change particle energy (which could, of course, be resupplied by an rf cavity). However, because of the small phase volume reduction by an "ideal" foil, scattering by a real foil would more than cancel the reduction in phase volume. (As a second historical footnote, it is interesting that the formulas for foil damping are the same as those for radiation damping of electrons. See H. G. Hereward, Brookhaven Symposium 1961, p. 222; with a comment by K. R. Symon.)

The work on foils showed that although a foil is non-Liouvillian, it is almost Liouvillian. However, a wedged foil was effective at interchanging radial and longitudinal phase space (which is why it superficially looked attractive). This is an interesting possibility in its own right. It had been proposed by L. Smith that cavities with electric fields which varied with radius might also have this capability, but N. Francis at MURA proved this not to be the case.[7]

Stimulated by these considerations and more particularly by the desire to develop a mathematical technique for handling self-field phenomena, R. L. Mills and I examined, in 1958, the limits of applicability of Liouville's theorem to particle beams. In this discussion we identified the need for neglect of small-angle collisions (which is employed in electron cooling) and the neglect of fluctuation phenomena (which is employed in stochastic cooling). Neither of us, however, had the slightest idea of how to circumvent the theorem.

In 1966, Budker introduced the idea of electron cooling, giving G. K. O'Neill credit for independent discovery of the concept.[9] In 1968, S. vander Meer conceived of stochastic cooling, although he did not write the work up until 1972.[10]

Now, in this brief review I have neglected to mention very much more work which provided the background against which were discovered the two successful concepts for cooling. In particular, mention must be made of the studies of radiation damping which provided much insight into cooling.[11]

III. Electron Cooling

The idea is, simply, to couple the proton beam, in a frame moving with the average longitudinal speed of the protons, to something with less transverse and less longitudinal energy (or roughly speaking temperature). Then by simple thermodynamics, one must have a cooling of the protons.

If the coupling is to a system which interchanges energy in the various degrees of freedom then one runs the risk that the "infinite" reservoir of longitudinal energy is coupled into the transverse motion or the longitudinal spread in motion. An example of this is the resistive wall instability where the wall resistance takes energy out of the average longitudinal motion while, at the same time, it transfers energy from the longitudinal to the transverse motion at an even higher rate and hence there is a net loss (in terms of cooling).

In plasma physics there are well-known formulas for exchange of energy amongst plasma components. From any standard text one may obtain for the non-relativistic regime, in the frame of average proton speed,

$$T^*_{eq} = \frac{3M_p m_e}{8(2\pi)^{1/2} n^* e^4 \log\Lambda}\left(\frac{kT^*_p}{M_p} + \frac{kT^*_e}{m_e}\right)^{3/2}, \quad (1),$$

where all quantities are in the moving frame and

T^*_p = proton temperature ($kT_p = 1/2 M_p v^{*2}_\perp$),

T^*_e = electron temperature,

n^*_e = density of electrons,

logΛ involves the Debye length,

τ^*_{eq} = equilibration time.

Assuming T^*_p dominates T^*_e (very cold electron beam), one obtains for τ_{eq} in the laboratory:

$$\tau_{eq} \approx \frac{\beta^{*3}\gamma^2}{200\, r_e r_p n_e c}, \qquad (2)$$

where r_e abd r_p are the classic electron and proton radii, n_e is the electron density in the laboratory, and β^* is the proton velocity (in units of c) in the moving frame. The factor of γ^2 is from transformation of n^*_e and τ^*_{eq}. For transverse temperature $\beta^* = \gamma\theta_{lab}$, where θ_{lab} is the angle of deviation of a proton from the average (or electron) direction. For a proton with a longitudinal deviation in momentum $\beta^* \equiv \Delta p/p$.

Thus one can see, especially for the cooling of betatron amplitudes, the strong, dependence upon γ, namely as γ^3. For damping of longitudinal phase space the γ dependence is weaker. Also, of course, one wants a high electron current so as to decrease τ_{eq}.

An alternative--and very simple--derivation of Eq. (2) may be obtained by considering elementary collisions between electrons and protons, but that is, of course, the basis for the quoted Eq. (1).

The inclusion of many complicating features, such as a strong longitudinal magnetic field, have been considered in recent years. Also, careful theoretical treatments have been given employing distribution functions. You will be hearing about this later in the Workshop. Finally, I want to emphasize the very extensive experimental work, leading to a demonstration of the practicality of this concept, which has been carried out at Novosibirsk.

IV. Stochastic Cooling

This technique employs the fluctuations in a beam of a finite number of particles to provide the cooling. The mean lateral position position, $\bar{x}$, of a section of the beam is sensed by a system with gain, g, and bandwidth, W. At some other point of the ring a correcting signal is applied to the beam so as to reduce $\bar{x}$. The correcting section is placed close enough to the pick-up station so that most of the particles detected by the pick-up are in the sample that is affected by the correcting element. The process can be repeated, effectively, if on subsequent passages through the pick-up, different particles are in the sample. In short, one wants little spread in particle transit time between pick-up and corrector (compared to 1/W) and a large spread in transit times between different encounters of the pick-up (compared to 1/W). In this case,

$$\tau_{damping} = \frac{2N}{W}(2g - g^2)^{-1}, \qquad (3)$$

where N is the total number of beam
A finite signal-to-noise ratio, $1/\eta$, modifies the factor of g^2 to $g^2(1 + \eta)$.

We may readily derive a formula for stochastic damping, by employing a simplistic model, which is very close to Eq. (3). Suppose the pick-up is of length ℓ, in a ring of radius R, containing N particles. Then there will be

$$n = \frac{N\ell}{2\pi R}$$

particles in the sample, and the centroid of this group will be

$$\bar{x} = \frac{1}{n}\sum_{i=1}^{n} x_i ,$$

Suppose the corrector changes each particle position x_i to $x_i - g\bar{x}$ where g is the gain of the system.

A measure of the beam spread is

$$\overline{x^2} = \frac{1}{n}\sum_{i=1}^{n} x_i^2,$$

since although the sample of n-particles has a non-zero centroid $\bar{x}$, the centroid of all N particles is zero. It is easy to compute that after the corrector, $\overline{x^2}$ changes to

$$\overline{x^2}\left[1 - (2g - g^2)\frac{\bar{x}^2}{x^2}\right].$$

Thus, if the correction is made once per revolution a characteristic time is

$$\tau_{damping} \approx \frac{N\ell}{\beta c}(2g - g^2). \qquad (4)$$

Clearly, $\ell/\beta c$ is close to the bandwidth W, while the numerical factor comes from a more careful definition of the characteristic time.

As in the case of electron cooling, much theoretical and experimental work has been done beyond that leading to Eq. (3). In particular, a great deal of experimental work, demonstrating the practicality of the concept, has been done on the ISR at CERN.

REFERENCES

1. D. W. Kerst et al, Phys. Rev. 98, 1153 (A) (1955).
   K. R. Symon & A. M. Sessler, CERN Symposium 1956, 44, (1956).
2. D. W. Kerst et al, Phys. Rev. 102, 590 (1956).
3. G.K. O'Neill, Phys. Rev. 102, 590 (1956).
4. A. M. Sessler, Internal MURA Note (May, 1956).

5. A. M. Sessler, Internal MURA Note (July, 1956).

6. D. B. Lichtenberg, P. Stehle & K. R. Symon, MURA Report (July, 1956).

7. L. Smith - Private communication
N. E. Francis, Internal MURA Report on Radial & Phase Motion in a Syndrotron (undated).

8. R. L. Mills & A. M. Sessler, MURA Report (October, 1958).

9. G. I. Budker, Orsay Symposium 1966, II-1.

10. S. van der Meer, CERN-ISR Internal Report (August, 1972).

11. F. E. Mills, Nucl. Instr. & Methods 23, 197 (1963).

APPENDIX

The paper is complete without the following Appendix material which consists of the transparencies shown at the Workshop (the marked parts were read aloud). They are included here to provide the reader with some appreciation for the spirit and character of the Workshop.

Attainment of Very High Energy by Means of Intersecting Beams of Particles

D. W. Kerst,* F. T. Cole,† H. R. Crane,† L. W. Jones,‡ L. J. Laslett,§ T. Ohkawa,‖ A. M. Sessler,¶ K. R. Symon,** K. M. Terwilliger,‡ and Nils Vogt Nielsen††

Midwestern Universities Research Association,‡‡ University of Illinois, Champaign, Illinois

(Received January 23, 1956)

IN planning accelerators of higher and higher energy, it is well appreciated that the energy which will be available for interactions in the center-of-mass coordinate system will increase only as the square root of the energy of the accelerator. The possibility of producing interactions in stationary coordinates by directing beams against each other has often been considered, but the intensities of beams so far available have made the idea impractical. Fixed-field alternating-gradient accelerators[1] offer the possibility of obtaining sufficiently intense beams so that it may now be reasonable to reconsider directing two beams of approximately equal energy at each other. In this circumstance, two 21.6-Bev accelerators are equivalent to one machine of 1000 Bev.

The two fixed-field alternating-gradient accelerators could be arranged so that their high-energy beams circulate in opposite directions over a common path in a straight section which is common to the two accelerators, as shown in Fig. 1. The reaction yield is proportional to the product of the number of particles which can be accumulated in each machine. As an example, suppose we want 10^7 interactions per second from 10-Bev beams passing through a target volume 100 cm long and 1 cm^2 in cross section. Using 5×10^{-26} cm^2 for the nucleon interaction cross section, we find that we need 5×10^{14} particles circulating in machines of radius 10^4 cm.

There is a background from the residual gas proportional to the number of particles accelerated. With 10^{-6} mm nitrogen gas, we would have 15 times as many encounters with nitrogen nucleons in the target volume as we would have with beam protons. Since the products of the collisions with gas nuclei will be in a moving coordinate system, they will be largely confined to the orbital plane. Many of the desired p-p interaction products would come out at large angles to the orbital plane since their center of mass need not have high speed in the beam direction, thus helping to avoid background effects.

Multiple scattering at 10^{-6} mm pressure is not troublesome above one Bev; but beam life is limited by nuclear interaction with residual gas to ~1300 seconds. Consequently, in about 1000 seconds the high-energy beam of 5×10^{14} particles must be established in each accelerator. The fixed-field nature of the accelerator allows it to contain beams of different energy simultaneously. It may be possible to obtain this high beam current in this time by using $\sim10^3$ successive frequency modulation cycles of radio-frequency acceleration, each cycle bringing up 5×10^{11} particles. It is encouraging to learn that Alvarez and Crawford[2] succeeded in building up a ring of protons by successively bringing up several groups of particles to the same final energy by frequency modulation in the 184-in. Berkeley cyclotron.

The number of particle groups which may be successively accelerated without leading to excessive beam spread can be estimated by means of Liouville's theorem.[3] One can readily convince himself that there is adequate phase space at high energy to accommodate

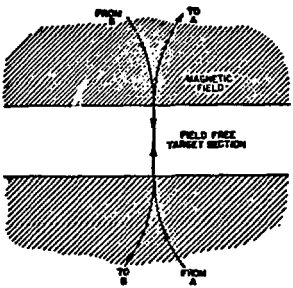

FIG. 1. The target straight section. B and A can be adjacent or concentric fixed-field alternating-gradient accelerators.

the necessary number, N, of particle groups. Assume for simplicity that synchrotron and betatron phase space are separately conserved, so that for the former

$$(\Delta p)_f(\Delta S)_f = N(\Delta p)_i(\Delta S)_i,$$

where ΔS and Δp are the arc length and momentum spread at injection and final energy. Then, employing the fact that $P \sim R^{k+1}$, where R is the radius and k is the field index, one obtains

$$N = 2(k+1)(\Delta R/R)(p_f/p_i)(\Delta S_f/\Delta S_i)(E_i/\Delta E_i).$$

Using typical numbers such as

$$(p_f/p_i) \sim 100, \quad k \sim 100, \quad R \sim 0.5 \text{ cm},$$
$$R \sim 10^4 \text{ cm}, \quad (\Delta E_i/E_i) \sim 10^{-3},$$

one finds that there is room for $N \sim 10^9$ frequency-modulation cycles.

The betatron phase space available is so large that it cannot be filled in one turn by the type of injectors used in the past which can inject 10^{11} particles. Thus there is the possibility of attaining and exceeding the yield used for this example by improving injection.

The more difficult problem of whether one can, in fact, use all of the synchrotron and betatron phase space depends in detail upon the dynamics of the proposed scheme and this is presently under study.

* University of Illinois, Urbana, Illinois.
† State University of Iowa, Iowa City, Iowa.
‡ University of Michigan, Ann Arbor, Michigan.
§ Iowa State College, Ames, Iowa.
‖ University of Tokyo, Tokyo, Japan.
¶ The Ohio State University, Columbus, Ohio.
** University of Wisconsin, Madison, Wisconsin.
†† Norwegian Institute of Technology, Trondheim, Norway.
‡‡ Supported by the National Science Foundation.

[1] Keith R. Symon, Phys. Rev. 98, 1152(A) (1955); L. W. Jones *et al.*, Phys. Rev. 98, 1153(A) (1955); K. M. Terwilliger *et al.*, Phys. Rev. 98, 1153(A) (1955); D. W. Kerst *et al.*, Phys. Rev. 98, 1153(A) (1955).

[2] L. Alvarez and F. S. Crawford, private communication.

[3] We are indebted to Professor E. Wigner who pointed out to us the importance of this consideration.

Storage-Ring Synchrotron: Device for High-Energy Physics Research*

GERARD K. O'NEILL
Princeton University, Princeton, New Jersey

(Received April 13, 1956; revised version received April 23, 1956)

AS accelerators of higher and higher energy are built, their usefulness is limited by the fact that the energy available for creating new particles is that measured in the center-of-mass system of the target nucleon and the bombarding particle. In the relativistic limit, this energy rises only as the square root of the accelerator energy. However, if two particles of equal energy traveling in opposite directions could be made to collide, the available energy would be twice the whole energy of one particle. Kerst, among others, has emphasized the advantages to be gained from such an arrangement, and in particular of building two fixed-field alternating gradient (FFAG) accelerators with beams interacting in a common straight section.

It is the purpose of this note to point out that it may be possible to obtain the same advantages with any accelerator having a strong, well-focused external beam. Techniques for beam extraction have been developed by Piccioni and Ridgway for the Cosmotron, and by Crewe and LeCouteur for lower energy cyclotrons.

In the scheme proposed here (see Fig. 1), two "storage rings," focusing magnets containing straight sections one of which is common to both rings, are built near the accelerator. These magnets are of solid iron and simple shape, operating at a high fixed field, and so can be much smaller than that of the accelerator at which they are used.[1] The full-energy beam of the accelerator is brought out at the peak of each magnet cycle, focused, and bent so that beams from alternate magnet cycles enter inflector sections on each of the storage rings. In order to prevent the beams striking the inflectors on subsequent turns, each ring contains

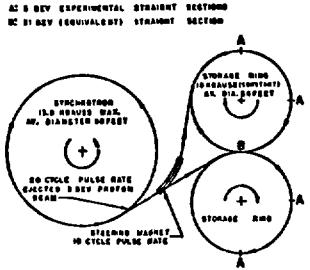

FIG. 1. Plan view of particle orbits in a hypothetical arrangement of storage rings at a 3-Bev proton synchrotron.

a set of foils, thick at the outer radius but thinning to zero about one inch inside the inflector radius. The injected beam particles lose a few Mev in ionization in the foils; so their equilibrium orbit radii shrink enough to clear the inflectors after the first turn. After several turns, the beam particles have equilibrium orbits at radii at or less than the inside edge of the foils.

The possibility exists of storing a number of beam pulses in these storage rings, since space charge and gas scattering effects are small at high energies. Preliminary calculations have been carried out on a hypothetical set of storage rings for the 3-Bev, 20 cycle per second Princeton-Pennsylvania proton synchrotron. Since the storage rings would be simple and almost entirely passive devices, their cost would be small compared with that of the accelerator itself. It was estimated that a pair of storage rings operating at 18 000 gauss with a 2 in.×6 in. good-n region would weigh a total of 170 tons. The magnet of the synchrotron itself would weigh 350 tons, and would be of much more complicated laminated transformer iron. In the event that one could obtain an average current of 1 microampere from the synchrotron, and an average particle lifetime of a few seconds for the storage rings, there would be about 1000 strange-particle-producing reactions per second at each of two beam crossover points, for an estimated 1.5-millibarn total cross section. The center-of-mass energy, 7.8 Bev, would be equivalent to that of a 31-Bev conventional accelerator. If storage rings could be added to the 25-Bev machines now being built at Brookhaven and Geneva, these machines would have equivalent energies of 1300 Bev, or 1.3 Tev.

If only one storage ring were used, tangential to the accelerator itself, the interaction rate would be reduced by a factor S/D, where S is the average number of beam pulses stored in each ring, and D is the fraction of time the accelerator beam is at full energy. The interaction rate would be proportional to S^2 if two storage rings were used.

The advantage of systems involving energy-loss foils is that they provide an element of irreversibility; with foils, the area in phase space available to a particle can be made to decrease with time. This makes it possible to insure that particles once injected will never subsequently strike the injector, no matter how long they may circulate in the storage ring. Preliminary work with a stabilized electronic analog computer indicates that foils may also allow the stable and irreversible capture of roughly half of the circulating particles by a fixed-frequency rf system, which in turn may allow the storage of a large number of beam pulses in each storage ring. It appears that a thin hydrogen jet inside the equilibrium orbit of a conventional synchrotron would, in some energy ranges, reduce radial betatron oscillations even when scattering is taken into account.

The major difficulties in the use of storage rings with foils may result from the amplification of radial betatron oscillations by the foils. Quantitative calculations of this effect have been carried out on the analog computer. It was found that the effect would be serious unless the initial injection to the storage rings could be very precise. However, calculations were also made on a system involving a second foil placed at the inner limit of the good-n region. This foil would move the particle orbits inward as soon as betatron oscillation became serious, and would then continue reducing the betatron oscillation amplitude until the foil itself was rotated out of the median plane. During the long interval (about 0.1 second, or 600 000 turns) before the next beam pulse, the betatron oscillations would continue to be reduced by a thin hydrogen "target" jet also at the radius of the second foil. The process of orbit shrinkage would stop when the particles were captured in stable synchrotron phase by a low-power fixed-frequency rf system; the reduction in betatron oscillations due to the hydrogen would continue. The rf system would define an equilibrium orbit just outside the radius of the hydrogen jet, so that particles whose betatron oscillation amplitudes had been reduced to low values would circulate in a high-vacuum region, where the mean lifetime for nuclear interactions would be long. When the moving foil returned to assist in the acceptance of the next beam pulse, all particles that had been captured by the rf in previous pulses would have small oscillation amplitudes, and so would miss the foil. In this way particles from many beam bursts could be concentrated in a small region, with very little deviation in energy or position.

The author takes pleasure in acknowledging very helpful discussions on this subject with Dr. M. G. White and Dr. F. C. Shoemaker. The assistance of Dr. I. Pyne in setting up problems for the GEDA computer of the Princeton engineering school is also very gratefully acknowledged.

* This work was supported by The Higgins Scientific Trust Fund.

[1] Between the dates of submitting this letter and its publication, it has come to the author's attention that the basic idea of a storage-ring synchrotron has also occurred, at about the same time, to W. M. Brobeck of the Berkeley accelerator group, and to D. Lichtenberg, R. Newton, and M. Ross of the MURA group.

16 May 1956

Memorandum to : Jim Snyder

From: A. M. Sessler

Topic: Proposed Digital Computer Program to Study the Coupling of Radial Betatron Oscillations; and Synchrotron Oscillations; in the Presence of Foils; and Non-slaunched, Non-Radially Terminating, Leakage Flux and Magnetic Effects Absent, R. F. Gaps.*

Motivation: 1) It appears important that we study the effects of coupling between orbital motion and synchrotron oscillations in order to be able to understand completely such things as R. F. knockout.

2) The Princeton people have made the important observation that it is possible to devise systems which are non-Liouvillian as far as the accelerated particles are concerned. This is readily reconciled with general theorems of dynamics by noting that the proposed schemes introduce other particles (electrons in foils) so that the total phase space is still conserved, or alternatively the accelerated particles are subject to dissipative forces. The possibilities opened up by the observation must be studied, since successful use of foils may allow a storage ring to be substituted for an accelerator--at a considerable saving in cost.

3) The separated sector accelerator has slaunched cavities, and some of the proposed R. F. schemes employ cavities which only extend over part of the radial aperture. It is important to study the effects these cavities may engender, but it was felt that the simpler problem in which these effects were ignored, should at least be formulated first. It may

*I am indebted to Dr. Laslett for constant encouragement and support during the writing of this title.

On the Non-Liouvillian Character of Foils

A. M. Sessler

July 11, 1956

Comments

I was unable to see Lichtenberg on my visit of July 10. Symon says Lichtenberg's results do not agree in detail with those presented here, but it is not clear to me that we are calculating the same quantity. Simply to form a basis for discussion during future visits to Madison I have written this material up. With the technical group in two locations, preliminary drafts with a high probability of included errors, seem unfortunately to be essential.

Lichtenberg has constructed an ingenious proof[1] that thin foils are almost Liovillian in character. He has shown by general arguments that the change in total phase space on passage through a foil is negligibly small. This author felt the need for a specific calculation in order to confirm the general result; as well as to obtain explicit formulas for the change in betatron, synchrotron, and total phase space on traversal of a foil. The results of these calculations have been outlined here.

I. Derivation

The starting point is a mathematical characterization of a foil and its effect on the betatron oscillation coordinates x and p, and on the energy of a particle. The transformation is given in a previous memorandum[2], but will

---

[1] Mura lecture of July 2, 1956, soon to be published.
[2] "A Proposed Digital Computer Program to Study Foils, etc." -- Memorandum to J. N. Snyder of May 16, 1956.

MODIFICATION OF LIOUVILLE'S THEOREM REQUIRED BY THE PRESENCE OF DISSIPATIVE FORCES*

D. B. Lichtenberg,+ P. Stahle,‡ and K. R. Symon*
Midwestern Universities Research Association

July 12, 1956

It has recently been suggested by O'Neill[1] that high current densities might be achieved in accelerators by the use of foils to reduce the volume in phase space occupied by a beam of particles. It is the purpose of this note to examine under what conditions such a compression of phase space can occur and whether the effect is large enough to be of any practical value in accelerators.

The equations of motion satisfied by a particle can be written

$$\frac{d}{dt}\frac{\partial L}{\partial \dot{q}_i} - \frac{\partial L}{\partial q_i} = Q_i$$

where the Lagrangian L includes all forces derivable from a potential, the Q_i are the forces due to the foil and the q_i are the generalized coordinates of the particle.

---

* Supported by the National Science Foundation, Office of Naval Research, and Atomic Energy Commission.

+ Indiana University.

‡ University of Pittsburgh.

* University of Wisconsin.

1. O. K. O'Neill, Phys Rev 102 1418 (1956).

If we define

$$p_i = \frac{\partial L}{\partial \dot{q}_i} ,$$

$$H = \sum_i p_i \dot{q}_i - L$$

we get

$$\left.\begin{aligned} \dot{q}_i &= \frac{\partial H}{\partial p_i} \\ \dot{p}_i &= -\frac{\partial H}{\partial q_i} + Q_i \end{aligned}\right\} \qquad (1)$$

We now consider a closed region V in phase space. The rate of change of this volume will be equal to the volume integral of its divergence:

$$\frac{dV}{dt} = \int \Pi_i \, dq_i \, dp_i \sum_i \left(\frac{\partial \dot{p}_i}{\partial p_i} + \frac{\partial \dot{q}_i}{\partial q_i} \right). \qquad (2)$$

Using Eq. (1), Eq. (2) becomes

$$\frac{dV}{dt} = \int \Pi_i \, dq_i \, dp_i \sum_i \frac{\partial Q_i}{\partial p_i}. \qquad (3)$$

Therefore to see what happens to a volume in phase space due to a foil, we need merely consider the form of the functions Q_i. Of special interest is the case of an ideal foil, defined as one which produces an energy loss but no scattering. If, furthermore, the energy loss depends on the path length through the foil, but not on the particle velocity, we may write

$$\underset{\sim}{Q} = Q(\underset{\sim}{r}, t) \frac{\dot{\underset{\sim}{r}}}{\dot{r}} = Q(\underset{\sim}{r}, t) \frac{(\underset{\sim}{p} - e\underset{\sim}{A}/c)}{|\underset{\sim}{p} - e\underset{\sim}{A}/c|}$$

where $\underset{\sim}{r}$ is the position of the particle and $\underset{\sim}{A}$ is the vector potential. By writing the time t explicitly, we take into account

that the foil need not remain in one position. Note that $Q(\underline{r}, t)$, is negative for a foil. With the above choice of Q we obtain

$$\sum_i \frac{\partial Q_i}{\partial p_i} = 2\,\frac{Q(\underline{r}, t)}{P} \qquad (4)$$

where $P = |\underline{p} - e\underline{A}/c|$ is the kinetic momentum of the particle. The factor 2 comes from the fact that we are considering the problem in three dimensions. If the effect of the foil on vertical oscillations is neglected, the factor is unity. Using Eq. (4), Eq. (3) becomes

$$dV/V = 2\,dt\;\overline{Q(\underline{r}, t)/P} \qquad (5)$$

where the bar indicates the space average of Q/P.

In most accelerators, the momentum spread of the beam is much smaller than the average momentum P of the particles. Therefore instead of Eq. (5) we may write

$$dV/V = (2/P)\,dP \qquad (6)$$

where $dP = \bar{Q}\,dt$ is the average momentum increment of a particle due to the foils in time dt. Integrating, we obtain, if the foils are the only source of momentum increment,

$$\frac{V_f}{V_i} = \left(\frac{P_f}{P_i}\right)^2 \qquad (7)$$

where the subscript i indicates the initial value and f the final value. It is apparent from Eq. (7) that the volume in phase space may be reduced by the use of an ideal foil, but that the average momentum of the particles must be reduced by an amount comparable to the reduction in phase space. To avoid this, an oscillator

can be used to supply the energy lost in the foil. Then the average momentum P is kept constant and, on integrating Eq. (6), we get

$$\frac{V_f}{V_i} = e^{-2\Delta P/P_i} \qquad (8)$$

where ΔP is the average total momentum loss in the foil.

An actual foil differs from an ideal foil in that the energy loss of a particle depends on the magnitude of the particle momentum. However, in the relativistic region this dependence is small and can be neglected so that Eqs. (7) and (8) still approximately hold.

In the non-relativistic region the energy loss goes approximately as the inverse square of the velocity so that the force becomes

$$\underset{\sim}{Q} = Q(\underset{\sim}{r},t)\,\underset{\sim}{P}/P^3.$$

Putting this expression for Q in Eq. (3) it turns out that $dV/dt = 0$. From Eqs. (7) and (8) it is apparent that the reduction of the volume in phase space depends only on the energy loss in the foil. Therefore, although foils of odd shapes and those which change with time may twist a volume in phase space, they are no more effective in reducing the volume than are uniform foils which produce the same average energy loss. In order to increase the density of particles in the beam by a factor n, a reduction in phase volume by a factor n is required, which from Eq. (8) implies a loss of momentum to the foil of

$$\Delta P = \frac{P}{2}\log n$$

which is comparable to P itself. An actual foil thickness sufficient to do this would produce more than enough scattering to cancel the compression in phase space obtained above.

MIDWESTERN UNIVERSITIES RESEARCH ASSOCIATION*

2203 University Avenue, Madison, Wisconsin

LIOUVILLE'S THEOREM FOR A CONTINUOUS MEDIUM WITH CONSERVATIVE INTERACTIONS**

R. L. Mills and A. M. Sessler
The Ohio State University, Columbus, Ohio

October 8, 1958

ABSTRACT

It is shown that for a continuous medium with conservative interactions the density in six-dimensional phase space is preserved as one follows the motion of the medium.

*AEC Research and Development Report. Research supported by the Atomic Energy Commission, Contract No. AEC AT (11-1) 384.

**Research supported in part by the National Science Foundation.

I. INTRODUCTION

The study of the motion of particles in an accelerator becomes a many-body problem when the interactions between particles are taken into account. It is thus important to investigate the possibility of establishing the validity--or approximate validity--of general dynamical theorems applicable to the n-body problem. Such a powerful theorem is the theorem proved here to be rigorously valid for continuous media, and asserted to be an extremely good approximate theorem for particles in an accelerator.

Liouville's theorem is a theorem which asserts that in a $2fN$ dimensional space (f is the number of degrees of freedom of one particle) spanned by the coordinates and momenta of all particles (called γ space), the density in phase is a constant as one moves along with any phase point. It is thus a statement about the density of points; each point representing a dynamical system. The systems constitute an ensemble and of course do not interact.

The theorem proven here refers to a system of many interacting particles, and asserts that in the 2f-dimensional space spanned by a single system of coordinates and momenta (called a μ space), the density in phase is a constant as one moves along with any phase point. It is thus a statement about the behavior of interacting particles, and thus really quite different from Liouville's theorem.

The validity of the theorem, as well as the limits of its validity, may readily be seen by the following intuitive argument:

Consider first a system of many particles, N. Suppose these particles are subject to external forces (which may even be time dependent), but there

are no interactions between the particles. Clearly density in phase in μ space is a constant of the motion as one follows the motion of a phase point. This follows then immediately from Liouville's Theorem in γ space, since with no interactions between particles μ space for N particles is simply γ space for a single particle.

Consider now a system of a great many particles N, with interactions between the particles. Imagine that the solution has been obtained so that we know the motion of all the particles as a function of time. Concentrate now on a "small" number of particles n, which initially are localized in μ space. We will define what "small" means shortly. Let all the other particles move along the trajectories appropriate to the solution of the N-body problem. If the interactions between one of the particles and the n particles can be neglected compared to the interactions between the N-n particles and one particle, then these particles are subject to "external forces" and by the first case the density in μ space is a constant as one moves along with the sample group of n particles. This is clearly true for any sample, and hence the theorem is established.

That is, as long as one has sufficient particles N, that a sample can be obtained of sufficiently small number of particles n, that the interactions between these particles and one of their number is negligible compared to the interactions between one of these particles and the N-n particles, while at the same time n is sufficiently large that fluctuation phenomena can be neglected, then the theorem is valid. In the rigorous proof given in the next section, the limit of a continuous medium is taken so that fluctuation phenomena

do not exist. For applications to particle accelerators where we consider a number of particles $N \simeq 10^{13}$ this approximation is very valid, corresponding to neglect of particle-particle collisions which throw a particle out of the accelerator, but not neglecting long range electromagnetic interactions which are responsible for space-charge limits, plasma oscillations, beam-beam interactions, and possible two-stream amplification mechanisms.

The practical importance of the theorem can be readily seen by limiting one's attention to systems which initially have a constant density in a restricted region of μ space, and no particles outside this region. (This is determined by the injection mechanism, and is a reasonable approximation to most situations). In this case, the N-body problem is completely characterized by the behavior of the boundary surface as a function of time. This surface satisfies a partial differential integral equation of the first order in at most 2f independent variables, so that the N-body problem((f N) differential equations of the second order) is greatly simplified. In particular, for problems involving one degree of freedom, the equation for the boundary curve as a function of time and one coordinate is quite amenable to analysis.

II. FORMAL PROOF

Let λ_i (i = 1, ---, 2f,) be parameters labelling the particles of the medium (2f dimensional phase space; this is the μ space).

$dn = \sigma\, d\lambda_1 \ldots d\lambda_{2f}$ = number of particles in 'volume' element $d\lambda$.

σ = constant 'density' with respect to λ .

Let $\pi_\alpha(\lambda)$ = momentum density

$= \sigma p_\alpha$

$q_\alpha(\lambda)$ = position of particle λ .

EUROPEAN ORGANIZATION FOR NUCLEAR RESEARCH

CERN/ISR-PO/72-31

STOCHASTIC DAMPING OF BETATRON OSCILLATIONS IN THE ISR

by

S. van der Meer

Geneva - August, 1972

SUMMARY

In principle, betatron oscillations could be damped by detecting and compensating statistical variations of the average beam position, caused by the finite number of particles present. It is shown that achieving useful damping in the ISR would be difficult with presently available techniques.

1. STOCHASTIC DAMPING

As is well known, Liouville's theorem predicts that betatron oscillations cannot be damped by the use of electromagnetic fields deflecting the particles. However, this theorem is based on statistics and is only strictly valid either for an infinite number of particles, or for a finite number if no information is available about the position in phase plane of the individual particles. Clearly, if each particle could be separately observed and a correction applied to its orbit, the oscillations could be suppressed. It is also well known to be possible to damp coherent betatron oscillations (where the beam behaves like a single particle) by means of pickup-deflector feedback systems. In the same way, the statistical fluctuations of the average beam position, caused by the finite number of particles, can be detected with pickup electrodes and a corresponding correction applied. In other words, the small fraction of the oscillations that happens to be coherent at any time due to the statistical fluctuations, can be damped.

After the beam would have passed through such a damping system (for which the name "stochastic damping" could perhaps be used), it would no longer present any coherent oscillations, and further damping would seem to be impossible. However, there are two effects that reintroduce randomness, and therefore some coherency:

STOCHASTIC COOLING THEORY AND DEVICES

S. Van der Meer
CERN

I. Principle of Stochastic Cooling

Stochastic cooling uses the spontaneous violation of Liouville's theorem that is always present in a beam with a finite number of particles. The system detects the corresponding fluctuations and acts on the beam (in a strictly Liouvillian way) so that the random density variations do not get a chance of averaging out.

The most efficient cooling would be obtained if each individual particle could be observed separately. In practice, this is quite impossible. Even with the fastest systems proposed up to now, the resolution is of the order of 10^5 particles.

In general, the feedback system detects one parameter of the particle motion (transverse position or phase) and acts on another one (transverse or longitudinal momentum). The analysis is often easiest by considering two effects occurring simultaneously:

a) Coherent effect: each particle is influenced coherently by its own signal.

b) Incoherent effect: blowup is caused by the signals from the other particles ("Schottky noise") or by the amplifier noise.

The coherent effect is proportional with the system gain , the incoherent one with its square. Therefore, it is always possible to choose a gain where the coherent one is predominant. By a proper choice of parameters this will result in cooling.

II. Mixing

The incoherent effect caused by noise depends on the noise spectrum. The particles will only be influenced by the noise frequencies that coincide with harmonics of their revolution frequency (for momentum cooling) or with one of the betatron sidebands (for betatron cooling). This is strictly true only if the particle frequencies are constant; any other frequency will then only cause a beating effect that does not increase with time. In practice, the frequencies change so slowly that it is still true.[1] The noise power density vs. frequency at each of the particle's harmonics is therefore the quantity on which the blowup depends.

The Schottky noise (from the other particles) covers certain frequency regions, the Schottky bands, that also contain the frequencies to which the perturbed particle is sensitive. The power density clearly depends on the frequency spread covered by these bands: the wider this is, the less power density one has. Also, since the width of these bands increases with the harmonic number, higher harmonics contribute less to the incoherent effect.

It often happens that within the bandwidth of the electronic system these bands are separated everywhere and do not overlap. In that case, each of the sensitive frequencies of the perturbed particle is inside a single Schottky band. This situation is often called "bad mixing."

Alternatively, the revolution frequency spread (or the harmonic numbers used) may be so high that the bands overlap and that each particle frequency is inside many different overlapping Schottky bands. This is called "good mixing." Intermediate situations may, of course, also exist.

Seen in the time domain, the signal (or "pulse") caused by a single particle will influence many other particles as well. If this sample of other particles changes its population from one revolution to the next because the revolution time spread is much larger than the pulse duration, we have good mixing. For the opposite case, the sample population changes only slowly. The incoherent effect is then also worse, because the perturbations from the same particle are correlated over more than one turn.

With good mixing, the incoherent effect depends on the total number of particles. Higher harmonic numbers contribute as much as lower ones, because, although the power density is lower, more harmonics overlap there. With bad mixing, the particle density vs. frequency at the revolution frequency of the perturbed particle is important. Higher harmonics are less important than lower ones. Especially in the case of momentum cooling, the resulting equations are then different in character, because the momentum cooling itself increases the density.

In practical cases (e.g., the cooling in the CERN $\bar{p}$ accumulator) the mixing is often bad. In the following analysis of momentum cooling, we shall assume this.

III. Momentum Cooling

We shall first assume that a beam pickup and a longitudinal kicker are used (Fig. 1). Each particle induces a pulse in the pickup that produces a pulse at the kicker . The density distribution is governed by the diffusion equation

$$\frac{\partial \psi}{\partial t} = -\frac{\partial}{\partial E}(F\psi) + \frac{\partial}{\partial E}\left(D\,\frac{\partial \psi}{\partial E}\right), \qquad (1)$$

where ψ = particle density dN/dE
E = particle energy
t = time
F = coherent acceleration rate $d\bar{E}/dt$
D = diffusion constant (incoherent term) $= 1/2\ (d\bar{E}^2/dt)$.

It is convenient to express F and D as a function of the complex system gain G_n at harmonic number n:

$$F = \frac{d\bar{E}}{dt} = 2ef_0 R \sum_n \mathrm{Re}(G_n) \qquad (2)$$

$$D = D_1 + D_2\psi \qquad (3)$$

$$D_1 = 2KTf_o R_K \sum_n |G_n|^2 \qquad (4)$$

(noise from an amplifier with a 3 dB noise figure)

$$D_2 = 2e^2 f_o{}^3 R^2 \frac{dE}{df} \sum_n \frac{|G_n|^2}{n} \qquad (5)$$

(Schottky noise).

The sums are extended over all harmonics of the revolution frequency f_o. The gain G is measured between the amplifier input and output (supposed to have equal impedance).

$$R = \sqrt{n_p R_p n_K R_K}$$

n_p, n_K, R_p, R_K = number and impedance of pickups, kickers

e, K, T = electron charge, Boltzmann constant, room temperature

Of course, around each harmonic number, G, and therefore F and D, may still vary with E. In fact, if F is independent of E, there is no cooling, but only a steady acceleration or deceleration, added to the blowup from the first term. Cooling will result if the coherent effect moves the particles into a direction where F decreases, so that they pile up there. This can be done in two ways:

a) by using a pickup whose sensitivity depends on position and therefore (if placed in a point with non-zero dispersion) on E. This method was first proposed by Palmer.[2]

b) by placing a filter in the feedback loop whose gain depends on frequency in the required way around each harmonic of the revolution frequency. Such a filter was proposed by Thorndahl.[3]

Equation (1) to (5) neglect the effect of feedback from the kicker via the beam towards the pickup. This is usually justified; a more complete theory where this is taken into account is being developed by F. Sacherer.

It is not easy to find solutions for the diffusion equation (1). Even if G depends linearly on E at each harmonic, an analytical solution seems impossible because of the dependence of D on ψ. It is therefore necessary to solve each particular case by numerical integration.

In practice, it is often possible to make the first term of (3) smaller than the second one. This means that the cooling rate is limited by the Schottky noise rather than by the amplifier noise, whose density is then below the Schottky noise density at the Schottky frequencies. Since, however, the amplifier noise is also present between the Schottky bands, it will normally give the largest contribution to the output power required. The available wide-band output power may restrict the cooling rate that can be obtained.

IV. Scaling

It is interesting to compare different cooling systems installed in different rings and starting with different initial distributions. We assume:

a) the initial distributions have the same shape.

b) the amplifier noise is negligible from the point of view of cooling.

c) the cooling is not limited by the available amplifier power.

d) the two systems compared have a similar frequency response (although the frequency scale may be different).

e) in both cases the gain is adjusted to the optimum value.

f) the variation of G with E is the same for both systems if scaled to the width of the initial particle distribution.

It can then be shown that the time scales as $N/(n_\ell{}^4 \Delta f)$, with

N = total number of particles

n_ℓ = number of revolution frequency harmonics within the passband

Δf = initial spread of revolution frequency.

We may also express this in machine parameters and find then a scaling factor $Nf_o/[W^2 |\eta|(\Delta p/p)]$, with

W = system bandwidth

$\eta = (\Delta f/f)/(\Delta p/p)$.

V. Use of Filters

If the dependence of the coherent factor F on the energy E is to be achieved by using the relationship between E and revolution frequency, we need filters that perform in a similar way around each harmonic of the revolution frequency. Such filters may be built using as elements transmission lines with a length equal to half the ring circumference. These lines may be either open or shorted at the far end. They then have an impedance

$$Z = jZ_L \tan(\pi f/f_o) \quad \text{for a shorted line}$$
$$\text{or} \quad Z = -jZ_L \cot(\pi f/f_o) \quad \text{for an open line} \qquad (6)$$

Therefore, the response of filters made with such elements is the same around each harmonic of f_o. Shorted or open lines behave like inductances or capacitances, respectively for positive $\Delta f/f_o$.

Since the width of the Schottky bands increases with the harmonic number, this behavior is not quite ideal. However, by combining these lines with lumped elements, filters may be made that give nearly the same characteristic vs. E at each harmonic. An example is given in Ref. 4.

A simple filter may be made as shown in Fig. 2. This filter has zero transmission at each harmonic of the revolution frequency corresponding to a given momentum value; in the neighborhood of these zeros, the transmission varies linearly with frequency. For a limited frequency range, this filter therefore behaves like a linear pickup, except that it is not sensitive to betatron oscillations.

Figure 3 shows Schottky scans obtained with momentum cooling, using such a filter (CERN ICE experiment). The density is proportional to the square of the vertical coordinate; the horizontal scale corresponds to the revolution frequency (or momentum).

The advantage of using filters instead of position-sensitive pickups to make F depend on E is that wide-band sum pickups may be made much shorter than position-sensitive ones. Also, the filter will have minimum gain at the frequencies where the particles will accumulate; it will therefore also diminish the influence of the amplifier noise on the cooled particles.

VI. Momentum Stacking

In the CERN $\bar{p}$ accumulator ring each antiproton pulse will be precooled by a momentum cooling system using the filter method. The particles will then be captured by a normal rf system and deposited at the top of a stack. This stack must be constantly cooled so that space is made free for the next pulse. The total momentum spread of the stack will then remain constant; its density will increase. Particles will migrate towards the bottom of the stack, where they will pile up. Clearly, the system gain at the bottom will have to be much lower than at the top. The optimum gain profile may be found by requiring the steepest possible density increase from top to bottom of the stack, while still maintaining a constant flux of particles migrating against this slope towards the bottom. This flux is

$$\phi = \frac{dN}{dt} = F\psi - D\,\frac{d\psi}{dE}. \qquad (6)$$

For simplicity, we now assume that the gain G is real (i.e., we assume perfect phase at all frequencies of interest). We also neglect the amplifier noise. Then $D = c_1\alpha^2\psi$ and $F = c_2\alpha$, where α is proportional to the system gain. Equating the flux to the required ϕ_o, and adjusting α so that $d\psi/dE$ becomes as steep as possible, we find

$$\alpha = 2\phi_o/(\psi c_2), \qquad (7)$$

i.e., the gain should be inversely proportional with density. The resulting optimum density profile is

$$\psi = \psi_o \exp\,[(E_o - E)/E_d], \qquad (8)$$

where E_o and ψ_o refer to the top of the stack, and

$$E_d = -4c_1\phi_o/c_2^2. \qquad (9)$$

This quantity determines the density gradient that may be obtained.

In practice, these expressions are modified by many detailed considerations, such as amplifier noise and imperfect phase. Still, the optimum stack profile found for the practical case of the $\bar{p}$ accumulator, where these effects were taken into account, is not dissimilar to Eq. (8). Figure 4 shows this profile and how it develops with time during stacking. The sudden increase in slope near the stack bottom is caused by the use of a feedback system with higher bandwidth in that region.

In fact, the very large density ratio between the top and bottom of the stack necessitates a corresponding gain ratio. This dependence of gain on energy will be obtained by the use of position-sensitive pickups in combination with filters. Three overlapping feedback systems are at present foreseen. Noise filters will be used to prevent that the high-gain systems for the top of the stack will produce too much blowup at frequencies corresponding to the bottom. A more detailed description is given in Ref. 4.

VII. Betatron Cooling

There are two important differences between momentum cooling and betatron cooling:

a) For momentum cooling, the filter method is possible because the frequency of the pickup signal is related to momentum. The dependence of frequency on betatron amplitude, on the other hand, is weak.

b) Mixing is connected with momentum spread. Therefore momentum cooling reduces the mixing, whereas betatron cooling does not.

Because the mixing is constant, Gaussian distributions will remain Gaussian, which simplifies the theory. However, no detailed analysis including the mixing in an exact way is available at present. We shall make the following simplifying assumptions:

a) The mixing is bad,

b) The feedback system has constant gain with zero phase shift over a bandwidth W.

c) The momentum distribution is square, with a total revolution frequency spread $\varepsilon = \Delta f/f_o$.

Because of the last assumption, the bad mixing will cause an increase in Schottky power density[1] by a factor $\Lambda f_o/\varepsilon W$, with

$$\Lambda = \sum_n 1/n,$$

summed over all harmonics of the revolution frequency within the passband.

The cooling rate then is (as in Ref. 5, but corrected for bad mixing)

$$\frac{1}{\tau} = \frac{W}{2N}\left\{2g - g^2\left(\frac{\Lambda f_o}{\varepsilon W} + \eta^*\right)\right\}, \qquad (10)$$

where g is the gain relative to the optimum gain for good mixing and zero amplifier noise, whereas η^* is equal to the ratio of amplifier noise to signal power.

The optimum value for g gives

$$\frac{1}{\tau} = \frac{W}{2N}\cdot\frac{1}{\frac{\Lambda f_o}{\varepsilon W} + \eta^*}. \qquad (11)$$

As the cooling proceeds, η^* increases because the signal power decreases. Therefore, even if g is continuously adjusted to keep track of this, the cooling rate will decrease.

In the CERN $\bar{p}$ cooling ring, betatron cooling will be done on the stack, so that the cooling rate need not be high. It will be limited mainly by the bad mixing; because of this, amplifier noise will not be a problem.

VIII. Pickups and Kickers

Wideband pickups and kickers used at present for stochastic cooling are of three types:

a) sum pickups or kickers with ferrite rings

b) transverse pickups or kickers formed of $\lambda/4$ directional couplers

c) high frequency devices of traveling wave type with coupling slots.

Sum pickups or kickers with ferrite rings surrounding the beam are used for momentum cooling. It is usually found that for practical momentum cooling systems the output power needed is important. Since it can be decreased by using many kicker gaps, the length of these gaps should be as small as possible. For instance, for the $\bar{p}$ accumulator we plan to use kickers containing 100 or 200 gaps. Since most of the output power is due to amplifier noise, we also must use a large number of pick-up gaps, increasing the signal so that the gain may be reduced and the amplifier noise power decreased.

For the same reason, the gap impedance should be high. This is, of course, the reason why a ferrite ring is used. Unfortunately, at high frequencies (a few hundred MHz) the best available ferrites have low permeability and high losses. Therefore, it is doubtful if much more than 50 Ω/gap, as in present structures, may be reached. The power dissipation and cooling of the ferrite in the kickers is also a factor to be taken into account. It may limit the output power even more than the availability and cost of high power wide-band amplifiers.

Transverse pickups and kickers are necessarily much longer. Typically, their length should be about $\lambda/4$ in the middle of the passband, so that they have a reasonable impedance throughout. Because of this length (e.g., 25 cm for a bandwidth of 200-400 MHz), it is usually difficult to find space for a great number of transverse pickups. The signal-to-noise ratio therefore tends to be low. As a consequence, betatron cooling of low intensity beams is slower than momentum cooling.

For frequencies above 1 GHz, where ferrite cannot be used any more, Faltin[6] has developed a wide-band pickup (or kicker) structure that essentially consists of a metal box around the beam with transmission lines arranged above and below it. Slots in the top and bottom of the box couple the beam to the waves traveling along these lines (see Fig. 5). The same structures may be used as a sum or transverse pickup by adding the signals on the lines in phase or with a 180° phase shift. Such structures have been successfully used at CERN both for betatron cooling and for stochastic acceleration.

References

[1] S. van der Meer, Influence of Bad Mixing on Stochastic Acceleration, CERN SPS/DI/PP/Int. Note 77-8.

[2] R. B. Palmer, Brookhaven National Laboratory, private communication (1975).

[3] G. Carron and L. Thorndahl, Stochastic Cooling of Momentum Spread by Filter Techniques in the Cooling Ring, CERN Technical Note ISR-RF/LT/PS, January 1977.

[4] Design Study of a Proton-Antiproton Colliding Beam Facility, CERN/PS/AA 78-3.

[5] H. G. Hereward, Statistical Phenomena-Theory, Proc. of the 1st Course of the International School of Particle Accelerators, Erice, 1976; CERN 77-13, p. 281.

[6] L. Faltin, Dissertation, T-U, Vienna, 1977. L. Faltin, Slot-Type Pick-Up and Kicker for Stochastic Beam Cooling, Nucl. Instr. and Methods 148, 449 (1978).

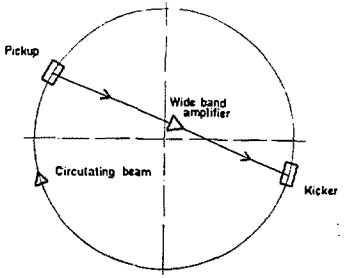

Fig. 1. Principle of stochastic cooling.

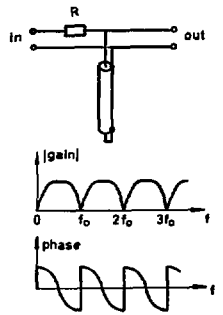

Fig. 2. A simple filter for momentum cooling.

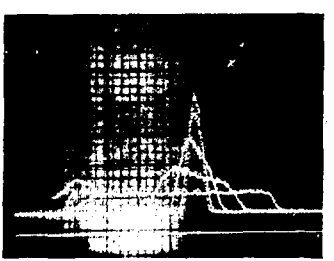

Fig. 3. Momentum cooling as obtained in the ICE experiment at CERN. Number of particles: 10^7. These Schottky scans represent the square toot of the density distributions. Successive scans were made at intervals of 1 minute.

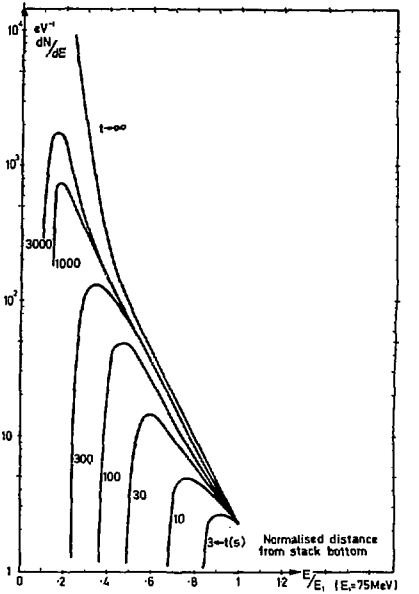

Fig. 4. Density distributions across the antiproton stack (CERN $p\bar{p}$ scheme).

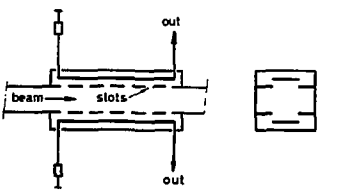

Fig. 5. Wide-band slot-type pickup.

TEVATRON USED AS $\bar{P}P$ COLLIDER

L. C. Teng
Fermi National Accelerator Laboratory

Assuming that electron cooling performs more or less as expected, we describe here how it will be used to obtain $\bar{p}p$ colliding beams in the Tevatron and give the expected performance.

I. Choreography

The present cooling ring is 2/7 the size of the Booster. For $\bar{p}p$, we shall assume that the ring is stretched to the same circumference as the Booster, as shown in Fig. 1. We start with standard acceleration of protons to 8 GeV in the Booster and injection into the Main Ring. Normally we fill the Main Ring to 2.5×10^{13} protons by 13 pulses from the Booster. For this operation, we can inject perhaps only 12 pulses to leave gaps for the rise time of the kickers. Then we accelerate the beam in the Main Ring to 80 GeV, the highest energy at which we can extract from a medium straight section. We extract one Booster batch at a time in synchronism with the Booster cycle (see Fig. 2). The 80-GeV protons strike a $\bar{p}$-production target and produce 5.18 GeV $\bar{p}$'s. The choice of energy is based on the following: the bunch spacing of the 80-GeV protons is 1/1113 of the Main-Ring circumference or 1/84 of the Booster circumference, but because of the energy (velocity) difference, the spacing of the $\bar{p}$'s from the target is necessarily smaller. To use the same Booster rf system for decelerating the $\bar{p}$'s, their bunch spacing must be 1/85 of the Booster circumference or their velocity 84/85 that of the 80-GeV protons. This gives a $\bar{p}$ energy of 5.18 GeV, which is, fortunately, a convenient and reasonable value.

Each Booster batch of $\bar{p}$'s is decelerated to 200 MeV and transferred to the cooling ring, where they are electron-cooled and stacked within a Booster cycle time. It takes 12 Booster pulses to empty the Main Ring of 80-GeV protons. The Main Ring is then returned to its 8-GeV injection field and the cycle starts over again in approximately 3 sec. The cooling and stacking of $\bar{p}$'s can go on for hours.

At the end, we fill the Tevatron with one Main-Ring pulse of 100-GeV (normal beam transfer energy from Main Ring to Tevatron) protons. The $\bar{p}$'s stored in the cooling ring are then bunched (by a small constant-frequency rf system in the cooling ring), accelerated in the Booster (with field reversed) and the Main Ring (counterclockwise), and transferred to the Tevatron (counterclockwise) at 100 GeV to join the already stored protons. The counter-circulating p and $\bar{p}$ beams are then both accelerated to 1000 GeV, and the low-β^* insertion energized for high luminosity colliding beams.

We will now discuss each of the processes involved quantitatively and in detail.

II. Antiproton Production

The cross section for forward production of 5.18 GeV $\bar{p}$'s with 80-GeV p's on H_2 target derived from Fermilab and ISR data, is about 50 mb/sr/($\Delta p/p$). The Booster acceptance at 200 MeV (40 π mm-mrad horizontal, 20 π mm-mrad vertical) translated to 5.18 GeV is 4π, 2π (the momentum ratio is just about 10). We have designed a beam transport using only quadrupole lenses which gives a β of 2.5 cm at the target. This gives an acceptance solid angle of

$$\pi\times\frac{\sqrt{4\times2}}{0.025}\times10^{-6} = 3.5\times10^{-4}\ \text{sr}.$$

Together with an acceptance momentum bite of $\Delta p/p = 3\times10^{-3}$, this gives

Cross section for accepted $\bar{p} = 5\times10^{-5}$ mb.

With a targeting efficiency of 1/3 (5-cm long W target) and a total cross section of 40 mb we get

$$\frac{N_{\bar{p}}}{N_p} = \frac{1}{3}\frac{5\times10^{-5}}{40} = 4\times10^{-7}.$$

In one hour, at 1 pulse/3 sec and 2.5×10^{13} p/pulse we get

$$N_{\bar{p}} = 10^{10}/\text{hr}.$$

III. Luminosity

For head-on collisions of two round Gaussian beams with standard deviations (rms beam widths) σ_p and $\sigma_{\bar{p}}$ the luminosity is given by

$$L = 3f\frac{n_p n_{\bar{p}}}{\epsilon_p+\epsilon_{\bar{p}}}\frac{N}{\beta^*},$$

where

- f = revolution frequency
- n_p, $n_{\bar{p}}$ = number of each particle per bunch
- N = number of bunches
- β^* = β at collision point
- ϵ_p, $\epsilon_{\bar{p}}$ = emittance of each beam

$$\left(\epsilon \equiv \frac{6\pi\sigma^2}{\beta}\right).$$

With

- $n_{\bar{p}} = 10^{10}$ (1 hour collection)
- $n_p = 2\times10^{10}$ (present normal operation)
- N = 1
- $\beta^* = 2.5$ m (see below)
- $\epsilon_p = 0.02$ π mm-mrad (at 1000 GeV)

$$\left(\epsilon_{\bar{p}} << \epsilon_p\right)$$

- f = 48 kHz.

We get

$$L = 1.8\times10^{28}\text{cm}^{-2}\text{sec}^{-1}.$$

To get a luminosity of $10^{30}\text{cm}^{-2}\text{sec}^{-1}$ we can collect $\bar{p}$ for 3 hours or increase the target efficiency, or both, to get $n_{\bar{p}} = 3\times10^{10}$. A scheme will be described later to collapse 8 (say) proton bunches into 1 bunch

with $n_p = 1.6\times10^{11}$ protons. We can further reduce β^* to 1 m in both planes. Altogether this gives a factor of $3\times8\times2.5 = 60$ and a luminosity of

$$L = 1.08\times10^{30}\,\text{cm}^{-2}\text{sec}^{-1}.$$

The discussions below will show that this luminosity can be obtained with a relatively high degree of confidence.

IV. Beam-Beam Tune Shift

The tune shift suffered by a $\bar{p}$ going through the high-density core of a Gaussian p bunch is given by

$$\Delta\nu_{\bar{p}} = \frac{3}{2}\frac{r_0}{\gamma}\frac{n_p}{\epsilon_p},$$

where $r_0 = 1.53\times10^{-18}$ m is the classical proton radius. With $n_p = 2\times10^{10}$ and $\epsilon_p = 0.02\ \pi$ mm-mrad at 1000 GeV ($\gamma \doteq 1067$) we get

$$\Delta\nu_{\bar{p}} = 0.0007.$$

Increasing n_p 8-fold we will have $\Delta\nu_{\bar{p}} = 0.0056$ which, although greater than the commonly accepted safe limit of 0.005, may nevertheless be tolerable for reasonably long beam lifetimes.

With a total of 3×10^{10} $\bar{p}$'s, we can divide them into 3 bunches with 10^{10} in each bunch. Thus we can still have the proton tune shift

$$\Delta\nu_p = \frac{3}{2}\frac{r_0}{\gamma}\frac{n_{\bar{p}}}{\epsilon_{\bar{p}}}$$

within safe limits while maintaining $\epsilon_{\bar{p}} << \epsilon_p$.

We have been considering only the tune shift caused by one beam bunch. There is some evidence that the tune shifts due to distant bunches do not add constructively and that it is only the tune shift per bunch which measures the damaging effects of the nonlinear field of one beam on particles in the other beam. In any case, we will show below that it is possible to keep the p and the $\bar{p}$ orbits separated everywhere except near the collision region, so that each particle sees indeed only one bunch of the other beam.

V. Low-β Insertion

The low-β insertion for the Tevatron is described in detail by D. E. Johnson in Fermilab TM-737, "Main Ring/Doubler Low-Beta Insertions," June 1977. We will mention here only that

(1) It is an antisymmetric insertion with 4 independently adjustable anti-pairs of quadrupoles. For antisymmetric insertion we always have $\beta^*_H = \beta^*_V$.

(2) The β^* value can be continuously adjusted from the normal 70 m down to less than 2.5 m. The β^* is tuned to a low value only after both the p and the $\bar{p}$ beams have been accelerated to 1000 GeV.

(3) When β^* is tuned to a small value, the dispersion η^* at the collision point is also reduced to some small value, typically less than 1 m. Hence the contribution to horizontal beam size from momentum spread is negligible.

VI. Orbit-Separating Bump Electrodes

With a normal tune of $\nu = 19.4$, we can separate the p and $\bar{p}$ orbits over most of the ring circumference by using electrostatic dipoles to bump them into 19 oscillations in opposite directions. The p and $\bar{p}$ orbits coincide over only the 0.4 tune advance, hence allowing head-on collisions.

If the orbit is bumped by an angle θ at β_E, the amplitude of the oscillation at β_{max} is

$$A = \sqrt{\beta_E\beta_{max}}\,\theta = \sqrt{\beta_E\beta_{max}}\,\frac{eE\ell/c}{p},$$

where E and ℓ are the field and the length of the bump electrode, for

$$\begin{cases} \beta_E = \beta_{max} = 100\ \text{m} \\ pc = 1000\ \text{GeV} \\ E\ell = 50\ \text{kV/cm}\times6\ \text{m} = 30\ \text{MV}. \end{cases}$$

We get

$$A = 3\ \text{mm}.$$

That is, the p and $\bar{p}$ orbits are separated by ±3 mm at the peak, which is adequate.

VII. Scheme to Collapse 8 Proton Bunches Into 1

We start by injecting 8 consecutive bunches of 2×10^{10} p/bunch into the Main Ring and accelerating them to 100 GeV. The Main Ring is then flat-topped. The longitudinal emittance of the beam has been measured to be about 0.1 eV-sec/bunch. (Some recent measurements give much higher values. The cause of this recent emittance growth is not yet known.) The total emittance of 8 bunches is, then, 0.8 eV sec $= 0.24$ (GeV/c) m.

We first debunch the 8 beam bunches adiabatically (see Fig. 3). After debunching the dimensions of the total occupied phase area (using physical coordinates Δz and Δp) are

$$\begin{cases} \Delta z_0 = 8\,\dfrac{2\pi R}{1113} = 45.2\ \text{m} \\ \Delta p_0 = \dfrac{0.24}{45.2}\ \text{GeV/c} = 0.00531\ \text{GeV/c}. \end{cases}$$

At the end of debunching, the 1113-harmonic cavities are all turned off and we abruptly turn on a set of rf cavities operating at a harmonic number much lower than 1113/8. We shall take 70. By rotating the phase area 1/4 of a phase oscillation in the central (linear) part of the stationary h = 70 bucket, we want to change the dimensions to

$$\begin{cases} \Delta z = \dfrac{70}{1113}\,\Delta z_0 = 2.84\ \text{m} \\ \Delta p = \dfrac{1113}{70}\,\Delta p_0 = 0.0845\ \text{GeV/c}. \end{cases}$$

The dynamics of the rotation gives

$$\begin{cases} \Delta z = K^{-1}\,\Delta p_0 \\ \Delta p = K\,\Delta z_0 \end{cases} \text{where } K \equiv \frac{mc}{R}\left(\frac{h}{2\pi}\frac{eV}{mc^2}\frac{\gamma}{A}\right)^{\frac{1}{2}}.$$

With h = 70, $\gamma = 107.6$, $\Delta = 1/\gamma_t^2 - 1/\gamma^2 = 0.00276$, to get K = 0.00187 (GeV/c)/m we need

$$V(h = 70) = 8.58 \text{ kV}.$$

The interesting parameters of the h = 70, V = 8.58 kV buckets are

Bucket height = 0.107 GeV/c
Bucket area = 6.11 (GeV/c) m
Phase oscillation wave number = $\nu_s = 5.11 \times 10^{-5}$
(0.10 sec for $\frac{1}{4}$ oscillation).

The rotated buckets having $\Delta z = 2.84$ m, $\Delta p = 0.0845$ GeV/c and containing 1.6×10^{11} protons are then transferred to the Tevatron and captured into the matched stationary buckets of the Tevatron with h = 1113 and V(h = 1113) = 1113/70×8.58 kV = 136.5 kV. These buckets have the same height (Δp) as the h = 70 buckets, but are only 70/1113 times as wide (Δz) hence 70/1113 times the area.

Although the calculation given here is rather simplistic, the beam should behave pretty much as described. The only worries are instabilities. Immediately after debunching, the momentum spread is $\Delta p_0/p = 5.31 \times 10^{-5}$, which may be too small to keep the beam stable against longitudinal instabilities. Various head-tail type of instabilities can also occur to the intense beam bunch of 1.6×10^{11} protons. All these should be examined in detail.

VIII. Incoherent Detuning of the Proton Bunches

At 100 GeV, the tune shift will be imagine dominated and given by

$$\delta\nu = \frac{r_0 R^2}{\nu\gamma} \frac{G}{g^2} \lambda,$$

where

- λ = linear density = $(1.6 \times 10^{11})/2.84$ m = 5.6×10^{10} m^{-1}
- g = half aperture = 1.5 in. = 0.038 m
- G = geometrical factor = $\pi^2/12$ (worst value corresponding to round beam in rectangular beam pipe).

This gives

$$\delta\nu = 0.023 \text{ (at the worst)}$$

which is entirely tolerable.

IX. General Considerations of Tevatron Aperture, Vacuum, and Impedances

1. The aperture requirement for $\bar{p}p$ operation is less demanding than that for either fixed-target operation (slow resonant extraction) or pp operation (momentum stacking a la ISR).

2. With cold-bore, the vacuum in the Tevatron is expected to be better than 10^{-11} Torr. Hence there will be no problem with neutralization, gas lifetime, or pressure-bump instability. The vacuum is essentially a "sealed" system. The cold vacuum-pipe wall acts as a very fast getter pump. One only has to make sure that the starting pressure and the leaks are reduced to such an extent that the pumping capacity of the pipe wall is not exhausted in too short a time. Presumably, warming-up and flushing the ring to rejuvenate the pipe wall once every 6 months is not too bad.

3. For most (not all) instabilities, the threshold given by Landau damping is proportional to

$$\frac{ZI}{\gamma},$$

where Z = impedance of the beam environment, I = beam current, and γ = beam energy. The increase in I can be offset either by increasing γ (higher energy) or reducing Z (improving the feedback system). Although the instabilities should be individually investigated in detail, at first glance none of them appear to impose any serious problem.

We conclude that, provided electron cooling works approximately as expected, the scheme described above should yield $\bar{p}p$ colliding beams in the Tevatron with a luminosity of $10^{30}\text{cm}^{-2}\text{sec}^{-1}$ at 1000 GeV×1000 GeV in a relatively straightforward manner.

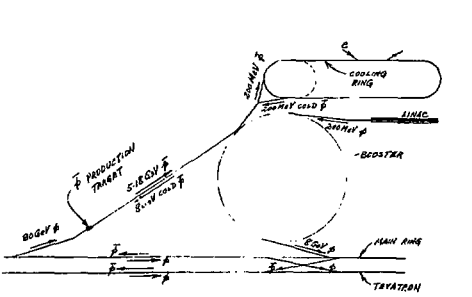

Fig. 1. The Cooling-Ring, Booster, Main-Ring, Tevatron complex showing the choreography for attaining $\bar{p}p$ colliding beams.

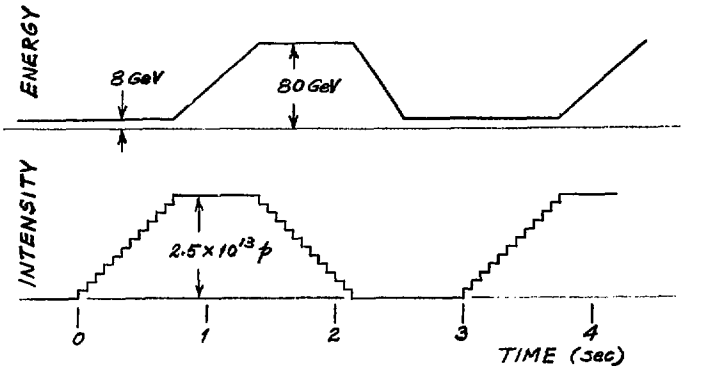

Fig. 2. The Main-Ring cycle during production-cooling-accumulation of $\bar{p}$'s.

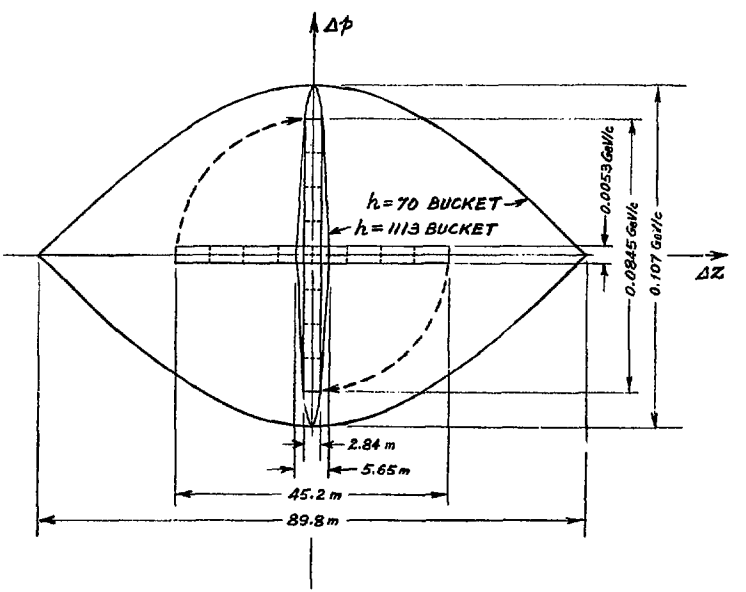

Fig. 3. Stationary rf buckets for harmonic numbers 1113 and 70 illustrating the scheme for collapsing eight proton bunches into one.

PROPOSED P-P COLLIDING BEAM FACILITY AT CERN

Roy Billinge
CERN

I. Introduction

Following the proposal of Budker and Skrinsky in 1966 and the subsequent experimental studies of electron cooling, Rubbia suggested various schemes for collecting antiprotons, injecting them in the SPS, accelerating them together with protons and colliding the beams at energies up to 270 GeV.

During 1976, working groups examined these possibilities and as a result a cooling experiment (ICE) and a study group were initiated. In the course of these studies, important advances were made in the theory of stochastic cooling. This technique, proposed by van der Meer in 1968 had seemed too slow for our application. However, some new techniques were proposed which, combined with the theoretical advances, indicated the feasibility of a fast pre-cooling of each injected pulse in momentum space before adding it to the stack.

Consequently, the initial proposal for a two-ring solution based on electron cooling was abandoned in favor of the present proposal. This decision has now been confirmed by the outstanding results of stochastic cooling tests on ICE.

II. Basic Parameters

A fundamental requirement on any proposed scheme was that its construction, testing, and operation should have a minimum impact on the existing research programs of the SPS and ISR. This alone indicates the need to use protons at PS energy for producing the antiprotons.

The basic scheme consists in directing 26 GeV/c protons from the PS on to a target. The antiprotons produced will be focussed and injected into a fixed-field cooling ring. Each injected pulse undergoes a rapid pre-cooling to reduce its momentum spread, after which it will be deposited by the rf system at the top of the stack. The stack is cooled continuously, both longitudinally and transversely so that particles slowly migrate to the bottom of the stack. The overall layout proposed is shown in Fig. 1.

To achieve the design luminosity of 10^{30} cm^{-2} sec^{-1} at 270 GeV/c it is necessary to collect, cool, and stack antiprotons for many hours. Studies of lifetimes in the SPS and feasible improvements to the average vacuum indicated that a luminosity lifetime of about 24 hours could be expected at 270 GeV/c. Consequently, the present design is based on collecting sufficient antiprotons in ~24 hours to reach luminosities of ~10^{30}.

Initial experiments with intense single bunches in the SPS indicate that about 10^{11} protons per 200 MHz bunch can be captured and accelerated, within invariant emittances of about 10π μrm. A low-beta insertion was designed which leaves free the space between two existing SPS quadrupoles (29m) and gives beta values of 4.7m horizontally and 1m vertically.

If we assume similar emittances for the antiprotons, applying the luminosity formula indicates a requirement to accumulate ~10^7 $\bar{p}$'s per second. With the present PS intensity of 10^{13} ppp, a cycle time of 2.6 secs, and collecting $\bar{p}$'s of 3.5 GeV/c, this can be attained within a momentum bite of ±0.75% and transverse emittances of 100π μrm.

III. Cooling Ring

The ring diameter must be as small as possible to minimize the stochastic cooling requirements. Since means exist to confine the protons in one quarter of the PS circumference, the cooling ring can have one quarter the diameter of the PS. At 3.5 GeV/c this allows a design with adequate space for injection, extraction, cooling, and diagnostic equipment.

To provide adequate "mixing" of particles η must be at least 0.1 (i.e., $\gamma_{tr} < 2.45$) which in a ring of average radius 25m implies an average $\alpha_p \approx 4.2$m. However, injection of the large emittance, large momentum spread beam requires α_p close to zero at the septum to minimize the "kick" strength required. Also the stacked beam must be screened from the injection kicker by means of a moveable shutter. To minimize the momentum separation required to achieve this, α_p at the injection kicker should be large. For similar reasons, the pre-cooling kickers have shutters and must be located at large α_p. In addition, to avoid blow-up of betatron oscillations the pre-cooling kickers are located in two regions of equal α_p separated by half a betatron wavelength. The focussing lattice designed to satisfy these conditions is shown in Fig. 2. The aperture requirements are based on the need to have a stacked beam with a total momentum width of 2.5%, an injected beam of 1.5%, both with horizontal and vertical emittances of 100π μrm and separated by a momentum "gap" of 1.8% (Fig. 3). The corresponding apertures are shown in Fig. 4 and the overall layout of the ring in Fig. 5.

IV. Some Limitations

In order to make use of the extracted beam line TT 60 for reverse injection to the SPS, a vertical emittance limit of $E_V = 1\pi$ μrm is imposed. With 6×10^{11} antiprotons in the cooled stack within this emittance, evaluation of intra-beam scattering following Piwinski's theory shows that the beam blow-up can be overcome by the stochastic cooling for a final horizontal emittance, $E_H = 1.4\pi$ μrm and a total momentum spread of $\delta p/p = 3\times10^{-3}$. This corresponds to a total bunch area of 5.63 eV sec.

The SPS rf system has a nominal frequency of 200 MHz and will be able to supply a peak voltage/turn of 8.8 MV. The traveling-wave structures accelerate only in one direction so that connecting half the cavities in the opposite sense allows the p and $\bar{p}$ beams to be treated separately with up to 4.4 MV/turn. For stationary buckets at 270 GeV/c this provides a bucket area of about 2 eV sec. This leaves no margin for dilution of the antiproton bunches

unless the number of bunches is 4 or more. The number of bunches proposed is 6, which leaves open the possibility of utilizing more than one of the 6 long straight sections for colliding-beam physics. Although this leaves some margin in the bucket area at 270 GeV/c, the area available near transition energy in the SPS is insufficient. Consequently it is proposed to accelerate each of the 6 bunches in 4 adjacent 200 MHz buckets up to high energy. There the 4 adjacent bunches will be coalesced into a single 200 MHz bucket.

V. Injection and Initial Acceleration Into the SPS

Many options exist for the detailed scheme of capturing the antiproton and proton bunches in the SPS and for their initial acceleration without incurring excessive Laslett Q shift. These are being studied both theoretically and experimentally at present.

The scheme proposed initially is to trap 1/6 of the stack in the cooling ring in a small bucket (h = 1), accelerate it to the injection/ejection orbit and then eject it along TT2A and down TT60 thence into the SPS.

The 6 bunches thus formed would be captured by a subsidiary rf system in the SPS running at 2.6 MHz (h = 60) with an initial bunch length of 80m. Subsequently, the shortened bunches would be recaptured and rotated at h = 210 in larger buckets. After this, each 5.7m long bunch is captured into the four adjacent 200 MHz buckets. Both proton and antiproton beams are then accelerated by the normal SPS rf system up to the required collision energy.

The main parameters of the proposed scheme are shown sequentially in Fig. 6.

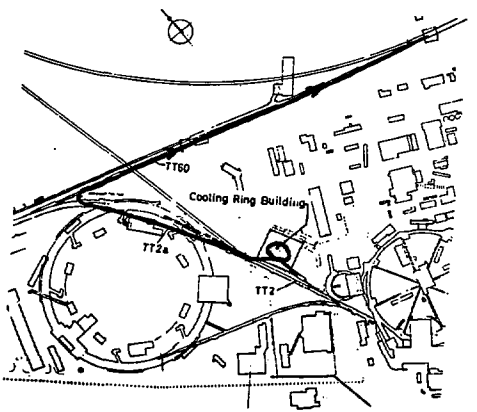

Fig. 1. Overall site layout

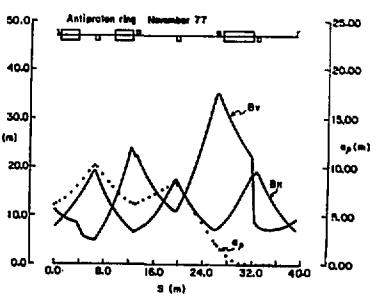

Fig. 2. Focussing lattice

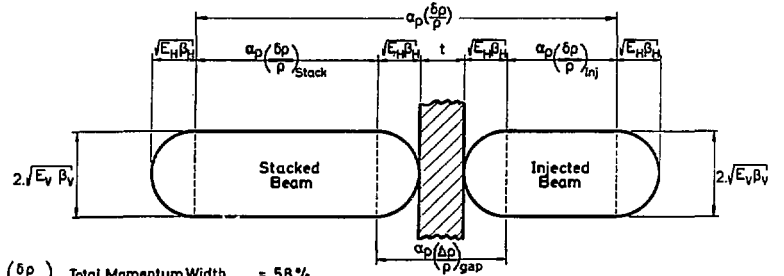

$\left(\frac{\delta p}{p}\right)$ Total Momentum Width = 5.8 %

(πE_v) Vertical Emittance = 100 π mm mr

(πE_H) Horizontal Emittance = 100 π mm mr

$\left(\frac{\delta p}{p}\right)_{st}$ Stack Momentum Width = 2.5 %

$\left(\frac{\delta p}{p}\right)_{inj}$ Injected Momentum Width = 1.5 %

Fig. 3. Machine acceptance

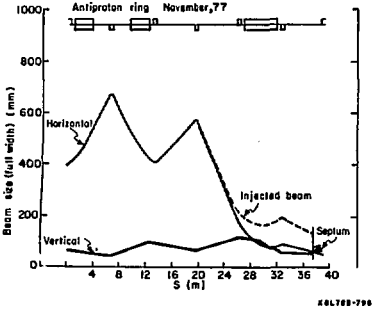

Fig. 4. Apertures

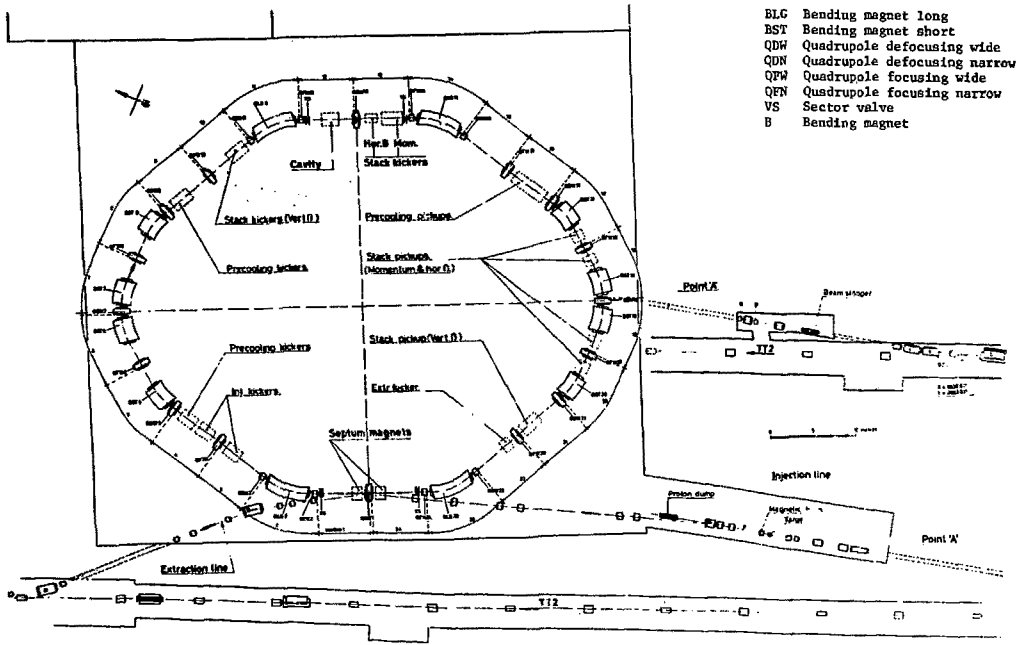

Fig. 5. General layout of the antiproton accumulator

MAIN PARAMETERS

10^{13} protons at 26 GeV/c each 2.6 secs.

⇩

2.5×10^{7} $\bar{p}$'s at 3.5 GeV/c within: -

$\frac{\delta p}{p} = \pm 7.5\%$

$E_\gamma = 100\pi\mu rm$

Pre-Cooling $\frac{\delta p}{p}$ from $\pm$ 7.5‰ to $\pm$ 1‰ in 2 secs.

⇩ X 24,000 in 18 hours.

Stack $\frac{\delta p}{p} = \pm$ 12.5‰: $E_H = 100\pi\mu rm$: $E_\gamma = 100\pi$

⇩

6×10^{11} $\bar{p}$ in $\frac{\delta p}{p} = \pm$ 1.5‰: $E_H = 1.4\pi\mu rm$: $E_\gamma = 1\pi\mu rm$.

⇩

Colliding Beams at 270 GeV/c

6 bunches p, $\bar{p}$ each 10^{11} and 1.5m long.

Interaction Region $\beta_H = 4.7m$: $\beta_V = 1.0m$

Emittances (E_H, E_V): $\left.\begin{matrix} \text{protons} & 6.9 \times 3.5 \\ \text{antiprotons} & 3.8 \times 1.9 \end{matrix}\right\} \times 10^{-8}\pi$ rad m.

Luminosity: 10^{30} cm^{-2} sec^{-1}

L. Lifetime 24 hrs at 2×10^{-9} Torr.

Fig. 6. Main parameters of the proposed scheme

$\bar{p}p$ SYSTEMS AT ISABELLE

Robert B. Palmer
Brookhaven National Laboratory
Upton, New York 11973

I. Introduction

As was stated by Lee Pondrom,[1] it is to be expected that pp interactions will be studied at CERN and at Fermilab several years before they will be studied at ISABELLE. Further, pp interactions will be studied at ISABELLE with far higher luminosities than pp. In the light of such observations, a pp program at BNL can only be justified if: 1) the luminosity is higher than at CERN/Fermilab; and 2) the luminosity is high enough for detailed comparison of pp and $\bar{p}p$ interactions. These requirements would seem to suggest a minimum acceptable luminosity of 10^{31}.

I will consider three schemes, or stages, with steadily increasing cost and complexity only the last of which really meets the above requirement. The step by step presentation enables one to study what the real limits are.

II. Basic Plan

The basic proposed arrangement is shown if Fig. 1 protons are taken from the AGS and stacked in the ISA ring @1 until a 6×10^{14} proton charge is achieved. These protons are bunched into one or a few short pulses, each is extracted, focused to a very small spot and targeted on a short irridium target. The antiprotons made are collected by a horn system and injected and held in a single bucket of a high frequency rf system in the second ring.

The process is repeated and the next bunch of antiprotons placed in the next rf bucket of the second ring and so on until all bunches are full.

Finally, the first ring is filled with protons in the other direction and $\bar{p}p$ interactions take place at the 6 intersection regions.

In this basic proposal no cooling is employed and the principles used to attain maximum luminosity are those that produce the highest possible antiproton phase space density from the target. These are: 1) the proton bunch used to target is as intense and as short in times as possible; 2) the target is as small as possible; and 3) the protons used to target are at the highest possible energy (see Fig. 2 and later discussion). It is an inevitable consequence of these conditions that the target will be heated to a very high temperature and will, in fact, evaporate. This we do not believe is a fundamental problem and it will be discussed again below.

The final luminosity of $\bar{p}p$ is a function of the crossing angle, bunching and so on, but if the crossing is tune shift limited and is at an intersection with the same β as that for pp then we can write the luminosity:

$$L_{\bar{p}p} = I_{pp} \times \frac{n_{\bar{p}}}{n_p}, \tag{1}$$

where $n_{\bar{p}}$ and n_p are the total number of $\bar{p}$'s and p's stored.

In practice one would employ stochastic cooling to reduce the vertical $\bar{p}$ emittance until it matched the p emittance. In this case standard crossing angles would be employed and the relation of Eq. (1) is obvious.

The number of $\bar{p}$'s made per proton on target can be written

$$\frac{\partial n_{\bar{p}}}{\partial n_p} \approx \frac{1}{\sigma_a} \cdot E\frac{\partial^3\sigma}{\partial p^3} \varepsilon \frac{\Delta p}{p} \pi p_\perp^2 \tag{2}$$

where σ_a is the total absorption cross section, $E\,\partial^3\sigma/\partial p^3$ is the invariant $\bar{p}$ production cross section, ε the targeting efficiency (taken as 0.3), $\Delta p/p$ is the momentum acceptance for $\bar{p}$'s, $p_\perp$ is the transverse momentum acceptance for $\bar{p}$'s.

Finally we can write the luminosity

$$L_{\bar{p}p} = L_{pp} \cdot \frac{\partial n_{\bar{p}}}{\partial n_p} \cdot m, \tag{3}$$

where m is the number of ISA cycles used to make $\bar{p}$'s (assuming that the stack used to make $\bar{p}$ has the same number of protons as that used for pp interactions).

The values of all these parameters for the case (I) we are discussing are given in Table I. I will now discuss these parameters in turn.

a) $L_{pp} = 10^{33}$ is that given at the high luminosity small crossing angle intersections in the current ISA proposal.

b) The invariant cross section is plotted in Fig. 2 taken from estimates made by Cronin,[2] the values plotted are for p momenta in the central region which would be 14 GeV for 400-GeV pp interactions. Since collection must take place above the ISA transition energy of 20 GeV, a correction has to be made. Assuming collection at 21 GeV and a $(1-x)^6$ dependence an invariant p production of 0.055 is obtained.

c) Target efficiency of 0.3 is taken, which corresponds to that obtained from a thick target. It is a conservative figure.

d) The momentum acceptance of 1.5% is that of the ISA ring used to capture.

e) The final parameters: the $p_\perp$, and the total number of cycles m used turn out to be related and in order to evaluate them we have to consider explosive targeting, and rf requirements; big enough subjects to justify sections of their own.

III. Targeting

If the actual target is thin enough then the apparent size of the target is a function of the angular acceptance of $\bar{p}$'s from that target, rising linearly with that angle. Under these circumstances, the transverse momentum accepted rises only as the root of the machine acceptance and we obtain:

$$\pi p_\perp^2 = \frac{2p^2A}{l} = \pi(175\ \text{MeV})^2, \tag{4}$$

where p is the captured momentum (21 GeV)

A is the ISA acceptance ($1.4\ \pi\ 10^{-6}$ meter steradians)

l is the length of the target (6 cm irridium).

The apparent target diameter is given by

$$d = \sqrt{\frac{2A}{1\pi}} = 0.4 \text{ mm}. \qquad (5)$$

The actual target cannot be greater than this value and the question must be asked: How long will such a target remain when hit by the protons? Will it remain long enough? This leads me into the question of target heating.

The temperature reached in the target may be estimated by

$$T = \frac{\partial E/\partial x}{k} \frac{n/h}{\rho \pi r^2} = 125{,}000°C, \qquad (6)$$

where $\partial E/\partial x$ = beam heating (22 MeV/cm)

n = number of p's per ISA fill (6×10^{14})

h = number of ISA bunches extracted separately (4)

k = specific heat of target (0.036)

ρ = density of target (19.3)

r = target radius (0.2 mm)

The $\partial E/\partial x$ estimate is certainly optimistic since it ignores secondary particles, but the k estimate is very conservative since at such temperatures there will be a high degree of ionization.

I have also ignored all cooling due to radiation and conduction which again makes it a conservative calculation. At best the order of magnitude is probably right so I continue.

The ion velocity at this temperature is:

$$v = \sqrt{\frac{2kT}{m}} = 0.24\ 10^6 \text{cm/sec}$$

and this better be less than r/t where t is the bunch length

$$t \leq 80 \text{ n seconds}$$

which brings one to the next question: Can the bunch be this short?

Longitudinal phase space conservation demands that

$$ht \frac{\Delta p}{p} = \text{constant } (\approx 6\times10^{-9} \text{ sec})$$

which gives for h = 4, t = 80 n sec

$$\frac{\Delta p}{p} = 2.0\%$$

This is the momentum spread in the proton beam just before targeting and is acceptable.

Finally, we must ask: What rf system is needed to make the bunch?

IV. RF Systems

The procedure to make such a short bunch would be to slowly lower the rf voltage until the buckets are half filled (V = 2 kV) and then apply an eighth harmonic saw-tooth shaped high voltage (800 kV) for a 1/4 synchrotron cycle. This is a lot of rf but not excessive in view of its use for a short pulse at a fixed frequency.

RF is also required to hold the $\bar{p}$ bunches. The requirements are

t = 80 n sec

$\frac{\Delta p}{p}$ = 1.5%

p = 21 GeV

p(transition) = 20 GeV

f = 10 M/hz.

The voltage needed turns out to be ≈130 kV, which is not unreasonable.

V. Luminosities

All we now need to obtain luminosities is the number of ISA cycles used (m) in Eq. (3).

If no cooling is used, then the filling will have to stop when all buckets of the p rf system are full. There are 120 buckets, 4 are filled per ISA cycle and thus the ring is full after

m = 30 cycles.

The final luminosity in this case is then

$$L_{\bar{p}p} = 0.6\times10^{30}.$$

This is a reasonable value considering that NO COOLING has been used to stack and the time required if the ISA were cycled every 6 minutes would be only 3 hours.

If stochastic cooling (momentum or transverse) is employed once every 3 hours and further stacking schemes are used (see '77 Summer Study), then the process can be repeated, say 10 times, and a luminosity of 0.6×10^{31} achieved after a stacking time of the order of 30 hours.

VI. Further Improvements

Further improvement in luminosity can not reasonably be obtained by further stacking since the time required is already excessive. We must restudy Eq. (2) and make our improvements there. Targeting must clearly be improved but there is a limit to what can be done. More can be gained if the $\Delta p/p$ can be increased and the $p_\perp$ acceptance increased. These can both be improved if a special 21-GeV capture and cooling ring is built. A $\Delta p/p$ of 6% would not be unreasonable and with A = 6π 10^{-6} m steradians $p_\perp$'s up to 350 MeV would be captured. The apparent target diameter would be increased to 0.8 mm, thus easing the target heating problem. The cycle now could involve a single proton bunch (h=1) that would be targeted and the p's captured and debunched in the transfer ring. During the following 6 minutes, as the ISA was refilled, the p's would be cooled and finally stacked in the second ring just prior to receiving a new p burst. The rate of $\bar{p}$ production would be 16 times that without the transfer ring and after 30 hours of stacking, a luminosity of 10^{32} might be achieved.

Conclusion

The figures given above may well be optimistic, but they indicate some basic points:

1) It is better to use high-energy protons to make p's.

2) The maximum possible $\Delta p/p$ and $p_\perp$ should be accepted and the latter requires a smaller acceptance (A) at high

momenta than low.

3) ISABELLE is well suited to meet these requirements, especially if a 21-GeV capture/transfer ring is built.

4) $\bar{p}p$ luminosities over 10^{31} should be achievable with reasonable stacking times.

Finally, one should remark that the $\bar{p}p$ interactions at ISABELLE would be with all the experimental advantages this would bring together with the greater ease of long-term storage and smaller tune-shift problems.

References

[1] L. G. Pondrom, Proc. 1977 BNL Summer Workshop, BNL 50721, p. 372.

[2] J. W. Cronin, Proc. 1977 Fermilab Workshop on Colliding Beams.

TABLE I

Options	I stack in ISA without cooling	II stack in ISA with cooling	III capture $\bar{p}$'s in transfer ring	
L_{pp}	10^{33}	10^{33}	10^{33}	$cm^{-2}sec^{-1}$
$\frac{1}{\sigma_a} E \frac{\partial^3 p}{\partial p^3}$	.055	.055	.055	GeV^{-2}
ϵ	.3	.3	.3	
$\frac{\Delta p}{p}$	1.5	1.5	6	%
$\pi_{p_\perp}^2$	$\pi(.175)^2$	$\pi(.175)^2$	$\pi(.35)^2$	GeV^2
m	30	300	300	
$L_{\bar{p}p}$	$.6\times10^{30}$	$.6\times10^{31}$	10^{32}	$cm^{-2}sec^{-1}$

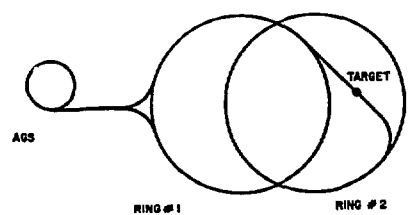

Fig. 1. $\bar{p}p$ arrangement at ISABELLE.

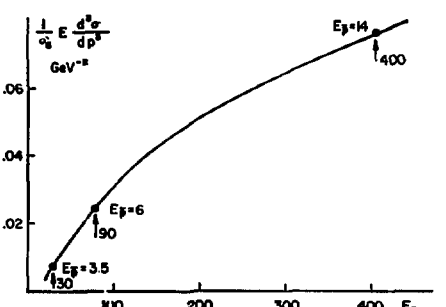

Fig. 2. Antiproton production versus proton energy.

REPORTS OF WORKING GROUPS

STOCHASTIC COOLING THEORY*

Frank J. Sacherer

CERN, Geneva, Switzerland

1. OPEN LOOP

Feedback from kicker back to PU via the beam is neglected. Consider momentum cooling as proposed by Thorndahl.[1] (See Fig. 1). A particle passing the PU induces a pulse which is amplified, filtered, and synchronized to arrive at the gap with the particle, correcting its energy by ΔE_c volts/turn. In the frequency domain, the single particle of charge e has a DC current ef_0 and AC components $2ef_0$ at each harmonic of the particle's revolution frequency f_0 (Fig. 2).

The periodic notch filter $H(\omega)$ insures that particles with too much energy are decelerated while particles with too little energy are accelerated, compressing the beam energy spread into the notches. If $G_n(E)$ is the voltage gain from preamp input to final amplifier output for harmonic n, including the filter, then

$$\Delta E_c = 2\, ef_0\, R \sum \mathrm{Re}\, G_n \qquad \text{(volts)} \tag{1}$$

where $R = \sqrt{R_{pu}R_k}$ is the mean of the PU and gap resistance, and the summation is over the harmonics in the system bandwidth.

The kicks from the other particles and the amplifier noise contribute heating terms. The noise density referred to the preamp input is shown in Fig. 3. It consists of white noise $2KT = 8.2\times10^{-21}$ watts/Hz, assuming a 3 dB noise figure, and Schottky noise of $2\, e^2 f_0^2 N R_{pu}$ watts per Schottky band, where N is the number of particles in the beam and Δf_0 is the spread in revolution frequencies. A single particle is driven only by the noise at harmonics of its own revolution frequency. Summing the noise density over harmonics, we find the rms energy charge per turn

$$\Delta E_{ic}^2 = \underbrace{2KT\, f_0 R_K \sum |G_n|^2}_{\text{amplifier noise}} + \underbrace{2e^2 f_0^3 R^2 \frac{N}{\Delta f_0} \sum \frac{|G_n|^2}{n}}_{\text{Schottky noise}} \quad (\text{volts})^2. \tag{2}$$

For non-square distributions, replace $N/\Delta f_0$ in (2) by dN/df_0. If the Schottky bands overlap (perfect mixing), $n\Delta f_0$ in the summation should be replaced by f_0.

*Shortened version of ISR report (1978) with same title.

The evolution of the particle distribution

$$\psi\,(E,t) = \frac{dN}{dE} \tag{3}$$

is governed by the Fokker-Planck equation

$$\frac{\partial\psi}{\partial t} = \underbrace{\frac{\partial}{\partial E}\left(\frac{\Delta E_c}{T_0}\,\psi\right)}_{\text{cooling}} + \underbrace{\frac{1}{2}\frac{\partial}{\partial E}\left(\frac{\Delta E_{ic}^2}{T_0}\frac{\partial\psi}{\partial E}\right)}_{\text{heating}} \tag{4}$$

where T_0 is the revolution period. This equation is nonlinear because ΔE_{ic}^2 depends on ψ, so a general analytic solution is ruled out, although stationary solutions are easy to find. The equation has been integrated numerically with the measured filter characteristics to compare with the ICE experiment at CERN.

For an ideal linear filtor,

$$\begin{aligned} \textstyle\sum \mathrm{Re}\, G_n &= n_\ell G \\ \textstyle\sum |G_n|^2 &= n_\ell G^2 \\ \textstyle\sum \frac{|G_n|^2}{n} &= \Lambda G^2 \end{aligned} \tag{5}$$

where $\Lambda = \sum \frac{1}{n} \sim 1$

and n_ℓ is the number of harmonics in the system bandwidth Δf, namely $n_\ell = \Delta f/f_0$. Let

$$\frac{\Delta E_c}{T_0} = \frac{2e\, f_0 R n_\ell G}{T_c} = -\frac{E}{\tau_0} \quad \text{volts/sec} \tag{6}$$

where τ_0 is the cooling time for a single particle with no noise present. Then with noise,

$$\Delta E_{ic}^2 = \frac{1}{2}\frac{N T_0^2}{n_\ell \tau_0^2}\left[\underbrace{\frac{\Lambda f_0}{n_\ell \Delta f_0} + \frac{2\, KT\, f_0}{2e^2 f_0^2 R_{pu} N}}_{\eta}\right] E^2 \tag{7}$$

where η is the average noise-to-signal ratio in each revolution frequency band. The second-moment of the Fokker-Planck equation becomes

$$\frac{1}{\sigma}\frac{d\sigma}{dt} = -\frac{1}{\tau_o} + \frac{3}{4}\frac{NT_o}{\eta_\ell \tau_o}\left[\underbrace{\frac{\Lambda f_o}{\eta_\ell \Delta f_o}}_{\substack{=1 \text{ for perfect mixing} \\ >1 \text{ for bad mixing}}} + \eta\right] \qquad (8)$$

where σ is the rms energy spread, and the decrease of Δf_o with time has been neglected. If the PU resistance is large enough, the amplifier heating term η can be neglected, and (8) becomes

$$\frac{1}{\sigma}\frac{d\sigma}{dt} = -\frac{1}{\tau_o} + \frac{3}{4}\frac{N\Lambda}{\eta_\ell^2 \tau_o \Delta f_o} . \qquad (9)$$

The Schottky heating is minimized by increasing the number of harmonics η_ℓ and the revolution frequency spread Δf_o via the machine dispersion.

The same analysis for betatron cooling yields

$$\frac{1}{\sigma}\frac{d\sigma}{dt} = -\frac{1}{\tau_o} + \frac{1}{2}\frac{NT_o}{\eta_\ell \tau_o}\left[\underbrace{\frac{\Lambda f_o}{\eta_\ell \Delta f_o}}_{=1 \text{ for perfect mixing}} + \eta\right] \qquad (10)$$

which is the usual result for the perfect mixing limit.[2] Here $\sigma^2 = \overline{x^2}$ and τ_o is the simple-particle damping time for no noise. The average noise to-signal ratio,[3] $\eta = \overline{r^2}/\sigma^2$, increases as σ is cooled because the amplifier noise is not filtered in this case, while the spread Δf_o in revolution frequencies remains constant.

2. CLOSED LOOP

So far, feedback from the kicker back to the PU via the beam has been neglected. When the Schotthy bands overlap (perfect mixing), any coherent modulation produced by the kicker on the beam smears out before it arrives at the PU, so the open-loop damping rates apply. For bad mixing, the coherent modulation does not decay, but remains approximately constant around the machine circumference. In this case, the damping rates and system stability are modified.

Consider the betatron damping system shown in Fig. 4. The amplifier noise x_n and Schottky noise x_S are assumed to be injected into the loop as shown, while x_B is the coherent signal on the beam due to the force F, $\omega_\beta = Q\omega_o$ is the betatron frequency, and Im $\Delta\omega$ is the damping rate for the coherent modes of beam oscillation. It is related to the single-particle damping rate by

$$\text{Im}\,\Delta\omega = \frac{N}{2\eta_\ell}\frac{1}{\tau_o} . \qquad (11)$$

A simple particle with revolution frequency Ω_i responds to the force F as

$$\ddot{x}_i + Q^2\Omega_i^2\, x_i = F \qquad (12)$$

where the dot signifies the co-moving derivative

$$\frac{d}{dt} = \frac{\partial}{\partial t} + \Omega_i \frac{\partial}{\partial \phi} . \qquad (13)$$

The single-particle response is therefore

$$\tilde{x}_i = \frac{\tilde{F}}{2\omega_\beta(\omega_i - \omega)} \qquad (14)$$

where the tilda indicates the Fourier transform and $\omega_i = (n \pm Q)\Omega_i$. The coherent signal on the beam is then

$$\tilde{x}_B = \frac{1}{N}\sum \tilde{x}_i = \frac{\tilde{F}}{2\omega_\beta}\underbrace{\frac{1}{N}\sum \frac{1}{\omega_i - \omega}}_{G(\omega)} , \qquad (15)$$

or

$$\tilde{x}_B = \frac{-\Delta\omega\, G(\omega)}{1 + \Delta\omega\, G(\omega)}(\tilde{x}_n + \tilde{x}_s) \qquad (16)$$

while the force acting on the beam is

$$\tilde{F} = \frac{-2\omega_\beta \Delta\omega}{1 + \Delta\omega\, G(\omega)}(\tilde{x}_n + \tilde{x}_s). \qquad (17)$$

The denominators in (16) and (17) are the usual transverse coasting-beam dispersion relations. A typical plot of the inverse of the beam transfer function for real ω is shown in Fig. 5. It deviates from the real axis when ω is within the band of incoherent frequencies ω_i, that is, within a Schottky band. The system is unstable if $\Delta\omega$ lies to the right of the hatched line.

The open-loop signals are reduced by the factor

$$T_n(\omega) = \frac{1}{1 + \Delta\omega\, G(\omega)} = \frac{G^{-1}(\omega)}{\Delta\omega + G^{-1}(\omega)} = \frac{\text{Num}}{\text{Den}} \qquad (18)$$

which is the ratio of the vectors shown in Fig. 5. The numerator is typically ~1/4 S where S is the total frequency spread for the Schotthy band in question, so significant signal reductions require coherent damping rates in excess of $\Delta\omega \sim 1/4\,S$. In fact, large reductions in the Schotthy signals are commonly observed when operating the betatron cooling systems at the ISR[3] or the ICE experiment, particularly for the lower frequency bands where the frequency spread is small. Even the relatively small feedback via parasitic coupling impedances produces a noticeable effect in the ISR, in this case reducing the area of the stable bands compared with the unstable bands. The noise heating terms in (4) should thus be multiplied by $|T_n|^2$ while the cooling term is multiplied by $\text{Re}T_n$. Detailed calculations have not been performed yet.

Similar signal reduction occurs for momentum cooling (Fig. 6). In addition, system stability is more critical because of the periodic notch filter. The poles and zeroes and response for a first-order filter are shown in Fig. 7. The high gain and changing phase near the poles may cause instability unless the total loop gain KHG including the beam is less than unity everywhere.

For bad mixing, the density and energy modulation on the beam due to the gap voltage u is

$$\tilde{I}_n(\omega) = e N \omega_o \int \tilde{\psi}_n \, dE \qquad (19)$$

$$\tilde{\psi}_n(E,\omega) = - j \frac{e}{T_o} \tilde{u} \quad \frac{\frac{d\psi_o}{dE}}{\omega - n\omega_o - nkE}$$

where the stationary beam distribution $\psi_o(E)$ is normalized to unity. Thus the beam transfer function is

$$G(\omega) = - 2\pi j \frac{Ne^2R}{T_o^2} \int \frac{\frac{d\psi_o}{dE}}{\omega - n\omega_o - nkE} dE \qquad (20)$$

which is approximately (exact for a Lorentz distribution)

$$G(\omega) \approx j\,nk \frac{Ne^2R}{(\omega - n\omega_o - j\sigma)^2 T_o^2} \qquad (21)$$

with Landau damping included. Here σ is the rms frequency spread for the nth Schottky band. The beam thus has second-order poles near each harmonic of the revolution frequency, and the beam response falls off as the square of the frequency outside the Schotthy bands.

The pole-zero diagram for the closed-loop transfer function is shown in Fig. 8. As the gain is increased, the poles move on the paths indicated. Eventually the system pole crosses into the right-hand-plane and instability results. As the pole approaches the axis, the noise power near the resonance increases, possibly saturating the amplifier. The simple pole in Fig. 7 is replaced by a pole-zero cluster, which is responsible for the signal reduction within the Schottky bands. This reduction is probably beneficial since it is largest for the low frequency Schottky bands which contribute most of the heating. This may explain why the momentum cooling observed in the ICE experiment is faster than expected from the open-loop transfer function.

For stack cooling, third-order or higher order filters are required to shield the accumulated beam from its own Schottky noise, yet provide enough gain on the injection orbit to compress the newly injected pulse within a few seconds. Since the beam response decreases as the square of the frequency, while the filter response increases as the cube, the overall gain increases with frequency, and eventually unity gain is likely to be exceeded. Quantitatively, the unity gain restriction

$$1 \geq |K\,H\,G| \qquad (22)$$

can be written as

$$1 \geq 2\pi \frac{Ne^2R}{T_o^2} KH(\omega) \int \frac{\frac{d\psi_o}{dE}}{\omega - n\omega_o - nkE} dE \qquad (23)$$

or

$$1 \geq \frac{Ne}{2\pi \eta T_o} \frac{V(E)}{nkE^2} \qquad (24)$$

where V(E) is the required single-particle energy change per turn,

$$V(E) = 2\,n_\eta \frac{e}{T_o} RKH(\omega) \qquad (25)$$

and the energy deviation E rather than frequency $\omega = n\omega_o + nkE$ is used. Requirement (24) cannot be satisfied for practical $\bar{p}$ collection schemes, thus ruling out the filter method for stack cooling.

This problem is less serious with the Palmer method of momentum cooling. The horizontal PU can be shaped as shown in Fig. 9 with a sensitivity F(E) that decreases approximately exponentially in the stack region, with

$$V(E) = 2\,n_\eta \frac{e}{T_o} F(E). \qquad (26)$$

The unity gain requirement is now

$$1 \geq 2\pi \frac{Ne^2}{T_o^2} \int \frac{F(E) \frac{d\psi_o}{dE}}{\omega - n\omega_o - nkE} dE$$

or (27)

$$1 \geq \frac{Ne}{n_\eta T_o} \int \frac{V(E) \frac{d\psi_o}{dE}}{\omega - n\omega_o - nkE} dE,$$

with the filtering inside the integral. The overall response decreases linearly with frequency. Van der Meer has pointed out that (27) is always satisfied to within a factor of order unity as long as the beam is cooled, that is, provided the cooling term in (4) is larger than the Schottky heating term.[5] Linear filters are also required in this case to reduce the amplifier noise in the stack region.

In summary, it seems that a complete theory of stochastic cooling that includes the effects of bad mixing is now available. Detailed calculations of cooling rates and system stability remain to be done.

ACKNOWLEDGMENT

This work was carried out with the active support and collaboration of Lars Thorndahl and Simon Van der Meer.

REFERENCES

[1] L. Thorndahl and G. Carron, Stochastic cooling of momentum spread by filter techniques in the cooling ring, CERN technical note, ISR-RF/LT/ps (1977).

[2] H. G. Hereward, "Statistical phenomena-theory," Erice lectures on Accelerator theory, CERN-77-13, 281 (1977).

[3] S. Van der Meer, Stochastic damping of betatron oscillations in the ISR, CERN-ISR-PO/FB-31 (1972).

[4] P. Bramham, G. Carron, H. G. Hereward, K. Hübner, W. Schnell, and L. Thorndahl, "Nucl. Instr. and Methods," 125, 201 (1975).

[5] S. Van der Meer, private communication (Oct. 1977).

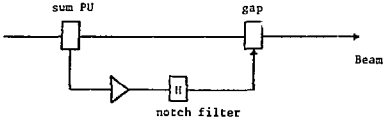

Fig. 1

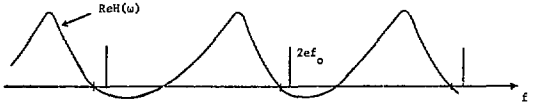

Fig. 2

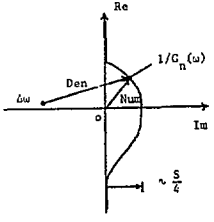

Fig. 3

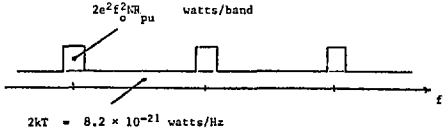

Fig. 4

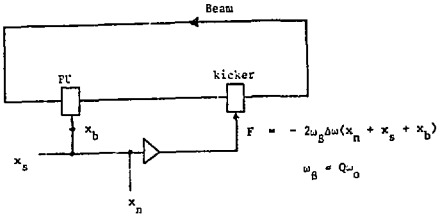

Fig. 5

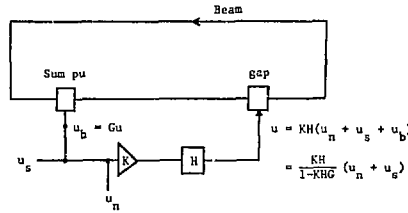

Fig. 6

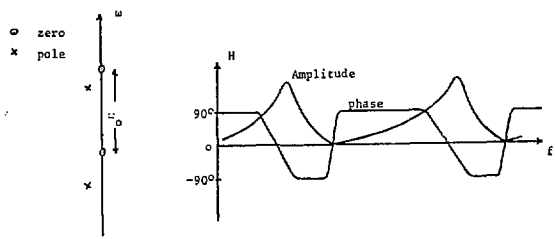

Fig. 7

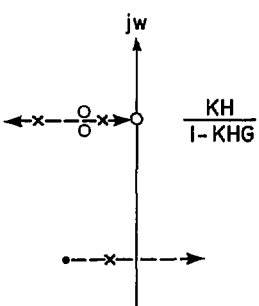

XBL 7810-11577

Fig. 8

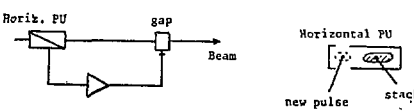

Fig. 9

RELATIVISTIC ELECTRON COOLING FOR HIGH LUMINOSITY PROTON-ANTIPROTON COLLIDING BEAMS AT VERY HIGH ENERGIES

C. Rubbia
CERN, Geneva, Switzerland

Electron cooling has been introduced by Budker[1] in order to extend to heavy particle beams most of the benefits of damping by synchrotron radiation, which is a very powerful tool in the process of accumulation and collision in e^+e^- storage rings. Assume an intense electron beam in contact with heavy particles (e.g. protons or antiprotons) stored in a ring. Provided the average electron and proton velocities are adjusted to be closely equal and the electron temperature (e.g. the residual kinetic energy of electrons in the frame moving with the common average velocity) is sufficiently small, in favorable conditions the proton temperature will decrease up to about twice the electron temperature. This means that the angular divergence of the stored proton beam θ_p will decrease eventually up to a value

$$\theta_p = \sqrt{\frac{2m}{M}}\ \theta_e ,$$

where θ_e is the angular divergence of the electrons, and m and M are respectively the electron and proton masses. A similar damping is expected to occur in the longitudinal motion.

As is well known, extensive experiments[2] carried out at Novosibirsk with the storage ring NAP-M have demonstrated cooling of 65 - MeV protons by electrons trapped in a solenoidal magnetic field. Their results are in satisfactory agreement with theory, once the specific properties of the proton and of the electron motions have been taken into account.

It is generally believed that because of the extremely fast energy dependence of the formula giving the cooling time, which for constant θ_p goes approximately as $\gamma^5\beta^4$, cooling with electrons is only possible at very low energies. In the present note, we discuss a number of practical arrangements in which we succeed in overcoming the large power-law effects by the reduced beam sizes and most important, the incredibly large current densities of electrons which can be obtained by synchrotron damping of the electron beam. We propose feasible schemes in which a relatively modest device can continuously cool protons and antiproton beams even at ultra-high energies like those in the CERN-SPS (γ=300) and in the Fermilab-ED (γ=1000) with remarkable improvements of beam stability and luminosity.

In order to understand the implications of electron cooling for $\bar{p}$-p colliders at high energies, we start with the formula giving the luminosity L for head-on collisions

$$L = \frac{f n^2 b}{4\pi \sigma_x \sigma_y} = \frac{f n^2 b}{4\pi\sigma^2} , \qquad (1)$$

where n is the number of particles in each of the b bunches, $\sigma_x = \sigma_y = \sigma$ is the beam rms cross section at the crossing point and f is the revolution frequency. On the other hand, the tune shift ΔQ coming from beam-beam interactions

$$\Delta Q = \frac{r_p n \beta^*}{4\pi \gamma \sigma^2} , \qquad (2)$$

where $\beta^* = \beta_x = \beta_y$ is the value of the beta function at the crossing point, $r_p = 1.53 \times 10^{-16}$ cm is the classical proton radius and γ the usual relativistic factor. Combining the two formulae we get

$$L = \frac{f \Delta Q \gamma nb}{r_p \beta^*} , \qquad (3)$$

where one can see that for a given ΔQ the luminosity is independent of the number of bunches and linearly proportional to the total number of particles N = bn. Setting $L = 10^{30}$ cm^{-2} sec^{-1}, $\Delta Q = 10^{-2}$, $\gamma = 280$, $\beta^* = 1$ m and f = 43.4 kc/s we get N = bn = 1.25×10^{11}. The corresponding invariant emittance E_o of the two beams, defined as the two s.d. point of the Gaussian approximation is easily evaluated

$$E_o = \frac{r_p n \beta}{\Delta Q} . \qquad (4)$$

In practice, cooling can be achieved with an electron beam stored in a small ring of elongated race-track shape running tangent to the protons and antiprotons along a straight section. In the simplified case of an electron velocity distribution uniform in three dimensions in the moving-particles frame, the damping time in the laboratory frame is given by the following general formulae

$$\tau_e = \frac{0.5}{r_p r_e c L} \frac{\gamma^2}{n_e \eta} \begin{cases} \theta_p^3 \beta^3 \gamma^3 & \text{for } \theta_p > \theta_e \\ (T_e/mc^2)^{3/2} & \text{for } \theta_p < \theta_e \end{cases} \qquad (5)$$

where r_p and r_e are the classic radii for the two particles, c is the speed of light, L=20 is the Coulomb logarithm, n_e is the density of electrons in the laboratory system and η is the fraction of the storage ring circumference with electron cooling. T_e is the electron temperature in the moving frame expressed in units of kinetic energy.

It is immediately apparent from this formula that if the beam is initially very cold, it is easy to keep it cooled. For a proton emittance as low as the one required by Eq. (4), it is expected that the proton

velocity in the particle frame will become lower than the rms velocity of the electrons. This, in turn is equivalent in the laboratory system to the condition $\theta_e \geq \theta_p$. The frictional force of the electrons on the protons is then proportional to the residual proton velocity in the particle frame and the damping constant τ_e due to the electron friction force is independent of the amplitude of the proton oscillations. For a velocity distribution of the electron beam spatially symmetric and Gaussian and a constant density over the cross section of the beam, the damping constant is given more precisely by the formula[2]

$$\tau_e = \frac{3}{2\sqrt{2\pi}} \frac{\beta \gamma^2 e}{r_p r_e \eta j L} \left(\frac{T_e}{mc^2}\right)^{3/2}, \quad (6)$$

where $T_e = \beta^2\gamma^2 mc^2\theta_e^2$ is the electron temperature and j is the current density.

Of course the central question is what electron current density and temperature we can achieve in practice. The proton beam has a very small (circular) cross section $q_p = \beta_o (E_o/\gamma\beta)$ where β_o is the (average) value of the beta function at the cooling straight section. Inserting $\beta_o = 60$ m, $\gamma\beta = 280$ and for the value of the emittance given in Eq. (4) for $n = 2 \times 10^{10}$ we find $q_p = 0.66$ mm^2. A practical electron beam will cover perhaps twice this area in order to insure convenient matching. For a reasonable number of bunches, the electron beam cross section can be only of order of a fraction of mm^2. Even relatively modest electron currents can be used to achieve substantial current densities.

A crucial feature of the cooling with relativistic electrons is the fact that the longitudinal temperature $T_{e\parallel}$ is insensitive to the laboratory energy spread. The Lorentz transformation from the laboratory to the moving particle frame is surprisingly favorable;

$$T_{e\parallel} = \frac{1}{2} m_e c^2 \left(\frac{\Delta p_e}{p_e}\right)^2_{rms} \quad (7)$$

For a relatively large momentum spread $(\Delta p/p)_{rms} = 10^{-3}$ in the laboratory frame, we find $T_e = 0.25$ eV! Likewise, the condition that the proton velocity in the moving frame should be no greater than the rms electron velocity becomes the laboratory condition $|\Delta p/p| \leq [(\Delta p_e)/p_e]_{rms}$, which is easily satisfied by the proton beam. On the other hand, substantial momentum spreads are needed to insure stability of both proton and electron bunches. For a parabolic distributions in line density and a peak current I_o, bunches are stable[3] provided

$$\left|\frac{Z}{n}\right| \leq 1.92\, \eta \frac{p}{I_o} \left(\frac{\Delta p}{p}\right)_{rms}, \quad (8)$$

where Z is the longitudinal impedance for the n mode and η is the usual factor relating the change in period to the change of momentum. For $|Z/n| = 20$ ohm (which can probably be achieved with a small weak focusing electron ring), $\eta = 0.7$ and $p_e = 143$ MeV/c, we get $I_e \leq 10$A. Applying the corresponding expression to the protons, with $|Z/n| = 25$ ohm, $\eta = 1.72 \times 10^{-3}$, $\Delta p/p = 10^{-3}$ we find $I_p \leq 36$A, which is a very safe value.

The transverse temperature $T_{e\perp}$ is directly related to the rms angular divergence. The requirement $T_{e\parallel} = T_{e\perp}$ gives $\theta_e^{rms} = 1/\sqrt{2}\,\beta\gamma)\,/(\Delta p/p)$. This equation requires very small angular divergence for the electrons and it is likely that at high energies one has to accept $T_{e\perp} \geq T_{e\parallel}$.

Cooling is needed at high energies in order to compensate for beam growth due to beam-gas scattering, higher-order resonances, longitudinal and transverse instabilities, intra-beam scattering and so on. In order to have a first-order estimate of the cooling rate which is required, we shall estimate simply the effect of the multiple scatterings with the residual gas. The time constant for beam growth due to multiple scattering in absence of cooling is given by [4]

$$\frac{1}{\tau_{ms}} = \frac{1}{\theta_p^2} \frac{d\theta_p^2}{dt} = \frac{K \beta_o}{\gamma\beta E_o} n_{ms}, \quad (9)$$

where $K = 4\pi^2[(m_e^2/c)\, r_e^2\, c\, G_{N2}\, (t/M)] = 1.08 \times 10^{-23}$ m^3 sec^{-1}, G_{N2} is tbe absolute gas factor for N_2 and n_{ms} the equivalent density of nitrogen atoms for multiple scattering. It is related to the equivalent multiple scattering preseure p_{ms} (Torr) by

$$n_{ms} = 1.93 \times 10^{25} [\mathrm{m}^{-3},\ \mathrm{K^o},\ \mathrm{Torr}] \frac{p_{ms}}{T}, \quad (10)$$

where T is the absolute temperature of the residual gas. For instance, setting $\beta_o = 60$ m, $P_{ms} = 10^{-9}$Torr, $T = 300$ K^o, $\gamma\beta_o = 280$ and $E_o = 3.2 \times 10^{-2}$ rad m, we calculate $\tau_{ms} = 2.14 \times 10^4$ sec.

The balance equation between the damping and diffusion processes (Langevin equation) has the form

$$\frac{d\theta_p^2}{dt} = -\frac{2\,\theta_p^2}{\tau_e} + \sum_1^n \left(\frac{d\theta_p^2}{dt}\right)_i, \quad (11)$$

where τ_e is the cooling time constant and $[(d\theta_p^2)/dt_i]$ is the diffusion rate for the corresponding process. The solution in case of cooling competing with just multiple scattering has been given in Ref. 2. The equilibrium value of the square of the mean proton angle is

$$\bar{\theta}_p^2 = 2\frac{m_e}{M}\theta_e^2 + \sqrt{18\pi}\frac{e\,c\,Z^2\,n_{ms}}{j\,\eta\,\beta^2}\frac{L_p}{L}\frac{m_e}{M}\left(\frac{T_e}{m_e c^2}\right)^{3/2} \quad (12)$$

where $L_p = \ln(133\, Z^{-1/3})$ is the Coulomb logarithm for scattering on the nucleus of charge Z.

Electron cooling will counteract Coulomb scattering if $\tau_s \approx \tau_e$. The corresponding electron current density is easily calculated combining Eq. (6) and Eq. (9)

$$j = 3.31 \times 10^{-20} \frac{\beta_o n_{ms} \gamma T_e^{3/2} \text{ (eV)}}{E_o \eta} A/m^2 \quad (13)$$

The minimum current density is inversely proportional to the equilibrium emittance of the proton beam E_o. Since the proton beam cross section and therefore the electron beam cross section are proportional to E_o, the total current is independent of the beam emittance. This is easily understood since a very small beam has a faster growth rate and therefore also needs more efficient cooling. As a numerical example, we can take the emittance from Eq. (4) for six bunches and insert the following numerical values in Eq. (13): $\beta_o = 60$ m, $n_{ms} = 4.65 \times 10^{13}$ ($P_o = 10^{-9}$ Torr), $\eta = 5 \times 10^{-3}$, $\gamma = 280$, $E_o = 3.2 \times 10^{-6}$ rad-m and $T_e = 0.5$ eV. We find $j = 0.57$ A/mm^2. The proton beam rms radius is $r_p = 1/2[(E_o\beta_o)/\beta\gamma]^{\frac{1}{2}} = 0.47$ mm. A reasonably well matched electron beam could have twice the rms radius of the protons, that is a cross-sectional area of about $\alpha_e = 2.8$ mm^2 or a total current $I_e = 1.56$A.

A transverse temperature of $T_{e\perp} = 0.5$ eV correspond to rms angular divergence $\theta_e = 1/\beta\gamma\,[T_e/(M_e c^2)]^{\frac{1}{2}}$ and for a rms radius of 0.66 mm, we find an invariant emittance (2 s. d.) $E_o = 4.1 \times 10^6$ rad-m, which is comparable to that of the protons. On the other hand, longitudinal temperature $T_{e\parallel} = 0.5$ eV corresponds to about $\Delta p/p_{rms} = 1.4 \times 10^{-3}$ which is substantially wide. An identical condition holds also for the proton beam.

We note that the previously indicated longitudinal impedance of $|Z/n| \simeq 20$ ohm for the electron ring, when combined with Eq. (8), gives us a maximum electron current of 20A, which is about fifteen times what is required to counterbalance the beam-gas collisions. Although other forms of instability of the electron beam still need to be investigated, it is likely that we shall end up with a lot of spare cooling capacity to counteract, if necessary, more virulent instabilities.

The tune shift ΔQ produced by the electron current on the proton beam limits the current density to the value

$$j \leq 2\,Q(\Delta Q)\,\frac{e\,c\beta^3\gamma^3}{\ell\,R_o\,r_p},$$

where $\ell = 20$ m is the length of the cooling region, R_o is the radius and Q is the tune of the SPS and other symbols have the same meaning as in the previous formulae. Setting $\Delta Q = 10^{-4}$ we get $j \leq 4.6\,10^3$ A/mm^2 which is safely beyond any practical value.

Lifetime of the beam in absence of other effects will be determined by nuclear collisions and single large-angle scatterings. The beam-gas lifetime for nuclear collisions is given by [5]

$$\frac{1}{\tau_{ns}} = \frac{1}{I}\frac{\sigma I}{dt} = 7.32 \times 10^2\, P_{ns}\ \text{(Torr)},$$

where P_{ns} is the residual N_2 equivalent pressure. For $P_{ns} = 10^{-9}$ Torr we find $\tau_{ns} = 1.37 \times 10^6$ s or about 16 days. The single Coulomb-scattering lifetime depends on the limiting aperture b_o.

The elastic Coulomb cross section of nuclei of charge Z for very small q^2 can be approximated as

$$\frac{d\sigma}{dq^2} = 270\,Z^2\ (\text{nb/GeV}^2) \times \frac{1}{q^4\,(\text{GeV})},$$

where $q^2 \simeq \theta^2 p^2$ is the q^2 in the scattering. Integrating the cross sections for all scattering angles larger than θ_o gives $\sigma = (270 \times 10^{-33} Z^2)/(p^2\theta^2)$. Replacing variables p and θ_o with more convenient quantities, we get

$$\frac{1}{\tau_{ss}} = 6.33 \times 10^3\ m^4 s^{-1}\ \text{Torr}^{-1}\ \frac{Z^2}{\gamma^2\beta^2\beta_o^2 b_o^2}\ P_{ss}.$$

Setting $b_o = 2$ mm for instance, we find $\tau = 4.88 \times 10^6$ sec or about 56 days.

The applicability of the scheme to the $\bar{p}$-p in the SPS is examined in more detail. The longer lifetime of beams suggests a longer collision time and therefore a longer accumulation time of $\bar{p}$'s. Assuming that 48 hrs is the largest time period over which accumulation can be practically envisaged, for the design performance of the source, [2] we set $N = nb \simeq 1.2 \times 10^{12}$ $\bar{p}$. Inserting this number in Eq. (3) and for standard values of β^* and $\Delta Q = 10^{-2}$ we get

$$L = 10^{31}\ \text{cm}^2\ \text{sec}^{-1}.$$

Longitudinal instabilities amongst other reasons suggest that individual bunches should not contain more than approximately 10^{11} particles. A preferable value could be 2×10^{10}, which has already been achieved, giving b = 60. Bunches are separated by about 115 m or 0.38 μs, which is acceptable for manipulation. The invariant emittance during collisions (at $\gamma\beta = 280$) is held constant with an appropriate balance between cooling and gas scattering to the value of Eq. (4), namely $E_o = 3.1 \times 10^{-6}$ rad-m.

The longitudinal area of bunches could be as large as 1.4 rad. For $V_o = 4.4$ MV and other standard rf parameters, we expect $\Delta p/p\,|_{full} = 1.8 \times 10^{-3}$ and a bunch length which is about 0.4 of the bunch separation. The rms betatron beam cross section in a middle of a straight section is $\sigma = 0.17$ mm^2. Note that the momentum spread gives an additional contribution to the width, which is $\Delta x = \Delta p/p \cdot \alpha_p = 3.6$ mm for $\alpha_p = 2$ m. We can either locate the cooling section in a straight section with $\alpha_p = 0$ or take advantage of the dispersion by matching it to an energy-modulated electron beam. The cooling time (assuming $\alpha_p = 0$) is given by Eq. (6)

$$\tau_e = \frac{4.81 \times 10^4\, T_e^{3/2}\ \text{(eV)}}{J(A/\text{mm}^2)}.$$

Assume an electron beam cross section which is four times the rms of the proton beam. Let us also take a maximum electron current of 4A at $\gamma\beta = 280$, corresponding to $p_e = 143$ MeV/c. Then $j = 4/(0.17 \times 4) = 5.9 A/mm^2$. For an electron ring which is approximately 50 m in circumference and electron and proton bunches of matched lengths, the average circulating electron current is then 50 mA, which is within the range of achieved performances. If the electron temperature is taken to be $T_e = 0.5$ eV, we find a cooling time $\tau_e = 2891$ sec, to be compared to the multiple-scattering lifetime of 21,400 sec. Clearly there is about a factor ten of safety.

In order to obtain a beam with the indicated transverse emittance, the design emittance of the accumulator ring has to be reduced a few times. This can be done by the cooling itself during the first few hours of collisions or by precooling at somewhat lower energy where the cooling time is greatly diminished.

Acknowledgements

I would like to express my appreciation to Drs. F. Mills, A. Ruggiero, and B. Palmer for very helpful comments and suggestions.

References

1. G. I. Budker, Atomnaya Energiya 22, 346 (1967).
2. G. I. Budker et al., BNL-TR-635 (Translation) and Particle Accelerators to be published.
3. E. Keil and W. Schnell, CERN-ISR-TH-RF/60-48 (1969).
4. G. Guignard, Yellow Report CERN-77-10.
5. Design Study of a proton-antiproton colliding beam facility, CERN-PS-AA 78-3 (1978).

COLLIDING BEAMS - LIMITATIONS/INSTABILITIES

A. G. Ruggiero and L. C. Teng

Fermi National Accelerator Laboratory

I. Fundamental Limitations on Luminosity

In principle, for moderate intensities, all coherent instabilities can be cured by modifying the impedance of the beam environment either passively or actively (feed-back). Self fields and beam-image forces, although extremely nonlinear, are not very rich in harmonics. They produce incoherent tune spreads that, if too large, will cause beam loss through resonances. The beam-beam forces, which are the most limiting, are however both nonlinear and rich in harmonics and cause the beam to blow up through a diffusion-like process. This stochastic process of beam growth can be counteracted only by some kind of cooling mechanism. For a crude measure of the magnitude of the beam-beam forces, one generally uses the linear tune shift. The achievable luminosity is then determined by the maximum beam-beam tune shift allowed.

For head-on collision of bunched beams, the luminosity is given by

$$L = \frac{n_p n_{\bar{p}}}{2\pi \left(\sigma_p^2+\sigma_{\bar{p}}^2\right)_H^{1/2} \left(\sigma_p^2+\sigma_{\bar{p}}^2\right)_V^{1/2}} fN,$$

where n_p and $n_{\bar{p}}$ are the numbers of particles (p or $\bar{p}$) per bunch, σ is the rms beam half-width (subscripts p for proton, $\bar{p}$ for antiproton, H for horizontal, V for vertical), f is the revolution frequency, and N is the number of bunches in each beam (same number in both beams). If parameters are identical in the horizontal and the vertical planes, we can write

$$L = \frac{f n_p n_{\bar{p}}}{2\pi\left(\sigma_p^2+\sigma_{\bar{p}}^2\right)} N,$$

or, in terms of the emittance $\epsilon \equiv 6\pi\sigma^2/\beta$, (assuming zero dispersion)

$$L = 3f \frac{n_p n_{\bar{p}}}{\epsilon_p+\epsilon_{\bar{p}}} \frac{N}{\beta^*}.$$

The beam-beam tune shifts per bunch are given by

$$\Delta\nu_p = \frac{3}{2}\frac{r_o}{\gamma}\frac{n_{\bar{p}}}{\epsilon_{\bar{p}}}, \quad \Delta\nu_{\bar{p}} = \frac{3}{2}\frac{r_o}{\gamma}\frac{n_p}{\epsilon_p},$$

where $r_o = 1.535 \times 10^{-18}$ m is the classical proton radius. Maximum luminosity is obtained when both beams are the same and limited by the same allowable tune shift. We can then drop the subscripts p and $\bar{p}$ and express both L and n in terms of $\Delta\nu$. This gives

$$\begin{cases} L = \frac{2}{3} f \frac{(\Delta\nu)^2}{r_o} \gamma \epsilon_o \frac{N}{\beta^*} \\ n = \frac{2\Delta\nu}{3r_o}\epsilon_o \end{cases} \qquad (\epsilon_o \equiv \beta\gamma\epsilon \text{ = normalized emittance; } \beta \sim 1)$$

If no cooling is applied during collision, a traditionally acknowledged safe upper limit for $\Delta\nu$ is 0.005, for a beam lifetime of few tens of hours. If *cooling is applied during collision through* heat exchanging with a cold electron beam, as suggested during the Workshop by C. Rubbia,[1] the upper limit of the tolerable $\Delta\nu$ can be raised before encountering a strong resonance effect or the stochastic limit (overlapping of resonances in one dimension). Here we will continue to take $\Delta\nu = 0.005$. The following table gives the parameters for the Fermilab Tevatron and the CERN SPS.

	Tevatron	SPS
f	48 kHz	43 kHz
γ	1067 (1000 GeV)	288 (270 GeV)
β^*	2.5 m	$\sqrt{1 \text{ m} \times 5 \text{ m}}$
ϵ_o	$15\pi \times 10^{-6}$ m-rad	$14\pi \times 10^{-6}$ m-rad
$\Delta\nu$	0.005	
n	1.0×10^{11}	1.0×10^{11}
L	(0.68×10^{30}) N cm^{-2}sec^{-1}	(0.17×10^{30}) N cm^{-2} sec^{-1}

To get $L = 10^{31}$cm^{-2}sec^{-1} we need approximately

N	15	60
nN	1.5×10^{12}	6×10^{12}

We conclude that a pp luminosity of 10^{31}cm^{-2}sec^{-1} is obtainable with moderate effort in the Tevatron, but is more difficult to attain in the SPS because of the lower beam energy. We next investigate the incoherent tune spread and the coherent instabilities that may be encountered by the somewhat intense proton beam bunches in the Fermilab scheme.

II. Transverse Incoherent Tune Spread

This is given by the Laslett formula (round beam)

$$\delta\nu = \frac{r_o\lambda}{\gamma}\left(\frac{\pi R}{\gamma\epsilon_o B} + \frac{G}{\nu}\frac{R^2}{g^2}\right),$$

where the first term in the parentheses is due to the self field, and the second term is due to the image field. For the Tevatron, the largest $\delta\nu$ occurs at 100 GeV. With

- γ = 107.6
- R = ring radius = 1000 m
- ν = betatron tune = 19.4
- g = aperture half-gap = 1 in. = 0.0254 m
- B = bunching factor, ratio of the bunch length to the bunch separation = 0.3
- G = geometrical factor = $\pi^2/12$ (rectangular beam pipe)

ϵ_o = normalized emittance = $15\pi \times 10^{-6}$ m
λ = average particle linear density
= $(1.0 \times 10^{11})/5.6\text{m} = 0.18 \times 10^{11}\,\text{m}^{-1}$
(rf wave length = 5.6 m),

we get

$$\delta\nu = 0.017,$$

which is a tolerable spread.

III. Longitudinal Individual - Bunch (Microwave) Instability

A beam bunch can experience second-order self-bunching at harmonics of the fundamental synchrotron frequency. The instability is described by a longitudinal impedance $|Z_n/n|$ in analogy to the coasting-beam case, where now the mode number n does not really have a precise meaning. If we give $|Z_n/n|$ the meaning of an equivalent impedance after summation over the beam spectrum, the following criterion for stability is commonly used.

$$|Z_n/n| \leq \frac{E/e}{eI_p} \Lambda \left(\frac{\Delta p}{p}\right)^2, \qquad (1)$$

where $\Lambda = \gamma_t^{-2} - \gamma^{-2} = 0.00276$, I_p is the peak current in the bunch and $\Delta p/p$ the full width at half maximum of the momentum distribution.

Equation (1) is a consequence of the Landau damping coming from a spread in the synchrotron frequency that is proportional to the square of the beam height.

By conservative extrapolation from beam observations in the Main Ring, we take

$$|Z_n/n| \sim 50 \text{ ohm}$$

For a Gaussian distribution with rms energy spread δ and rms length σ,

$$\frac{\Delta p}{p} = 2.355\,\frac{\delta}{E}$$

and

$$I_p = \frac{N\sqrt{2\pi}}{\sigma} I_b,$$

with I_b the average current per bunch. Combining these, we have the result that Eq. (1) transforms to

$$\sigma\delta^2 \geq 6 \times 10^{15}\ \text{eV}^2\,\text{m}$$

which we have calculated for 1000 GeV and for the parameters of section I, since this is the worst case for a bunched beam.

For instance, if $\delta/E = 10^{-4}$, then

$$\sigma \geq 60 \text{ cm}$$

or, in terms of bunch area S (= $6\sigma\delta/c$),

$$S \geq 1.2 \text{ eV-sec.}$$

This condition should be easily satisfied.

Another critical situation is at 100 GeV just after a single proton beam pulse is debunched, when $\Delta p/p$ is smallest. At this time, one should use the coasting beam criterion, which is still of the form (1) if we replace the peak current I_p with the total beam average current I_o.

We have $I_o = 0.47$ A, and by taking $|Z_n/n| = 50$ ohm again, the stability condition gives

$$\frac{\Delta p}{p} \geq 1.7 \times 10^{-4},$$

which is about three times larger than one would expect from a longitudinal emittance of 0.1 eV·s. The required final momentum is obtained by letting the bunches blow up in a controlled fashion (with a bunch spreader) up to approximately 0.35 eV·s as is presently done in the Main Ring.

IV. Longitudinal Bunch-To-Bunch Instability

Each beam bunch can oscillate in various modes, m, of the longitudinal oscillation. The wake field of the oscillation of one bunch can affect all following bunches and cause a bunch-to-bunch instability at some mode number μ. This instability is stabilized by Landau damping from a spread $\delta\Omega$ in phase oscillation frequency within a bunch.

Sacherer[2] has calculated the complex shift $\Delta\omega_m$ of the angular synchrotron frequency. It depends on the longitudinal coupling impedance and on the spectrum of the beam. By the approximation of an impedance that increases linearly with frequency, namely when Z_n/n, as defined in the previous section, is constant,[3] one has simply

$$\left|\frac{\Delta\omega_m}{\Omega}\right| < \sqrt{m}\,\frac{I_o\,|Z_n/n|\,N^2}{2\pi h B^3 V \cos\phi_s}, \qquad (2)$$

where Ω is the angular phase oscillation frequency, I_o the average current in N bunches, h the harmonic number, V the peak rf voltage and ϕ_s the stable synchronous phase. Equation (2) applies in the limit in which spurious sharp resonances have been eliminated or shifted; otherwise the shift is given by [4]

$$\frac{\Delta\omega_m}{\Omega} = \frac{Z_s\, I_o\, N}{2\pi h B V \cos\phi_s}\, F_m, \qquad (3)$$

where Z_s is the resonance shunt impedance, and F_m a form factor that measures the excitation of the beam. At worst, $F_m = 1$. We take also $\phi_s = 0$.

The stability condition [4] is

$$\frac{\sqrt{m}}{4}\,\delta\Omega \geq |\Delta\omega_m| \quad \text{for (2)}$$

and

$$\frac{\delta\Omega}{4} \geq |\Delta\omega_m| \quad \text{for (3)}$$

The spread in $\delta\Omega$ arises from the nonlinearities of the particle motion within a rf bucket. If the

bucket is not full, one has

$$\frac{\delta\Omega}{\Omega} \simeq \frac{\phi_o^2}{16}$$

for a bunch with half-length ϕ_o expressed in rf radians.

At the same time,

$$B = \frac{2\phi_o N}{2\pi h}$$

Taking $|Z_n/n| = 50\Omega$, V= 1 MV and 0.75 mA per bunch, we derive from (2) the following condition on the bunch length.

$$\phi_o \gtrsim 1.7 \text{ rad}$$

which, because of the way we have derived it, does not depend on the number of bunches.

From our experience in the Main Ring, spurious modes occur mostly in the rf cavities and can be easily damped down to a few tens of kΩ. If we take Z_3 = 30 kΩ, we derive from (3) the following condition on the bunch length.

$$\phi_o \gtrsim 0.1\, N^{1/3} \text{ rad},$$

which is less stringent than the previous one.

If shorter bunch length is desired, one can either stablize the shorter bunch by using a Landau cavity or at least eliminating the $N^{1/3}$ multiplier by spacing the N bunches asymetrically around the ring, so that their wake fields do not add constructively.

V. Transverse Individual-Bunch Instability (Head-tail Instability)

This instability can generally be controlled by properly adjusting the chromaticity $\xi = \Delta\nu/(\Delta p/p)$ Above transition, setting $\xi < 0$ will make most of the m>0 modes stable (depending on the impedance structure) leaving only the monopole mode m = 0 unstable. The m= 0 mode is that in which the beam bunch oscillates transversely as a rigid body and can easily be damped with a feedback circuit as is done in the Main Ring. In the absence of Landau damping, the growth time is proportional to n/γ. Although the number of particles per bunch n is increased by a factor 5 compared with the present operation of the Main Ring, this factor is compensated by the increase in γ. Therefore we do not expect that the feedback damper will have to be very different from the one now used in the Main Ring.

VI. Transverse Bunch-to-Bunch Instability

The dipole case (m = 1) was studied long ago by Courant and Sessler[5] and the throbbing modes (any m) by Lee, Mills, and Morton.[6] More recently, Sacherer[7] has unified the theories of the transverse instabilities including also the head-tail effect by combining the effects of short and long-range wake fields and taking into account the non rigidity of the bunches. The result of this general theory is that the instability causes a complex shift of the betatron angular frequency which is given by

$$\Delta\omega_m = \frac{1}{1+m}\,\frac{i}{2\nu\omega_o}\,\frac{eI_b}{\gamma m_o L}\,\frac{\sum_p Z_\perp(\omega)\, h_m(\omega-\omega_\xi)}{\sum_p h_m(\omega-\omega_\xi)} \qquad (4)$$

where m is the internal bunch mode, $i = \sqrt{-1}$, ω_o the angular revolution frequency, ν the betatron tune, e the particle charge, I_b the average current per bunch γm_o the relativistic mass, L the full bunch length, $Z_\perp$ the "transverse impedance" of the surroundings which has to be calculated at the angular frequencies

$$\omega = (p + \nu)\,\omega_o$$

where $-\infty < p$, integer $< +\infty$ for a single bunch or several bunches oscillating independently, and p = μ + kN, $-\infty < k$, integer $< +\infty$ for coupled motion of N bunches, μ being then the bunch to bunch mode number. In addition,

$$\omega_\xi = \nu\omega_o\,\frac{(\Delta\nu/\nu)/(\Delta p/p)}{|\gamma_t^{-2} - \gamma^{-2}|}$$

and $h_m(\omega)$ are Sacherer's functions[7] which give weights for the contribution of the beam sprectrum.

The transverse impedance $Z_\perp$ can be approximated for circular geometry in terms of the longitudinal impedance Z_n/n used in section III above[7] as

$$Z_\perp = \frac{2c}{b^2}\,\frac{Z_n/n}{\omega/n}. \qquad (5)$$

where b is the vacuum-chamber radius.

The beam is made stable by providing a spread in time $\delta\nu$ (Landau damping) such that

$$\omega_o\,\delta\nu \gtrsim \Delta\omega_m \qquad (6)$$

In the approximation that Z_n/n is constant, and anomalous, parasitic modes have been reasonably damped, $Z_\perp$, (5), is a constant and can be taken out of the summation at the r.h.s. of (4). This gives[8], by taking the worst case, m=0 and by making use of (2),

$$\Delta\nu \gtrsim \frac{eI_b}{\nu\omega_o^3}\,\frac{c^3\,|Z_n/n|}{E\,L\,b^2}. \qquad (7)$$

If this condition is satisfied, the beam is certainly stable, provided spurious impedance resonances are properly damped, but the opposite is not necessarily true. With this very conservative procedure, the stability condition (7) does not depend on the two instability mode numbers m and μ. Inserting the same numbers as before, we have

$$\Delta\nu \gtrsim \frac{0.03}{L\,(\text{in m})} \qquad \text{(at 100 GeV)} \qquad (8)$$

If the bunch length L > 2m as required in section IV, the corresponding tune spread should be attainable. Eventually a slow damper similar to the

one presently used in the Main Ring can be used to damp dipole bunch-to-bunch modes. Higher modes m require less spread than (8).

VII. Conclusion

The overall conclusions are, for the high-intensity proton bunches in the Fermilab scheme

1. If the longitudinal emittance is larger than 0.35 eV-sec per bunch, there will be no trouble in adiabatic debunching in the Main Ring at 100 GeV.

2. The head-tail instability can be controlled in the usual manner by adjusting the chromaticity and using the feedback damper.

3. Harmful spurious resonances in the rf cavities must be shorted to impedances below, say, 30 kΩ. Then, as long as the beam bunches are longer than approximately 2 m, there will be no trouble with either longitudinal or transverse bunch-to-bunch instabilities. Eventually a Landau cavity can be used to shorten the bunches.

4. A bunch spreader is required for the Energy Doubler to adjust the final bunch area to the threshold of instability.

References

1. C. Rubbia, contribution to this conference.
2. F. J. Sacherer, CERN/Si-BR/72-5 (1972).
3. A. G. Ruggiero, Proceedings of the 1975 ISABELLE Summer Study, Vol. II, p. 539.
4. F. J. Sacherer, IEEE Transactions on Nuclear Science, NS-20, No. 3, p. 825, June 1973.
5. E. D. Courant, A. M. Sessler, Rev. Sci. Instr. 37, 1579 (1966).
6. M. J. Lee, F. E. Mills and B. L. Morton, SLAC-76, Aug. 1967.
7. F. J. Sacherer, Proc. IXth Intern. Conf. on High-Energy Accelerators, Stanford 1974, p. 347.
8. A. G. Ruggiero, Proceedings of the 1975 ISABELLE Summer Study, Vol. II, p. 545.

$\bar{P}$ PRODUCTION CHARACTERISTICS AND COLLECTION SYSTEMS

David Cline
Fermi National Accelerator Laboratory, Batavia, Illinois 60510
and
University of Wisconsin, Madison, Wisconsin 53706

I would like to report on the work of the target group.[1] Most of these ideas are old, but it is interesting to review them.

First I should say that the amount of data that exists on antiproton production is still too small. We really need to measure this. It has not been very fashionable for experimenters at Fermilab or the SPS to make measurements of low-energy antiproton production with high-energy beams. It has simply not been interesting, but I think it is now. I think it is extremely important. Nevertheless, I think we have a good phenomenological feeling for the relevant parameters in the production. The invariant cross section, as far as one can tell, probably peaks at $x = 0$, which means that there is probably a very broad maximum in the cross section for producing antiprotons of momentum such that $x = 0$ for a given laboratory energy.

The second thing is that there seem to be two nuclear effects that one can observe: (1) There is very little evidence for absorption of the antiprotons inside the nucleus itself.[2] This is not an understood physical phenomenon, but it doesn't seem to hurt in going from low-Z materials, low-A materials, to high-A materials. (2) On the other hand, there is evidence that if you are near threshold for production of antiprotons (you can find this from the work at CERN, Deckers et al.) that the cross section may be a factor of two larger per nucleon and heavy nuclei. So there is a gain by going to heavy nuclei, aside from just making targets that are shorter. Again, this should be measured.

The Production Cross Section Variation with Energy

For example, the existing data that are relevant to Fermilab for the Fermilab scheme using GeV/c antiprotons follows the production curve in Fig. 1. It seems to have a broad maximum as far as one can tell and continues flat up to very high energies. If these data are compared with the predictions of the Stanford-Wang formula, the results are plotted in Fig. 2. The group tried to understand to what extent these phenomenological models give the same general features. The cross sections probably follow a rule of thumb something like this. As a function of laboratory energy, the cross section for 3 GeV/c, which is roughly the momentum to be used at CERN, has a sharp threshold. This is the point of $x = 0$ where the cross section has roughly reached its maximum or the knee in the curve and probably goes up slowly after that. The results at 6 GeV/c follow Fig. 1 and probably higher momenta like 20 GeV/c will reach a larger asymptotic value than 6. A. Kernan has parameterized the $x = 0$ data as shown in Fig. 3.

As can be seen, a very high energy machine would continue to gain in cross section given the same acceptance of the collector. However, the gain is relatively smaller the larger the energy, as seen from Fig. 3. One might have naively thought that if you go to very high energy, you get many more lower energy particles, but that appears not to be true. The factor between 6 GeV/c and 3 GeV/c is between 5 and 10. Thus the Fermilab scheme antiproton production cross section and the CERN scheme anti-proton production cross sections are quite different. The acceptance of the CERN collector must be larger if the same number of $\bar{p}$ are to be collected/hour.

The Production Cross-Section Variation with Transverse Momenta

Another characteristic of the production is the $p_\perp$ distribution, which as everybody knows, has a falloff something like $e^{-6p_\perp}$. Let me show you two examples of that. At 6 GeV/c $\bar{p}$ momentum, the angular distribution is plotted in Fig. 4.[4] There is a cutoff near 300 MeV/c. There will be little gain by building devices that collect all the way up to high $p_\perp$ because the yield of antiprotons is decreasing. The point is that you do not gain in trying to collect $p_\perp$ of 1 GeV/c because there is not much yield beyond that, as far as we can tell. Figure 5 shows the differential cross section for 9 GeV/c produced by 200 GeV/c incident protons.[4] It is expected that the characteristic will be the same in the two cases.

From these distributions, we can get an idea of the ideal $\bar{p}$ yields that can be obtained from these $\bar{p}$ collector systems. We work backwards and compare the ideal yield and compare what has been calculated through a realistic focusing system and targetry and find out how close we have come to the ideal. We can write

$$\frac{N_{\bar{p}}}{N_p} = \frac{1}{\sigma_a} E \frac{d^3\sigma}{dp^3} \frac{dp_\parallel}{E} \pi dp_\perp^2,$$

where σ_a is the absorption cross section, $dp/E = \delta p/p$ the momentum bite and $dp_\perp^2$ the transverse momentum bite.

For an ideal transverse momentum collection, $\pi dp_\perp^2 \approx \pi(0.3)^2$ which gives

$$N_{\bar{p}}/N_{p_{ideal}} = \frac{\pi(0.09)}{\sigma_a} \frac{Ed^3\sigma}{dp^3} \frac{\delta p}{p}.$$

We can estimate the ideal yields as[5]

$$N_{\bar{p}}/N_p = 1.1 \times 10^{-5} \text{ CERN}$$
$$(\approx 2.2 \text{ with Fermi momentum effects})$$
$$= 2.8 \times 10^{-5} \text{ Fermilab}$$
$$= 1.5 \times 10^{-2} \text{ and } \delta p/p_{\text{Fermilab}}$$
$$= 0.3 \times 10^{-2}.$$

The $N_{\bar{p}}/N_p$ values for CERN and Fermilab are within a factor of two. Even though we started with a factor of 5-10 in cross sections, the larger momentum acceptance of the CERN machine has made up for that.

We caution, however, that these estimates are still for hydrogen. If the Fermi momentum effect is included, going to a heavier target at CERN will get another factor of 2.[5] But there is not much to be gained beyond that. The ideal collection yield of those two schemes will be roughly the same. The momentum acceptance offsets the change in cross section. At CERN it is necessary to take a larger momentum bite because the cross section is smaller.[5]

We can estimate the ideal yield of $\bar{p}$/sec at the two machines assuming

$$\langle N_p \rangle = 10^{13}/\text{sec} \quad \text{Fermilab}$$

$$\langle N_p \rangle \quad \text{CERN}$$

$$\langle N_{\bar{p}} \rangle_{\text{Ideal}} = 2.8\times10^{8}\ \bar{p}/\text{sec} = 1.0\times10^{12}/\text{hour} \quad \text{Fermilab}$$

$$\langle N_{\bar{p}} \rangle_{\text{Ideal}} = 7\times10^{7}\ \bar{p}/\text{sec} = 2.5\times10^{12}/\text{hour} \quad \text{CERN}$$

If these ideal yields could be reached, the number of $\bar{p}$ collected would be 10^{12} $\bar{p}$/hour (Fermilab) and 2.5×10^{11} $\bar{p}$/hour (CERN). Obviously such intense sources would lead to the possibility of high-luminosity $\bar{p}p$ storage rings.

The point of the discussion is that the ideal yields are large. Now when you go through the document of the CERN scheme or go through the numbers we come up with at Fermilab you find the actual calculated yields into our devices are considerably lower than this.[5-8]

Compare these ideal yields with the expected values of "realistic" targets and collection system at Fermilab and CERN.

$$\langle N_{\bar{p}} \rangle_{\text{Real}} = 1.2\times10^{10}/\text{hour} \quad \text{Fermilab}$$

$$\langle N_{\bar{p}} \rangle_{\text{Real}} = 3.6\times10^{10}/\text{hour} \quad \text{CERN}$$

In the first case, the ideal yield is 83 times larger and in the second case the ideal yield is 7 times larger. An interesting question is "where is the missing factor?" Part of it is almost certainly the transverse momentum acceptance of the Fermilab Booster, but a large factor seems to come from the effects of finite-size targets.

Target Efficiency and Depth of Focus of the Beam Transport

Consider a point target and, in a simple-minded way, assume that the average angular production angle of the antiproton is 30 milliradians, and the spot size is 0.1 mm. Then the emittance of the "beam" should be $3\pi\times10^{-6}$ mrad. In principle, the design acceptance of the Booster at Fermilab for 200-MeV protons is 4π versus $2\pi\times10^{-6}$.[7,8] In principle, the system would thus collect almost all the antiprotons that are available into the Booster, if you can make the spot size small enough. The problem is doing this in practice, practice.

We find empirically that $N_{\bar{p}}/N_p$ for the Fermilab system, which is the one I know best, is 2×10^{-7} compared to the theory which gives 2×10^{-5} so there is a factor of 83 between what is possible and what we expect to realize.[6,8] Some of that factor of 83 is due to the acceptance of the real Booster. We should put in the real Booster size, which is 2.65π by $1.3\pi\times10^{-6}$. There is a factor of 3 to 5 just in Booster acceptance, but there is still a factor of 20 to 30 left, which we could have gotten in principle with a point target, but which we do not get in practice. That it is sort of illustrated by calculations that George Chadwick has been doing for a tungsten target, focusing down the spot to 0.2 by 0.1 mm (Fig. 6).[6] As a function of target length, the yield into the Booster is shown in Fig. 6.[6] The target-length effect is an enormous effect. As a function of target length, there is little gain after 4 or 5 cm. (Four or five cm is 1/3 of an absorption length.) So the yield does not even peak out at one absorption length; it peaks out at 1/3 of an absorption length. We are really not using the protons wisely, let alone collecting all the antiprotons. So it seems that there is some gain to be made if we can find a way of reducing the effects of long targets. The group discussed the possibility of a better depth-of-focus system and we were very fortunate that Roy Blumberg was here, because he has been thinking about such systems for some time.[9]

It is a simple idea, at any given point, such as point B in the target, the emittance may look like the presentation in Fig. 7. But at point A at the end of the target, the emittance will be larger. So when all the points in the target are added, the phase space looks like that shown in Fig. 7. We want to match into a phase space that looks like a circle, but the finite length target blows up the emittance. One idea (I think it is probably the only credible one that I've heard so far) that might help increase the depth of focus is to use a pulsed wire.[9] This concept is just beginning. We haven't done nearly enough work on this, but it is at least very promising. The idea is to use a wire of length L and radius b with a current I through it. The field in the wire then increases like r, up to the surface, falls off like 1/r outside the surface. With a wire of 1 mm radius and 30,000 A the magnetic-field B at the surface is about 4T. Inside the wire, the focusing is like that of an ideal lens whose focal length varies with radius. We do not yet know how much of the focusing is done inside and outside the wire in the actual Monte Carlo calculations. But outside the wire, or at the surface, in order to trap particles of 300 MeV/c then BL should be about 1.6 T-m, for 300 MeV/c, a B of 4 T would give you 25 cm, so you would trap the antiprotons at a wavelength of 25 cm. In fact, a more careful calculation gives particles starting out with angles θ_0 being bent straight by θ, and going straight, as given by the formula in Fig. 8.

Blumberg has done calculations (and I emphasize this is preliminary) for a target length of 35 cm and a radius of 1 mm or 0.3 mm. The angular distribution and yield versus current for the calculations are shown in Figs. 9 and 10. There is a peak in the yield as

shown in Fig. 10.[9,10] The Sanford-Wang formula was used in this estimate; it is probably not entirely correct, but probably not so far off either. With no current in the wire, the yield is shown in Fig. 9. With current in the wire and viewed at the end of the wire, the particles are pushed down in angular distribution, so that the number within 20 mrad is considerably larger than it was for the zero-current case. Of course, the size of the beam is somewhat larger and we do not yet know how large it is. As a function of current, the yield peaks at 30 kA; it continues to increase, then it falls off and never increases again. This is roughly a quarter of a wavelength for the system. The particles have crossed over again at larger currents. In fact, some of them are always crossing over, because they start at different parts of the target, and therefore apparently the yield does not increase again because the particles have gone back through the wire and are being absorbed. Note that it is not necessary to go to extremely high currents to get a large effect. It is actually very simple to see how this works. In the limit that the phase space is blown up by a finite target length, but all the particles are trapped, the phase space is rotated as illustrated in Fig. 7. The magnetic field simply rotates the phase space and in principle could keep it as small as a point-like phase space.

What increases in yield might be expected over the present target systems?[7] Consider the Fermilab case, where target heating is not likely to be important. If a two absorption length target can be used, compared to one-quarter length that is used at present, an increased yield by some factor, perhaps 3 to 4, would result, so the better depth of focus immediately allows the use of a longer wire. The yield increases up to the optimal absorption length, which is perhaps two. There is probably an increased brightness or increased yield in the angular region accepted by the Booster. That could perhaps give a factor of four, but we do not know that factor yet and additional calculations are essential. There is also the possibility, according to the calculations of Blumberg, that longer wires will result in the collection of antiprotons from secondary interactions. It isn't clear how much this would give, but Blumberg believes it may give you as much as a factor of 1.5 to 2. It is probably again something that will have to be measured. If we are allowed to multiply all these factors (which we are probably not) a factor of 18 increase would result.

What is the future of the target studies? First, we need more calculations; I think we should also make a wire to test, but I think the conclusion is that better targets and focusing systems might give a factor of yield of 4 to 20, and that is certainly worth pursuing. This could lead to increased luminosity of a factor of ten in $\bar{p}p$ storage rings.

References

[1] The people working in the group were D. Berley, R. Blumberg, D. Cline, A. Kernan, T. Kycia, and D. D. Reeder.
[2] L. Pondrom, private communication.
[3] D. Deckers et al., Phys. Rev. 137, B962 (1963).
[4] T. Rhoades, private communication; A. Kernan, private communication.
[5] Design Study of a Proton-Antiproton Colliding Beam Facility CERN/PS/AA 78-3.
[6] G. Chadwick, Considerations on the Antiproton Production Beam, private communication.
[7] Booster Synchrotron, Fermi National Accelerator Laboratory Internal Report TM-405, Edited by E. L. Hubbard, 1973.
[8] D. Cline et al., Collecting Antiprotons in the Fermilab Booster and Very High Energy Proton-Antiproton Interactions, Fermi National Accelerator Laboratory Internal Report TM-689, 1976.
[9] L. N. Blumberg and A. E. Webster, IEEE Trans. Nucl. Sci. NS-24, 1539 (1977).
[10] R. Blumberg, private communication.

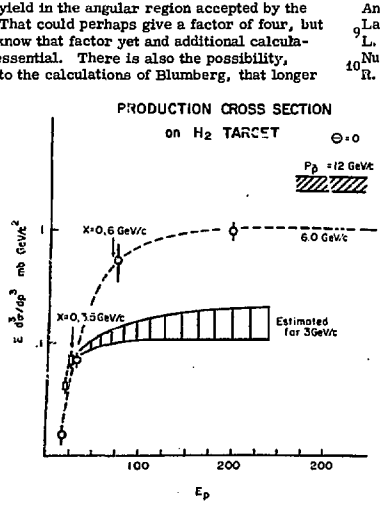

Figure 1

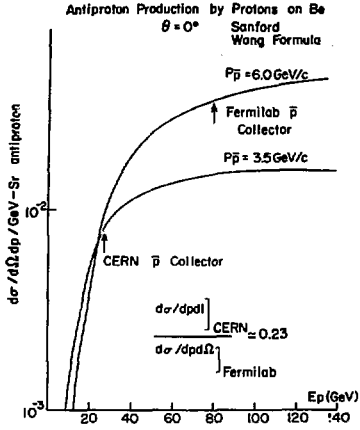

Figure 2

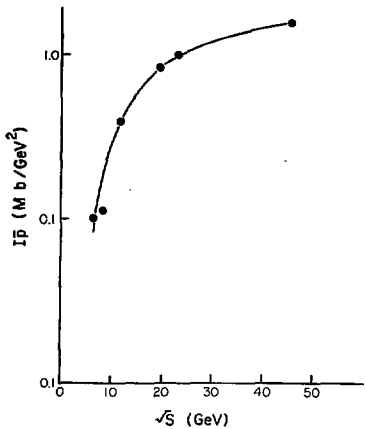

Figure 3

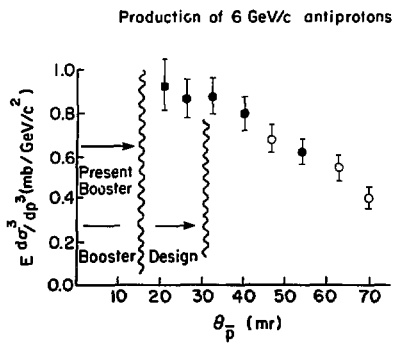

Figure 4

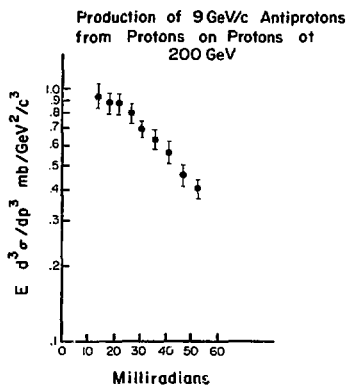

Figure 5

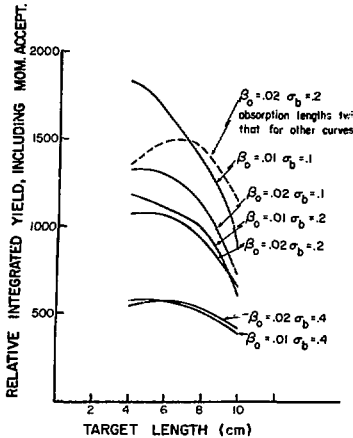

Figure 6

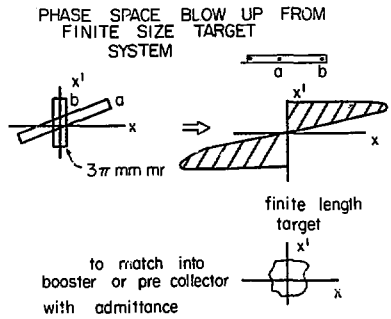

Figure 7

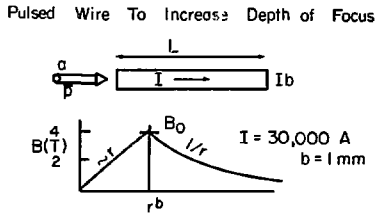

Figure 8

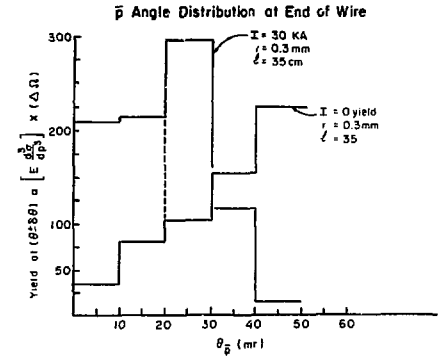

Figure 9

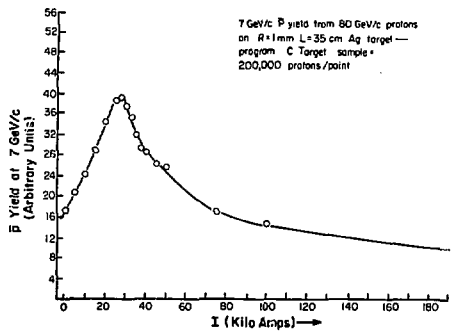

Figure 10

DETECTORS; RELATION OF DETECTORS TO PROTON-ANTIPROTON MACHINES

S. Fung, Lawrence W. Jones, L. Pondrom,
G. Salvini and A. Tollestrup

Reported by G. Salvini
CERN

We started our discussions on detectors for Proton-Antiproton interactions at high energy with some general considerations, but we soon turned to more practical aspects.

I. Philosophical Considerations and General Aspects.

We assume the following working hypothesis:

- There has been until now and there will be in future a continuity of heavier masses and higher energy levels at any c. m. energy we shall reach, at least in this century.
- Energy resolution of the apparatus will always be an important and a limiting factor at all energies ($\Delta M/M$; $\Delta E/E$; $\Delta P/P$ etc.); present-day resolutions are far from being satisfactory.
- High luminosity (L) will always be important; adequate detectors for high L have still to be invented.
- The quality of the machines is today perhaps better than that of the detectors for them. The ratio (cost of detector)/(cost of machine) should increase, in order to get detectors adequate to the progress of the accelerators.
- Proton-Proton and Proton - Antiproton interactions will be very different on the important points at all energies. The comparison between the two will always be essential to our understanding.

The following question has been considered in our working group: is it conceivable to build a Super Detector, looking at all 4π solid angle, capable of recognizing all particles, and "socially relevant" in the sense that it can supply many groups of physicists with pictures, as the bubble chambers did in the past? Or we must rather admit that in this case that the dream of a 4π universal detector is impossible, and specialized different detectors in a variety of configurations will be *more important? We went back to this point after a* concrete discussion on existing projects.

II. Relation of Detectors to Proton - Antiproton Machines.

It is important to discuss and plan colliders and detectors in strict collaboration. Among the reasons for this, we recall:

- The Luminosity per bunch is today limited by the detector capacity to support the huge number of hadronic interactions. At CERN, with 6 $p\text{-}\bar{p}$ bunches and a total luminosity $L = 10^{30}\ cm^{-2}\ s^{-1}$, we can have *d*ble interactions in the same crossing in approximately 20 per cent of the cases. This is very close to a maximum acceptable limit, when one wishes to measure all particles and energies (total calorimetry). Total calorimetry will be of great importance, for instance, for the evaluation of the charged masses decaying with the emission of one neutrino.
- The time interval between the $p\text{-}\bar{p}$ bunches is also relevant. If it is less than one microsecond, it can seriously trouble observation by drift-chamber techniques (for instance in an experiment like proposal P92[1]).
- The measurement of the total energy in a detailed balance (total calorimetry) may require either long straight sections (for instance $\geq 2 \times 50$ meters at 1000 + 1000 GeV) or "calorimetrization" of low-beta quadrupoles by inserting layers of scintillators between the iron plates. The shape of the donut and the level of the vacuum inside will obviously be important. We must keep in mind that $p\text{-}\bar{p}$ interactions approximately 40% *of the energy will flow through angles of* $\lesssim$ *10 milli*radians. In fact, typical values of the angle of emission of the particles in the forward jets will be:

$\theta_i \sim (0.3\ GeV/p_i(GeV))$ (Average angle of emission of a particle in the forward jet);

$\theta_0 \sim M_{\pi^0} / E_{\pi^0}$ (minimum angle of emission of the photons in π^0 decay);

$\theta_{Bi} = \ell / R = 0.3\ \ell\ B/p_i$ (angle of emission of a charged particle of momentum p_i when leaving magnetic field of the apparatus, if it is a dipole). In the case of P92[1] it is $\sim 0.6/p_i$.

Typical resulting angles for the most energetic particles in the forward cones are of order 5 milliradians. For a donut diameter of 10 cm, this corresponds to a straight section length of 10 m or more.

Note that the idea of pursuing the forward particles along and between low-beta quadrupoles is justified when considering the value of the angles θ_p, $\theta_{\bar{p}}$ of protons and antiprotons in the beam:

$$\theta_p \sim \frac{0.15}{\sqrt{\beta}}\ ;\ \beta = 0.5\ m;\ \theta_p \sim 0.2\ \text{milliradian}.$$

Our conclusions have been summarized in the sketch of Fig. 1.

III. Some Specific Apparatuses for Proton - Anitproton Experiments.

The CERN P92 proposal,[1] already described in this workshop, is (see Figs. 2 and 3) an example of a 4π detector to measure momentum, energy and ionization of each produced particle. Complete calorimetry and analysis at very small angles are planned, by extending the central apparatus with smaller calorimeters and wire chambers.

Another experiment [2] has been proposed at CERN for the SPS $p\bar{p}$ facility. The main purpose is to study production and decay of the $W^{\pm}$ and Z^0 bosons. It must be remarked that a small azimuthal wedge in the central region is instrumented to cover other aspects of $p\bar{p}$ collisions, like free-quark production and structure of large transverse-momentum jets.

A number of detectors being proposed at Fermi Lab have been discussed in our working group. The program at Fermi Lab is to reach an optimum design for a modest-cost detector suitable for studies of either $p\bar{p}$ or pp collisions up to 2 TeV in the center of mass, at luminosities in the range $10^{28} - 10^{31} cm^{-2} s^{-1}$. The time schedule for assembling the detector is about three years, so that it will be available for physics in 1980-81. This roughly parallels the scenario for construction of the Energy Doubler. The search for the $W^{\pm}$ and Z^0 intermediate bosons, although by no means the only experiment of interest, has served as a test case for the evaluation of the performance of the detector.

The study made by the Hitlin group at the 1977 Fermilab Summer Study serves as one of the points of departure. Of course the design at CERN and PETRA are also very useful. Four proposals are being pursued in competition, and one of them or one combination among them, will be selected for the task. These proposals are as follows:

a. A calorimetric detector (see Fig. 4a) without a magnetic field, emphasizing hadronic-energy measurements in a heavy-concrete and scintillator segmented calorimeter, and electron gamma-ray energy measurements in lead-scintillator shower counters. Lithium-foil transition-radiation detectors will be used for additional π-e discrimination. Total weight is about 1200 tons, with very good solid-angle coverage.

b. A toroidal magnetic detector. It will have a 1.5-m diameter field-free region around the pipe, followed by a superconducting toroid 5m long, with inner radius 0.75 and outer radius 1.5 m. The inner field is 1.8 T. The opaque space, because of the shadows of the coils and support will be about 10% in azimuth. Calorimeters will be outside the magnet. Total weight with end caps is about 2500 tons (see Fig. 4b).

c. A small solenoidal detector with a magnetic field of 1 T over a 1 m radius, 5 m long. Field uniformity will be insured by iron pole tips. The iron return can be used as hadron calorimeter.

d. A large solenoidal detector with a magnetic field of 2 T, and a radius of 2 m and total length of at least 5 m. The iron return will be again used as part of the large hadron calorimeter. This large device can be rotated around a vertical axis to allow its use as a dipole for small-angle physics. Its weight will be about 4000 tons. (Fig. 5)

The main claim in favor of option a. is cost and simpler analysis. In favor of option b. is the large field-free region surrounding the beam pipe. Options c. and d. are similar, apart from scale and resolution, and hence cost. Decreasing the product BL^2, where L is a typical chord of the charged-particle arc, decreases the momentum p_0 at which the resolution reaches its largest (worst) value, and where the resolution from the magnet trajectory equals that from the calorimetry. (See Fig. 6.)

IV. Use of a Magnetic Field in the Detectors.

We think that a low magnetic field may be much better than having no field at all, because of the physics advantage of recognizing the sign of the particle up to 50-100 GeV, to measure charge asymmetries, which can be clear and strong in $p\bar{p}$ collisions, [1] when for instance charged $W^{\pm}$ bosons are produced.

Some of us gave a brief look at a magnetized-iron calorimeter, and suggest that a system capable of determining muon momenta to 20% is possible, together with tracking and otherwise good calorimetric energy determination of hadrons, photons and electrons. That concept is illustrated in Fig. 7. It is a simple rectangular box of 1 in. iron plates spaced at 0.5 in. intervals, with a minimum path length in the iron of 1 m. The region around the interaction point would contain tracking chambers and lead scintillator shower detectors. Both the box and the end caps will be magnetized by 10^4 ampere-turns wound at the corners of the box to B=2 T. Large external drift chambers will observe the deflection of muon candidates.

V. Resolution in Energy and Masses.

As we said, we assume that a better resolution will always be extremely useful, independently of today's theoretical speculations. It is important to recall that beyond 200 GeV c.m., only the proton-proton and proton-antiproton colliders will remain to give us the farthest information of our universe of energy and momentum. The miracle of 1 - MeV resolution obtained at SPEAR, Frascati, Doris with the J-ψ particle will not be possible again, for it was due to the precision in energy of the $e^+ e^-$ beams at 2 GeV. Up to 200 GeV c.m. the future $e^+ e^-$ rings will allow a total resolution (for neutral vector bosons) of 200 MeV, due to the precision of the $e^- e^-$ beams. Beyond that energy, we shall depend on detection of the produced particles. The best resolution today with 4π detectors is $\Delta M/M \, (\Delta E/E) = 1$ GeV for completely identifiable particles. A sketch of the situation is given in Table I.

We express the opinion, perhaps rather obvious, that the best efforts of the physicists must be devoted in the coming years toward the goal of reaching a resolution of approximately 0.2 GeV with a detector even at the highest energies and masses of the produced particles.

VI. Back to the Universal 4π Detector

a. Some of us firmly believe that one, full 4π detector (that is, an instrument which allows in each interaction the measurement of the energy or momentum of each particle, the charge, identification of the neutral particles, the ionization of each particle) will be necessary, although expensive. An instrument like this

means a large effort in cost and some hope of having many physicists divided into different groups to explore millions of detailed interactions, as in bubble chambers. There are of course, advantages over bubble chambers of trigger, statistics, precision in momenta and ionization.

These beautiful hopes still need some "caveat". In fact we must temper consideration of this large ambitious detector with the recollection that similar projects in the past have on occasion proven more difficult than anticipated. Moreover, we must admit that there are specific requests which cannot be easily extended to the full solid angle, like polarization, structure of jets, refined masses of stable and unstable particles. All this demands some kind of arm spectrometer. But before developing this point, we make a comment connected to the hopes which arose in the work shop, regarding the future luminosities of a $p-\bar{p}$ ring.

A large increase of the luminosity, for instance to the level $L = 10^{31 - 32}$ cm^{-2}s^{-1} as indicated by Carlo Rubbia in his talk of March 29, could mean that even at 90° and p_t values of $\geq$ 30 GeV, we can get

$$10^{-(33-34)} \times 10^{(31-32)} \times 10^{5} = 10^{(2-4)} \text{events/day,}$$

particles or jets, entering a small-angle well-prepared detector.

We could in this way in a reasonable time have at our disposal some 10^5 particles coming from the deep core (if there is one) of the proton-antiproton interactions. If we stick to the hypothesis made in point 1 above, that in the most important aspects pp and $p\bar{p}$ interactions shall be very different, then the high luminosity of $p\bar{p}$ colliders will be very welcome, even necessary, independent of any record luminosity of pp.

b. In this optimistic view of a high luminosity, a spectrometer external to a 4π detector can study secondaries with much more sophisticated particle identification than possible with a 4π detector. Questions which such a detector could study would include:

- search for massive, stable particles; search for quarks;

- a quantitative study of K, π, p, $\bar{p}$, n differential production spectra;

- unambiguous identification of muons through momentum and velocity as well as range.

This dector should incorporate:

- Magnetic deflection
- Cerenkov counter
- Good dE/dx measurements
- A good calorimeter
- Time of flight
- Perhaps transition-radiation analysis

The experiments at CERN already reported have proposed an azimuthal wedge [2] or central opposite windows [1] in order to make a refined analysis of the particles emitted. Another CERN proposal [3] is particularly studying the instrumentation of the 90° holes in the P92 proposal [1], in order to separate the particles of a jet and to observe individual quarks, even if associated with high multiplicity.

An example of a fine small-angle detector is given in the Aspen 1977 Summer study [4]. Their spectrometer is 7 m overall in length, and would for instance extend 7 + 3 = 10 m from the interaction point if attached to large-angle CERN experiments.

VII. An Optimistic Touch.

Before closing, let us give a glance toward the future, with the optimism inspired from the discussions and findings of these last three days. Let us assume that future detectors will succeed, that it will become possible with a luminosity $L = 10^{32}$ cm^{-2}s^{-1} to separate and recognize an interesting object (like the heavy boson) in a jungle of hadrons and photons, which are more abundant by a factor 10^{10} or more. Let us assume also that in the 1980's we shall be able to get masses in the 100 - 1000 GeV/c^2 range with resolutions $\Delta M \leq 0.2$ GeV/c^2, and that new masses and objects will come out (our working hypothesis in section 1).

Then, after a few years of operation with the Fermi Energy Doubler or Isabelle, perhaps in 1990, the physicists could have at disposal a series of masses, as given f. i. in Fig. 8. Particles like Z^0 and $W^{\pm}$ and Higgs particles will have been studied in detail by the powerful $e^+ e^-$ colliders. But we insist again that beyond the limit of 200 GeV in the center of mass the pp and $p\bar{p}$ will be the only colliders capable of detecting a possible new spectroscopy of very high masses, as far from us today and perhaps as intriguing as Quasars are for the astronomers. Notice in Fig. 8 that the yields per day become comparable with what expected for neutral bodies from $e^+ e^-$ rings.

These perspectives bring us again to the main point of this summary: the pp and $p\bar{p}$ machines will soon be alone in exploring new domains, and an improvement in resolution and scope of the particle detectors around them will be of fundamental importance.

References

1. A 4π solid angle detector for the SPS used as a Proton Antiproton collider. CERN / SPSC/78-06 (SPSC/P92) Jan. 30/78.
2. Proposal to study Antiproton Proton interactions at 540 GeV c. m. CERN/SPSC/78-08 (SPSC/P93) Jan. 31/78.
3. Search for Quarks at the Proton Antiproton collider CERN/SPSC/78-16 (SPSC/P97.) Feb. 6/78.
4. Fermilab 1977 Summer Study; page 179 and Foll. Volume 2.

Table I. Resolution ΔM In The Measurement Of Masses and Widths.

Particle	$\Delta M_{e^+e^-}$ Resolution in Mass From e^+e^- Colliders	ΔM_{H} Resolution From $p\bar{p}$ Colliders	$\Delta M_H / \Delta M_e$
$J\psi$	1 MeV	30 MeV	~ 30
$W^{\pm}$	60 MeV	~ 1000 MeV	~ 15
W^{o}	150 MeV	~ 1000 MeV	~ 6
M (>200)	No e^+e^- collider available	1 - 2 GeV ?	

Notice that for possible masses $M \geq 200$ GeV / c^2 the pp and $p\bar{p}$ colliders will be the only machines available. It will be of paramount importance to get $\Delta M \sim$ 200 MeV in future detectors.

REQUESTS

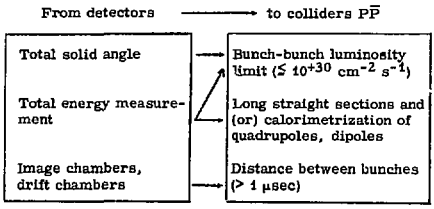

Fig. 1. The requests of the detectors to the parameters of the $P\bar{P}$ collider, in case a very large or total solid angle is requested.

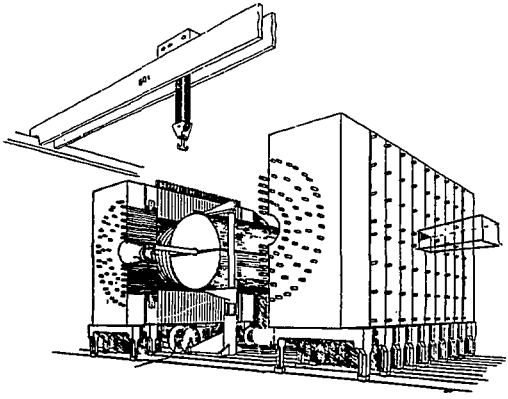

Fig. 2. The 4π detector proposed at CERN (Ref. 1); artist's view.

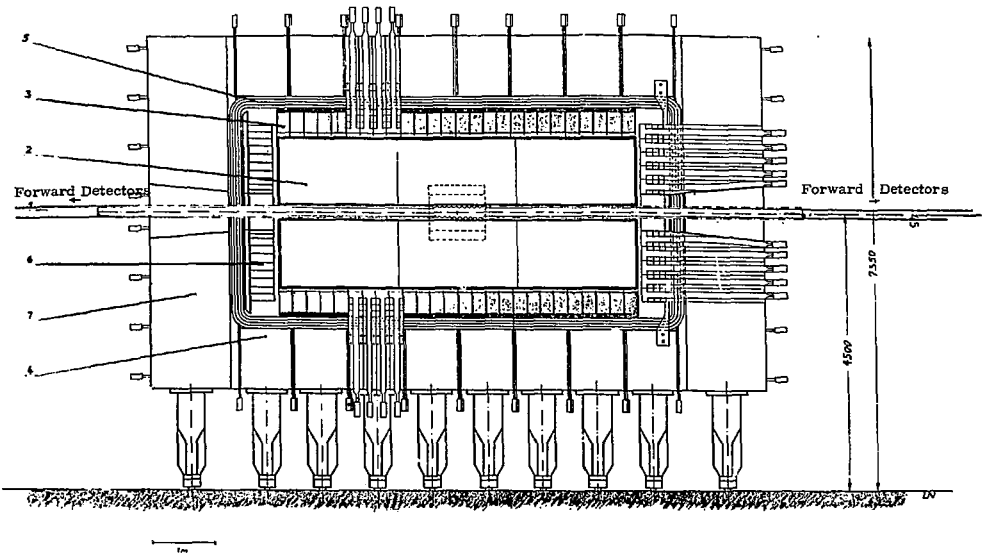

Fig. 3. The proposed 4π detector at CERN, side view. Legend: 1) vacuum chamber; 2) vertex chambers; 3) electromagnetic (e. m.) detectors; 4) hadron calorimeters and return yoke; 5) Al coil; 6) forward e. m. detectors; 7) end caps.

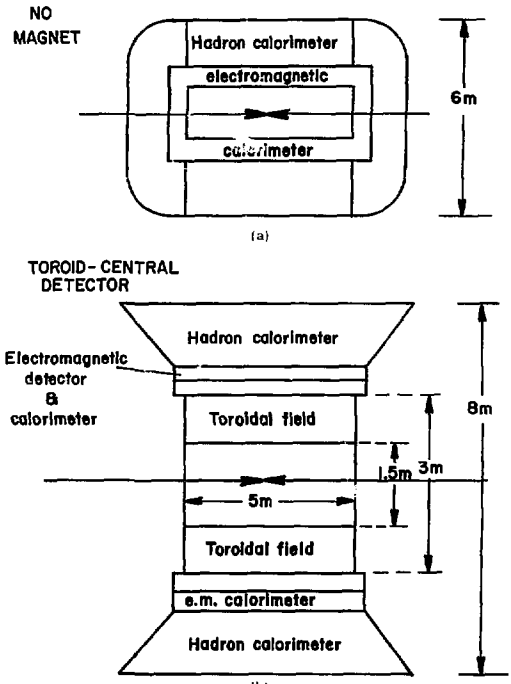

Fig. 4(a). A calorimetric solution, without magnetic field (Fermilab). (b) A solution with magnetic field produced by toroidal coils (Fermilab).

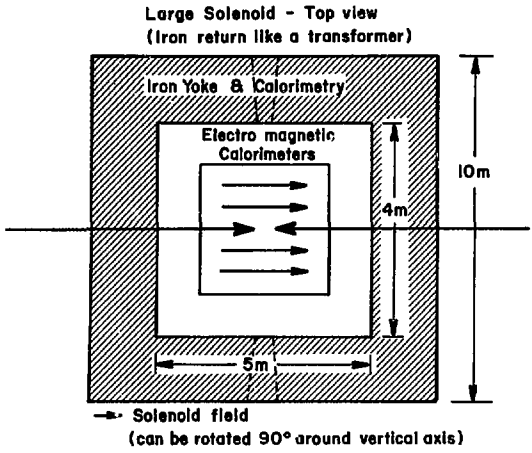

Fig. 5. The proposal at Fermilab with an high field solenoid.

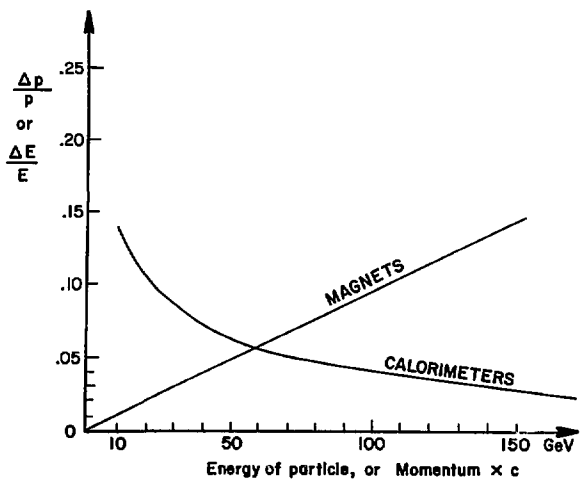

Fig. 6. The energy resolution with calorimeters compared with the resolution obtained with a magnet. Most expensive solutions will have the crossing point at higher energies. In the case of Ref. 1, the crossing is around 50 GeV.

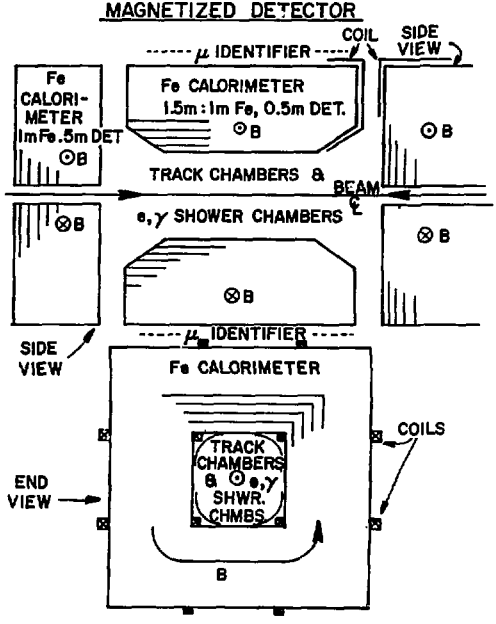

Fig. 7. Calorimetrization and magnetization of the iron, in order to measure the momentum of nonhadronic charged particles (like the muons) emitted in $\overline{P}P$ interactions.

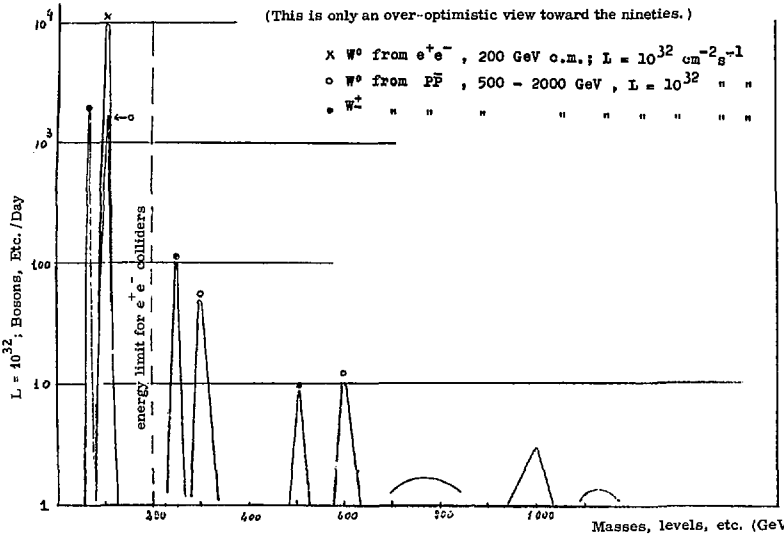

Fig. 8. An over-optimistic view of possible masses discovered in the eighties by e^+-e^- colliders, CERN SPS, Energy Doubler, Isabelle.

CONTRIBUTED PAPERS

ARE WE BEATING LIOUVILLE'S THEOREM?

A. G. Ruggiero
Fermi National Accelerator Laboratory

I. Introduction

During the last two years or so, because of the renewed interest in various techniques of beam stacking, such as electron cooling, stochastic cooling, synchrotron radiation, charge exchange, etc., people have been heard to wonder how such techniques could work when Liouville's theorem states that the phase-space area of a beam is preserved. People have made statements like "Liouville's theorem has been beaten," "we went around Liouville," "Liouville's theorem does not apply here," "Liouville's theorem is valid only if you take all the universe into account," and so on. People have even been heard to comment that Liouville's theorem has been proven wrong. But the majority were simply mystified by what they see as a conflict between what Liouville's theorem implies and what is apparent from the beam handling of the various cooling and stacking techniques. Most of the confusion is caused, I believe, by the fact that people make Liouville say things he never meant!

About twenty years ago, the Liouville question was also raised in connection with studies of devices which could produce a damping mechanism for protons similar to the synchrotron radiation for electrons. At that time, effort was devoted to generalization of Liouville's theorem to include dispersive systems and systems of interacting particles.[1] We will not deal here with these relatively more recent findings, but will confine our analysis to the simple form of the Liouville theorem as it was originally formulated. The confusion mentioned above can be removed by simply inspecting how the theorem of Liouville works with the beams of charged particles that we usually accelerate or store.

II. Liouville's Theorem

Liouville published his work[2] in 1837. It is, of course, not easy to find the original paper, but Liouville's theorem is discussed in many books on statistical mechanics. The discussion in the Ehrenfest's book[3] is particularly concise and close to the original.

Let us see what the theorem says. To make things simpler, let us consider only one particle which has motion described by three pairs of canonical variables (q_i, p_i, $i = 1, 2, 3$) and by the Hamiltonian function $H(q_i, p_i, t)$,

$$\dot{q}_i = \frac{\partial H}{\partial p_i} \qquad \text{and} \qquad \dot{p}_i = -\frac{\partial H}{\partial q_i} \,. \qquad (1)$$

Consider also the six-dimensional phase space of coordinates q_i and p_i ($i = 1, 2, 3$). Assign to the particle some initial conditions, that is a point P of the phase space that it occupies at the initial time t_0. One can solve the equations of motion (1) with the assigned initial conditions and calculate the trajectory of the particle in the phase space. We assume this trajectory is closed and elliptically shaped, as shown in Fig. 1. We can repeat this operation indefinitely for every set of initial conditions, that is, for every point P taken as the starting point. By doing this, we have filled the phase space with an infinitely large number of trajectories which describe the motion of the same particle which assumes different initial conditions.

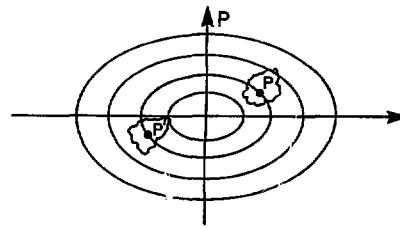

Fig. 1. The phase space

Consider now a region surrounding a particular point P. This region has volume V and includes an infinitely large quantity of points that we can regard as possible initial conditions of the particle at time t_0. For continuity reasons, all these points will occupy another region surrounding P' at a later time t. This second region can be calculated by solving the equations of motion (1) for each initial condition around P and marking the corresponding particle position at the time t. Obviously, because of the uniqueness of the solution of (1) there is a one-to-one correspondence between the points around P and those around P'. Liouville's theorem states that the volumes of the two regions are the same and equal to V. The proof of the theorem is relatively easy if one reminds oneself that the equations of motion in the Hamiltonian form (1) are equivalent to coordinate transformations with a Jacobian equal to unity. Thus Liouville's theorem can be stated also as follows: The streaming of the image points in the phase space as given by Eq. (1) generates a continuous point transformation, which transforms each six dimensional region into another one of the same volume. This is true at every time t at which we stop our process, and no matter what the initial volume V of the region surrounding P.

III. The μ-Space of a Physical System

Let us consider now a system of N particles like the beam of charged particles we usually deal with in accelerators or storage rings. The motion of each particle is again described by the equations (1). We assume the particles are not interacting with each other so that the Hamiltonian H will depend only on the coordinates of the particle under consideration. At the initial time t_0, the particles will occupy specific locations in a six-dimensional phase space similar to the one we described above and that we call μ-space. The previous space was used to represent the motion of the same particle with different initial conditions, whereas μ-space is used to show the trajectories of several different particles. By solving the equations of motion (1), we then have N trajectories in μ-space, one for each particle, as shown in Fig. 2. One can take a picture of μ-space at

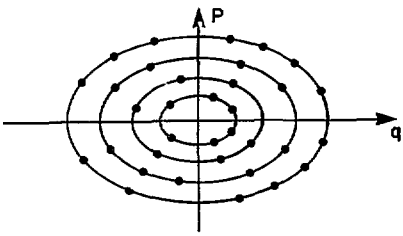

Fig. 2. The μ-space

a given time t and one sees N image points, each describing the location of one particle. Two particles cannot occupy the same location at the same time. There are at most N trajectories; several particles can share the same trajectory.

Even when N is very large but finite, μ-space is practically empty in contrast to the space of Sec. II which is continuously filled with all the possible trajectories of a single particle. It is therefore not obvious how useful the application of Liouville's theorem is to μ-space. One can in principle divide μ-space in six-dimensional cells, each large enough to contain a very large number of particles and yet small enough so that the coordinates do not change appreciably across their volume. With these requirements, one can then define reasonably well the particle *density in phase space, which is the number of particles* in a particular cell. This is a local average process and is very sensitive to fluctuations from cell to cell. The fluctuations are relevant to the statistical mechanics of a gas, but we will not deal here with them.

If the number of particles N becomes infinite, because they cannot occupy the same location at the same time and because they do not interact with each other, there is no difference noticeable between μ-space and the space we described in Sec. II. Each real particle is represented in the same way as a standard single particle with proper initial conditions. Thus with the above assumptions Liouville's theorem applies also to the μ-space of a real (continuous) system of particles. In particular, the cells could be made infinitesimally small and the density measured by a distribution function $\psi(q,p)$, which when multiplied by the volume element dqdp of the cell gives the number of particles. As defined, ψ is a continuous distribution. It is a consequence of Liouville's theorem that

$$\frac{d\psi}{dt} = 0,$$

which can also be written as

$$\frac{\partial\psi}{\partial t} + \sum_{i=1}^{3} \left(\dot{q}_i \frac{\partial\psi}{\partial q_i} + \dot{p}_i \frac{\partial\psi}{\partial p_i} \right) = 0, \qquad (2)$$

a special case of the Vlasov equation for non-interacting particles. It is quite legitimate to make use of Eq. (1) for $\dot{q}_i$ and $\dot{p}_i$ in the left-hand side of (2).

Thus for a system of $N = \infty$ non-interacting particles it is possible to define a density ψ in μ-space and apply Liouville's theorem. The streaming of the image points is governed by the Vlasov equation (2) and statistical-fluctuation considerations do not apply here.

IV. A Beam of a Finite Number of Particles

Suppose that the system is again made of an infinitely large number of particles but they are all confined initially in a finite volume V of the μ-space, so that outside this region $\psi = 0$. Liouville's theorem states that the volume V is preserved during the motion of the system. A real beam of charged particles is always made of a finite number N of particles, but it is quite common to make the approximation of a continuous distribution, which implies $N \to \infty$. With this approximation, it is possible to define a volume V of the phase space constantly occupied by the beam and which is often called the beam emittance. But a closer view of the distribution of the particles of a real beam as shown in Fig. 2 shows that since each particle occupies a zero-volume element of space and there is a finite number of particles, the actual volume occupied by the beam is zero. One can avoid this inconsistency by dividing the μ-space in cells as explained above, and consider only those cells that at a given time are occupied by particles. The sum of the volumes of all these cells can be defined as the beam emittance in the case that N is finite. Similarly, a density function ψ can also be introduced by taking the ratio of the number of particles in a given cell to the volume of the same cell. So defined ψ is a discontinuous function that can be approximated by a smooth one.

If the number of particles in a cell is sufficiently large and uniformly spread, their image points in the μ-space can be thought as representatives of typical possible replicas, at some time t, of the reference particle. All the particles that occupy a particular cell at an initial time t_0 are expected to occupy at a later time t another one with the same volume, apart from statistical fluctuations. Thus one would expect that Liouville's theorem applies also to the case of systems with a finite number N of particles. One would conclude this after having applied local

averages as we have described, and, again, apart from statistical fluctuation. These are basically the arguments that make people consider an actual beam of N particles as a Liouvillean system, and so define a distribution function ψ and apply the Vlasov equation (2) to it. Hence, one is encouraged to make the statement that the beam phase-space volume (or area) is preserved.

V. Example of Conservative Systems That Do Not Preserve Phase-Space Area

In the following, we want to give two examples which show that, despite the fact that the motion is conservative and described by a Hamiltonian function, the phase-space area of a beam of a finite number N of particles, defined with the average process described above, is not preserved.

First example. Consider the case of Fig. 3, which shows a debunched beam in the longitudinal phase space of variables φ, the phase angle in rf units, and $\Delta p/p$, the relative momentum deviation. Suddenly an rf cavity system is turned on to bunch the beam. The rf voltage creates a stationary bucket whose separatrix is shown in Fig. 3. The motion of the particles changes from a simple drift along the angle-axis to an oscillation around the center O of the bucket. The oscillation frequency is maximum for particles with small amplitude, that is in the neighborhood of O, and decreases moving toward the edge of the bucket; near the separatrix, the phase oscillation frequency becomes very small, practically zero. In Fig. 3, we show the shape of the beam after several phase oscillations. The filamentation is caused by the difference of oscillation frequencies. We have shown with continuous lines the boundary of the beam. The area which is stretched between them would be the area of the beam in the case it is made of an infinitely large number N of particles. This area is invariant, because of Liouville's theorem, and equal to the area of the original strip. In this case, which deals with the beam as a continuous medium, one can calculate the shape of the beam bunch by means of the Vlasov equation (2). As the motion proceeds, the number of fans of the filamentation increases. The beam looks like a long ribbon wrapped on itself in a spiral motion; the ribbon length gets longer and also more and more narrow to preserve the area. This characteristic should always be recognizable for a continuous beam no matter for how long one observes it.

If the beam is instead made of a finite number N of particles, at a particular time the average distance of the particles in one spiral equals the distance between two adjacent spirals. When this happens, as is shown in the last of Fig. 3, the bucket looks as if it is homogeneously filled with particles and any regular structure due to the initial beam ribbon has disappeared. Thus, for practical purposes, after some time (which depends on N) the beam occupies a new area that is larger and that equals the bucket area. One can reach this conclusion by applying the local average process to define the beam area, once at the beginning when the beam is still debunched and then later when the beam has been bunched.

Second example. If we reverse the process described above, we obtain even further increases of the beam phase-space area if the beam is made of a finite number N of particles. To this purpose, consider the pictures of Fig. 4. We start with some number of beam bunches filling up the corresponding accelerating rf buckets. Then suddenly the rf voltage is turned off and the motion of the particles is changed from circulatory around the center of the bucket to rectilinear along the angle-axis. Suppose that particles with larger momentum move faster than those at lower momentum; then the bunches will elongate leaving their center at rest. At a certain instant, the stretching causes overlapping of neighboring bunches and the beam is observed as debunched in the real space. Actually there is still "rf structure" of the beam in the longitudinal phase space after considerable stretching of the initial bunch ellipses. In fact, if the beam is made of an infinitely large number of particles, the "rf structure" will never disappear. In this case, one can apply the Vlasov equation (2) to calculate the beam shape and infer that the beam area is an invariant. The beam bunches, as shown in Fig. 4, get longer but narrower so that their area at any time equals the initial area they had before starting this debunching process.

On the other hand, if the beam is made of a finite number N of particles, at a certain time the rf structure vanishes. This occurs when the average distance between particles equals the distance between the bunch strips. The time required to reach this situation is called "decoherence time" and clearly depends on N. Thus after the decoherence time, the beam is fully debunched not only in time but also in the longitudinal phase space.[4] Application of the averaging process to determine the beam area shows that the final area is larger than the original one when the beam was still bounded.

With the two examples above, we have shown two cases where the beam phase-space area is not preserved. The reason is the finiteness of the number of particles in the system, which is in contradiction with the major requirement to fulfill for Liouville's theorem: the system must be equivalent to a continuous medium. For those systems where N is finite, it is not always possible to make use of the Vlasov equation (2).

VI. The Stacking and Cooling Techniques

At this point the reader should have a reasonably good idea of what a real physical beam of charged particles looks like and what the implications are of Liouville's theorem in this connection. The most important aspect that one should not forget is that the beam is made of a finite number of particles. The beam area is then defined only as a local average process. Indeed, in practice, beam sizes are measured with devices which count the number of particles in one interval or bin, the equivalent of the cell that we described above.

With this in mind, one should then be able to understand how it is possible to reduce the beam size with "cooling" techniques and yet have Liouville theorem's still apply.

If the beam is made of a finite number of

particles, there are large empty regions surrounding the image points of the μ-space (see Fig. 2). There is no reason and no limitation in principle why one cannot fill up these empty regions with more particles if one can find a way. The Liouville theorem would certainly not be contradicted. The question is how it is technically possible to add more particles without perturbing the motion of those that are already there. For instance, if a kicker magnet is used to bring more particles into an area of the phase space already occupied by some particles with the same charge, the same magnet would kick the latter particles out. But if the charge of the particles to be kicked in is opposite to that of the particles already in the storage, then one can manage to kick the entire beam including the fresh pulse by the same amount and in the same direction. This is the principle on which the negative-ion injection is based. One does not "go around" or "beat" Liouville's theorem here; it simply does not apply. If the original beam was made of an infinite large number of particles so that no empty regions in the phase space were available, there would be no way to stack more particles, even with the negative-ion injection method.

Similarly, there is no reason and no limitation in principle why one cannot take a particle at the edge of the beam and place it in an empty region in proximity to the beam center. When this is repeated several times and for all the particles, the beam area can be made as small as wanted, in principle zero. Stochastic cooling is based on this principle. But again if the beam is a continuous medium, that is $N \to \infty$, the reduction of the beam size would not be possible. Indeed it is well known that there is no cooling for $N \to \infty$, since no signal would be provided by the beam (no statistical fluctuations!).

The other two techniques, electron cooling and cooling by synchrotron radiation, are based on entirely different principles than negative-ion injection and stochastic cooling. In these cases, particles suffer energy variations that do not depend on the beam intensity and distribution, but on the properties of the medium they travel through. The motion of these particles then cannot be derived from a Hamiltonian and therefore Liouville's theorem does not apply. One can of course write equations of motion which can again be interpreted as a continuous point transformation in a proper phase space, but now the Jacobian of the transformation is not unity, and phase-space area is not preserved under this transformation. This is true for a continuous system whose distribution function must satisfy a different kind of continuity equation than (2), the Fokker-Planck equation.[5]

There is a difference between the effects of synchrotron radiation and the electron cooling. In the former case, all the particles experience a systematic energy loss which depends on their energy, whereas in the latter particles experience an energy variation which changes sign across an equilibrium value of the particle energies. Because of this difference, in the case of radiation, the energy loss has to be compensated with an external rf cavity, whereas in the electron cooling there is no need of energy compensation. Actually it is well known that it is the addition of the rf cavity that gives synchrotron-radiation damping.[6] But in either case the damping time does not depend on the beam intensity, as in stochastic cooling.

It is not clear whether the dynamics of stochastic cooling can be theoretically described by a continuity equation similar either to the Vlasov equation or to the Fokker-Planck equation, which are based on the assumption of a continuous beam, whereas the principle of the cooling is based on the fact that the beam is made of a finite number of particles.

Acknowledgements

I am very much indebted to F. T. Cole for patiently having read, commented and corrected this paper.

References

[1] A. M. Sessler, contribution to this conference.
[2] J. Liouville, J. Math. Pures. Appl. 2, 16 (1837).
[3] Paul and Tatiana Ehrenfest, The Conceptual Foundations of the Statistical Approach in Mechanics, translated by M. J. Moravesik, Cornell University Press, 1959.
[4] S. Pruss and F. Turkot, private communication, Fermilab, 1976. Such effect has indeed been observed in connection of the slow spill extraction out of the Main Ring. Particles are extracted according to their momentum. Also when the rf was turned off, experimentalists complained about a persistent rf structure in their spill. If the beam, though, was let coast in the ring for a time equivalent to the decoherence time, the rf structure was no longer observed in the extracted beam.
[5] S. Chandrasekhar, Rev. Mod. Phys. 15, 1 (1943).
[6] M. Sands, SLAC-121, Stanford, Nov. 1970.

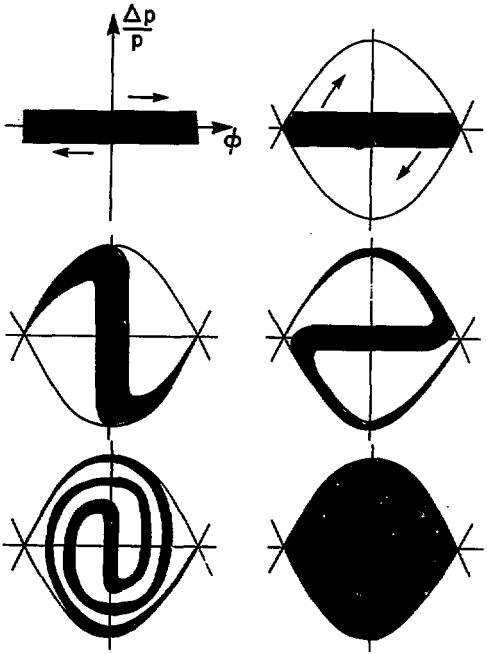

Fig. 3. RF capture.

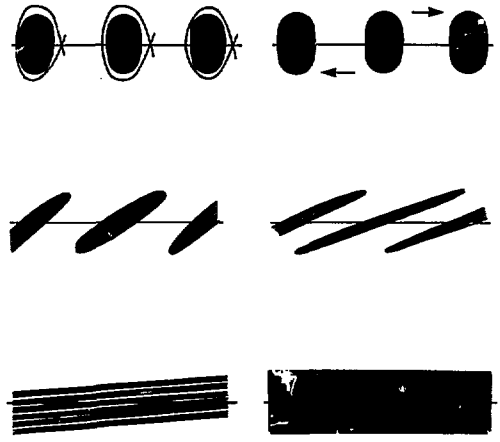

Fig. 4. Beam debunching.

Dup

LUMINOSITIES OF PROTON-ANTIPROTON COLLIDING BEAMS

D. Berley
Department of Energy, Washington, D. C.

and

M. Month
Brookhaven National Laboratory

The purpose of this paper is to compare the luminosities achievable with the proton-antiproton collision schemes proposed by CERN and by Fermilab. Estimates have been made by both CERN[1] and Fermilab[2,3] groups but these estimates have not been made with a consistent set of assumptions. A comparison of the potential performance of the two schemes at present is therefore not possible. We are motivated not only by the need for a realistic assessment of the many details entering but also by a hope that a deep understanding of the factors contributing to the luminosity may lead to improvements which in turn could result in increased luminosity. Using the antiproton schemes proposed,[1,2] we find that the luminosity at 1000 GeV/c of the Fermilab Doubler as a $\bar{p}$-p collider is 3.4×10^{29} and the luminosity of the SPS at 270 GeV/c as a $\bar{p}$-p collider is 1.0×10^{30}.

I. Accumulation of Antiprotons

The number of antiprotons produced in a stationary target and accepted in a collection channel is

$$N_{\bar{p}} = \frac{d^2N}{dP\,d\Omega}\,\Delta p\,\Delta\Omega\,\eta_{tgt}\,N_p,$$

$\frac{dN}{dP\,d\Omega}$	number of antiprotons produced per unit solid angle per unit momentum per interacting proton
Δp	momentum acceptance of the collector
$\Delta\Omega$	solid angle acceptance of the collector
η_{tgt}	target efficiency
$N_{\bar{p}}$	number of antiprotons produced
N_p	number of protons incident on target.

To estimate the antiproton production cross section we use the review of Cronin[4] which discusses antiproton production through $pp\rightarrow\bar{p}x$. No measurements exist in the kinematic region to be used and the work of Cronin contains the best available information and extrapolations. The antiproton production rate is related to the invariant cross section

$$\frac{d^2\sigma}{dpd\Omega} = \frac{p^2}{E}\left(E\frac{d^3\sigma}{dp^3}\right)$$

p and E are the antiproton momentum and energy. The antiproton cross sections are believed to be largest when the antiproton is at rest in the barycentric system of the incident nucleons.

The solid angle which can be accepted by the channel depends upon the target dimensions and the desired beam emittance. The beam emittance (phase space area) is

$$\epsilon_V = \pi\theta_V h$$
$$\epsilon_H = \pi\theta_H w$$

h, w are the target half height and half width
θ_V, θ_H are the vertical and horizontal half angles of emission

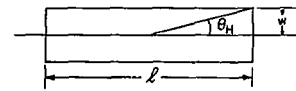

Fig. 1

The target width should be no larger than the antiproton beam size at the end of the target as shown in Fig. 1:

$$w \simeq \tfrac{1}{2}\ell\theta_H.$$

Similarly,

$$h \simeq \tfrac{1}{2}\ell\theta_V.$$

Under these simple assumptions

$$\theta_H^2 = \frac{2}{\ell}\frac{\epsilon_H}{\pi}$$
$$\theta_V^2 = \frac{2}{\ell}\frac{\epsilon_V}{\pi}.$$

The solid angle is

$$\Delta\Omega = \pi\theta_H\theta_V,$$

or

$$\Delta\Omega = \frac{2}{\ell}\sqrt{\epsilon_H\epsilon_V}$$

We use the emittances of the SPS design report[1] and the existing Fermilab Booster.[5]

The momentum acceptance of the channel depends upon the properties of the accumulator. In the CERN case, the momentum acceptance of the transfer lines and machine are designed to be maximum and there are simply no other restrictive constraints. The Fermilab case is quite different. The primary constraint here is the Booster rf acceptance, its operating cycle and the rf manipulation needed to achieve the design goal of $\Delta p/p = \pm 0.15\%$ at 6.1 GeV/c However, given that the Booster can accept $\Delta p/p = \pm 0.15\%$ at 6.1 GeV/c with a bunching of a factor of 10 "on the fly" and "without significant change in the booster operating modes for p acceleration and $\bar{p}$ deceleration," then it appears possible to accomplish this and still end up with a "coasting beam momentum spread" of $\Delta p/p = \pm 0.15\%$ at the low energy end, this being the Booster acceptance at 200 MeV. The difficulties though should not be underestimated. Some change in the rf cycle could be required and recall that this must be done at short intervals, there being about 1 sec between the p acceleration phase and the $\bar{p}$ deceleration phase. Also handling, observing and controlling high intensity p's and low intensity $\bar{p}$'s alternately could pose problems.

The target efficiency, η_{tgt}, depends upon the target length. When the target length is one interaction mean free path and when reabsorption of the antiprotons in the target is taken into account, the maximum target efficiency is ~ 30%. The acceptance of the channel will not be uniform over the length of the target and over the transverse dimensions of the target. The additional losses may lower the efficiency by a factor 2. We therefore choose

$$\eta_{tgt} = 0.15.$$

The parameters of the CERN and Fermilab designs are shown in Table I.

From these parameters the number of antiprotons is calculated. The ratio $N_{\bar{p}}/N_p$ is shown in Table II(a). Assuming that the Fermilab accelerated proton intensity will double by the time the $\bar{p}p$ collider is built and assuming that the PS intensity also increases from its present value we have calculated the number of antiprotons which would be produced per day. These are shown in Table II(b).

The ratios of the factors used in the antiproton production rate calculation are also shown in Table II. Fermilab has considerable advantage in using high energy protons to produce the antiprotons but the Booster, in which the antiprotons are collected, has a small aperture and works to the disadvantage of Fermilab. For completeness, we show in Table III the parameters involved in $\bar{p}$ accumulation that we consider reasonable compared with those that have been assumed by Fermilab.[2]

II. Luminosity and Tune Shift

The luminosity of two bunched beams colliding head on is given

$$L = \frac{2 N_p N_{\bar{p}} f}{M \left[\beta_H \beta_V \left(\epsilon_{Hp} + \epsilon_{H\bar{p}}\right)\left(\epsilon_{Vp} + \epsilon_{V\bar{p}}\right)\right]^{\frac{1}{2}}}$$

N_p	number of protons stored
$N_{\bar{p}}$	number of antiprotons stored
M	number of bunches
f	frequency of revolution
β_H, β_V	horizontal and vertical β functions at the interaction region
ϵ_{Hp}, ϵ_{Vp}	horizontal and vertical proton beam emittances
$\epsilon_{H\bar{p}}$, $\epsilon_{V\bar{p}}$	horizontal and vertical antiproton beam emittances

The luminosity is computed with the parameters listed in Table IV. We find a luminosity of 3.4×10^{29} cm^{-2} sec^{-1} for the Fermilab scheme at 1000 GeV/c and 1.0×10^{30} cm^{-2} sec^{-1} for the CERN scheme at 270 GeV/c. Our calculation of the luminosity for the CERN ring is in agreement with their result given in their design report.[1]

To increase the luminosity, the number of particles in the beams can be increased, the number of bunches decreased, the β values decreased or the beam emittances decreased. This can be done until the beam-beam tune shift for the collisions exceeds the value where stable beam storage can be sustained and instabilities result in a rapid loss of luminosity. The tune shift is given by

$$\Delta\nu_{V,H} = \frac{2 r_p N}{\gamma} \sqrt{\frac{\beta_{V,H}}{\epsilon_{V,H}}} \frac{1}{\left(\sqrt{\epsilon_V \beta_V} + \sqrt{\epsilon_H \beta_H}\right)}$$

$\Delta\nu$	linear beam-beam tune shift at a given collision point
r_p	classical proton radius
N	number of particles in each bunch of the "other" beam
γ	beam energy in units of the proton rest mass

We note the horizontal and vertical beam ½ - sizes are

$$a = \sqrt{\beta_H \epsilon_H / \pi}$$
$$b = \sqrt{\beta_V \epsilon_V / \pi}.$$

We note that the beam-beam limit can be taken roughly to be given by

$$(\Delta\nu)_{limit} < 0.01.$$

The tune shifts are computed with the parameters of Table V. The tune shifts per collision are about a factor of 2 below the maximum allowed. Without the antiproton emittances, the beam-beam tune shifts for protons cannot be computed. For equal numbers of p's and $\bar{p}$'s the proton tune shift for Fermilab would of course be much higher than for antiprotons since the $\bar{p}$ emittances are so much smaller. However, in this paper we have found the $\bar{p}$ collection rate to be sufficiently low at Fermilab that this is probably not an issue. Since the number of p's exceeds the number of $\bar{p}$'s by a factor of 18, the emittances of the $\bar{p}$ beam would have to be less than 18 times smaller for the proton beam tune shift to become significant compared to the antiproton tune shift.

III. Conclusions

The luminosity which would be produced by the CERN $\bar{p}$-p colliding beam is about 3 times that proposed by Fermilab. The major advantage of the CERN proposal is that the acceptance of the cooling ring is 60 times that of the Fermilab proposal. The damping time for stochastic cooling, used at CERN is independent of oscillation amplitude. The momentum and solid angle acceptance can be made as large as the practical limit determined by the magnetic storage ring. At Fermilab the aperture of the Booster is roughly matched to the volume in momentum space that can be cooled by the electron beam during one acceleration cycle.

The limitation on acceptance at Fermilab is therefore imposed nearly equally by the Booster acceptance and the electron cooler.

The antiproton production cross section is larger when the antiprotons are produced with high-energy incident protons. The Fermilab proposal has the advantage of higher incident proton energy.

REFERENCES

[1] Design Study of a Proton-Antiproton Colliding Beam Facility, CERN report CERN/PS/AA 78-3, 1978.

[2] Design Report - Fermilab Cooling Experiment, Fermilab, November 1977.

[3] L. Teng, Introductory talk at this Workshop.

[4] J. W. Cronin - Antiproton Production at Rest in the Center of Mass, 1977 Summer Study on Colliding Beam Physics at Fermilab, Volume I, p. 269.

[5] D. Cline, Introductory talk at this Workshop.

Table I. Antiproton Production and Acceptance Parameters.

	E_p GeV/c^2	$p_{\bar{p}}$ GeV/c	$E\frac{d^3\sigma}{dp_{\bar{p}}^3}$ mb/GeV^2	$\Delta p/p$	ϵ_H mm-mr	ϵ_V mm-mr	ℓ_{tgt} cm	$\Delta\Omega$ μsr
Fermilab	80	6.1	0.7	3×10^{-3}	2.6π	1.3π	5	73.5π
CERN	26	3.5	0.2	1.5×10^{-2}	100π	100π	4.5	4444π

Table II.(a) Antiproton Collection Rates - Collection Factors

	$\frac{d^2N}{dpd\Omega}$ sr^{-1}GeV^{-1}	Δp GeV/c	$\Delta\Omega$ sr	η_{tgt}	$\frac{N_{\bar{p}}}{N_p}$
Fermilab	0.111	0.0186	$73.5\pi \times 10^{-6}$	0.15	7.15×10^{-8}
CERN	0.0475	0.0525	$4444\pi \times 10^{-6}$	0.15	192.4×10^{-8}
Fermilab/CERN	6.34	1/2.82	1/60.46	1	1/26.9

Table II. (b) Antiproton Collection Rates - Rates

	N_p/pulse	$N_{\bar{p}}$/pulse	sec/pulse	$\bar{p}$/hr	$\bar{p}$/day
Fermilab	3.3×10^{13}	2.36×10^{6}	6	1.42×10^{9}	3.40×10^{10}
CERN	1.0×10^{13}	1.92×10^{7}	2.6	2.66×10^{10}	6.38×10^{11}
Fermilab/CERN	3.3	1/8.1	2.3	1/18.8	1/18.8

Table III. Comparison of Parameters Used in $\bar{p}$ Accumulation.

Parameter	Fermilab (optimistic)	This Paper
p (GeV/c)	6.1	6.1
$\Delta p/p$	3×10^{-3}	3×10^{-3}
Δp (GeV/c)	0.018	0.018
ϵ_H (mm-mrad)	4π	2.6π
ϵ_V (mm-mrad)	2π	1.3π
$\Delta\Omega$ (μsr)	111.4π	73.5π
$d^2\sigma/dpd\Omega$ (mb/sr/GeV/c)	8.07	4.33
η_{tgt}	0.33	0.15
σ_{tot} (mb)	40	39

For $N_{\bar{p}}/N_p$ Computation

	$\frac{d^2N}{dpd\Omega}$ ($\bar{p}$'s/sr/GeV/c/int.p)	Δp GeV/c	$\Delta\Omega$ sr	η_{tgt}	$N_{\bar{p}}/N_p$
This Paper	0.11	0.18	73.5π	0.15	7.1×10^{-8}
Fermilab	0.20	0.18	111.4π	0.33	4.3×10^{-7}
Fermilab/This Paper	1.82	1.0	1.52	2.20	6.1

Table IV. Luminosity

Parameter	Fermilab	CERN SPS
E (GeV)	1000	270
N_p	6×10^{11}	6×10^{11}
$N_{\bar{p}}$ (1 day accumulation)	3.4×10^{10}	6×10^{11}
f_{rev} (kHz)	47.8	43.4
M (no. of bunches)	6	6
β_H (m)	2.5	4.7
β_V (m)	2.5	1.0
ϵ_{Hp} (mm-mrad)	$1.42\pi \times 10^{-8}$	$6.9\pi \times 10^{-8}$
ϵ_{Vp} (mm-mrad)	$1.03\pi \times 10^{-8}$	$3.5\pi \times 10^{-8}$
$\epsilon_{H\bar{p}}$ (mm-mrad)	$<<\epsilon_{Hp}$	$3.8\pi \times 10^{-8}$
$\epsilon_{V\bar{p}}$ (mm-mrad)	$<<\epsilon_{Vp}$	$1.9\pi \times 10^{-8}$
L ($cm^{-2}sec^{-1}$)	3.4×10^{29}	1.0×10^{30}

Table V. Beam Beam Tune Shift in a Single Collision

Parameter	Fermilab	CERN SPS	
	$\Delta\nu_H = \Delta\nu_V$ (antiproton)	$\Delta\nu_V$ (proton)	$\Delta\nu_H$ (proton)
N (particles/bunch)	1×10^{11} (proton bunch)	1×10^{11}	1×10^{11} (antiproton bunch)
β_V (m)	2.5	1.0	1.0
β_H (m)	2.5	4.7	4.7
b (mm)	0.16	0.138	0.138
a (mm)	0.19	0.423	0.423
γ	1066	288	288
$\Delta\nu$	4.1×10^{-3}	4.4×10^{-3}	6.8×10^{-3}

Dup

EFFECT OF THE SEXTUPOLE DISTRIBUTION ON THE MOMENTUM APERTURE IN THE SMALL COOLING RING LATTICE AT FERMILAB*

M. Month and H. Wiedemann.†
Brookhaven National Laboratory
Upton, New York

In the process of cooling and accumulating antiprotons for use in p-$\bar{p}$ collisions, rings must be designed with a large usable momentum aperture, on the order of 3% or larger. Since long straight sections and dispersionless regions are generally required, the sextupole field correction system for "chromatic aberration" is an important aspect of the overall lattice design.

The Fermilab small cooling ring, whose purpose is to demonstrate the feasibility of cooling and accumulating protons (and antiprotons) with electrons, is a particularly simple system. We will use this lattice to show the sensitivity of the momentum aperture to the sextupole correction system distribution.

The lattice is basically a racetrack arrangement with two arcs and two dispersionless straight sections. The arcs are each composed of roughly 2 FODO cells and momentum match regions where the dispersion is brought to zero. There is also a "high dispersion" small straight in each arc. This straight section is used for a kicker needed for injection when phase displacement stacking is employed. The long straight sections are cooling regions where the electron beam can be injected and extracted. In the first Fermilab tests only one electron beam is used, thus destroying the two-fold lattice periodicity. The electron beam has a focusing action on a proton beam and we take the strength to be given by $\Delta \nu \sim 0.1$.

The arcs, as we have said, each have 2 FODO cells. Thus, there are four appropriat. locations for sextupoles per superperiod, two having their effect mostly on the vertical chromatic aberrations (SD sextupoles), and two horizontal sextupoles, SF. We treat 2 cases:

A) a single SF and a single SD per superperiod - $\Delta \nu \sim 0.1$.

B) two SF and two SD per superperiod, powered in series - $\Delta \nu \sim 0.1$.

To see the effect of the sextupole distribution, we plot in Fig. 1 the tune as a function of momentum for orbits across a 3% momentum spread. The sextupole strengths are chosen to give a zero linear chromaticity. The corresponding β-function variations are shown in Fig. 2 and the dispersion function variations are given in Fig. 3.

Contrasting A) and B) we can see the dramatic impact of an added sextupole, that is, of smoothing the sextupole distribution. We might also conjecture that if there is the future expectation of lengthening the straight sections and adding more electron beams ("tromboning" the small cooling ring), there should be some thought given to the possibility of a more elaborate sextupole field correction system.

*Work performed under the auspices of the U. S. Department of Energy.

†Stanford Linear Accelerator Laboratory.

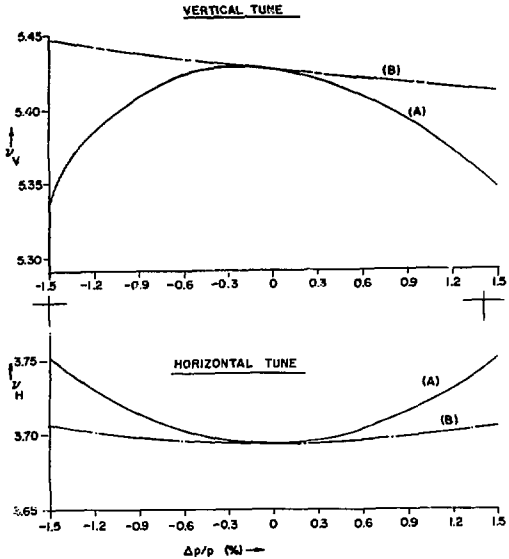

Fig. 1. Tune versus momentum (A) single F and D sextupoles per superperiod; (B) two SF and two SD sextupoles per superperiod (in series).

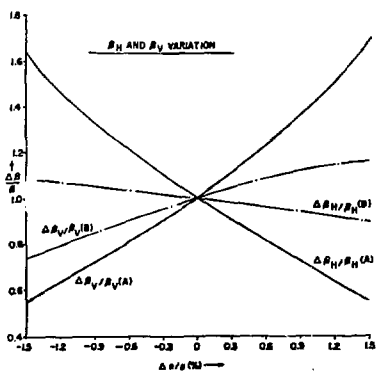

Fig. 2. β function versus momentum (A) single F and D sextupoles per superperiod; (B) two SF and two SD sextupoles per superperiod (in series).

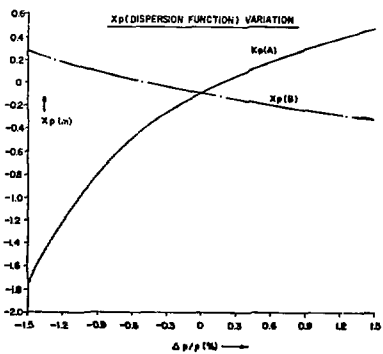

Fig. 3. X_p (Dispersion Function) versus momentum.

Dup

ELECTRON COOLING OF HIGH ENERGY BEAMS*

M. Month
Brookhaven National Laboratory
Upton, New York

The purpose of this short note is to clarify the relationship between electron cooling time and beam energy[1] and also to see how the nature of the electron beam enters. In particular, we want to know whether it is electron total current or current density that is significant. There is no attempt here to include any measure of sophistication, such as the effect of a solenoid field, but simply to use Coulomb scattering and statistical equilibrium. For simplicity, we take the 3 phase spaces (horizontal, vertical and momentum) to have equal occupied areas and use the terminology for the transverse case.

Thus, we can use Skrinsky's expression for the e-folding cooling time,

$$\tau = \frac{\pi}{2}\left(\frac{m}{M}\right)\frac{e\,\beta\,\gamma^2}{L\,r_p^2\,\eta\,I a}\,E^3, \qquad (1)$$

where β, γ are the usual relativistic parameters, the unitless velocity and energy,

m, M are the electron and proton mass,

e is the unit of electric charge (1.6×10^{-19}C),

r_p is the classical proton radius (1.54×10^{-18}m),

L is the Coulomb logarithm depending on the minimum impact parameter; we take L = 20, and

η is the ratio of length of electron cooling region to the circumference of the proton (antiproton) ring.

We assume that the electron beam and proton beam are matched in space, this being the optimum configuration, where we expect the above expression for the cooling time to apply. Thus,

a is the radius of the proton beam in the cooling region, and

E is the invariant emittance of the proton beam.

E is defined without the notorious "π", i.e.,

E = Area/π in phase space. In particular,

$$E = \beta\,\gamma\,\theta\,a,$$

with θ the 1/2-divergence of the proton beam, proportional to the square root of the beam temperature.

The variable I is the total electron current.

In the form (1), the basic nature of the electron cooling process is exposed:

1) Cooling depends most critically on the invariant emittance, $\tau \propto E^3$. This is a very important point, since E is generally a property of the source of particles and as the beam passes from machine to machine as it is accelerated to higher and higher energies, E is in principle invariant, but in practice the effective emittance will increase in response to the vagaries of the real world. Real beams tend to have $E > 20\times10^{-6}$ rad-m. In fact, one of the best high energy beams is to be found at the ISR, where with a great deal of vertical shaving, a value $E_y \lesssim 10\times10^{-6}$ rad-m is attained. This is all in accordance with Liouville's Theorem which tells us that the effective invariant emittance will not decrease in the real world-M- will not, that is, unless through some process which is unusual for particle beams, such as interaction with an electron beam having a thermal equilibrium level much lower than that of the proton beam. Thus, we have an interesting dilemma. If we take proton beams as nature provides, or if we accept antiproton beams at the production target of large solid angle, electron cooling will tend to be a very long process, since E will be a large number. It is the irony of electron cooling that it works best for beams that don't really need it!

2) The energy dependence is given by

$$\tau \propto \beta^{3/2}\,\gamma^{5/2}\left[\text{since } a \propto (\beta\gamma)^{-1/2}\right].$$

Thus, cooling times could conceivably be "reasonable" for very low energy proton beams.

3) The cooling time is increased as the ratio of cooling length to ring circumference is reduced. As the energy of the proton (antiproton) ring is increased, it takes a larger ring to store them. Thus, η is smaller for higher energy, which further decreases the cooling rate.

4) The cooling rate is proportional to the total electron current and not the transverse current density. Once the total current is given, the transverse density needed can be deduced from the size of the proton beam which is to be cooled. Thus, in principle, very small high density electron beams available from electron storage rings do not appear to be useful in the context of the discussion given here.

To get a feeling for the order of magnitude of cooling times we might achieve, consider a 50 GeV beam with an invariant emittance equal to that of the best proton beam available; that is, $E=20\times10^{-6}$ rad-m. Let us also take a cooling length of 20m in

the Fermilab ring, giving $\eta = 20/(2\pi \times 1000) = 3.2 \times 10^{-3}$. Assuming a β-function value, $\beta^* = 50$ m over the 20 m cooling length, we have:

$$a = \left(\frac{E\,\beta^*}{\beta\gamma}\right)^{1/2} = 4.3 \text{ mm},$$

with $\gamma = 53$. Thus, the cooling time is:

$$\tau = 4.6 \times 10^6 \text{ sec}/_{I(\text{amps})} = 53.4 \text{ days}/_{I(\text{amps})}.$$

Thus, for an electron beam of 50 A peak current matched to the proton beam, the e-folding cooling time is $\tau = 1.1$ days. This corresponds to a current density in the electron beam, $n_e = I/\pi a^2 = 86$ A/cm^2 and an average electron current of 5 A (if bunching is 10 to 1). This is a very high current indeed.

It thus appears to be impractical to consider using electron cooling at high energies for the purpose of cooling and accumulating antiprotons. However, if we already have "cold" proton and antiproton beams, it might be conceivable to use electron beams from storage rings for the purpose of sustaining constant luminosity and perhaps limiting beam loss and, therefore, background. Thus, if we managed to attain a cold beam of emittance 10 times less than we assumed - i.e., $E = 2$ μrad-m, then the cooling time for a 50 A electron current is reduced to 92 sec. Thus, in such a situation, blow-up processes occurring on a time scale of the order of 100 sec can, to some extent, be "damped". However, even such an application is not trivial and the conditions for stability of both electron and proton stored beams must be carefully studied. Furthermore, it should be remembered that these "high density" (low emittance) p and $\bar{p}$ beams must be formed at low energy where electron cooling is practical. Thus, space charge limitations at low energy become a factor.

We could imagine a system combining stochastic cooling at large amplitudes followed by electron cooling to maintain the small size reached. Such a system does not appear to be very promising; in any case, consideration of this subject is outside the intentions of this paper.

---

*Work performed under the auspices of the U. S. Department of Energy.

1. Most of the results given here can be deduced from a 1971 BNL report, R. L. Gluckstern, Electron Cooling of Protons in ISABELLE, CRISP 71-24 (1971).

Dup

BEAM SEPARATION FOR p-$\bar{p}$ COLLISIONS IN A SINGLE RING IN THE MULTIBUNCH MODE*

D. Berley,† A. A. Garren‡ and M. Month
Brookhaven National Laboratory
Upton, New York

e^+e^- storage rings are operated with very few bunches. Designing for a very high volume density gives the optimum luminosity limited by the beam-beam interaction. A value of the tune shift of 0.03-0.06 per bunch interaction is normally assumed in the design stage. Operating e^+e^- rings tend to achieve this.

p-$\bar{p}$ single ring operation presents a different situation in that such high tune shifts may not be stable. Normally, it is assumed that proton tune shifts should be limited to ~ 0.005, an order of magnitude smaller than for electrons. For head-on collisions, coupling the three phase space dimensions, the limit could well be less than this value. In any case, it is clear that some gain could be visualized by dividing the available beam into a sequence of bunches. Then, if the limit is determined by the tune shift per bunch, a luminosity increase at a given collision region could be attained. For a given number of particles per bunch, the luminosity will increase linearly with the number of bunches while the tune shift per bunch remains unchanged. However, as the number of bunches is increased, the number of collision points around the ring also increases. For n bunches, there are in fact 2n collision regions. Because, in general, there is no symmetry of collision points, it is not clear that the relevant limitation is the tune shift per bunch. We could indeed guess that under such conditions as would be present either at Fermilab or the SPS at CERN, the total tune shift per revolution might be a more relevant parameter reflecting the performance limitation. Thus, some means of separating the beams at points where no experiment is being performed seems to be an important feature for a p-$\bar{p}$ colliding beam ring.

For many bunches, it does not seem to be a practical solution to separate the beams locally by a group of electrostatic deflectors. The energy of the beams is too high and the number of units required would be too high. A feasible arrangement would not appear to be possible. Thus, both at Fermilab and at the SPS, it has been proposed to use a different method. By exciting a betatron oscillation in some appropriate, localized region, one could create a specific collision point while at the same time cause the p and $\bar{p}$ beams to oscillate in opposition so that their orbits meet at only a small number of points, roughly given by twice the tune, 2ν. This situation is depicted schematically in Fig. 1.

Thus, we have 2n collision points and ~ 2ν orbit crossings. The question is: what oscillation amplitude, i.e., what deflector strengths are required so that the beam separation at all undesired collision points is sufficient to prevent harmful beam-beam interaction? Furthermore, we might ask if we can reasonably expect to reach the goal of sufficient separation in the existing machines for a large number of bunches.

These questions are, of course, difficult to respond to and we will not attempt any general answer. However, by performing a simplified calculation for the Fermilab situation, perhaps some feeling for the difficulties involved will become clearer.

We consider the case of 6 bunches of p's and $\bar{p}$'s. There are, therefore, 12 points of collision. Three deflectors are sufficient to give the situation sketched in Fig. 1. Since the total tune is about 19.4, we expect about 38 orbit crossings around the ring. Thus, if the collisions were randomly distributed, there would, in general, be a couple of places where the orbits would come very close. In fact, we might expect that unless extraordinary measures were taken (some symmetry) this type of situation could not be avoided.

To be a little more quantitative, take the following model:

Consider i interaction points from D1 to D2 and a phase advance between these points of $2\pi\nu_R$ (ν_R is a tune slightly reduced from $\nu = 19.4$). Then, for the ℓth collision point, the beam separation is given by,

$$\Delta_\ell = 2\theta\,\beta \sin\frac{2\pi\nu_R}{i}\,\ell,$$

where β is the average β-function, θ is the effective deflector kick, and we have assumed the phase advance to be linear in distance, which is only roughly valid.

If we take a deflector field of E = 50 kV/cm and a length L = 6 m, then for a beam of momentum p = 1000 GeV/c, the deflection angle is,

$$\theta = EL/P = 3\times 10^{-5} \text{ radians.}$$

For $\beta \approx R/\nu \approx 50$ m, $\nu_R = 19.4\text{-}0.25 = 19.15$ and i = 11, we have for the separation at collision ℓ,

$$\Delta_\ell = 3 \sin(3.4818\,\pi\ell) \text{ (mm)}.$$

We list in Table 1 the values of Δ_ℓ for $\ell = 1$ through 11.

Table 1. Beam Separation at Collision Points

Collision Point ℓ	Beam Separation Δ_ℓ (mm)
0	C*
1	3.00
2	0.34
3	2.96
4	0.68
5	2.88
6	1.01
7	2.76
8	1.32
9	2.61
10	1.62
11	2.43

Before commenting on the results in Table 1, we might ask what the desired separation is. Let us take a beam of normalized emittance, E = 30 μrad-m (Emittance = phase space Area/π). For a 1000 GeV beam, this gives for β = 50 m a 1/2 beam size, b = 1.19 mm or an rms size, σ = 0.6 mm. We might guess that the required separation is 10 σ or 6 mm. Then we would need at least twice as much kick as assumed above. However, even if we take 5σ as being sufficient, it becomes clear from Table 1 that most of the points violate this condition. In fact, there are points where the phase advance is such that essentially no separation results - points 2 or 4 in the case computed here—almost independent of the amplitude of the betatron oscillation.

A more accurate calculation using the Doubler lattice yields results not differing essentially from those in Table 1.

---

*Work performed under the auspices of the U. S. Department of Energy.

†U. S. Department of Energy.

‡Lawrence Berkeley Laboratory.

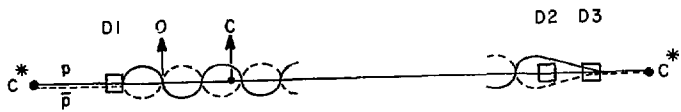

Fig. 1. Beam separation by localized set of Electrostatic Beam Deflectors. D1, D2, D3 = deflectors. C* = desired collision point. O = orbit crossing. C = undesired collision point.

Dup

NOTE ON BEAM-BEAM TUNE SHIFT IN SINGLE RING MULTI BUNCH MODE*

M. Month
Brookhaven National Laboratory
Upton, New York

If many identical counter-rotating bunches of protons and antiprotons are stored in a single ring, they will have identical orbits. Therefore, for n bunches, there will be 2 n collisions at 2n equally spaced locations around the ring. A particle of one beam will then be influenced by a periodic sequence of 2n strongly nonlinear forces caused by the n bunches in the other beam.

Let $\Delta\nu_I$ be the tune shift at some collision point I. Now the tune shift for the entire orbit is:

$$\Delta\nu \text{ (Total)} = \sum_{I=1}^{2n} \Delta\nu_I .$$

The question is: Is this total tune shift relevant to the problem of beam stability? The answer is: not in general. What we are trying to describe is a nonlinear force and the nonlinear force is described by its "strength", $\Delta\nu_I$, for each bunch interaction individually. It is not at all clear that the sum of the individual $\Delta\nu_I$ is the significant quantity.

If, however, all th collisions are identical, meaning that the β-values are the same at all points where the bunches meet, then it might be argued that $\Delta\nu_0$, the beam-beam tune shift per collision is the true measure of the strength of the nonlinear force. The reasoning is that although there is more nonlinear force, this is cancelled by the effect of the symmetric distribution of the force along the orbit. Said another way, although the strength of resonances increases with more collisions, the density of resonances (in tune space) is decreased by the symmetry. This point is very difficult to verify in detail on theoretical grounds, but experiments at Adone have shown that there could be some validity to the claim. With 3 bunches, the beam-beam limit, the tune shift for rapid beam blow up, was not proportional to the total shift. It was also not proportional to the tune shift per bunch, but rather somewhere in between, suggesting a more complicated relationship between the beam-beam limit and the tune shift distribution around the orbit. This is true even in the case of a symmetric distribution.

On the other hand, the situation at both FNAL and the SPS is quite different. In these cases, the beam configuration at the collision points are not symmetric, but differ from one collision point to the other. The theoretical argument related to the decrease of the density of resonances (due to symmetry) does not strictly apply. We might expect, therefore, that the effect of the nonlinear forces would be better described by the total tune shift rather than the tune shift in any given bunch collision.

We might conclude that at FNAL or the SPS the addition of bunches can only provide increased performance at some collision point if the bunches are well separated at all other collision points!

---

*Work performed under the auspices of the U. S. Department of Energy.

ELECTRON BEAM COOLING - PROSPECTS OF RIBBON-TYPE E-BEAMS

F. Krienen

CERN, Geneva, Switzerland

Some time ago we made an exercise to find out how an electron beam cooling device would look if you had to cool antiprotons with very large momentum bite. In the device described below the 100 MeV antiprotons will concentrate at the lower end of its momentum range. The spot size will of course depend on the electron temperature.

I. General Description

The beam profile of the antiprotons in the cooling straight sections is 700 mm wide and 136 mm high. The electron beam will cover the antiproton beam in the width, i.e., 700 mm, whereas the height will be 80 mm. This profile will be maintained all the way from cathode to collector in order to keep the transverse temperature of the electrons as low as possible. The momentum spread in the antiproton beam requires the corresponding momentum spread in the electrons, i.e., ±6%. This can be achieved by surrounding the electron beam with a wire cage, in which the wires are parallel with the electrons. Each wire is kept at the appropriate potential, creating inside the cage a potential distribution so that the electrons entering the cage are post-accelerated.

The total potential difference across the cage is 15 kV; the higher potential is at the outside of the cooling ring. The magnetic guiding field in the straight sections is uniform and parallel to the electron velocity; its value is 600 G. The solenoid creating this field has a circular section with a bore of 1 m, so that there is ample space to stiffen the flat vacuum tank and to accommodate high-voltage feedthroughs and other diagnostic means. The electron beam must bypass the lattice elements of the storage ring. Hence the electron beam is bent in at the upstream end of the cooling straight section and bent out at the downstream end of the cooling straight section. The bending is achieved by a toroidal magnetic field on which is superimposed a weak dipole field of about 2.6 G which has actually a small gradient in order to minimize the transverse temperature.

The torus is a substantial piece of equipment, for it has to accept the antiproton beam as well. The bending radius of the torus is 3.15 m at the center of the electron beam. The bore of the torus is 2.75 m, the angle of bending is 45°. The electron beam in one upstream bypass is actually in line with the electron beam in the preceding downstream bypass. Hence it is possible to daisy-chain the electron beams of the four cooling sections so that we need only one electron gun and one collector. The acceleration of the electrons to the final energy will be in magnetically confined flow. The cathode of the gun will be of the dispenser type and will be built up of rectangular slabs to obtain the required cathode emitting area of 700 × 80 mm.

The cathode has the conventional Pierce-type focusing electrodes ensuring uniform current density of 0.2 A cm^{-2}, and a set of four focusing slits of the resonant type. The electrons leaving the last slit will be post accelerated to assume the potential in the wire cage. Upon entering the collector region they will be decelerated by the same amount so that they pass the magnetic shunt with approximately equal energy. The magnetic shunt exerts an outward force on the electrons so that the collector is appreciably wider than the original electron beam. This facilitates collection of electrons at a potential only a few kilovolts above the cathode potential and minimizes the electron backstream.

Considerable attention has been given to the problem of space charge neutralizing the electron beam. Partial space-charge neutralization, to the amount of $(1 - \beta^2)$, would keep the electron paths parallel to the beam axis. However, the potential gradient in the cage seems to be prohibitive in achieving permanent trapping of (+ ve) ions. As the current density is relatively low, the peripheral transverse energy is about 1.2 eV and decreases with the square of the distance from the median plane. If, on the other hand, a system were devised in which the electrons moved in a field-free tank with initially the proper velocity spread across the beam, perfect space charge neutralization becomes a must, for otherwise a small resulting drift would mix the high and low velocity electrons in the long run.

Hence space-charge neutralization seems to be out of the question. The potential gradient in the cage would also produce a vertical drift coupled to appreciable transverse energy. However, this motion can be suppressed by superimposing a weak vertical magnetic field on the longitudinal guiding field, thus the resultant magnetic field is slightly tilted. The tilt field is proportional to dp/dx and amounts to about 1.4 G. This correction persists also in the torus: it is added to the field of the same sign needed for the bending proper, totalling about 4.0 G. The tilt fields are produced by a cage of current wires coaxial with the center line of the electron beam and outside the vacuum tank, which in addition allows small corrections to be made to ensure optimum parallelism of the electron beam and the antiproton beam. The circulating antiprotons receive in the toroids alternating vertical kicks of about 44 mrad. Vertical displacement of the large quadrupoles adjacent to the toroids would compensate for this. The above measures ensure that the electron beam apparatus is symmetric with respect to the (horizontal) median plane, which facilitates construction and alignment.

II. Magnetic Field

Figure 1 shows the assembled guiding magnets. There are four cooling solenoids of 11 m length, four bypass solenoids of 10.9 m length, and eight

toroids of 45° bending angle and 2.47 m length as measured along the mean radius of 3.15 m. One of the bypass solenoids is interrupted to accommodate gun, collector, and vacuum pumps. The solenoidal field is 600 G. The toroidal field is matched to the same value at a radius of 3.15 m. The current density in the copper coils is conservative, 3 A mm^{-2}. The effective copper thickness is 16 mm. A return mild steel shield is foreseen. The flux density in the shield will be 10 times the internal field. The shield will effectively protect the electron beam from stray fields and from the leads powering the coils. The coil will be moulded in the shield. The coil structure is sufficiently stiff to be supported from the ground in two V blocks. Solenoids are bolted to the toriods by means of flanges.

Table 1 gives particulars about the amount of copper, steel, and power. Figure 2 shows a section of the current wire cage which provides the tilt magnetic field; maximum currents are of the order of 5 A. The idea is to have independent control in each of the solenoids or toroids.

III. Vacuum System

Figure 3 shows the assembled vacuum tanks. There are four cooling vacuum tanks of 11 m length, four bypass vacuum tanks of 18.9 m length, and eight manifolds which are located in the toroids. In the bypass tank which houses the gun and the collector are located additional vacuum ion pumps. The manifold is built to accommodate ion getter pumps plus some titanium sublimation pumps. Each vacuum tank is aligned within its corresponding solenoid or toroid. The vacuum tank flanges will be flush with the magnet flanges. There will be a simplified bellows structure on each pair of vacuum flanges in order to handle small misalignments. Each flange will have double sealing with prevacuum in between. The high vacuum side will be metal to metal, the low vacuum side will be viton. The 11 m tank would weigh about 1800 kg (stainless steel), the 19 m tank about 3000 kg, and the manifold 1500 kg. The total tank volume is 30 m^3. The total length of the metal-to-metal seal is about 60 m.

IV. Velocity Cage

Figure 4 shows some details of the cage in which the potential gradient is made to achieve a velocity spread of the electrons. The strips are supported on alumina spacers, which are screwed in the vacuum tank walls. Mini conflats assure vacuum tightness of the bolt holes. The strips are daisy-chained from tank to tank by means of spring contacts. In the first and last tank the strips are individually brought out by means of multiple feedthroughs. In this way complete control of the potential distribution inside the cage can be obtained. Figure 5 shows the equipotential plot in the cage, taking into account the space-charge electric field.

V. Gun

Figure 6 shows a section of the cathode and the resonant focusing slits. The design is based on the computer calculations of the circular beam of the ICE gun. Clearly the linear device with which we are concerned in this proposal needs reconsideration. Although the post acceleration program has still to be developed, the expectation is that this will give positive results as the electrons are already at 90% of their final velocity. The cathode is presumably one of the most delicate parts of the system. Preliminary discussions with a potential manufacturer resulted in a design in which the tungsten dispenser cathode is subdivided into rectangular slabs of 8 mm thickness, 20 mm width, and 70 mm height. Each slab has two holes in which is located a protected bifilar heater. A filament lifetime of 10,000 hours seems to be feasible. (This would be higher if oxide cathodes were utilized.) The slabs are assembled in submodules, which in turn are mounted on a molybdenum carrier. The carrier is kept at about 600°C and is mounted in its turn on a water-cooled copper base via stainless-steel studs.

The crucial part seems to be the thermal expansion which could result in bending and warping of the emitting surface. The tantalum Pierce-type focusing electrode is heat sunk so as to avoid spurious electron emission, and is mounted with heat conducting studs on the copper base. The resonant focusing slits are water-cooled to avoid damage to these electrodes in case of mal-steering of the electron beam. The flat tank being located in a round coil facilitates the high-voltage feedthrough of the various electrodes. The applied voltages are maximum of the order of -60 kV with respect to ground. Some consideration will be given to decreasing the current density, in case the tune shift of the antiproton beam is larger than can be handled. Table 2 shows some of the parameters of the gun.

VI. Collector

Figure 7 shows some details of the collector structure. The nominal current is 112A so that the power in the beam is over 6 MW. To sink this power into the collector would certainly be very difficult and wasteful. However, one can recuperate most of the power by deceleration of the electrons. To this end the collector is kept at a potential slightly higher than that of the cathode. The expectation is that between 1 and 2 kV is manageable. Secondary emission can be minimized by choosing the appropriate collector surface treatment. The magnetic field in the collector cavity is greatly reduced by means of a magnetic shunt. The so ensuring vertical component of the magnetic field would bend the electrons outwards so that the collector cavity is appreciably higher than the original height of the electron beam. The small magnetic field in the collector volume is further shaped by additional current wires in order to have the lateral velocity of the electrons reduced to a small value of the order of 100 eV at the point of impact with the collector. Table 2 shows some of the parameters of the collector.

VII. Power Supply

The power supply for the cathode potential is well stabilized to 3×10^{-5}. The rated current is 100 mA, although the cathode draws in theory no current at all. It would be advisable to make this power supply short-circuit proof. The same applies to the slit anodes; their stability is 10^{-3} and rating 10 mA. The collector power supply is rated for 150 A, 2 kV, and is stabilized to 10^{-2}. The wire cage power supply provides the appropriate potential to the wires by means of a voltage divider. Its rating is 20 kV, 100 mA, and is stabilized to 10^{-4}. The filament power supply is rated 30 V, 500 A. A separation transformer is needed to bring the collector power supply and the filament transformer on cathode potential. The rating is 380/380, 400 kVA, 50 Hz. All components at cathode potential are housed in a high-voltage Faraday cage which is surrounded by a grounded Faraday cage. The volume of the former is about 120 m^3.

VIII. Control System

It is at this stage rather difficult to specify the precision with which parameters have to be controlled. Indeed the purpose of the ICE experiment is to ascertain which parameters are critical and which are not. Consequently, some of what follows may have to be amended as the ICE experiment progresses. Clearly the relative velocity of electrons and antiprotons is the most important quantity to be controlled. This would entail precise control of the cathode potential and the cage potential. The latter could possibly be approached with a b-parameter fit. Magnetic guiding field, anode slits, and collector potentials are presumably of lesser importance. The vertical magnetic correction must be adapted to the potential gradient in the cage, and a horizontal component might be necessary to correct for misalignment and temperature effects. Diagnostic means to find out the whereabouts of the beam will have to be developed. Another part of the control would be the switching-on procedure. Apart from the interlocks, which are trivial, one should envisage adjusting the applied voltages to the magnetic field, since the latter scales with the square root of the potential to achieve minimum excursions of the electrons around their guiding centers. Without control, the electrons could hit the anode slits during the switching-on time. In this case, current protection of the anode voltages would trip the high voltage.

TABLE 1: Guiding field

	Quantity	Weight (ton) each
11 m cooling solenoid	4	Cu 5.12 Fe 7.57
19 m bypass solenoid	4	Cu 8.84 Fe 13.07
Toroid	8	Cu 3.12 Fe 15.34

IX. Diagnostics

The efforts made so far in this field are mostly concerned with the effect the electron beam has on the coasting protons. Extrinsic effects as such are not within the scope of this section; rather, we discuss briefly the essential measures to ensure the correct functioning of the device. Now the power in the beam is of the order of 6 MW, although the heat content in the beam is only 6 joule. The first number tells us that permanent landing of the electron beam on some part other than the collector would damage the device. Hence fast switching-off will be in demand. Presumably, crowbarring the cathode to ground with a triggered spark gap would be possible. The spark gap would trigger on excessive current in the slit anodes, the wire cage, and in the cathode power supply. A pick-up electrode surrounded by a guard electrode is common practice in monitoring properties of an electron beam. In the present device this is only possible under pulsed conditions. Also this can be done with triggered spark gaps. A rise-time and fall-time of about 10 μsec seem within reach, and pulse lengths of up to 1 msec can be tolerated. Several movable probes would be needed to indicate the position of the electron beam. Instabilities with a time structure could be detected on the elements of the wire cage, and possibly a small but fast electric or magnetic disturbance working on the electron beam could, via the signals on the wire cage, tell the position of the beam. Intrinsic transverse temperature control has as yet not found a practical solution, but hopefully synchrotron radiation or the scattering of laser light on the spiralling electrons would some day or another show results.

TABLE 2: Gun and Collector

Cathode potential	-51.4	kV
Filament voltage (rated)	36	V
Filament current (rated)	500	A
1 anode slit potential	-31.4	kV
2 anode slit potential	-23.9	kV
3 anode slit potential	-12.2	kV
4 anode slit potential	-2.9	kV
perveance	7.610^{-6}	$AV^{-3/2}$
Current density	2900	A m^{-2}
Total current	112	A
Collector potential (nominal)	2	kV
Collector power (nominal)	224	kW

X. Some Pertinent Formulas

Solenoid

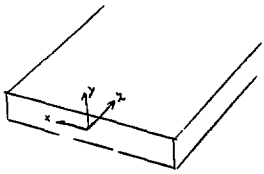

Toroid

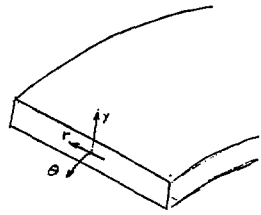

Potentials	Rectangular coordinate solenoid	Cylindrical coordinate toroid
Magnetic guiding field	$A_x = B_z y$	$A_y = \mu_0 I \ln r/(2\pi)$
Self magnetic field	$A_z = -\frac{1}{2}\mu_0 j y^2$	$A_\theta = f(r,y)$ (elliptic integral)
Vertical tilt field (e.g., bending)	$A_z = -B_y' x$	$A_\theta = \frac{1}{2}B_y r$
Space charge electric field	$\phi = -jZy^2/(2\beta_\parallel)$	$\phi = -jZy^2/(2\beta_\parallel)$
Cage electric field	$\phi = -E_x x$	$\phi = -E_r r$

Current density $j = 2000$ A m^{-2}

Vacuum impedance $Z = 377\ \Omega$

Relative velocity $\beta_\parallel = 0.44 \pm 6\%$

Peripheral space charge potential (with respect to the median plane) $\phi = 1370$ V

Drift angle (horizontal) $\sigma = v_x/v_z = jZy(1 - \beta_\parallel^2)/(\beta_\parallel^2 B_z c)$

Peripheral drift angle $\sigma_{max} = 5.9 \times 10^{-3}$ rad

Peripheral drift temperature $E_\perp = \frac{1}{2} mc^2 \beta_\perp^2 = 1.74$ eV

Tilt field $B_y = -(1/e)(dp/dx) = 1.41 \times 10^{-4}$ tesla (p = electron momentum)

Cage electric field $E_x = E_r = \beta c B_y = 18$ kV m^{-1}

Magnetic bending field $B_y = p/(eR) = 2.65 \times 10^{-4}$ tesla ($R = 3.15$ m) to be added to tilt

Budget electron cooling device in KSF

	Weight (ton)	Unit price	Quantity	Subtotal	Total
11 m cooling solenoid	12.69	214	4	856	
19 m bypass solenoid	21.91	369	4	1476	
Toroid	18.46	213	8	1704	
					4036
11 m vac. tank (cooling)	SS 1.76	70	4	280	
19 m vac. tank (bypass)	SS 3.04	114	4	456	
Toroid	SS 1.50	60	8	480	
					1216
Wire cage				280	
Gun				240	
Collector				120	
					640
Power supplies 500 kVA incl. cooling				400	
Faraday cage				100	
Manual control				100	
Remote control				200	
Cabling				100	
					900
Vacuum pumps					200
			Grand Total		6992
Power bill (in kW)					
11 m cooling solenoid		102	4	408	
19 m bypass solenoid		177	4	708	
Toroid		70	8	560	
					1676
Collector (nominal)					224
Power hut					100
			Grand total		1400

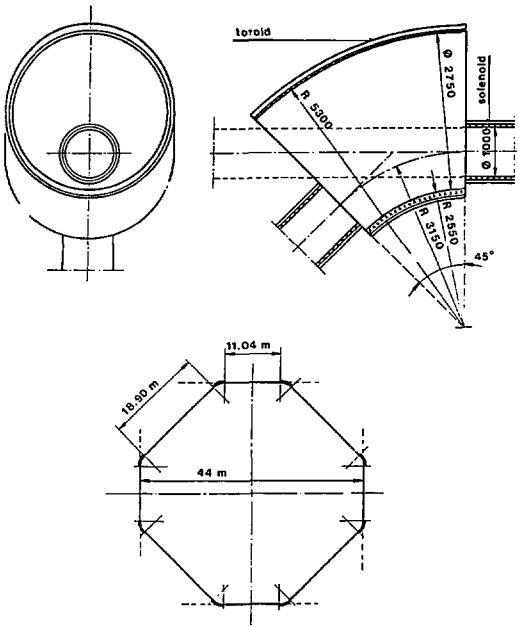

Fig. 1. Guiding magnets

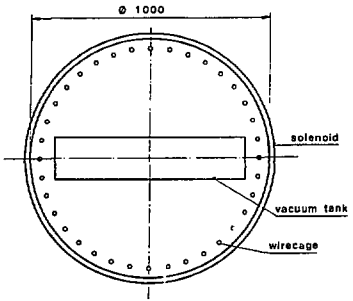

Fig. 2. Wire cage (magnetic)

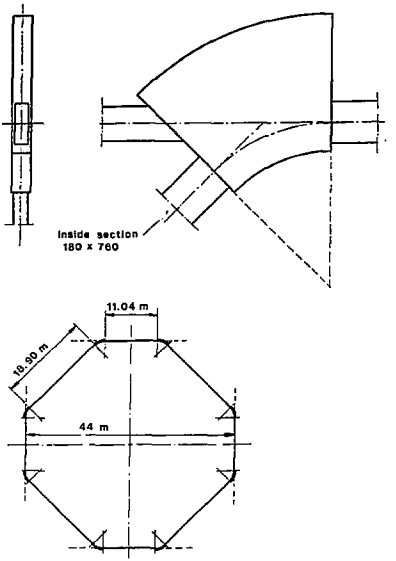

Fig. 3. Vacuum tank

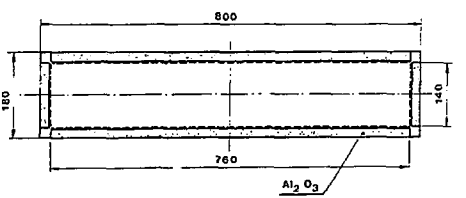

Fig. 4. Wire cage (electrostatic)

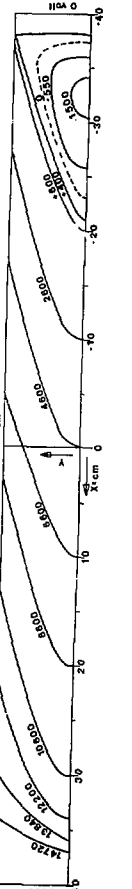

Fig. 5. Equipotential plot (including space charge)

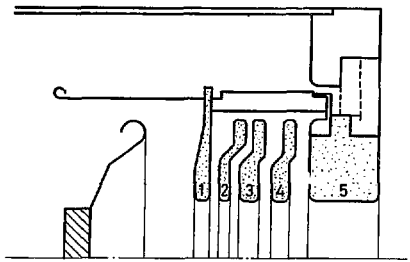

Fig. 6. Gun

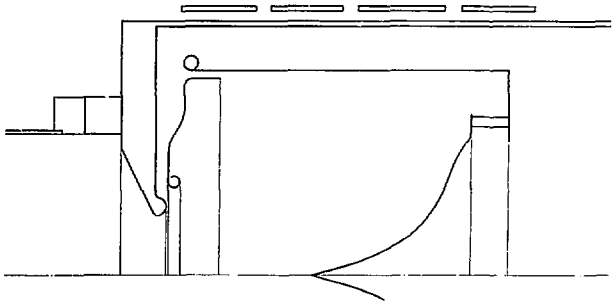

Fig. 7. Collector

ACCOMMODATING STOCHASTIC COOLING AT FERMILAB

P. McIntyre and A. Ruggiero
Fermi National Accelerator Laboratory

Considerable interest has been focused on the possibility of using stochastic cooling to augment or replace electron cooling in an ultimate $\bar{p}$ source at Fermilab. Unfortunately, there is a mismatch between the "natural" $\bar{p}$ production cycle time and the cooling (or precooling) time using stochastic cooling. We calculate here the extent of the mismatch and suggest a possible way of resolving it.

The $\bar{p}$ production cycle using electron cooling proceeds as follows:

1. Fill the Main Ring with $N_p \geq 2\times10^{13}$ protons, and accelerate to 80 GeV ($t_p \sim 1.6$ sec);

2. Extract a Booster-length bunch of protons and target to make $\bar{p}$'s;

3. Decelerate $\bar{p}$'s in the Booster and transfer to the cooling ring;

4. Cool $\bar{p}$'s and accumulate (t_c).

Steps 2, 3, and 4 are repeated 13 times until all protons have been targeted. The average $\bar{p}$ accumulation rate is $R_{\bar{p}} = N_{\bar{p}}\,\eta/T$, where $\eta = N_{\bar{p}}/N_p$ is the $\bar{p}$ yield and $T = 13\,t_c + t_p$ is the production cycle time. For electron cooling, we expect to achieve $t_c \sim 50$ msec, $T \sim 3$ sec, and $\eta \sim 2\times10^{-7}$. This corresponds to a $\bar{p}$ collection rate $R_{\bar{p}} = 1.3\times10^{6}$/sec.

Stochastic cooling is characterized by larger phase space acceptance but longer cooling time than electron cooling. CERN expects to achieve $t_c \sim 2$ sec (stochastic momentum cooling), $T \sim 2.5$ sec, $N_p \sim 10^{13}$, $\eta \sim 2.5\times10^{-6}$, corresponding to a collection rate $R_{\bar{p}} = 1.0\times10^{1}$/sec.

To realize stochastic $\bar{p}$ cooling and accumulation at Fermilab, one could use a production cycle similar to the one for electron cooling:

1. Fill the Main Ring with $N_p \geq 2\times10^{13}$ protons, and accelerate to 80 GeV ($t_p \sim 1.6$ sec);

2. Extract a Booster-length bunch of protons and target to make $\bar{p}$'s;

3. Stochastically cool the $\bar{p}$'s and accumulate successive production cycles until all N_p protons have been targeted.

Long-term accumulation could be accomplished in the stochastic cooling ring itself (the CERN scheme) or by decelerating the stochastically cooled $\bar{p}$'s from each production cycle to 200 MeV and accumulating them in a separate electron cooling ring.

We can now compare the $\bar{p}$ yield using stochastic cooling to that using electron cooling. The cycle time is much longer with stochastic cooling:

$$T = 13\,t_c + t_p \sim 28 \text{ sec!}$$

The $\bar{p}$ yield for the same phase-space acceptance at Fermilab would be greater by a factor of 4 than that of the CERN design due to the higher energy of the targeted protons: $\eta \sim 10^{-5}$. This yield is 50 times greater than that using electron cooling. The collection rate would be $R_{\bar{p}} = 7.0\times10^{6}$/sec. Most of the increased $\bar{p}$ yield is used simply to compensate for the ($\times10$) longer production cycle time, yielding only modest ($\times5$) improvement in $\bar{p}$ collection rate.

This mismatch could be largely overcome by using the Energy Doubler/Saver ring to momentum-stack protons at 80 GeV prior to extraction and targetry. Assuming a 10-turn stack, we obtain $N_p = 2\times10^{14}$;

$$T = 13\,t_c + 10\,t_p \sim 46;\quad R_{\bar{p}} = 4.3\times10^{7}/\text{sec}.$$

In effect the use of momentum stacking makes the $\bar{p}$ production time (~2 sec/stack for 10 stacks) match the cooling time (2 sec per bunch for 13 bunches), as was the case for electron cooling. This in turn allows efficient use of the increased phase space acceptance.

A crucial requirement for this scheme is clearly a 10-turn stacking capability in the Energy Doubler. Also, the $\bar{p}$ production target must survive the impact of $\sim10^{13}$ 80-GeV protons.

STOCHASTIC COOLING WITH NOISE AND GOOD MIXING

A. G. Ruggiero
Fermi National Accelerator Laboratory

I. Introduction

In this note we shall make a few observations and derivations of the stochastic cooling theory. We shall work in the time domain as it was originally proposed by Van der Meer[1] and later amplified by Hereward,[2] This approach is called old-fashioned by some, a term which I do not understand. The new-fashioned method is to carry out the analysis in the frequency domain. This I believe to be a matter of taste and costum, but the two methods are equivalent and ought to give the same result. After all, a system frequency response can be replaced by an equivalent Green's function, and impedances and phase factors can be replaced by amplification and delay coefficients.

The ingredients that are required can be summarized as follows:

(i) A proper definition of the beam signal. This includes a single-particle signal as well as the signal produced by the surrounding ones. Several people like to distinguish the two contributions and call the latter beam or Schottky noise. I believe that this is relevant only up to some point, as we shall see later.

(ii) A proper definition of the noise from the amplification chain. This is a wide-band noise, also called "white" noise. Its spectrum is constant and its effect is completely random. It is quite different from the beam noise, which is not "white," but has a preferential frequency distribution. The integration of the beam-noise spectrum actually leads to a correlated time-dependent signal. To some, the term beam noise could be misleading. Thus one can expect different effects of the system noise and of the beam noise. It is not obvious that they should be simply added to each other.

(iii) Systematic loop errors. We give a few examples: the center of the beam can slowly move from turn to turn, or conversely the pickup device is not centered on the beam center; in the case of the notch filter device, the reference revolution frequency is not accurately determined. These errors would eventually lead to beam "heating" in the same way as the loop noise does.

(iv) Mixing of the signal. This is a crucial issue. Mixing is strongly beam-momentum dependent. Good mixing is achieved in the limit of $\gamma=1$. For large momentum the focusing of the ring is important; one would like to have a transition energy as low as possible. Mixing plays an important role in stochastic-cooling theory and one can draw different conclusions about cooling beams at diferent momenta that at first might sound contradictory. For example, in a bad mixing situation (large momentum) it seems preferable to work in a higher frequency range and momentum cooling seems to be more effective than betatron cooling. At the other end, in the limit $\gamma\to1$, betatron cooling and momentum cooling are equally effective because the mixing situtation is bettor.

In all papers on stochastic cooling, one finds the statement that the method does not depend upon beam momentum. I believe this is not correct; not only does the mixing have a strong energy dependence, but also the electronic gain required for a given cooling rate is reduced at least with the first power of the beam momentum. Mixing also enters again in the cooling rate itself, since bad mixing leads to lower rates.

I believe these considerations are very relevant and should be taken into account in designing a large p-$\bar{p}$ colliding device. In this note, we shall look eventually to the case of good mixing, that is, the low momentum case. I believe that partial mixing can also be included in the following time domain, old-fashioned theory, but we shall leave it out for the moment.

Another reason to investigate the low-momentum case is that because we plan to carry out an experiment at Fermilab on the Electron Cooling Ring, we need to become acquainted with the technique.

II. The Stochastic Cooling Loop

The stochastic cooling loop is shown in Fig. 1.

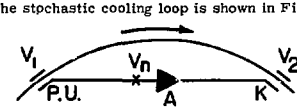

Fig. 1 The cooling loop

A fast beam detector PU is located somewhere around the ring. The pickup and the electronics which supply it have a characteristic rise time τ, so that if there are N particles uniformly spread around the ring, at any given time it is possible to observe a sample of n particles with

$$n = \frac{\tau}{T_0} N = \frac{\tau I}{e}, \qquad (1)$$

where T_0 is the revolution period and I the beam current. From the pickup we expect a voltage V_1 which is modulated with time by the beam with resolution τ. We can write,

$$V_1 = s I \tau \bar{z}, \qquad (2)$$

where s is the sensitivity and $\bar{z}$ the beam signal, which could be the average displacement from a reference orbit of the n particles simultaneously detected or their off-momentum value as it is measured, for example, by the notch-filter technique at CERN. Because we are interested in the case of full mixing, we do not have to be specific about the beam signal; the following considerations apply to either betatron or momentum cooling. Nevertheless, the signal could be a combination of stochastic, coherent, and error contributions which are all function of time.

We do not have to specify the nature of the beam detector but we remark that, since it has to be broadband, its response is proportional to the instantaneous number of particles $I\tau$ as shown in (2).

The pickup voltage V_1 is amplified by a chain of amplifiers and applied to a beam kicker K. This could be either an electrostatic or magnetic deflector for the transverse cooling or a broadband cavity for momentum cooling. Its effect is to modify the motion of the same sample of beam that was measured at the pickup location by an amount which is proportional to the signal $\bar{z}$,

$$V_2 = \kappa\,(\beta p)(g\bar{z}), \tag{3}$$

where κ is a factor which measures the effectiveness of the kicker and g is the dynamic gain, which is the fraction of the signal which is actually damped with the voltage V_2. On the r. h. side of (3) we explicitly show the dependence on the momentum p and velocity β of the beam.

In the following, we assume that the delay between the pickup and the kicker is properly adjusted to guarantee that one is deflecting the same beam sample that has been detected and by the proper amount. We also assume the bandwidths of the pickup and kicker are matched to each other and that, as a consequence, there is no dependence on either I or τ or any of their conbinations on the r. h. side of (3).

Denoting by A the electronic amplification, we have

$$V_2 = AV_1 . \tag{4}$$

Combining (2), (3) and (4) gives

$$A = g\,\frac{\kappa\beta p}{sI\tau}, \tag{5}$$

which shows the relation between A and g, but also the dependence of the required amplification A for a given gain g on the beam momentum and current and on the system bandwidth. We note, though, that the gain g itself could depend on the beam current and the system bandwidth as we shall see later.

Equation (5) is the result that is crucial to our considerations and we will return to it later.

III. Front-End Noise

In the previous section we have analyzed how the beam signal is handled; in the present one we want to deal with another source of signal: the noise which is generated at the front-end of the amplification chain. As shown in Fig. 1 the noise figure is given by a front-end voltage V_n. This voltage is also amplified and applied to the kicker, and the beam at location K does not have the capability of discriminating between the contribution of the beam (V_2) and the noise contribution (AV_n). The beam will experience a total voltage $V_2 + AV_n$ and the system will interpret it as being caused by an equivalent beam signal $\bar{z} + r$ at the location of the pickup. From (2) we derive

$$V_n = sI\tau r, \tag{6}$$

where r is the equivalent beam displacement induced by the noise voltage V_n - observe that this quantity does not depend on the dynamic gain g or on the system amplification A; Eq. (6) represents the only relation which ties r to V_n. The reader should also note the fact that the beam current I and the risetime τ enter the r. h. side of (6).

There is a crucial difference between $\bar{z}$ and r. In the time domain, this difference can be expressed by observing that $\bar{z}$ has a strong autocorrelation, whereas r, being a white noise, is completely uncorrelated in time. By the frequency domain, this is made even more apparent by noting that r has a frequency -independent spectrum, whereas the frequency contained of $\bar{z}$ is lumped around harmonics of the revolution frequency.

The beam signal $\bar{z}$ ultimately leads to a cooling time T_D which is not expected to depend on the noise signal r. On the other hand, r causes a beam diffusion which is made quite visible, for instance, by opening the circuit on Fig. 1 between the P. U. and the K locations in front of the amplifiers. The two effects will eventually balance off to a minimum size that the beam can reach, which is given by the product of the cooling rate and the diffusion constant due to the noise. The characteristic time required to reach this final value is still given by T_D. We emphasize here the analogy of the two effects of damping and diffusion to synchrotron radiation in electron storage rings.

IV. Beam Dynamics

We take a particle in the beam as reference and follow its motion turn by turn. At one particular turn, the m-th, it will be crossing the beam pickup and will be detected together with n other particles Each particle in the sample gives a signal z_i (i=1, 2, ---, n) and the total signal is

$$\bar{z}_m = \frac{1}{n}\sum_i z_i ,$$

where the index m refers to the m-th turn. This sample at the same time has an emittance which can be described by

$$\sigma_m^2 = \frac{1}{n}\sum_i z_i^2 .$$

*We assume that all the n particles travel to*gether between P. U. and K. That is, that no mixing occurs. Then all the particles are kicked by the same amount When the kick is translated to the location of the pickup (we shall always compare the beam at the same location) the coordinate z_i of each particle is modified as follows

$$z_i \to z_i - g\,(\bar{z}_m + r),$$

where we have included both the beam signal and the noise signal. This will have caused the emittance of the sample to change to

$$\sigma_{m+1}^2 = \frac{1}{n}\sum_i (z_i - g\bar{z}_m - gr)^2 \tag{7}$$
$$= \sigma_m^2 - (2g-g^2)\,\bar{z}_m^2 + g^2r^2 - (2g-g^2)\,r\bar{z}_m$$

and for beam bary center

$$\bar{z}_{m+1} = \frac{1}{n} \sum_{1}^{n} (z_1 - g\bar{z}_m - gr)$$

$$= (1-g)\,\bar{z}_m - gr. \qquad (8)$$

When the reference particle is back to the location of the pickup on the next turn, we assume it has lost its companions during the previous turn and is surrounded by n new, different particles (full mixing).

In this way, a new signal is generated and the cycle is repeated again. Since the reference particle will enter different beam samples, one can assume that (7) applies as an average over several turns to the entire beam. In this approximation one does not expect any correlation between r and $\bar{z}$ and therefore the last turn at the right-hand side of (7) does not give any contribution.

Taking m, the number of turns, as a continuous independent variable, we derive the following differential equations from (7) and (8).

$$\frac{d\sigma^2}{dm} = g^2 r^2 - (2g - g^2)\,\bar{z}^2 \qquad (9)$$

$$\frac{d\bar{z}}{dm} = -g\bar{z}, \qquad (10)$$

where, for the last equation, we have assumed that the average value of r is zero.

We have not specified what $\bar{z}$ is. For instance, it could be caused by a coherent beam oscillation with no relation to the beam size σ. In this case, one integrates (10) to get

$$\bar{z} = \bar{z}_0\, e^{-gm}, \qquad (11)$$

which is the usual coherent-oscillation damping formula. The damping rate is given by the gain g, as one would have expected by definition. Insertion of (11) into (9) gives

$$\sigma^2 = \sigma_0^2 + g^2 r^2 m + \frac{2-g}{2}\,\bar{z}_0^2\,(e^{-2gm} - 1).$$

The second turn at the right-hand side is the diffusion term due to the noise, the last the damping of the apparent emittance due to coherent oscillations (the actual beam emittance does not change).

Note that the turn $g^2\bar{z}^2$ on the right-hand side of (9) has also been called the beam noise turn because it adds positively to the system noise $g^2 r^2$. This definition is arbitrary; this term will also be there when $\bar{z}$ is a coherent oscillation, which we can hardly qualify as noise.

The case of interest is when $\bar{z}$ is a pure stochastic signal due to the finite number n of particles in the beam sample. This signal will change randomly from sample to sample with an expectation value given by

$$\bar{z}^2 = \frac{\sigma^2}{n}. \qquad (12)$$

In this situation, we can disregard Eq. (10) and replace r^2 on the right-hand side of (9) by its expectation value. This is justified by the approximation that (9) applies in average over several turns. We obtain

$$\frac{d\sigma^2}{dm} = g^2 r^2 - \frac{2g - g^2}{n}\,\sigma^2. \qquad (13)$$

More generally, one should have also included errors and have written (12) as

$$\bar{z}^2 = \frac{\sigma^2}{n} + z_r^2.$$

But one can combine the effect of z_r^2 with r^2 and probably ignore it as long $z_r^2 << r^2$. We shall assume in the following that is indeed the case.

Eq. (13) was first derived by Hereward,[2] but he integrates it in a curious way. He introduces the quantity

$$\eta = \frac{r^2}{\sigma^2/n} = \frac{\text{noise power}}{\text{signal power}} \qquad (14)$$

and assumes that η is a constant. This could be an approximation at the beginning of the cooling and for slow cooling, when indeed the beam signal does not change much. But in fast cooling σ^2 would change rapidly, whereas r^2 remains constant. In this regime, η can no longer be regarded as a constant.

Eq. (13) can in fact be integrated to give the general solution

$$\sigma^2 = \sigma_\infty^2 - (\sigma_\infty^2 - \sigma_0^2)\,e^{-\alpha m}, \qquad (14')$$

where

$$\sigma_\infty^2 = \frac{ngr^2}{2-g} \quad \text{and} \quad \alpha = \frac{2g - g^2}{n} \qquad (15a \text{ and } b)$$

The solution (14) is also plotted in Fig. 2

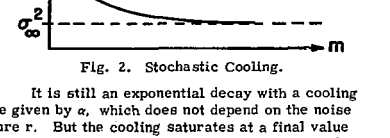

Fig. 2. Stochastic Cooling.

It is still an exponential decay with a cooling rate given by α, which does not depend on the noise figure r. But the cooling saturates at a final value σ_∞ which depends on the noise. When the noise disappears the final size also vanishes.

It is possible that the factor η, Eq. (14), is relatively small at the beginning of cooling, because the beam signal is larger. But toward the end of the cooling, the situation reverses; the noise signal predominates and the factor η cannot be ignored.

Inspection of (15) shows conflicting requirements for the gain g. From one side, one would like

to have fast cooling which requires a large g, possibly g=1. On the other side, if cooling has to be effective, the final size σ_∞^2 should be small which require a small g. The case g=1 would work if

$$\sigma_\infty^2 = \frac{nr^2}{2} \ll \sigma_o^2 .$$

This requires small front-end noise V_n and large bandwidth.

The theory we have outlined above applies only to the case of good mixing. Nevertheless, we may expect that some of the conclusions, at least qualitatively, apply also to the case of bad mixing. For instance, the solution should still have the form of Eq. (14') as sketched in Fig. 2, provided that the cooling rate α and the final beam size σ_∞^2 are properly defined to include a mixing coefficient. One would expect the cooling rate to become smaller and the final beam size to become larger. Thus good mixing represents the optimal situation.

It should be possible to treat the bad mixing case with the approach outlined here by splitting $\bar{z}$ in Eqs. (9) and (10) in two contributions, one from the old particles which still remain with the test particle and one from the new ones which are just refilling the sample under consideration.

V. Consequenses of our Analysis

The conclusion of our analysis can be drawn by combining Eqs. (1), (5), (6) and (15), and

$$T = \text{cooling time} = T_o/\alpha .$$

Several of these equations can be combined to give the following

$$A = g\frac{\kappa\beta p}{es\tau} \tag{16}$$

$$T_D = \frac{\tau}{g}\frac{IT_o/e}{(2-g)} \tag{17}$$

and

$$\sigma_\infty^2 = \frac{gV_n^2}{(2-g)s^2e\tau I} . \tag{18}$$

The next step is to eliminate g from (16) and derive two equations from (17) and (18)

$$\frac{T_D}{T_o} = \frac{\tau I_o^2/4e}{I_o - I} \tag{19}$$

$$\sigma_\infty^2 = \frac{\bar{\sigma}^2 I_o}{I_o - I} , \tag{20}$$

with

$$I_o = \frac{2\kappa\beta p}{As\tau} \tag{21}$$

and

$$\bar{\sigma}^2 = \frac{AV_n^2}{2es\kappa\beta p} \tag{22}$$

These are all the equations that are required to design a cooling loop. They give the cooling time and the final beam size in terms of the machine revolution period T_o, the beam momentum p, the system bandwidth $1/\tau$, the front-end noise V_n, the electronic gain A and the two parameters s and κ which are the sensitivity of the pickup and the effectiviness of the kicker. These equations are quite general.

One has cooling when $s\kappa A > 0$ and $I < I_o$, in which case also $\bar{\sigma}^2 > 0$.

Observe that in the limit of small current, the cooling time is independent of the beam intensity and the system bandwidth

$$\frac{T_D}{T_o} = \frac{\kappa\beta p}{2esA} \tag{23}$$

and

$$\sigma_\infty^2 = \bar{\sigma}^2 \qquad \text{for } I \ll I_o .$$

When I approaches I_o the cooling time becomes infinite and there is no more cooling. The final beam size also diverges because of the diffusion caused by the noise. Observe that there are some conflicting requirements on the electronic gain A, as one can see by inspecting (22) and (23): faster cooling is obtained with larger A, which also causes a larger final beam size. In the limit of small current there is also no dependence on the system risetime.

Our result (19) might seem strange and in contradiction with previous results. This was known under the form of Eq. (15b): for a constant dynamic gain g the cooling rate is proportional to the system bandwidth and to the inverse of the beam intensity. One has cooling only if

$$0 < g < 2 .$$

For practical purposes g is given by (5). Since A is usually a large number, it is the quantity that is kept constant, so that g increases with I. When $I > I_o$ then $g > 2$ and one does not have cooling anymore.

VI. The Experiment at Fermilab

An experiment on stochastic cooling has been proposed at Fermilab, to be carried out in the Electron Cooling Ring at a momentum of 644 MeV/c. The three loops, horizontal (H), vertical (V) and momentum-wise (P) are shown in Fig. 3.

The two loops for damping betatron oscillations have the following parameters:

$s = 200\ V^2 \cdot m \cdot nsec$
$k = 0.05\ V/m \cdot (eV/c)$

and

$\tau = 2nsec$ (200 MHz bandwidth)
$A = 10^6$ (120 db)
$V_r = 10\ \mu V$,

which gives

I_o = 91mA
T_D = 228 sec for $I << I_o$
$\bar{\sigma}$ = 4.6 mm.

The final beam size corresponds to an emittance of $3\pi 10^{-6}$ m (for 95% of the beam). The initial one could be $10\text{-}20\cdot\pi\cdot 10^{-6}$m. The sensitivity figure s given above is for a standard pair of electrodes 6 in. long with a 45° cut. The kicker could also be made of a pair of deflecting electrodes of the same length.

Observe that toward the end of the cooling the ratio of the noise power to the beam signal power, Eq. (14) is given by

$$\eta = \frac{I_o - I}{I},$$

as one can derive from (6) and (20). Thus in the limit of $I << I_o$, one has $\eta >> 1$ and most of the power required is given by the contribution of the noise. If the deflecting plates are matched to an impedance of 50 ohms, with a gain of 120 db and a front end noise of 10μV, the power required is 2W, probably marginal.

References

1. S. Van der Meer, CERN/ISR-PO/72-31.
2. H. G. Hereward, Proc. of the first Course of the International School of Particle Accelerators, Erice, Nov. 1976, page 281. (Hereward made more contributions, but unfortunately they have not all been published).

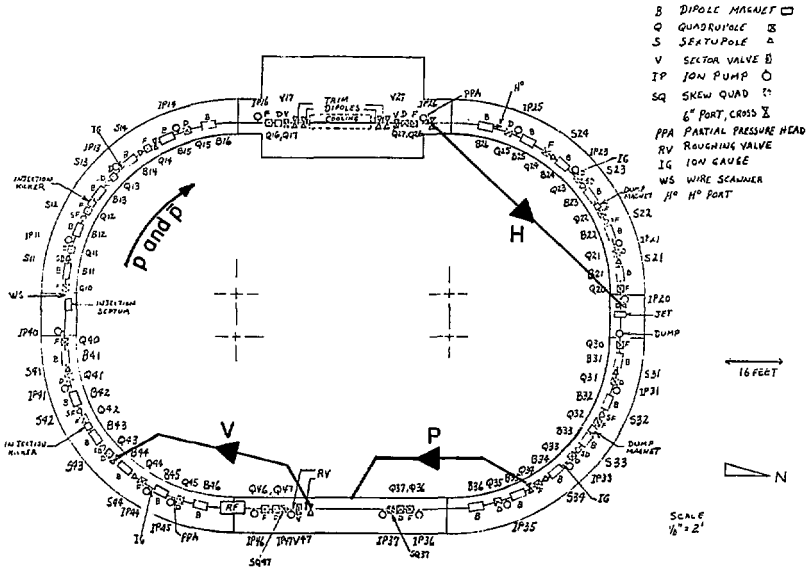

Fig. 3. The stochastic cooling loops for the electron cooling ring.

PROTON COOLING BY RADIATION

R. R. Wilson
Fermi National Accelerator Laboratory

The emission of electromagnetic radiation by electrons moving in magnetic fields (synchrotron radiation) is well understood and has many beneficent effects, such as in the damping of synchrotron and betatron oscillations in circular accelerators or in storage rings. Because the radiation depends inversely upon the fourth power of the mass of the radiating particle (protons radiate less than electrons by a factor of about 10^{13}) synchrotron radiation has as yet been negligible in proton accelerators. However, as proton energies grow ever higher, we eventually will reach a level at which the radiation will become large enough to be effective in damping orbit oscillations.

We can directly take over the theory of synchrotron radiation by electrons as given by Schwinger.[1] The rate of emission is given by

$$E_r = (2\omega e^2/3R)\,|\beta^3/(1-\beta^2)^2|\,, \qquad (1)$$

which for protons becomes

$$E_r = 7.8 \cdot 10^{-12}\, E^4/R, \qquad (2)$$

where the energy emitted per turn E_r and the proton energy E are measured in TeV and the radius of curvature R due to the magnetic field is in kilometers. For the Tevatron, where the radius of curvature is about 0.8 km, the energy radiated per turn is only about 10 eV per turn. At 10 TeV, assuming twice the magnetic field of the Tevatron, E_r would be 200 keV per turn, which is beginning to be significant.

Can such radiation provide cooling of betatron oscillations? The damping coefficient of synchrotron oscillations is given approximately by $2E_r/E$, and of the vertical oscillations by $E_r/2E$. The radial oscillations grow exponentially by the same factor, but can be coupled to synchrotron oscillations to provide overall damping. Thus for the 1 TeV case, if only this damping obtained, then the vertical size of the beam would be reduced by half in about 50 days. For the 10 TeV example, the halving time would be about 5 hrs, which is more significant.

We must also not forget the possibility that coherent effects will enhance the radiation.[2,3] Coherence will occur when the packets of protons are comparable in size to the wavelength of the radiation. The characteristic wavelength, λ_c, of the rather broad distribution of frequencies of the radiation by protons is given in centimeters by

$$\lambda_c = 3.5 \cdot 10^{-4}\, R/E^3. \qquad (3)$$

For the Tevatron with a proton energy at 1 TeV, λ_c is about 3μ.

L. I. Schiff calculated[4] the additional loss per particle per revolution due to coherent radiation in the absence of metallic shielding and found that it is given by

$$\Delta E = \frac{e^2}{R}\, N\, \phi\, 4/3, \qquad (4)$$

for N protons in a gaussian distribution having an angular width of ϕ between the 1/e points. Much of the enhanced radiation is in the microwave region and will be reduced by surrounding metal shielding. Schiff also made a calculation that would apply when the orbit of the particle is midway between two parallel metallic plates. He found for this case that the above result (4) should be reduced by a factor of $5(a/R)^2$ where a is the distance from orbit to plate.

In the Doubler each "bucket" of protons is a narrow pencil, typically about 30 cm long and a few mm in diameter. Hence we might expect some coherent enhancement of the radiation. There are about one thousand buckets, each of which will contain about 10^{10} protons. Hence the extra coherent radiation by each proton will be about 100 eV/turn. Although this may be significant in producing a quite measurable signal, it is not at all clear that it will contribute very much to the damping of random betatron oscillations. Of course, if the center of mass of the coherent bunch is executing a coherent betatron oscillation then that will be dampened. Because any coherent bunch will have a randomly distributed component of protons (proportional to $\sqrt{n}$) executing coherent betatron oscillations, the coherent radiation of the fluctuation from the average will produce a kind of "stochastic" cooling, although of negligible magnitude.

Let us consider briefly the limitation by synchrotron radiation of the growth of a proton beam caused by multiple coulomb scattering of the proton by residual gas. The mean squared height of the beam, $\overline{y^2}$, grows by scattering at a constant rate, i.e., $d\overline{y^2}/dt = a$. That growth is damped by radiation as $dy/dt = -by$, which can be rewritten $d\overline{y^2}/dt = -2b\overline{y^2}$. Without making a distinction between y^2 and $\overline{y^2}$, the sum of the two terms can be set to zero as a rough condition for the asymptotic size, y_o, which is then given by $y_o^2 = a/2b$. Evaluating the constants a and b by the usual approximate relationships gives

$$y_o^2 \approx 10^9\, \frac{R^4}{Qp\, E^5}\, \frac{km}{TeV}$$

where Q is the number of betatron oscillations per turn and the pressure p is in Torr. For a room temperature equivalent pressure of about 10^{-8} Torr of N_2, the beam in the Tevatron would damp down to a height of about 1 mm if it had an infinite lifetime. For larger machines, say E > 5 TeV, or for a better vacuum, the radiation damping would become really effective in reducing the asymptotic size of the beam - a more exact calculation is indicated.

REFERENCES

[1] J. Schwinger, Phys. Rev. 75, 1912 (1949).

[2] A. G. Ruggiero, Fermi National Accelerator Laboratory Internal Report TM-730, April, 1977. The author has considered the Main Ring and the Energy Doubler as a source of synchrotron radiation with special application to the measurement of beam size.

[3] R. Coissen, Opt. Commun. 22, 135 (1977) and Nucl. Instrum. Methods 143, 241 (1977). The author has studied modifications of the spectrum due to non-uniform fields.

[4] L. I. Schiff, Rev. Sci. Instrum. 17, 6 (1946).

NONLINEAR ELECTRON-PROTON INTERACTIONS DURING ELECTRON COOLING

A. G. Ruggiero
Fermi National Accelerator Laboratory

I. Introduction

Electron cooling is the method by which antiprotons will be stored and stacked in the Fermilab $p\bar{p}$ scheme. In the storage ring, either protons or antiprotons will be under the influence of an intense electron beam which occupies a small fraction of the ring circumference. Thus each particle will receive a kick turn after turn which can in good approximation be taken as lumped. The cooling is due to the microscopic structure of the electron beam, that is, to scattering by a large but finite number of electrons. The electron beam can also be regarded as a solid, continuous charge distribution with which one associates a rigid, continuous field. We are interested in the effect of this field on the stability of the motion of the p or $\bar{p}$ particles. This is also called the beam-beam effect which is measured by the beam-beam tune shift. In first approximation, the electron beam can be regarded as a quadrupole with the same focusing action in both planes (focusing for protons, defocusing for antiprotons). Such a quadrupole, when regarded as a perturbation to the lattice of the storage ring, causes primarily a shift of the betatron-oscillation frequencies.

If the electron beam is assumed to have a uniform transverse charge and current distribution, its only effect is betatron tune shift, which is common to all the particles with oscillation amplitude smaller than the electron beam radius. For a non-uniform distribution, a non-linear effect is expected which might cause, in absence of cooling, stochastic behavior of the particle motion which can then be expressed as a diffusion process for the entire beam of hadrons. Such an effect might eventually limit the capability of the electron cooling itself.

According to the design specification, the cathode of the electron gun which generates the electron beam is carefully built to give the most uniform distribution possible. In this case, the linear tune shift can be easily compensated by retuning the quadrupoles of the storage ring. Here we are interested in the case when the electron beam does not have a perfect uniform distribution. We have intentionally exaggerated the beam shape to a Gaussian distribution with a standard-deviation size of 2 cm in both planes in order to test the sensitivity of the primary beam to nonlinearities.

Though the two beam travel in the same direction and the electric field and magnetic field counteract each other, nevertheless, the cancellation is minimal because of the low proton-beam kinetic energy (200 MeV). For an electron current of 25 A and an interaction length of 5 m, the tune shifts are

$$\Delta\nu_x = 0.065 \qquad (\beta_x^* = 20.4 \text{ m})$$

$$\Delta\nu_y = 0.090 \qquad (\beta_y^* = 35.7 \text{ m})$$

II. Method of Calculation

The beam-beam effect is difficult to calculate analytically, so we planned for a numerical simulation of the particle motion under the influence, turn after turn, of a nonlinear lens (the electron beam). The program was developed at Fermilab[1] to investigate beam-beam effects in other colliding-beam situations. After having checked that we do not lose much information from statistical fluctuation between 1000 and 100 particles, we have taken 100 particles for our computation. To each particle we associate four initial conditions: x, x', y, and y'. These are taken randomly with a distribution which describes the proton beam at the crossing location. Our simulation consists in applying simultaneously to all the particles a series of a large number of cycles. Each cycle simulates one revolution and is made of two steps. In the first step, we apply to the particle coordinates a linear transformation with a 4×4 matrix which describes the linear lattice of the storage ring. For its determination we supply β_x, β_y, α_x, and α_y at the crossing point and the two phase advances per turn, the fractional part of the two betatron tunes ν_x and ν_y. The second step simulates the nonlinear kick when crossing the electron beam. For each particle we change z' by

$$\Delta z' = -\frac{4\pi}{\beta_z^*}\Delta\nu_z \frac{1-e^{-u^2}}{u^2} z, \qquad (1)$$

where z can be either x or y and

$$u^2 = \frac{x^2+y^2}{2\sigma^2}.$$

At the same time x and y are unchanged.

Equation (1) is derived in the approximations that β^* does not change across the electron beam length l, and that $\beta^* >> l$.

Every 1,000 turns, four histograms of 20 channels corresponding to the four coordinates are prepared and displayed. Then averages, standard deviations, minimum and maxima are calculated and printed out. We always found that the histograms approximately reproduce a Gaussian distribution. Thus we take the standard deviation as a measure of the beam size. The tracking always takes 50,000 turns which correspond to 40 msec of actual time. At the end, the final beam size is taken by averaging over the last 5,000 turns. The damping due to the electron cooling is not applied during the simulation.

III. The Results

These are shown in Table I through Table VI (see following pages).

TABLE I: $\nu_x = 0.57$, $\nu_y = 0.52$. The final beam size σ and angle ψ are shown versus the initial emittance ϵ, which is defined for 95% of the beam. One observes a shrinking of the beam size at the cost of increasing the angles by a factor two. This is merely due to the betatron mismatch. The increase in angle should eventually be taken into account for setting the initial conditions of the electron cooling.

TABLE I.

ϵ_x	ϵ_y		σ_x	ψ_x	σ_y	ψ_x
$\pi 10^{-6}$ m			mm	mrad	mm	mrad
40	20	(a)	11.0	0.56	10.7	0.30
		(b)	9.7	0.72	8.1	0.73
		(c)	9.4	0.71	8.2	0.72
20	20		6.8	0.51	8.4	0.71
10	10		4.6	0.37	5.8	0.54
5	5		3.2	0.27	4.0	0.40
1	1		1.5	0.12	1.8	0.18

[a] No beam-beam tune shift applied. One thousand particles taken.
[b] Beam-beam tune shift applied. One thousand particles taken.
[c] One hundred particles taken.

TABLE II: $\epsilon = 10\pi\ 10^{-6}$ m. The electron beam is not centered by x_B to the center of oscillation of the protons. No effect of the beam separation has been found.

TABLE II.

x_B	σ_x	ψ_x	σ_y	ψ_y
mm	mm	mrad	mm	mrad
-	4.6	0.37	5.8	0.54
2.5	4.7	0.37	5.8	0.54
5	4.9	0.36	5.8	0.53
7.5	4.9	0.38	6.0	0.51
10.	5.0	0.38	6.0	0.51

TABLE III: The electron beam is displaced from +2 cm to -2 cm in N turns. There is no variation in the beam size and angle. The small differences between the numbers shown in this table and in Table II are due to a minor change of β_x^* and β_y^* in our simulation.

TABLE III.

N	σ_x mm	ψ_x mrad	σ_y mm	ψ_y mrad
1000	5.9	0.40	5.9	0.49
4000	6.7	0.43	5.9	0.49
10000	6.3	0.42	5.9	0.49
20000	6.7	0.48	5.9	0.49
50000	6.7	0.47	6.1	0.48
∞	5.9	0.40	5.6	0.50

TABLE IV: Same simulations of Table III but now the tunes have been changed to

$\nu_x = 0.70$ and $\nu_y = 0.456$.

TABLE IV.

N	σ_x mm	ψ_x mrad	σ_y mm	ψ_y mrad
1000	30.4	1.43	79	1.7
4000	22.5	1.22	74	1.6
10000	28	1.45	71	1.6
20000	22.5	1.17	72	1.4
50000	19.2	1.05	78	1.2
∞	31.3	1.62	80	1.8

The beam size and angle increase are large, as is also shown in Fig. 1. One notices here a linear increase of σ with time at a rate of 5.3×10^{-4} mm/turn. Thus there is definitely a strong tune dependence. This may be caused by the nonlinear mismatch, nonlinear coupling and periodic crossing of resonances induced by the electron beam.

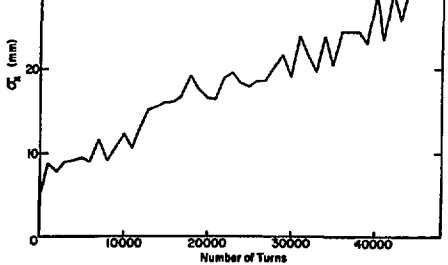

Fig. 1

Care should be taken to tune the storage ring properly to avoid these effects.

Another case is shown in Fig. 2. The electron beam is now moved more slowly (N = 50,000). The beam size at the end is down to the initial value, but one should note the increase in between.

TABLE V: The tunes are set to the original values. The electron beam center is made to oscillate horizontally according to the equation.

$$x_B = a \sin\left(2\pi \frac{n}{N}\right) + x_0.$$

No effect of the periodic movement of the electron beam, either centered or displaced, has been found.

TABLE V.

a mm	N	mm	σ_x mm	ψ_x mrad	σ_y mm	ψ_y mrad
-	-	-	4.5	0.38	5.9	0.55
1	10	-	4.4	0.40	5.9	0.55
1	100	-	4.6	0.37	5.9	0.56
1	1000	-	4.3	0.40	5.9	0.55
5	10	-	4.3	0.40	5.8	0.55
5	100	-	4.6	0.37	5.8	0.57
5	1000	-	4.5	0.38	5.9	0.56
1	10	1	4.5	0.38	5.8	0.56
1	100	1	4.6	0.38	6.0	0.54
1	1000	1	4.4	0.39	6.0	0.55

TABLE VI: The two beams are centered but the two betetron tunes change periodically according to the equation

$$\nu_x = 0.57 + \Delta\nu \cdot \sin(2\pi n/N)$$

$$\nu_y = 0.52 - \Delta\nu \cdot \sin(2\pi n/N).$$

This can either simulate phase oscillations and the machine chromaticity or power-supply ripple. Very large beam size (and angle) increases are now

TABLE VI.

$\Delta\nu$	N	σ_x mm	ψ_x mrad	σ_y mm	ψ_y mrad
-	-	4.5	0.38	5.9	0.55
0.010	10	6.6	0.48	10.0	0.86
	100	4.5	0.39	6.0	0.54
	1000	4.6	0.38	5.9	0.56
0.015	10	50	2.8	84	2.4
	100	4.6	0.38	6.0	0.57
	1000	5.0	0.47	5.2	0.52
0.020	10	76	3.9	108	3.0
	100	118	6.0	368	7.6
	1000	141	7.5	925	19.0
0.030	10	126	7.2	176	5.2
	100	207	10.9	208	10.6
	1000	187	10.0	604	20.5
0.100	10	116	6.7	150	3.9
	100	179	11.2	360	10.2
	1000	195	11.2	507	13.5

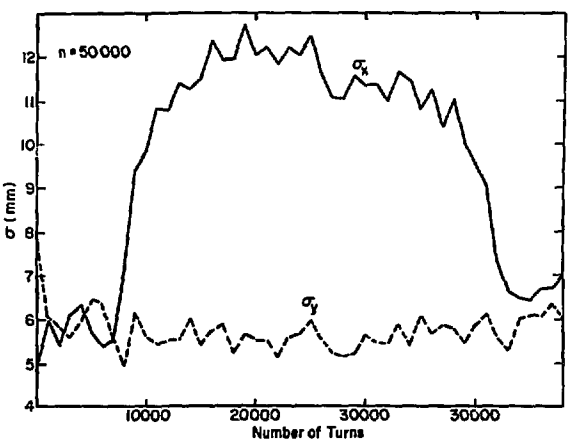

Fig. 2

noticed. Some cases are shown in Figs. 3 and 4. The beam size increases with $\sqrt{t}$ as is seen for the bottom curve of Fig. 4, where the dashed line is indeed a $\sqrt{t}$-curve. The diffusion coefficients $d\sigma^2/dt$ are shown in Table VII in units of m^2/sec. There is an increase of the diffusion with $\Delta\nu$ and N. For $\Delta\nu \lesssim 0.01$, no diffusion was observed, at least for the time explored during the computation.

TABLE VII.

$\Delta\nu$/N	10		100		1,000	
	x	y	x	y	x	y
0.010	-	-	-	-	-	-
0.015	65.1	186	-	-	-	-
0.020	149	305	366	3,562	523	22,515
0.030	417	814	1,127	1,137	920	11,601
0.100	353	587	843	3,409	1,000	6,776

References

1 A. G. Ruggiero, Fermi National Accelerator Laboratory FN-293 and FN-293A, May and June 1976. Also, IEEE Trans. Nucl. Sci. NS-24, 1893 (1977).

IV. Conclusions

If proper care is taken, beam-beam effects can be greatly reduced. Of course our simulation was applied only for a very short period of time (40 msec) and we did not prove the stability of the beam over long times (several hours) at all. On the other hand, we used a model for the electron beam where non-linearities have been intentionally pronounced. Eventually one would expect a distribution close to flat. The other effect which still requires investigation is the limitation of the electron cooling process by nonlinear beam-beam interaction. This effect also should be easily simulated with our computer code and we plan to do so in the near future.

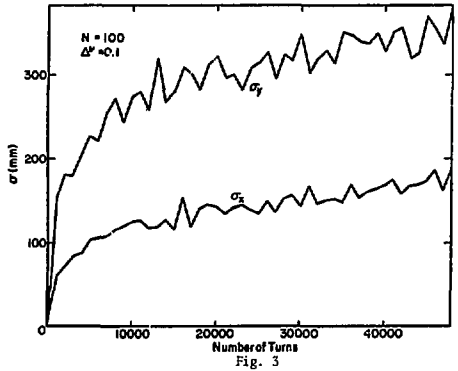

Fig. 3

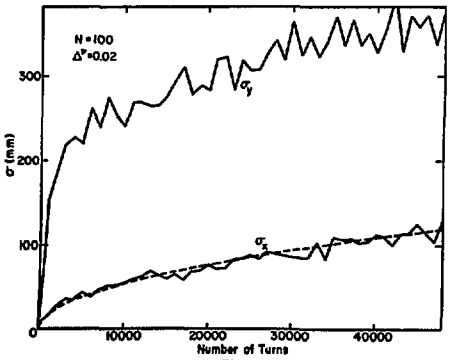

Fig. 4

BEAM STABILITY CONSIDERATIONS DURING ELECTRON COOLING

A. G. Ruggiero
Fermi National Accelerator Laboratory

I. Introduction

The method of cooling protons (and antiprotons) with an electron beam with the same velocity substitutes the damping effect of the synchrotron radiation for electron beams. At first sight one might think that proton beams can be cooled down to practically vanishing size. The only limit that was taken in the past (and, I would say, rather roughly) is the temperature of the electron beam.

Actually operation of electron cooling at low momentum is expected to be very sensitive to the final beam density, because space-charge and beam-stability limits are rather rapidly reached at low energies. Therefore, in this paper we calculate the beam-stability and space-charge limits for the electron-cooling experiment that is planned for Fermilab at 200 MeV kinetic energy. We find that the beam can be cooled down only to densities (longitudinal as well transverse) comparable to those presently obtainable with a proton beam circulating in the Booster at 200 MeV. Thus for very small intensities, one can also expect very small emittances, but if the beam current is raised the final equilibrium emittance must also increase. The equilibrium is given by the balancing two effects: the cooling damping and the space charge and collective phenomena that would make the beam blow up again. These effects do not interfere with the collection of antiprotons, because electron cooling makes space for new beam pulses. But once intensities similar to those we operate the proton beam are reached one should also expect the same emittance value for the antiproton beam.

In the following we estimate the beam stability against well-known theories.

II. Self-Bunching of the Coasting Beam

The scheme for $\bar{p}$ collection at Fermilab considers a combination of electron cooling and rf stacking. In this section we deal with stability against self-bunching of the stack. A crucial parameter for this sort of instability is the longitudinal impedance. The contribution from the self-field is

$$\frac{Z}{n} = i\,\frac{Z_0}{2\beta\gamma^2}\left(1 + 2\,\lg\frac{b}{a}\right) \sim 1\ k\,\text{ohm}, \qquad (1)$$

where Z is the equivalent impedance at the harmonic number n, $Z_0 = 377$ ohm, and a and b are respectively the beam and pipe radii. Observe that this impedance is large and therefore likely predominant compared with any other wall contribution. It is a pure positive reactance (anti-inductance) and does not cause any instability below transition energy, provided that it is the only existing one.

The stability diagram[1] is shown in Fig. 1, where,

$$U' - iV' = -i\,\frac{2eI\beta^2 Z/n}{\pi\,|\eta|\,E\left(\frac{\Delta E}{E}\right)^2}$$

and

I = beam current
$\beta = v/c$
$\eta = 1/\gamma_T^2 - 1/\gamma^2$
E = total particle energy
$\Delta E/E$ = full energy spread at half maximum of the energy distribution

The various curves correspond to different distributions:

1. Lorentzian
2. Gaussian
3. 5th-order parabola
4. 4th-order parabola
5. 3rd-order parabola
6. Squared cosine
7. 2nd-order parabola
8. Truncated cosine
9. 1st-order parabola

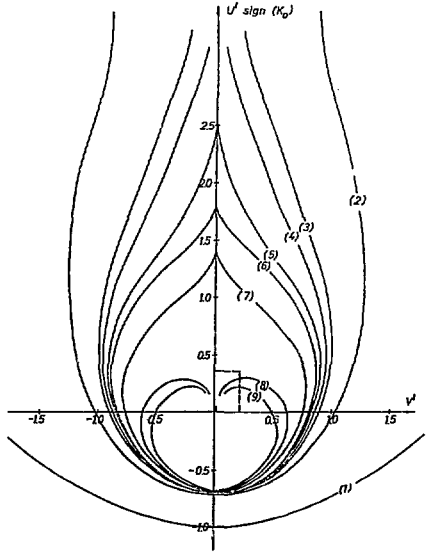

Fig. 1. Longitudinal stability diagram.

In our case $\gamma < \gamma_T$; thus one takes $k_o > 0$.

It is hard to make a judgement on beam stability since this depends very much on the energy distribution. The self-impedance (1) is very large and can hardly be reduced by an inductance. The only possible effect which can cause an instability is a resistance which moves the impedance along the V' -axis. In fact one has instability for a given distribution when *the impedance point lies outside the boundary curve* for that distribution shown in Fig. 1. Since U' is rather large, a small amount of resistance can move the point outside the stability diagram for practically all the distribution functions except the Lorentzian one.

In any case, the stability criterion is [2]

$$\left|\frac{Z}{n}\right| < \frac{E|\eta|}{eI\beta^2}\left(\frac{\Delta E}{E}\right)^2 .$$

If we take I= 2mA, equivalent to $N = 10^{10}$ particles $\Delta E/E = 10^{-5}$, corresponding to a longitudinal electron-beam temperature

$$T_{\parallel} = 0.4 \text{ eV}$$

we obtain

$$|Z/n| \sim 120 \text{ ohm}.$$

Thus the beam could be very unstable.

For 1 KΩ impedance, the threshold is

$$(\Delta E/E)_{th} = 3 \times 10^{-5}. \qquad (2)$$

Since the cooling is a relatively slow process and one begins with a spread much larger than (2), it would also represent the final beam spread. If the operation is less adiabatic, it is proper to make use of the overshoot formula

$$\left(\frac{\Delta E}{E}\right)_{\text{final}} \left(\frac{\Delta E}{E}\right)_{\text{initial}} = \left(\frac{\Delta E}{E}\right)_{th}^2$$

to calculate the final spread $(\Delta E/E)_{final}$. If one takes $(\Delta E/E)_{initial} = 10^{-5}$, then

$$(\Delta E/E)_{final} = 10^{-4},$$

quite a reasonable number.

III. Transverse Stability of the Stacked Beam

Because of the very small momentum of the beam, in this case the self-field is also predominant.

Define the transverse impedance

$$Z_{\perp} = \frac{iRZ_o}{\beta^2\gamma^2 a^2} + \frac{2ZR}{b^2(n-\nu)\beta}$$

$$= \text{self-field} + \text{wall impedance}$$

Uncooled Beam

Let us consider first the case in which the beam is not cooled transversely, but it is eventually in momentum. Then we take

R = machine radius ~ 22 m
a = 1 cm
b = 3 cm
ν = betatron tune ~ 4

and we have

$$Z_{\perp} = \left(i\,1.7 \times 10^8 + 8.5 \times 10^4 \frac{Z}{n-\nu}\right) \Omega/\text{m}$$

where Z is the wall impedance at $(n-\nu)$ times the revolution frequency. The wall effect is negligible provided that

$$\frac{Z}{n-\nu} << 2\text{K}\Omega,$$

which we expect to be the case.

The tranverse impedance $Z_{\perp}$ has the effect of causing a shift of the betatron oscillation angular frequency [3]

$$\Delta\omega = i\,\frac{ecZ_{\perp}I}{\nu\gamma^4\pi E_o}$$

E_o = 938 MeV, rest energy. With only the self-field contribution, the shift, though large, is nevertheless real and the beam is stable against collective instabilities. Yet a very small resistive-wall impedance makes the shift complex and, eventually, the beam unstable. One observes here an analogy of behavior with the longitudinal case discussed in the previous section.

If we take I = 2mA and $|Z_{\perp}| = 170$ MΩ/m then

$$|\Delta\omega| = 2 \times 10^3 \text{ s}^{-1}.$$

The beam is made stable by providing enough spread at the offending frequency $(n-\nu)\omega_o$; ω_o being the angular revolution frequency, so that [3]

$$\Delta|(n-\nu)\omega_o| > |\Delta\omega|.$$

(1) Stabilization from revolution frequency spread. This requires

$$(n-\nu)\frac{\omega}{\beta^2}|\eta|\frac{\Delta E}{E} > 2 \times 10^3 \text{ s}^{-1}.$$

The smallest number we can conceive for $\Delta E/E$ is 10^{-5}, which equals the longitudinal temperature of the electron beam. In practice, $\Delta E/E$ will be larger either because of intra-beam scattering or because the beam is longitudinally unstable. In this last case, we have an upper limit of 1×10^{-4} from the overshoot criterion. All the modes

$n > \nu + 12$ for $\Delta E/E = 10^{-5}$
$n > \nu + 1$ for $\Delta E/E = 10^{-4}$

are stable. The lower modes could be damped with electronic feedback. The bandwidth required is at most 15 MHz. With a slightly larger $\Delta E/E$, the entire mode spectrum can be made stable and there will not be any need of a damper system that can ultimately interfere with the stacking operation.

(ii) Stabilization from tune spread. This requires

$$\Delta\nu > \frac{|\Delta\omega|}{\omega_o} = \frac{2\times 10^3}{\omega_o} = 2.5 \times 10^{-4}.$$

This is a rather small spread. The tune shift due to the crossing with the electron beam is as large as 0.06 and a fraction of this is presumably a spread across the beam. There are also contributions from the beam emittance ϵ and the non-linearities of the guide field around the ring.

(iii) Stabilization with chromaticity. The amount of chromaticity

$$\xi = (\Delta\nu/\nu)/(\Delta p/p)$$

required depends on the energy spread as is shown in the following table.

Beam	$\Delta E/E$	$\xi \rightarrow \Delta\nu = 2.5 \times 10^{-4}$
Long. stable and cooled	10^{-5}	-2.2 (too large)
At the threshold of long. stabil.	3×10^{-5}	-0.73
Overshoot	1×10^{-4}	-0.22

It is required to blow up the beam somewhat longitudinally to get moderate chromaticity.

In general, the stability condition is

$$\Delta\left|(n-\nu)\frac{\omega_o}{\beta^2}\eta\frac{\Delta E}{E} + \nu\frac{\omega_o}{\beta^2}\xi\frac{\Delta E}{E} + \omega_o K\epsilon\right| > |\Delta\omega|.$$

To avoid cancellation, all the three terms must have the same sign. Since only the terms $n > \nu$ are unstable and $\eta < 0$ below the transition energy, the chromaticity ξ and the octupole strength K ought to be negative. This of course is relevant only when the three contributions to the spread are of the same order.

Transversally Cooled Beam

The radius of such a beam could be much smaller than what we have considered above. A final size a = 1 mm corresponds to an electron-beam temperature of 0.4 eV. In this case, Z_1 and $\Delta\omega$ are one-hundred times larger and pose serious concerns about the stability of the cooled beam. The amount of time spread which is now required is about 0.025, too large to be attained with reasonable chromaticity or octupole. An electronic feedback damper should have a band width larger than 60 MHz, rather hard to make.

Things can improve considerably if one lets the beam blow up further longitudinally, say up to

$$\frac{\Delta E}{E} = 1 \times 10^{-3},$$

which is the maximum the Booster rf system can accept. With this spread, all the unstable modes are given by

$$n - \nu \lesssim 12$$

which could be stabilized with a 15 MHz damper.

Of course, the other alternative is to give up transverse cooling completely and rely only on longitudinal cooling.

IV. Growth Rates

Most of the concern of course goes to the case in which the instabilities grow so fast that one can disregard the electron cooling itself. Eventually electron cooling might have the nice feature that it damps those instabilities which grow slowly compared to the cooling time.

The instability growth rate, in the absence of Landau damping is essentially given by the resistive part R_n of the impedance. In the limit when R_n is small compared with Z_n, one has

$$\frac{1}{\tau_n} \sim \frac{R_n}{|Z_n|}\,|\Delta\omega|,$$

where $|\Delta\omega|$ is the frequency shift. This would suggest that as long as $\tau_n >> \tau$, the cooling time, the beam should be stable.

There are some uncertainties about τ; thus we take

$$\tau_n \geq 1 \text{ second}.$$

This condition, applied to the transverse case, is actually independent of the beam size. For the transverse case

$$|\Delta\omega| = 2 \times 10^3 \text{ s}^{-1}$$

$$\frac{Z_n}{n} = \frac{b^2\beta Z_1}{2R} \sim 2\ \text{K}\Omega$$

and one derives

$$\frac{R_n}{n} < 1\Omega.$$

If this condition is satisfied, the transverse cooling process is presumably fast enough to damp any coherent oscillation.

V. Bunched Beam

There are only two situtation where the beam is bunched:

(i) During stacking - Each pulse has a much lower intensity, approximately 2μA, which corresponds to 10^7 ppp. The spreads of each of these pulses that

are not yet cooled, are also considerably larger. Thus we do not expect any transverse or longitudinal instability in this situation. Bunch-to-bunch instabilities should also not play a major role.

(ii) rf capture of the beam after stacking. If the coasting beam criteria are met when the average current is replaced by the peak current, the individual bunch modes as well as the bunch-to-bunch modes are stable. It is thus important to bunch the beam at a resonably low bunching factor, possibly 2 or 3, and extract the beam as rapidly as possible. Unfortunately, injection of the beam in the Booster will not soften the situation. The beam spreads are bound to increase to overcome the instabilities.

A final momentum spread up to 10^{-4}-10^{-3} can be expected. The transverse emittance will also grow but will be likely to be within the Booster acceptance.

VI. Incoherent Space Charge Limit

The incoherent space charge induces a betatron tune shift that is given by[4]

$$\Delta\nu = -\frac{rFN}{(\pi\epsilon_V\beta\gamma)\left(1+\sqrt{\frac{\epsilon_H}{\epsilon_V}}\right)\beta\gamma^2 B}$$

$$F = 1 + \frac{b(a+b)}{h^2}\left\{\epsilon_1\left[1+B(\gamma^2-1)\right] + \epsilon_2 B(\gamma^2-1)\frac{h^2}{V^2}\right\}$$

N = total number of particles in the ring
$r = 1.5347\times10^{-18}$ m
B = bunching factor (< 1)
b = mean semi-minor beam axis (vertical)
a = mean semi-major beam axis (horizontal)
2h = vertical vacuum-chamber aperture
2w = horizontal vacuum-chamber aperture
2v = height of magnet gap.

ϵ_1 (~0.2) and ϵ_2 (~0.4) are the Laslett image coefficients. ϵ_V and ϵ_H respectively the vertical and horizontal emittance.

For our case it is a good approximation to take

$$F = 1$$

$$\epsilon_H \sim \epsilon_V = \epsilon$$

$$\epsilon = a^2/\bar{\beta} \text{ with } \bar{\beta} = R/\nu \sim 5 \text{ m}.$$

For a transversally-cooled beam a ~ 1 mm (equivalent to the electron beam temperature $T_\parallel$ = 0.4 eV) and

$$\epsilon = 0.2\times10^{-6} \text{ m},$$

which gives

$$\Delta\nu = 2.1\times10^{-12} \text{ N/B}.$$

For a 10 mA beam

$$\Delta\nu = 0.02/B.$$

If during the final rf capture of the stack B ~ 1/5, then $\Delta\nu$ = 0.1 which may be reasonable.

VII. Conclusion

It seems that the cooled beam is too unstable to reach the spreads which are in equilibrium with the electron beam. Because of longitudinal and transverse instabilities the final spreads (momentum spread and transverse emittance) will be somewhat larger. The final values will probably equal the threshold values of the various instabilities, provided the cooling process is adiabatic enough. Otherwise "overshoot" will occur. Nevertheless, even in this case the final growth should be small enough to lead to emittances and spreads easily accepted by the Booster.

References

1. A. G. Ruggiero and V. G. Vaccano. ISR-TH/68-33 CERN, 1968.
2. E. Keil and W. Schnell, ISR-TH-RF/69-48 CERN, 1969.
3. F. J. Sacherer, Proc. 9th Int. Conf. on High Energy Accelerators p. 347, SLAC, Stanford, Cal.
4. L. J. Laslett, Proc. 1963 Summer Study on Storage Rings, BNL 7534, p. 324, Brookhaven National Laboratory, New York.

ANTIPROTON MOMENTUM COMPACTOR-DEBUNCHER LINAC

Lawrence W. Jones
University of Michigan
Department of Physics
Ann Arbor, MI 48109

The momentum acceptance of the Fermilab booster for 5.18 GeV$\bar{p}$'s limits the accepted $\bar{p}$ momentum spread to $\delta P/P = 3 \times 10^{-3}$. It is noted here that a larger momentum spread from a $\bar{p}$ production target may be accepted if a short linac section is used to give the $\bar{p}$'s an energy kick following a drift space from their production target, so that their time of arrival at the linac is related to their momentum error.

The scenario would be as follows: first the 80 GeV protons in the MR would be debunched (not necessarily completely) and then rebunched tightly at a high frequency f by a linac section. Then the extracted protons would strike the $\bar{p}$ production target in tight bunches, e.g., spread in time by $\lesssim 0.1\ f^{-1}$. Then a drift space Z would follow (occupied by the $\bar{p}$ beam transfer optics). Finally, a linac section, also at f and phased with the section in the main ring, would transmit the central particles of each spread bunch at 0° phase angle but would accelerate the late particles and decelerate the early particles in order to leave an ongoing beam debunched in time (over $\lesssim \pi$ radians) but homogenized in momentum. This beam is then inflected into the booster for deceleration and cooling.

The time dispersion of particles starting simultaneously after drifting a distance z meters in terms of their energy difference is given by

$$\delta t = \frac{\delta z}{c} = \frac{\delta\gamma}{\gamma^3}\frac{z}{c}, \qquad (\gamma \gg 1),$$

so that

$$\frac{dE}{dt} = \frac{E_o\gamma^2 c}{z}, \quad \left(\frac{\delta\gamma}{\gamma} \cong \frac{dE}{E_o}\right).$$

This energy spread can be compensated by an energy kick from the linac section where, from the linac rf,

$$\frac{dE}{dt} = 2\pi\ f\ E_L,$$

and E_L is the peak energy of the linac.

The momentum spread which can be compressed is just $2E_L$ for a maximum, although the linear portion of dE/dt is ~ 2/3 of that. Combining the two above expressions,

$$2\pi\ f\ E_L = \frac{E_o\gamma^2 c}{z},$$

or

$$z = \frac{E_o\gamma^2 c}{2\pi f E_L}.$$

As a numerical example, consider 5.18 GeV $\bar{p}$ ($\gamma = 6.51$) with a 3% momentum spread compressed by a linac section of 1.0 GHz. The linac energy E_L would have to be at least 0.015 x 6 GeV = 90 MeV.

To preserve a greater region of linear dE/dt, E_L = 130 MeV. These values give

$$z = 121 \text{ meters}.$$

The 3% momentum spread will be compressed to a fraction of 3% corresponding to the tightness of the 1 GHz bunching of the protons; if they are bunched to $1/20 \times 10^{-9}$ sec (1.5 cm), the 3% should compress to about 0.2% $\Delta p/p$.

There are some questions. The rf on-time required for the high frequency bunching hardware in the main ring is long, corresponding to a phase oscillation period at that frequency. Of course only one booster batch need be bunched each booster extraction cycle (60 millisec, the rf could be on for 1.5 μsec and off for 19 μsec each revolution). The second, debunching rf, would only need to be on for 2 μsec.

The path length dispersion from the betatron phase space in the $\bar{p}$ beam transport must be small compared to the energy-related dispersion. Hence if the beam crosses the axis at 10 mr, the path length spread of extreme rays is $\sim \frac{2}{3}\frac{\theta^2}{2} \cong 3 \times 10^{-5}$. This corresponds to $\delta E/E_o = 1.26 \times 10^{-3}$.

If the rf systems are reasonable, technically and economically, it seems that a scheme such as this could gain a factor of 10 in $\bar{p}$ flux and require minimal new construction or engineering. In particular, this could obviate the need for a stochastic cooling ring.

HIGH-ENERGY ELECTRON COOLING

A. G. Ruggiero
Fermi National Accelerator Laboratory

Introduction

Electron cooling at high energies with an electron beam circulating in a storage ring was proposed a long time ago,[1] but the idea was dismissed with a premature judgment of the impossibility of achieving a reasonably fast cooling rate with the beam density available. For instance, the present Fermilab[2] scheme has a projected cooling time of 50 msec with an electron current density of 1 A/cm^2 at $\beta = 0.566$. At larger energies, because of the strong dependence of the cooling rate on the beam momentum, a reasonable cooling rate can be obtained only with very high electron densities. Recently C. Rubbia[3] pointed out that indeed such large densities are available in stored electron bunches. An average beam current of 100 mA already would correspond to a peak current of tens of amperes. The beam transverse size can be made quite small, down to a millimeter or even less, giving a local density of thousands of A/cm^2 or more.

Rubbia's second point was that at high energies, electrons radiate, so whatever momentum is transferred to them by cooling a proton or antiproton beam will be carried away as radiation, allowing the electron beam to preserve its size, though at the cost of some enlargement.

Finally, the third thing pointed out by Rubbia is that at high energies fast cooling rates are not necessarily required.

There are two possible applications of the high-energy electron cooling:

1. It could be possible to raise the beam-beam limit from the canonical number of $\Delta\nu = 0.005$ to, say, $\Delta\nu = 0.02$. This would increase the luminosity by an order of magnitude. Indeed larger $\Delta\nu$ values cause shortening of the beam lifetime because of a hypothetical Arnol'd diffusion process. The effects of this process can eventually be balanced with electron cooling.

2. The one-beam lifetime itself, even in the absence of the second one, could be too small due to processes like gas scattering. The "heating" of the proton beam caused by such a process could then be balanced off by taking the "heat" away from the beam by means of "electron cooling."

In the following we shall look in more detail at the feasibility of high-energy cooling, especially in the context of an experiment for the Main Ring with the aim of lengthening the beam lifetime. Although some approximation in our approach cannot be avoided, we are nevertheless mostly interested in a self-consistent solution which takes into account the behavior of the equilibrium of the proton (antiproton) beam as well as the electron beam, which we assume is circulating in a storage ring.

At the end, we also look at the features of the electron storage ring which, as one would expect, is mostly made of wiggler magnets.

Electron and Proton Beams in Absence of Cooling

The high-energy electron cooling scheme is the one outlined in Fig. 1. There are two rings: one could be identified with the Main Ring where protons are circulating at a constant energy E_p and the other

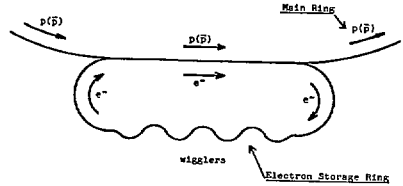

Fig. 1. High energy electron cooling plan.

with an electron storage ring at energy E_e. The two energies are adjusted so that the two beams have the same velocity. The two rings also share a long straight section of length ℓ where proton bunches and electron bunches travel together in the same direction. We make the obvious assumption that the two kinds of bunches are roughly matched in size and length.

In the following we shall denote by subscripts "e" and "p" the quantities which refer respectively to the electrons and to the protons.

In the absence of interactions between the two beams, we can write the following equations for the rms beam emittance ($\epsilon = \sigma^2/\beta$)

$$\frac{d\epsilon_p}{dt} = D_p \qquad (1)$$

$$\frac{d\epsilon_e}{dt} = -\frac{2}{\tau}\epsilon_e + D_e. \qquad (2)$$

We assume both beams are round, namely, that they have the same horizontal and vertical emittance.

In the absence of diffusion-like processes and of damping effects, the emittances are normally considered invariants. The diffusion coefficient D_p on the right-hand side of (1) is primarily given by gas scattering and similar effects. This diffusion is not compensated by damping and will cause a linear increase of the beam emittance with time. The beam size increase will stop when the beam edge has

reached an aperture limitation; after that particles will be continuously lost. In observations in the Main Ring, the following was found[4]

$$D_p = 5 \frac{P_{Torr}}{P_{GeV/c}^2} \text{ m/sec.}$$

At 100 GeV, with a pressure of about 5×10^{-8} Torr, this would correspond to $D_p = 0.25\times10^{-10}$ m/sec.

In Eq. (2), τ is the synchrotron radiation-damping time and D_e the quantum-fluctuation diffusion coefficient. The electron beam would have an equilibrium emittance which is given by

$$\bar{\epsilon}_e = \tfrac{1}{2}\tau D_e. \qquad (3)$$

This equilibrium value is reached in the e-folding time $\tau/2$.

Observe that τ and D_e depend strongly not only on the beam energy but also on the electron-beam storage ring lattice.[5]

The Electron-Cooling Effect

We want now to modify Eqs. (1) and (2) to include the beam-beam interaction, which is supposed to lead to "cooling" of the proton beam at the cost of some "heating" of the electron beam.

Because of the large energy and since the electron beam is already focused by the lattice quadrupoles and rf cavities, we do not have to take into account space-charge effects on the trajectory of the electrons, and we do not have to guide their motion with a solenoid as is done at lower energies. In addition, one can easily verify that at larger energies

$$\theta_{\parallel} << \gamma\theta_{\perp},$$

where $\theta_{\parallel}$ and $\theta_{\perp}$ are respectively the longitudinal and transverse relative momentum spreads. This is true for both beams. Thus we are in the situation of a longitudinal flattened ellipsoidal distribution of velocities. In this case, the transverse-energy exchange between the two beams depends only on the transverse emittance of both beams and, therefore, can be decoupled from the longitudinal-energy exchange. In this approximation, the usual formula for the damping rate of the transverse velocity is[6]

$$\frac{1}{\tau_p} = \frac{3\pi e^4 L}{m_p m_e c^4} \frac{\eta_p}{\beta^4\gamma^5} \frac{I_e/e}{a_e^2\theta_e^3}, \qquad (4)$$

where m is the rest mass of a particle, L is the Coulomb logarithm, η_p is the ratio ℓ/C_p, where C_p is the proton ring circumference, the fraction of the circumference over which cooling takes place, I_e is the electron beam current within the bunch, and a_e is the electron beam radius. We are assuming here that beam bunches are cylindrical in shape with uniform particle distributions.

Equation (4) applies to the case of uniform velocity distribution within the electron beam ellipsoid and for proton transverse velocity less than the transverse velocity spread of the electron beam. For the other case, θ_{1e} at the denominator of the right-hand side of (4) should eventually be replaced with $\theta_{\perp p}$. To represent a more realistic distribution function with slopes, we shall replace

$$\theta_e^3 \to (\theta_e^2 + \theta_p^2)^{3/2} \qquad (5)$$

in the denominator of the right-hand side (4). One should then also introduce a factor $\lesssim 1$ which depends on the distribution. Since this factor is not much different from unity, it will be neglected in the following.

An expression similar to (4), combined with (5), applies also for the electron beam, provided τ_p is replaced with τ_e, m_p with m_e, but not vice versa, and η_p, I_e and a_e are replaced respectively with η_e, I_p, and a_p. Since the electron storage ring is smaller than the proton ring, and the lengths of the rings are chosen to synchronize the traversals of bunches, the ratio η_e/η_p is given by the ratio of the number of proton bunches to the number of electron bunches.

We shall also assume that along the common straight section the β values of the two rings are constant and we denote them with β_e^* and β_p^*. From the definition of emittance (square of rms beam size/β^*) then we have

$$a^2 = \epsilon\beta^* \qquad \text{and} \qquad \theta^2 = \epsilon/\beta^*, \qquad (6)$$

which we can use in the right-hand side of (4).

Disregarding any other processes than the interaction between the two beams, the emittance equations are

$$\frac{d\epsilon_p}{dt} = -\frac{2}{\tau_p}\left(\epsilon_p - \frac{m_e}{m_p}\epsilon_e\right) \qquad (7)$$

$$\frac{d\epsilon_e}{dt} = -\frac{2}{\tau_e}\left(\epsilon_e - \frac{m_p}{m_e}\epsilon_p\right), \qquad (8)$$

where τ_p is given by (4) combined with (5) and (6) and τ_e by a similar derivation. Equations (7) and (8) are equivalent to the energy exchange between two gases put in contact at different temperatures. Equilibrium is reached when the two temperatures are equal. In our case the beam temperature is given by $m\epsilon$. The times τ_p and τ_e are equivalent to the relaxation times to reach equilibrium.

Observe that in terms of temperature, the relaxation times for the two beams would be the same, but in terms of emittances as shown by (7) and (8) the dependence on the masses is

$$\tau_p \sim m_p m_e \qquad \text{and} \qquad \tau_e \sim m_e^2.$$

Thus the electron beam "heating" time is at least 2000 times smaller than the proton beam "cooling" time.

When (4), (5), and (6) are combined together, they show that τ_p and τ_e depend on the beam emittances ϵ_e and ϵ_p.

Self-Consistent Solution at Equilibrium for Both Beams

Let us now combine Eqs. (1) (2) with (7) and (8). We obtain

$$\frac{d\epsilon_p}{dt} = D_p - \frac{2}{\tau_p}\left(\epsilon_p - \frac{m_e}{m_p}\epsilon_e\right) \tag{9}$$

$$\frac{d\epsilon_e}{dt} = D_e - \frac{2}{\tau}\epsilon_e - \frac{2}{\tau_e}\left(\epsilon_e - \frac{m_p}{m_e}\epsilon_p\right). \tag{10}$$

The solution of these equations will determine ϵ_e and ϵ_p as function of time. Their equilibrium, asymptotic values $\epsilon_{p\infty}$, $\epsilon_{e\infty}$ are calculated by setting the right-hand side of Eqs. (9) and (10) equal to zero.

Let us rewrite (9) and (10) by putting the dependence of ϵ_e and ϵ_p more explicitly

$$\frac{d\epsilon_p}{dt} = D_p - \kappa_p \frac{\epsilon_p - \frac{m_e}{m_p}\epsilon_e}{\epsilon_e\left(\frac{\epsilon_e}{\beta_e^*} + \frac{\epsilon_p}{\beta_p^*}\right)^{3/2}} \tag{11}$$

$$\frac{d\epsilon_e}{dt} = D_e - \frac{2}{\tau}\epsilon_e - \kappa_e \frac{\epsilon_e - \frac{m_p}{m_e}\epsilon_p}{\epsilon_p\left(\frac{\epsilon_e}{\beta_e^*} + \frac{\epsilon_p}{\beta_p^*}\right)^{3/2}}, \tag{12}$$

where

$$\kappa_p = \frac{6\pi e^3 L \eta_p I_e}{m_p m_e c^4 \beta^4 \gamma^5 \beta_e^*} \tag{13}$$

and

$$\kappa_e = \frac{6\pi e^3 L \eta_e I_p}{m_e^2 c^4 \beta^4 \gamma^5 \beta_p^*}. \tag{14}$$

At equilibrium we have

$$\epsilon_p = \frac{\epsilon_0 \epsilon_e}{\epsilon_e - \bar{\epsilon}_e}, \tag{15}$$

where $\bar{\epsilon}_e$ is given by Eq. (3) and

$$\epsilon_0 = \tfrac{1}{2}\left(\tau \frac{\kappa_e}{\kappa_p}\frac{m_p}{m_e}\right) D_p = \tfrac{1}{2}\tau_0 D_p. \tag{16}$$

It is reasonable to assume that, at equilibrium $\epsilon_e >> \bar{\epsilon}_e$; then the proton beam emittance is given by (16) and τ_0 would represent the proton beam "cooling" time near equilibrium.

From (13) and (14) we derive

$$\tau_0 = \tau\left(\frac{m_p}{m_e}\right)^2 \frac{\eta_e}{\eta_p}\frac{\beta_e^*}{\beta_p^*}\frac{I_p}{I_e}. \tag{17}$$

Observe the factor $(m_p/m_e)^2$, which is quite crucial for our analysis: one power of the ratio enters because the ratio of proton time τ_p to the electron time τ_e is proportional to m_p/m_e, and the second power comes from the last term on the right-hand side of (12), which represents heating of the electron beam, which must be coped with by synchrotron-radiation damping (τ).

The balance equations (11) and (12) apply in the case that the two beams are matched in size and velocity spread (at least approximately). If one wants to fulfill this condition, then $\epsilon_e \sim \epsilon_p$ and $\beta_e^* \sim \beta_p^* = \beta^*$. If one also observes that $m_p\epsilon_p >> m_e\epsilon_e$ (that is, the proton beam is always "hotter" than the electron beam) then at equilibrium the electron beam emittance is given by

$$\epsilon_e = \frac{\kappa_p}{D_p}\frac{\beta^{*3/2}}{\epsilon_0^{1/2}}. \tag{18}$$

Application to the Main Ring and CERN SPS

Let us consider the example of the Main Ring at 100 GeV. The electron-beam energy is then 50 MeV. The proton beam emittance, before gas scattering starts to dilute it, is

$$\epsilon_p = 2.2\times10^{-8}\ \text{m} \tag{19}$$

and the diffusion coefficient

$$D_p = 0.25\times10^{-10}\ \text{m/sec.}$$

If we want to "cool" the beam so that it preserves its initial emittance, then the cooling time required from Eq. (16) is

$$\tau_0 = 1.76\times10^{3}\ \text{sec.} \tag{20}$$

From (18), setting $\epsilon_e = \epsilon_0$ and taking $\beta^* \sim 70$ m, as it is in the present Main Ring medium or long straight section, we derive

$$\kappa_p = 1.4\times10^{-25}\ \text{m/sec.} \tag{21}$$

Let us take $\ell = 10$ m for the interaction length; then $\eta_p \simeq 1.6\times10^{-3}$. In addition, $L = 15$. Then we derive from (13) and (21)

$$I_e \simeq 8\ \text{A}, \tag{22}$$

after having assumed $\beta_e^* \sim \beta_p^* \sim 70$ m. The above is the peak current within the electron bunch. It is a reasonable number.

. With 10^{10} protons per bunch, the peak current in the Main Ring is about 1 A.

Let us assume that the number of proton bunches equals the number of electron bunches properly synchronized, so that

$$\eta_e/\eta_p = 1.$$

Then we derive from (17) and (20) the required radiation damping time

$$\tau = 4.4 \text{ msec.} \qquad (23)$$

This number is rather small.

The same calculation could be repeated for the CERN SPS. Here it seems that D_p is an order of magnitude smaller, because of better vacuum.[7] If all the other parameters remain unchanged, as effectively they are, then the required radiation damping time is also an order of magnitude larger, say around 40-50 msec.

One can repeat the same calculation for larger proton energies, say 200 GeV rather than 100 GeV. If one adopts the same procedure, which is to "freeze" the proton beam emittance to its invariant value, then

$$\epsilon_0 \sim 1/p \qquad (p, \text{ beam momentum})$$

and presumably

$$D_p \sim 1/p^2.$$

From (16) then

$$\tau_0 \sim p$$

whereas from (18) (with $\epsilon_e \sim \epsilon_0$)

$$\kappa_p \sim 1/p^{7/2}.$$

From

$$I_e \sim p^{3/2},$$

and, in conclusion, leaving I_p unchanged, from (17), we derive that the required radiation-damping time increases with the beam momentum as

$$\tau \sim p^{5/2}. \qquad (24)$$

Thus, at 200 GeV, for instance, τ = 25 msec. At the same time the electron beam energy also increases and reaching the required damping time is easier. Thus this scheme is better at higher energy.

Electron Storage Ring

In order to achieve a reasonable radiation damping time at low electron energy, wiggler magnets have to be inserted in the electron ring.

Let us consider the case of E_p = 100 GeV which would correspond to E_e = 50 MeV.

The electron storage ring could have the shape shown in Fig. 2. Let us define one wiggler unit as the combination of magnets that gives a total bending angle

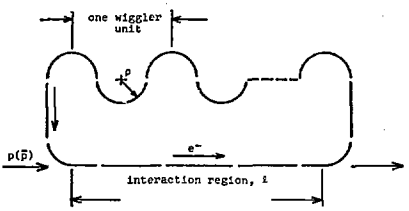

Fig. 2. Electron storage ring and wiggler.

of 2π and let us assume that there are n such units. The radiation damping time is

$$\tau = T_e \frac{E_e}{U_e}, \qquad (25)$$

where T_e is the revolution period and

$$U_e = 88.5 \frac{E^4_{e(\text{GeV})}}{\rho_{e(\text{m})}} \eta \text{ keV/turn} \qquad (26)$$

is the energy loss per revolution, ρ_e being the bending radius in the wiggler magnets. The magnetic rigidity of the electrons at 50 MeV is 1.67 kG·m; therefore, if we take a bending field of 10 kG, which might already be too large for wigglers, then we have

$$\rho_e = 0.167 \text{ m.}$$

From (24)

$$U_e = 3.3 \text{ n} \quad \text{eV/turn.}$$

As is shown in Fig. 2 the circumferential length of the electron storage ring will be mostly determined by the space required for the wiggler magnets. We can write

$$C_e \approx 2 \times 2\pi \rho_e \eta$$

$$T_e = \frac{C_e}{c} = \frac{4\pi\rho_e\eta}{c}.$$

Inserting these expressions in Eq. (23), we find that the radiation damping time is independent of the number of wigglers. The result is that the radiation damping time cannot be smaller than 100 msec, twenty times more than what is required [Eq. (21)] for Fermilab, but only two times larger than what is required for CERN.

If one takes

$$C_e \sim 30 \text{ m}$$

then one would require about 14-15 wigglers.

If the proton beam momentum p is increased, then obviously the electron beam momentum must also increase. Then one has the following dependence on the momentum p

$$\rho_e \sim p$$
$$U_e \sim p^3$$
$$T_e \sim p^3,$$

which gives

$$\tau \sim 1/p. \qquad (27)$$

The radiation damping time reduces only linearly by increasing the momentum of the proton beam. In addition, the number n of wigglers for the same storage ring circumference C_e would decrease as 1/p. At the same time, the required damping time versus beam-beam momentum is given by (22).

For the Main Ring at Fermilab, a balance between the required damping time (22) and the damping time that can be achieved (25) for an electron storage ring circumference of 30 m is reached at E_p = 250 GeV, which corresponds to E_e = 125 MeV. The damping time is about 40 msec and about six wigglers are required.

Thus, in conclusion, the project looks feasible.

References

[1] G. I. Budker, At. Energ. [Sov. J. At. Energy] 22, 346 (1967).

[2] The Fermilab Electron Cooling Experiment Design *Report, Fermilab, November* 1977.

[3] C. Rubbia, Relativistic Electron Cooling for High Luminosity Proton-Antiproton Colliding Beams at Very High Energies, contributed paper to the Berkeley Beam Cooling Workshop, March 27-31, 1978.

[4] I. Gaines, Proc. 1977 Aspen Summer Study on Colliding Beam Physics at Fermilab, Vol. 1, p. 115.

[5] M. Sands, The Physics of Electron Storage Rings, An Introduction, SLAC-121, November 1970.

[6] Ya. S. Derbenev and A. N. Skrinsky, Particle Accelerators 8, 1 (1977).

[7] E. J. N. Wilson, private communication (1978).

ATTENDANCE AT THE WORKSHOP

ALONSO, Jose	LBL
BERLEY, David	DOE
BILLINGE, Roy	CERN
BLUMBERG, Leroy	BROOKHAVEN
CLINE, David	FERMI
COLE, Francis T.	FERMI
CHO, Yanglai	ARGONNE
COOPER, Richard	LOS ALAMOS
COURANT, Ernest	BROOKHAVEN
DONALDSON, Rene	FERMI
FUNG, Sun Yiu	U.C. RIVERSIDE
GARREN, Alper	LBL
GILBERT, William	LBL
GLATZ, Joerg	LBL
GRUNDER, Hermann	LBL
HERRMANNSFELDT, Wm.	SLAC
JONES, Lawrence	U. OF MICHIGAN
JOHNSON, David	FERMI
KAINIS, Juris	LBL
KERNAN, Anne	U.C. RIVERSIDE
KERNS, Quentin	FERMI
KHOE, Tat K.	ARGONNE
KIM, Hogil	U. OF MARYLAND
KIMURA, Yoshitaka	KEK - JAPAN
KRINEN, Frank	CERN
KYCIA, Thaddeus	BROOKHAVEN
LAMBERTSON, Glen	LBL
LANCASTER, Henry	LBL
LASLETT, Jackson	LBL
LAWRENCE, George	LOS ALAMOS
LEEMANN, Beat	LBL
LEEMANN, Christoph	LBL
LEITH, David W.G.S.	SLAC
LOFGREN, Edward J.	LBL
MC INTURFF, Alfred	BROOKHAVEN
MC INTYRE, P.	FERMI
MILLS, Frederick E.	FERMI
MINARD, Marie-Noel	SLAC
MONTH, Melvin	BROOKHAVEN
PALMER, Robert B	BROOKHAVEN
PONDROM, Lee G.	U. OF WISCONSIN
REEDER, Don	U. OF WISCONSIN
RUBBIA, Carlo	CERN
RUGGIERO, Alessandro	FERMI
SACHERER, Frank	CERN
SALVINI, Giorgio	CERN
SELPH, Frank	LBL
SMITH, Lloyd	LBL
STAPLES, John	LBL
STEVENSON, Robert	LBL
TENG, Lee C.	FERMI
TOLLESTRUP, Alvin	FERMI
VAN der MEER, Simon	CERN
VOELKER, Ferd	LBL
WALLENMEYER, William	DOE
WIEDEMANN, Helmut	SLAC
WILSON, Robert	FERMI
WILSON, Ted	CERN
YOUNG, Donald E.	FERMI

APPENDIX
SOURCE INFORMATION FOR THE $P\bar{P}$ SCHEMES

dup.

APPENDIX A

Producing Massive Neutral Intermediate Vector Bosons with Existing Accelerators(*)

C. Rubbia and P. McIntyre
Department of Physics
Harvard University
Cambridge, Massachusetts 02138

and

D. Cline
Department of Physics
University of Wisconsin
Madison, Wisconsin 53706

Abstract

We outline a scheme of searching for the massive weak boson ($M = 50 - 200$ GeV/c^2). An antiproton source is added either to the Fermilab or the CERN SPS machines to transform a conventional 400 GeV accelerator into a $p\bar{p}$ colliding beam facility with 800 GeV in the center of mass ($E_{eq} = 320{,}000$ GeV). Reliable estimates of production cross sections along with a high luminosity make the scheme feasible.

Submitted to Physical Review Letters
March 1976

The past ten years have seen remarkable progress in the understanding of weak interactions. First there is the experimental discovery of $\Delta S = 0$ weak neutral currents,[1] which when contrasted with the previous limits on $\Delta S = 1$ neutral current decay processes[2] leads to the suggestion of additional hadronic quantum numbers in nature.[3] Strong evidence now exists for new hadronic quantum numbers that are manifested either directly[4,5] or indirectly.[6] The experimental discoveries are complemented by the theoretical progress of unified gauge theories.[7,8] These developments lead to the expectation that very massive intermediate vector bosons (50 - 100 GeV/c^2) may exist in nature.[7,8] The search for these massive bosons require three separate elements to be successful: a reliable physical mechanism for production, very high center of mass energies, and an unambiguous experimental signature to observe them. In this note we outline a scheme which satisfies these requirements and that could be carried out with a relatively modest program at existing proton accelerators.

We first turn to the production process. We concentrate on neutral bosons because of the extremely simple experimental signature and because production is largely dominated by a single production resonant pole in the particle-antiparticle cross section. The best production reaction would of course be:

$$e^+ + e^- \to W^o \begin{cases} \to e^+ + e^- \\ \to \mu^+ + \mu^- \\ \to \text{hadrons} \end{cases} \qquad (1)$$

where a sharp resonance peak is expected for $2E_{e^+} = 2E_{e^-} = M$. In the

Breit-Wigner approximation near its maximum we get:

$$\sigma(e^+e^- \to W^o) \simeq \frac{3}{4} \pi\lambda^2 \frac{\Gamma_i \Gamma}{(2E - M)^2 + \frac{\Gamma^2}{4}} \qquad (2)$$

where Γ_i, Γ are the partial width to the initial e^+e^- state and the total width, respectively. The decay widths into e^+e^- (and $\mu^+\mu^-$) pairs can be calculated in the first order of the semi-weak coupling constant: $\Gamma_{e^+e^\pm} \cong \Gamma_{\mu^+\mu^-} = 1.5 \times 10^{-7} M_W^3$ (GeV). For M = 100 GeV, $\Gamma_{e^+e^-} \simeq 150$ MeV, which is surprisingly large. The total width is related to the above quantity by the branching ratio $B_{e^+e^-} = \Gamma_{e^+e^-}/\Gamma$ which is unknown. Crude guesses based on quark models suggest $B_{e^+e^-} \simeq 1/10$, giving $\Gamma = 1.5$ GeV or $\Gamma/2E = 1.5\%$ for M = 100 GeV/c^2. At the peak of the resonance, $\sigma(e^+e^- \to W^o, 2E = M) = 3\pi\lambda^2 B_i \simeq 2.10^{-31}$ cm^2. Neutrino experiments[9] have found that $M_{W^+} > 20$ GeV/c^2. Therefore, if $M_{W^o} \sim M_{W^+}$, the neutral intermediate boson is out of reach of existing e^+e^- storage rings.

A more realistic production process is the one initiated by proton-antiproton collisions:

$$p + \bar{p} \to W^o + \text{(hadrons)}$$

which, according to the quark (parton) picture, proceeds by a reaction analog to (1), except that now incoming e^+ and e^- are replaced with q and $\bar{q}$. Strong support to the idea that W's are directly coupled to spin 1/2 point-like constituents comes from neutrino experiments[10] and from semi-leptonic hadron decays.[11] Furthermore neutrino experiments provide the necessary structure functions and have set limits[9] (> 20 GeV) on any nonlocality in the parton form factor. The main

difference with respect to e^+e^- is that now the kinematics is largely smeared out by the internal motion of q's and $\bar{q}$'s. The average center of mass energy squared of the $q\text{-}\bar{q}$ collision is roughly[12]:

$$< s_{q\bar{q}} > \sim S < x_q >_p < x_{\bar{q}} >_{\bar{p}p}$$

where S is the center of mass energy squared of the $\bar{p}p$ system and $< x_q >_p$ ($< x_{\bar{q}} >_{\bar{p}}$) is the mean fractional momentum of q's($\bar{q}$'s) in the proton (antiproton). From the neutrino measurements[9] and $< x_q >_p = < x_{\bar{q}} >_{\bar{p}}$ we find $< s_{q\bar{q}} > \sim 0.04\ S$. For $M = 100\ \text{GeV}/c^2$ this suggests $S \geq 2 \times 10^5\ \text{GeV}^2$ or $\sqrt{S} \geq 450$ GeV. The production cross section can be evaluated by folding the (narrow) resonance (2) over the q and $\bar{q}$ momentum distributions:

$$\sigma(q\bar{q} \to W^0 \to \mu^+\mu^-) = 3\pi\lambda^2 \frac{\Gamma_{q\bar{q}}}{\Gamma} \cdot \frac{\Gamma_{\mu\mu}}{\Gamma} \cdot \frac{dN}{dE}(E = M) \cdot 2\Gamma \qquad (3)$$

where $\frac{dN}{dE}$ is the probability (per unit of energy) of finding a $q\bar{q}$ collision with center of mass energy E, and the other symbols have the same meaning as in (2). Note that $\frac{\Gamma_{q\bar{q}}}{\Gamma} \simeq O(1)$ is a model-dependent parameter. The resultant cross section is $\sigma(p\bar{p} \to W^0 + \text{hadrons} \to \mu^+ + \mu^- + \text{hadrons}) \simeq 6\pi\lambda^2 \frac{\Gamma_{q\bar{q}}}{\Gamma} \frac{dN}{dE}(E = M) \cdot \Gamma_{\mu\mu} \cong 10^{-32}\ \text{cm}^2$. The numerical value is given for $M = 100\ \text{GeV}/c^2$, $\sqrt{S} = 500$ GeV and $\frac{\Gamma_{q\bar{q}}}{\Gamma} = 1/2$. This derivation of the cross section exposes the basic simplicity of the assumptions and gives the order of magnitude of the expected cross section. More sophisticated calculations give similar results.[12] We note that calculations of $W^\pm$ production in proton-proton collisions are very uncertain in contrast to the present one due to the apparent small antiparton content in the nucleon and the unknown distributions of this component.[13]

We turn now to the question of the experimental observation.

The cleanest experimental signature for the program outlined here is:

$$\bar{p} + p \to W^{o} + \text{hadrons}$$
$$\qquad\qquad \downarrow \mu^{+} + \mu^{-}$$

with the observation of a peak in the $\mu^{+}\mu^{-}$ invariant mass spectrum with the cross section of equation (3). A modest magnetized iron detector system is adequate to detect the high energy decay muons ($P_{\mu} \sim 50$ GeV) in the center of mass system. Electromagnetic production of $\mu^{+}\mu^{-}$ pairs is expected to be suppressed by a factor of $\lesssim (\alpha^2/G^2M_W^4)$. Note that a similar suppression is expected to hold for any hadronic vector meson. Note also that the production and decay of charged vector bosons is more problematic since the decay sequence

$$\bar{p} + p \to W^{+} + X$$
$$\qquad\qquad \downarrow \mu^{+} + \nu_{\mu}$$

leads to one muon and a missing neutrino which is difficult if not impossible to detect. In many previous discussions it has been assumed that the W^{+} would be produced with very little transverse momentum with respect to the incident beam direction and therefore the transverse momentum of the decaying μ would exhibit a sharp peak at $p_{\mu\perp} \sim M_W/2$.[14] Present evidence in case of the production of massive strongly interacting vector bosons (i.e., J/ψ) indicate that the parent is produced at relatively large $p_{\perp}$ and therefore the Jacobian peak is largely smeared out.[15] There is no obvious reason why the production of massive intermediate vector bosons should not follow the same behavior.[16] Without a sharp structure in the $p_{\mu\perp}$ distribution, a crucial experimental signature for the W^{+} is absent.

We now briefly outline the scheme of transforming an existing

proton accelerator into high luminosity $p\bar{p}$ colliding beams[17] using standard vacuum ($p \approx 10^{-7}$ Torr) and the separate function magnet system. The main elements are (1) an extracted proton beam to produce an intense source of antiprotons at 3.5 GeV/c, and (2) a small ring of magnets and quadrupoles that guides and accumulates the $\bar{p}$ beam, (3) a suitable mechanism for damping the transverse and longitudinal phase spaces of the $\bar{p}$ beam (either electron cooling[18] or stochastic cooling[19]), (4) an R.F. system that bunches the protons in the main ring and in the cooling ring, (5) transport of the "cooled" R.F. bunched $\bar{p}$ beam back to the main ring for injection and acceleration. A long straight section of the main ring is used as $p\bar{p}$ interaction region. A schematic drawing of these elements for the FNAL accelerator is presented in Fig. 1. The main parameters of the scheme are summarized in Table I.

The luminosity for two bunches colliding head-on is estimated using the relation

$$L = N_p N_{\bar{p}} \phi / a$$

where N_p and $N_{\bar{p}}$ are the number of protons and antiprotons circulating in the machine, respectively, ϕ is the revolution frequency and a is the effective area of interaction of the two beams. N_p is taken as 10^{12} protons in one R.F. bunch. The value of N_p is limited by the maximum allowed beam-beam tune shift ($N_p = 10^{12}$ for $\Delta\nu = 0.01$). We have verified the longitudinal stability of the bunch, the phase area growth due to R.F. noise, the transverse wall instability, the head-tail effect and non-linear resonances, including those arising from beam-beam interactions. None of these effects appears to be important.[20] We note that $N_p = 10^{12}$ corresponds to $i_{av} = 10$ mA and

$i_{peak} \simeq 25A$ for $\ell_{bunch} = 2.5m$ and that the Brookhaven AGS currently accelerates twelve bunches of similar characteristics.

The production of antiprotons at 3.5 GeV is done with protons from the same accelerator and with an overall efficiency $\bar{p}/p \simeq 4 \times 10^{-6}$. In order to reach $N_{\bar{p}} = 3 \times 10^{10}$ we need 750 pulses with 10^{13}ppp. About 10 seconds must elapse between pulses in order to clear away the freshly injected antiprotons.[21] Therefore the formation of $\bar{p}$'s would take of the order of few hours.

In order to make the beam as small as possible one can reduce the value of the betatron function in the collision point ($\beta_v \simeq \beta_h = 3.5m$) and make the momentum compaction factor close to zero.[22] Then for standard beam emittances[23] and $E_p = E_{\bar{p}} = 250$ GeV we calculate $L = 5 \times 10^{29}$ cm^{-2}sec^{-1} for $N_{\bar{p}} = 3 \times 10^{10}$. In order to observe one event/hour at our estimated cross section we require a luminosity of 3×10^{28} cm^{-2}sec^{-1}. If the more pessimistic cross section of 10^{-33} cm^2 is used, a luminosity of 3×10^{29} cm^{-2}sec^{-1} is needed which is still appreciably less than the calculated value. Finally, the half-life of the luminosity due to beam-gas scattering is about 24 hours for an average residual pressure of 0.5×10^{-7} Torr.

We would like to acknowledge Drs. T. Collins, R. Herb, S. Glashow, E. Picasso, G. Petrucci, N. Ramsey, L. Sulak, L. Thorndahl, and S. Weinberg for helpful discussions and suggestions.

TABLE I. - List of Parameters

1. MAIN RING (Fermilab)

- Beam momentum	250 (400) GeV/c
- Equivalent laboratory energy for ($p\bar{p}$)	133 (341) TeV
- Accelerating and bunching frequency	53.14 Mc/s
- Harmonic number	1113
- R.F. peak voltage/turn	3.3×10^{6} Volt
- Residual gas pressure	$< 0.5 \times 10^{-7}$ Torr
- Beta functions at interaction point	3.5 m
- Momentum compaction at int. point	~ 0 m
- Invariant emittances ($N_p = 10^{12}$)	
- longitudinal	3 eV s
- transverse	$50\ \pi\ 10^{-6}$ rad m
- Bunch length	2.3 m
- Design luminosity	5×10^{29} (8×10^{29}) $cm^{-2}.s^{-1}$

2. ANTIPROTON SOURCE (Stochastic Cooling[21])

- Nominal stored $\bar{p}$ momentum	3.5 GeV/c
- Circumference of ring	100 m
- Momentum acceptance	0.02
- Betatron acceptances	$100\ \pi\ 10^{-6}$ rad m
- Bandwidth of momentum stochastic cooling	400 Mc/s
- Maximum stochastic accelerating R.F. voltage	3000 V
- Bandwidth of betatron stochastic cooling	200 Mc/s
- Final invariant emittances ($N_{\bar{p}} = 3.10^{10}$)	
- longitudinal	0.5 eV s
- transverse	$10\ \pi\ 10^{-6}$ rad m

Figure Caption

Fig. 1. General layout of the $p\bar{p}$ colliding scheme. Protons (100 GeV/c) are periodically extracted in short bursts and produce 3.5 GeV/c antiprotons which are accumulated and cooled in the small stacking ring. Then $\bar{p}$'s are reinjected in an R.F. bucket of the main ring and accelerated to top energy. They collide head-on against a bunch filled with protons of equal energy and rotating in the opposite direction.

References

*Work supported in part by the U. S. Energy Research and Development Administration.

1. F. J. Hasert et al. and A. Benvenuti et al., papers submitted to the Sixth International Symposium, Bonn (1973), F. J. Hasert et al., Phys. Letters 46B, 138 (1973), A. Benvenuti et al., Phys. Rev. Letters 32, 800 (1974).
2. U. Camerini, D. Cline, W. Fry and W. Powell, Phys. Rev. Letters 13, 318 (1964), M. Bott-Bodenhausen et al., Phys. Letters 24B, 194 (1967).
3. S. L. Glashow, J. Iliopoulos and L. Maiani, Phys. Rev. D2, 1285,
4. B. Aubert et al., "Experimental Observation of $\mu^+\mu^-$ Pairs Produced by Very High Energy Neutrinos", in Proceedings of the Seventeenth International Conference on High Energy Physics, London, 1974 and in Neutrinos - 1974, AIP Conference Proceedings No. 22, edited by C. Baltay (American Institute of Physics, New York, 1974), p. 201. A. Benvenuti et al., Phys. Rev. Letters 34, 419 (1975), ibid. 34, 597 (1975).
5. J. von Krogh et al., "Observation of $\mu^-e^+K_s^o$ Events Produced by a Neutrino Beam", submitted to Phys. Rev. Letters; J. Blietschau et al., "Observation of Muon-Neutrino Reactions Producing a Positron and a Strong Particle", submitted to Phys. Letters.
6. J. J. Aubert et al., Phys. Rev. Letters 33, 1404 (1974), J. E. Augustin et al., Phys. Rev. Letters 33, 1406 (1974).

7. S. Weinberg, Phys. Rev. Letters 19, 1264 (1967).

8. A. Salam in Elementary Particle Physics (edited by N. Svortholm, Almquist and Wiksells, Stockholm, 1968), p. 367.

9. A. Benvenut et al., "Test of Locality of the Weak Interaction in High Energy Neutrino Collisions" to be submitted to Phys. Rev. Letters (March 1976).

10. See for instance A. de Rujula: Quark Tasting with Neutrinos. Proceedings 1976 Coral Gabl Conference, Miami, Florida, January 1976.

11. L. M. Chunet, J. M. Gaillard and M. K. Gaillard, Physics Reports 4C (1972), 5.
M. Roos, Phys. Letters, 36B (1971) 130.

12. Drell-Yan, Phys. Rev. Letters 25, 316 (1970), Pakvasa, Parashar, and Tuan, Phys. Rev. D10, 2124 (1975), S. M. Berman, Bjorken, Kogut, Phys. Rev. D4, 3388 (1971), G. Altarelli et al., Nucl. Phys. B92, 413 (1975), and R. B. Palmer, Paschos, Samios and Wang, BNL preprint J634.

13. A recent estimate of the antiparton content of the nucleon has been obtained using antineutrino scattering data below 30 GeV and is reported by A. Benvenuti et al., "Further Data on the High-y Anomaly in Inelastic Antineutrino Scattering", submitted to Phys. Rev. Letters (Feb. 1976).

14. Y. Yamaguchi, Nuovo Cim. 43, 193 (1966); L. Lederman and B. Pope, Phys. Rev. Letters 27, 765 (1971).

15. B. Knapp et al., Phys. Rev. Letters 34, 1044 (1975), Y. M. Antipov, et al., IHEP 75-125, Serpukhov (1976), F. W. Büsser et al., Phys. Letters 56B, 482 (1975), K. W. Anderson et al., submitted to Phys. Rev. Letters (1975), D. C. Hom et al., submitted to Phys. Rev. Letters (1976).

16. F. Halzen, private communication.

17. There are also various schemes for producing at modest cost a pp colliding beam machine of sufficient energy to produce the intermediate vector bosons. One such scheme is to collide the Fermilab main ring with the projected energy doubler ring (Cline, Richter, and Rubbia, private communication with R. R. Wilson, 1975); another scheme is to collide the Fermilab main ring with a small ring of 25 GeV protons (J. K. Walker et al., proposal submitted to Fermilab, 1976).

18. G. I. Budker, Atomic Energy 22, 346 (1967).
G. I. Budker, Ya. S. Derbenev, N. S. Dikansky, V. I. Kudelainen, I. N. Meshkov, V. V. Parkhomchuk, D. V. Pestrikov, B. N. Sukhina, A. N. Skrinskiy, Experiments on Electron Cooling, paper presented at the National Conference, Washington, March 1975.

19. L. van der Meer, CERN-ISR-PO/72-31 August 1972 (unpublished).
P. Braham et al., NIM 125, 156 (1975).
L. Thorndahl, CERN-ISR-RF/75 (unpublished).

20. See, for a complete discussion, M. Month, in Proceedings IX International Conference on High Energy Accelerators, SLAC, May 1974, page 593.

21. L. Thorndahl, CERN-ISR, RF/75 and C. Rubbia, report in preparation.

22. An electron target for NAL, in Proceedings 1973 NAL Summer Study, Vol. 2, page 21.

23. T. Collins, private communication.

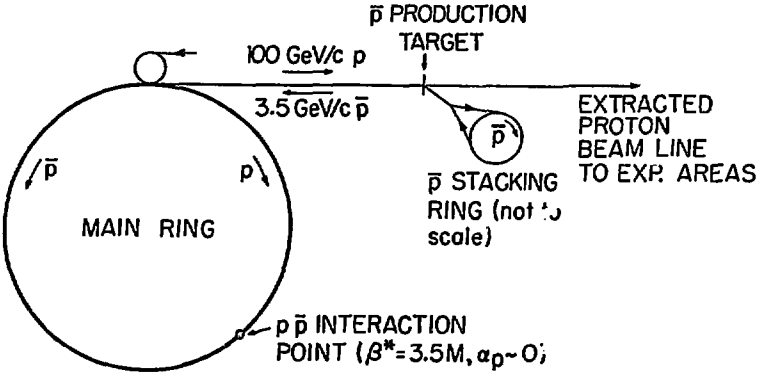
p̄ PRODUCTION TARGET
100 GeV/c p
3.5 GeV/c p̄
EXTRACTED PROTON BEAM LINE TO EXP. AREAS
p̄
p̄ STACKING RING (not to scale)
p̄
p
MAIN RING
p p̄ INTERACTION POINT (β*=3.5M, αp~0)

Fig. 1

CERN/PS/AA 78-3
27.1.1978

APPENDIX B

DESIGN STUDY OF A PROTON-ANTIPROTON COLLIDING BEAM FACILITY

FOREWORD

The idea of studying proton-antiproton collisions in storage rings has tempted physicists for a long time; in fact, the first suggestions in this direction were made before proton storage rings existed. The luminosity that could be hoped for was, unfortunately, not high enough for most experiments.

The development of beam cooling techniques has changed this, because cooling permits the accumulation of antiprotons in a storage ring over a long time, as pointed out by Budker and Skrinsky in 1966. C. Rubbia, during 1975 and 1976, worked out various antiproton collection schemes. His proposal was to inject the antiprotons into the SPS and accelerate them, together with protons, to 270 GeV, which is the maximum energy at which it can store particles continuously.

During 1976, two working groups examined the technical aspects of the scheme and the possibilities of $p\bar{p}$ physics. As a result, an experiment (ICE) on stochastic and electron cooling was initiated, and in parallel a study group was formed to prepare the present detailed design for a $p\bar{p}$ facility, using the SPS as a storage ring. During the study, it appeared that at a little extra cost the antiprotons could also be injected into one of the ISR rings. This feature was therefore added without, however, including any modifications to the ISR that might be required as a consequence.

The participants in this study are listed in Appendix A.

CONTENTS

I. INTRODUCTION

1.1 Choice of cooling method

Cooling is necessary for collecting a large number of antiproton batches in a storage ring and for compressing their phase space volume to a size acceptable to the SPS. In the present design, the following figures are relevant :

Phase space area	Accepted by cooling ring	Accepted by transfer channel and SPS
Longitudinal	350 mrad	72 mrad
Horizontal	100π mm.mrad	1.4 π mm.mrad
Vertical	100π mm.mrad	1 π mm.mrad

The figures for the cooling ring refer to a single antiproton pulse; for obtaining the design luminosity of 10^{30} cm^{-2} s^{-1}, about 24,000 pulses must be superimposed in phase space.

Two cooling methods (electron cooling and stochastic cooling) exist. Rubbia's earliest proposals (1975) assumed stochastic cooling; the stacking was to be done in betatron space[1]). The fast initial cooling needed for stacking appeared to be difficult in the presence of an intense stack and so a proposal using two separate rings emerged. With the then existing techniques this solution seemed somewhat marginal.

After the successful experiments by Budker's group at Novosibirsk[2]), electron cooling appeared to promise higher intensities. One of its important features is that the cooling rate does not depend on intensity; on the other hand, for obtaining a sufficiently high rate with acceptable electron beam currents, the antiproton energy must be low (e.g. 100 MeV). Since at this energy few antiprotons are produced, deceleration is required and after stacking, the antiprotons would have to be accelerated again for injection into the SPS.

This also resulted in a two-ring design, including complicated beam transfer and radiofrequency systems. This design was evaluated in detail during 1976 and 1977[3]. In parallel, however, stochastic cooling was further studied with the specific aim of arriving at a design with a single d.c. operated ring.

This work resulted in a better understanding of the stochastic cooling theory. Some methods were also discovered that promised better cooling. In particular, stacking was found to be easier in momentum space than in betatron space. A method was devised for precooling each injected pulse separately before adding it to the stack. In the meantime, many experiments were performed at the ISR. Although the cooling rate in these experiments was about three orders of magnitude below what is needed for precooling in the antiproton ring, they tend to confirm the existing theory. The same theory predicts a sufficiently high rate in the antiproton ring, mainly because of the larger revolution frequency spread and the smaller number of particles, but also because many more pick-up electrodes and a higher wide-band output power will be available.

The present design, therefore, is based on stochastic cooling using a single ring.

1.2 General description

Protons of 26 GeV/c from the PS will be directed onto a target. The antiprotons produced there will be focused and injected into the cooling ring that will work at a fixed field corresponding to a nominal momentum of 3.5 GeV/c. Each injected pulse will undergo a first rapid cooling treatment to reduce its momentum spread (precooling). It will then be deposited by a radio-frequency system at the top of a stack which has a slightly lower momentum than the injected beam. The stack is cooled continuously, both longitudinally and transversely. As a result, the particles will slowly migrate to the bottom of the stack, where finally a beam of sufficient density will be formed.

The same radiofrequency system then captures a certain fraction of this stack at a time in a single bunch and accelerates this back to the extraction orbit, which is the same as the injection orbit. This bunch will then be extracted and transferred to the SPS. For the design luminosity of 10^{30} cm^{-2} s^{-1}, six bunches, each containing 1/6 of the stack, will be transferred successively within a fraction of a second.

The ring will be located in a new building to be situated near the transfer tunnel TT2, downstream of the PS Booster complex (Fig. 1.1). The extracted antiprotons will follow the existing tunnels TT2a and TT60. Some of the existing extraction elements of the SPS will be used for injecting the antiprotons. Six bunches of antiprotons will be accelerated by four PS type cavities. The protons will be injected between 10 and 14 GeV/c and the bunches matched to the existing 200 MHz RF system at 18 GeV/c. The latter then takes the protons and antiprotons up to e.g. 270 GeV/c, where they will stay as long as their lifetime permits. The beams will be kept bunched in order to increase the interaction rate at the straight section(s) where the experiments will be performed. A low-beta section will further increase the luminosity.

Transfer to the ISR (ring 1) follows the normal route through TT2. In fact, the beam towards the SPS will cross the PS-ISR beam; a bending magnet at the crossing point is all that is needed to direct the antiprotons towards the ISR.

1.3 Choice of the main parameters

1.3.1 Proton source and primary momentum

The antiprotons could be produced by protons from either the PS or the SPS. At SPS energies, the production rate could be about four times as high as that from 26 GeV/c protons. However, the interference with normal SPS physics would be strong; during the long accumulation periods, the SPS would not be available for other purposes. Simultaneous $\bar{p}$ collection and $p\bar{p}$ experiments in the SPS would also be excluded.

With the PS as a proton source, the collection of antiprotons can go on in parallel with the normal PS, ISR and SPS operation. The PS acceleration cycles for $\bar{p}$ production could be interleaved with cycles for SPS or PS physics or for filling the ISR. A minimum repetition period of 2.6 seconds has been assumed for the present design, but this could of course be increased, depending on other users of the PS machine. Faster repetition is excluded by the precooling requirements.

1.3.2 Diameter of the ring

Single-turn extraction of the protons from the PS will normally produce a pulse with a duration of 2.1 μs. It would be difficult to inject a stream of antiprotons of this duration into a ring smaller than the PS itself, since multiturn injection is not possible because of the large phase space volume occupied by the antiprotons.

However, as will be discussed in Section 5, it is possible to inject the protons from the PS Booster into the PS in such a way that only one quarter of the PS circumference is filled. Thus, the cooling ring may have one quarter of the PS diameter (i.e. 50 m) and still accept all antiprotons produced.

The circumference of the extraction orbit will be made exactly equal to 1/44 of the SPS circumference. This will simplify the rf synchronization between the two machines.

1.3.3 Antiproton momentum

Although it would seem that with 1/4 of the PS circumference the cooling ring could work at up to 7 GeV/c, this appears to be impractical for several reasons :

a) As may be seen from Fig. 1.2, a relatively large fraction of the circumference is needed for injection, extraction, cooling and diagnostic equipment. This alone would prevent the use of a momentum higher than 3.5 GeV/c.

b) The output power needed for the precooling stage increases with the square of the momentum. It would be difficult to increase it much beyond the figure foreseen at present (25 KW, 150-400 MHz bandwidth).

c) The 152° bend in the transfer line to the SPS requires only a small addition to the existing tunnels if the momentum is 3.5 GeV/c. Any increase would result in more interference with the SPS programme because of the extra civil engineering work that would be needed.

For these reasons the figure of 3.5 GeV/c has been chosen, even though it is well below the usual SPS and ISR injection momenta.

1.3.4 Momentum spread and emittance of the injected $\bar{p}$ beam

The total number of particles accepted is proportional to the momentum spread and to the square root of the emittance in each plane*.

Consideration of the influence of these parameters on the apertures required and on the power needed for the precooling system led to the following figures :

Horizontal and vertical emittance	100π mm.mrad
Momentum spread	± 0.75%

Fig. 2.4 shows the actual apertures resulting from this choice. These depend of course on the lattice adopted, which will be discussed in more detail in Section 2.

---

* This is somewhat unusual; with constant phase-plane density at the target one would expect it to increase with the first power of the emittances. It is due to the imperfect matching that can be achieved with a target which is long compared to the β value at its centre.

1.4 Expected performance

The rate at which antiprotons can be accumulated and the luminosity obtained in the SPS are the two most important performance figures. To a certain extent they are independent, since accumulation could go on during normal SPS operation and the time needed is therefore not a critical parameter. Nevertheless, very large accumulation times would be inconvenient and also increase the risk of sudden beam loss due to random failures. Moreover, an accumulation time not longer than the useful lifetime in the SPS would simplify operation.

For this reason, the luminosity estimate is based, admittedly somewhat arbitrarily, on a time of accumulation of 24 hours.

Further assumptions are : a repetition period of 2.6 s and a PS intensity of 10^{13} protons per pulse. The number of antiprotons accepted per cycle will then be 2.5×10^{7}. After 24 hours of operation, taking into account transfer losses, occasional PS stops, etc., the total number of antiprotons accumulated will be 6×10^{11}.

These will be distributed over six bunches and collide in the SPS with six proton bunches.

The luminosity will be :

$$L = \frac{2 N_p N_{\bar{p}} f_r}{M \left[\beta_H \beta_v \, (E_{Hp} + E_{H\bar{p}})(E_{vp} + E_{v\bar{p}}) \right]^{\frac{1}{2}}}$$

With the values of table 1.1, we find

$$L = 10^{30} \text{ cm}^{-2} \text{ s}^{-1}$$

TABLE 1.1

N_p	total number of p	6×10^{11}
$N_{\bar{p}}$	total number of $\bar{p}$	6×10^{11}
f_r	revolution frequency	43.4 KHz
M	number of bunches	6
β_H	horizontal betatron function at the interaction point	4.7 m
β_v	vertical betatron function at the interaction point	1.0 m
E_{Hp}	proton emittances at 270 GeV/c	$6.9 \times 10^{-6}\pi$ rad m
E_{vp}	proton emittances at 270 GeV/c	$3.5 \times 10^{-6}\pi$ rad m
$E_{H\bar{p}}$	antiproton emittances at 270 GeV/c (allowing for blow-up by a factor 1.5)	$3.8 \times 10^{-6}\pi$ rad m
$E_{v\bar{p}}$	antiproton emittances at 270 GeV/c (allowing for blow-up by a factor 1.5)	$1.9 \times 10^{-6}\pi$ rad m

It must be made clear that the luminosity depends on many different features. It is not excluded that the initial value could be smaller and that the design figure would only be reached after an initial development period.

2. LATTICE AND APERTURES

2.1 Introduction

The lattice of the antiproton ring must fulfil the requirements both for storage and stochastic cooling. In contrast with conventional storage rings, the injected beam will have very large transverse emittances and momentum spread. Also the stochastic cooling process requires that "mixing" of a sample of particles occurs due to their spread in revolution frequency. This implies a large average value of the momentum compaction function α_p. Clearly these two characteristics combine to give very large radial beam sizes.

2.2 Injection and storage requirements

To permit the injection of the large emittance, large momentum spread beam, the focusing structure must be such as to minimise the "kick" strength required. For this reason the injection septum must be located in a region where α_p is close to zero. In addition, to avoid perturbing the stacked beam, it must be screened from the injection kicker by means of a moveable shutter. To permit this, the stack and the injected beam are separated in momentum by an amount Δp. This is shown in figure 2.1 and it can be seen that for a shutter thickness t and horizontal beam emittance πE_H, the momentum separation is given by

$$\frac{\Delta p}{p} = \frac{1}{\alpha_p} \left[t + 2 \sqrt{E_H \beta_H} \right]$$

where α_p and β_H are the values of the momentum compaction and betatron functions at the shutter position. Clearly this momentum separation contributes to the apertures required around the ring so that it is important to design the lattice such that $\alpha_p = 0$ at the septum position and its value at the injection kicker (i.e. 90^0 of horizontal phase advance downstream) is as close as possible to the maximum value.

2.3 Stochastic cooling requirements

Each injected pulse of antiprotons is subjected to a fast "pre-cooling" of its momentum spread. As in the case of the injection kickers, the pre-cooling kickers have shutters to confine their effect to the injected beam. Hence they must be located in a region of high α_p. However, each time a particle receives an impulse δp its closed orbit is shifted by an amount $\alpha_p \frac{\delta p}{p}$ and statistically this would blow up the betatron oscillations and counteract the betatron cooling. This effect must be avoided by providing two regions of equal and high α_p separated by a half wavelength of betatron oscillation so that the impulse can be applied in two halves without inducing any betatron motion.

To provide adequate "mixing" of particles, the absolute value of the dispersion in revolution frequency f, given by

$$\eta = -\frac{\delta f/f}{\delta p/p} = \frac{1}{\gamma_t^2} - \frac{1}{\gamma^2}$$

should be at least 0.1 which corresponds to a maximum transition energy $\gamma_{tr} < 2.45$ or an average α_p of 4.2 m in a ring of average radius 25 m.

2.4 Lattice design

In summary the basic requirement on the focusing and bending structure is for a ring one quarter the circumference of the PS, with a nominal momentum of 3.5 GeV/c, a transition energy $\gamma_{tr} < 2.45$ and a large amount of straight section space. To achieve the large average value of α_p with zero at the injection septum, the momentum compaction function should rise as quickly as possible after this and stay at a high value elsewhere in the ring.

Many types of focusing structure were examined: separated function, combined function and hybrid. Two possible solutions were found, namely a triplet type as in the PS Booster or a FODO type. Careful comparison of these showed that although the triplet lattice had lower betatron function values in the bending regions, the peak α_p and large momentum width combined to give excessively large quadrupole apertures. This in turn reduced the available gradient and increased the quadrupole length at the expense of free straight section space.

It has been shown[4] that in a "smooth" FODO lattice with equal bends it is possible to produce a region of $\alpha_p = \alpha'_p = 0$ by adjusting the bending angles in adjacent cells. Two independent variables were required so that choosing one of the bending angles as zero fixed both the phase advance and the remaining bend. Using this approach a lattice was designed which satisfies all the above conditions. The main parameters are given in table 2.1 and the betatron functions are plotted in figure 2.2.

The betatron tunes $Q_H = 2.29$, $Q_V = 2.28$ are in a region of the working diagram which is free of non-linear resonances up to seventh order (Fig. 2.3). Variations of the vertical tune do not affect the momentum compaction function but horizontally the maximum and minimum values change by :

ANTIPROTON RING 12 PERIODS D/2 F D/2 AGS VERSION 75.03 24/11/77 16.44.58

CIRCUMFERENCE = 156.49200 2 HALF SUPERPERIODS STRAIGHT MAGNETS ALL VALUES AT EXIT OF ELEMENTS

NO	ELEM	L(M)	DIST(M)	ANG(MR)	K(1/M2)	BETAV(M)	BETAH(M)	ALPHAV	ALPHAH	MUV/2PI	MUH/2PI	ALPHAP(M)	ALPHAP'
INITIAL			0.0000			10.54954	7.12218	0.00000	0.00000	0.00000	0.00000	6.03343	.000000
1	D	.2700	.2700	0.00000	.2180866	10.38958	7.24630	.58931	-.46215	.00409	.00600	6.08146	.354211
2	S1	.4625	.7525	0.00000	0.0000000	9.86109	7.73127	.52674	-.54296	.01169	.01627	6.25333	.356211
3	P1	1.4450	2.1975	222.54630	0.0000000	8.16361	9.63145	.61878	-.78297	.03746	.04282	6.92394	.579680
4	P1	1.4450	3.6425	222.54630	0.0000000	6.36350	12.21056	.58825	-1.02298	.06061	.06391	7.91481	.803150
5	S2	2.6080	6.2505	0.00000	0.0000000	4.72994	18.79452	.03711	-1.45576	.14645	.09151	10.00842	.803150
6	F	.2700	6.5205	0.00000	-.2940930	4.82729	18.08575	-.40624	.02113	.15746	.09377	10.11839	.002793
7	F	.2700	6.7905	0.00000	-.2940930	5.16840	18.67203	-.87216	1.50622	.16612	.09604	10.01082	-.796019
8	S2	2.6080	9.3985	0.00000	0.0000000	12.03465	12.63101	-1.76660	1.04615	.21976	.12388	7.92958	-.798019
9	P1	1.4450	10.8435	222.54630	0.0000000	17.11651	9.38998	-1.66680	.79169	.23581	.14540	6.94607	-.574550
10	P1	1.4450	12.2665	222.54630	0.0000000	21.44048	7.66404	-1.24916	.64720	.24782	.17276	6.28281	-.351060
11	S1	.4625	12.7710	0.00000	0.0000000	22.67372	6.97652	-1.30678	.46320	.25131	.18343	6.11341	-.351050
12	D	.2700	13.0410	0.00000	.2180866	23.02201	6.64790	.62365	.01534	.25318	.18567	6.06703	.007658
13	D	.2700	13.3110	0.00000	.2180866	22.56644	6.95978	1.35259	-.43155	.25506	.19501	6.11723	.365309
14	S3	1.9935	15.3045	0.00000	0.0000000	17.76216	9.35771	1.10354	-.77133	.27091	.23564	6.84546	.365309
15	S3	1.9935	17.2980	0.00000	0.0000000	13.84664	13.11033	.65449	-1.11110	.29120	.26444	7.57372	.365309
16	S3	1.9935	19.2915	0.00000	0.0000000	10.93849	18.21763	.60544	-1.45088	.31709	.28502	8.30196	.365309
17	F	.2700	19.5615	0.00000	-.2940930	10.85223	16.61450	-.28367	-.00849	.32105	.28735	8.31141	-.205465
18	F	.2700	19.8315	0.00000	-.2940930	11.24925	18.22667	-1.19728	1.43463	.32495	.28967	8.14298	-.949916
19	S3	1.9935	21.8250	0.00000	0.0000000	16.86249	13.17360	-1.62652	1.10615	.34606	.31021	6.24932	-.949916
20	S3	1.9935	23.8185	0.00000	0.0000000	24.23510	9.25409	-2.05977	.76567	.36377	.33879	4.35556	-.949916
21	S3	1.9935	25.8120	0.00000	0.0000000	33.30706	7.06615	-2.49101	.43119	.37495	.37600	2.46201	-.949916
22	D	.2700	26.0820	0.00000	.2180866	34.12695	6.95610	-.52950	-.02143	.37622	.38414	2.22444	-.812122
23	D	.2700	26.3520	0.00000	.2180866	33.87268	7.09154	1.46550	-.47542	.37748	.39026	2.02230	-.687256
24	S4	.5053	26.8573	0.00000	0.0000000	32.41571	7.61609	1.41855	-.66277	.37990	.40123	1.67506	-.687256
25	P2	2.4850	29.3423	340.30557	0.0000000	22.67174	11.38642	2.27330	-.98415	.39451	.44337	.41677	-.343628
26	P2	2.4850	31.8272	340.30557	0.0000000	11.14034	17.21082	2.09578	-1.40553	.41950	.47123	.00000	.000000
27	S4	.5053	32.3325	0.00000	0.0000000	9.14611	18.67523	1.65123	-1.49266	.42747	.47571	.00000	.000000
28	F	.2700	32.6025	0.00000	-.2940930	8.36513	19.08490	1.06193	-.01353	.43240	.47798	.00000	.000000
29	F	.2700	32.8725	0.00000	-.2940930	7.96276	18.68964	.36437	1.46697	.43768	.48025	.00000	-.000000
30	S3	1.9935	34.8660	0.00000	0.0000000	7.09396	13.51106	.08149	1.13077	.48035	.50027	.00000	-.000000
31	S3	1.9935	36.8595	0.00000	0.0000000	7.33300	9.67292	-.20139	.79456	.52492	.52816	.00000	-.000000
32	S3	1.9935	38.8530	0.00000	0.0000000	8.69988	7.17521	-.48427	.45836	.56507	.56662	.00000	-.000000
33	D	.2700	39.1230	0.00000	.2180866	8.83133	7.05211	-.00000	-.00000	.56996	.57268	.00000	-.000000

DP/P	COSMU(H)	Q(H)	QPRIME(H)	BETAMAX(H)	COSMU(V)	Q(V)	QPRIME(V)	BETAMAX(V)	XMAX(H)	GAMMA TR.
0.0000	.61114	2.2907	-2.8139	19.0858	.63782	2.2798	-1.2676	34.1270	10.1184	2.4347
-.0500	.60793	2.2920	-2.8196	19.7266	.62999	2.2831	-1.2776	35.1430	-.4769	2.5487
-.0400	.60923	2.2915	-2.8164	19.5029	.63297	2.2818	-1.2758	34.9568	-.3865	2.524[illegible]
-.0300	.61014	2.2911	-2.8143	19.2783	.63518	2.2809	-1.2739	34.7613	-.2935	2.5005
-.0200	.61073	2.2909	-2.8132	19.0543	.63669	2.2803	-1.2719	34.5571	-.1980	2.4778
-.0100	.61105	2.2907	-2.8130	19.0271	.63755	2.2799	-1.2698	34.3454	-.1001	2.4559
.0100	.61105	2.2907	-2.8157	19.2611	.63755	2.2799	-1.2652	33.9029	.1022	2.41[illegible]3
.0215	.61076	2.2909	-2.8188	19.4787	.63663	2.2803	-1.2624	33.6394	.2223	2.391[illegible]
.0300	.61046	2.2910	-2.8220	19.6488	.63556	2.2808	-1.2603	33.4416	.3126	2.3754
.0400	.61001	2.2912	-2.8265	19.8579	.63393	2.2814	-1.2577	33.2063	.4206	2.3569
.0500	.60950	2.2914	-2.8318	20.0758	.63191	2.2823	-1.2550	32.9691	.5303	2.3390

TIME = .216 SECONDS

Table 2.1 Lattice Parameters

$$\Delta\alpha p_{max} = -23\ \Delta Q_H \quad (m)$$

$$\Delta\alpha p_{min} = 8.3\ \Delta Q_H \quad (m)$$

2.5 Off-momentum orbits

A sextupole scheme which to a first order cancels the machine chromaticity in both planes, has been calculated. The sextupole components will be incorporated into the profile of the quadrupoles, and the required strengths are $K'_F = -0.048\ m^{-3}$ and $K'_D = 0.057\ m^{-3}$. With these conditions the residual variation in tunes within a momentum range of ± 3% is such that

$$\Delta Q_H < 4 \times 10^{-4} \quad \text{and} \quad \Delta Q_V < 1 \times 10^{-3}$$

over most of the aperture. An additional small correction to the quadrupole profile will create a slight over compensation of the natural chromaticity near the bottom of the stack in order to suppress the transverse resistive wall instability. This will only be required at the end of cooling, when nearly all particles will be at the bottom of the stack. A normal sextupole type correction would cause an undesirable Q variation across the aperture.

2.6 Apertures

The aperture requirements are based on the need to have a stacked beam with a total momentum width of 2.5%, an injected beam of 1.5%, both with horizontal and vertical emittances of 100π mm.mrad and separated by a momentum "gap" of 1.8% (see figure 2.1). This gives a total acceptance needed of 5.8% in momentum and 100π mm.mrad transverse emittances. The corresponding beam sizes in one quadrant of the machine are shown in figure 2.4. Since the machine lattice has reflection symmetry at the injection region, it was decided to use a split septum magnet which can then serve in common for injection and extraction. The resulting beam apertures in the injection region are also shown in figure 2.4 and the beam geometry around the septum in figure 4.5.

2.7 Intensity-dependent effects

At the end of the stacking period, some intensity-dependent effects may become noticeable. These will be discussed below, assuming the following stack parameters :

$$\Delta p/p = \pm 1.5 \times 10^{-3}$$
$$E_H = 1.4\ \pi \text{ mm.mrad}$$
$$E_V = 1\ \pi \text{ mm.mrad}$$
$$N = 6 \times 10^{11}$$

2.7.1 Intra-beam scattering

This is the most important effect. It has been evaluated following Piwinski's theory [5]. The blow-up is a function of the momentum spread and the transverse emittances. For the values above, the blow-up times are

horizontally : 0.5 h.
vertically : 23 h.
longitudinally : 2.4 h.

The horizontal and longitudinal blow-up rates increase rapidly if either $\Delta p/p$ or the horizontal emittance are decreased. The vertical rate depends mainly on $\Delta p/p$ and on the vertical emittance. As it happens, the effect is just small enough to be overcome by the stochastic cooling.

2.7.2 Incoherent tune shift

The direct effect (without images) will be at most

$$\Delta Q_V = -0.0025$$

The contribution from images is somewhat more difficult to estimate because the shape of the vaccum chambers is complicated and not yet completely defined. However, a rough estimate shows that the image effects

will be about 10 times smaller than the direct effect, because of the small dimensions of the stack compared to the vacuum chamber aperture. Partial neutralization of the stack due to ionisation of the residual gas will further reduce this effect.

2.7.3 Transverse instability

The main contribution to transverse instability will come from the frequency shift corresponding to the incoherent space charge effect. To increase the Landau damping, we shall shape the quadrupole profile so as to make the chromaticity slightly positive at the bottom of the stack. A chromaticity value of 0.2 can be obtained locally in both planes without exceeding a Q spread across the stack of 0.01. This spread must be kept small to avoid losses on resonances, since the particles migrate slowly towards the bottom of the stack.

Even with this chromaticity we still expect that the lowest modes will be unstable at the final stack density. An active feedback system covering the range 1-25 MHz will therefore be provided for each plane.

Other contributions to the instability will be less important. Both the resistive wall effect and the low frequency effect of cross-section variations will be negligible. Resonances of cavity-like objects do not seem dangerous because at the high frequencies concerned the Landau damping is sufficiently strong. Only the coupling impedance due to special objects (pick-ups, kickers) may have to be watched. No great problems are expected, however.

2.7.4 Longitudinal instability

The condition for longitudinal stability will be most stringent when 5 batches have been extracted and the last one, still with its initial density, remains. Under this condition, we have according to the Keil - Schnell criterion [6] :

$$\frac{Z/\!/}{n} < 840\ \Omega$$

The contributions to Z/n from the negative mass effect (25 Ω) and from the resistive wall (< 2 Ω) will be negligible. Resonant cavity-like objects do not seem dangerous, but will have to be watched and maybe damped in some cases.

The main contribution will probably come from the kickers for momentum cooling of the stack (see Section 5). Because of the ferrite rings surrounding the beam and the loading by the external circuit, these will appear to the beam as an inductance L and a resistance R connected in parallel. The inductance is proportional to the ferrite cross-section, which is determined by the requirement that at the lowest frequency used for stochastic cooling (250 MHz) the value of ωL should be large compared to R. For instance, with R = 50 Ω, ωL = 500 Ω at 250 MHz, and with 70 rings, the contribution to Z/n from ωL will be 250 Ω, independent of frequency. The parallel R will only reduce this value.

2.7.5 Ion-antiproton oscillations

This effect is discussed in Section 7.1

3. MAGNET SYSTEM

3.1 Magnet design

The magnet system must provide very wide apertures and yet occupy a minimum of azimuthal space. All elements are designed to operate DC but may be laminated or built from plates for ease of fabrication.

Two types of dipole bending magnets are proposed. The large angle magnets in the region of small momentum dispersion occupy most of the free space between consecutive quadrupoles. In this way it is possible to achieve the required deflection at a field level of 1.6 T so that a simple H magnet with flat coils can be used. Elsewhere the very wide apertures together with the need to leave as much free space as possible, led to a window-frame design with a field level of 1.8 T. The cross-sections of these dipoles are shown in figures 3.1 and 3.2 and the main parameters listed in table 3.1.

After allowing for closed orbit deviations, vacuum chamber wall and thermal insulation around the vacuum chamber, the magnet gaps are such that the H and window-frame versions require equal excitations. This is maintained by designing the magnetic circuits with an equal degree of saturation, so that they can be powered in series. The number of excitation turns was then chosen to give a current below 2,000 amps to keep cable costs down. Further considerations include : the number of parallel water cooling circuits, the total ring voltage, coil fabrication costs, and the need to locate about one quarter of the ampère-turns of the window-frame type coil inside the pole gap.

The quadrupoles will be of two types with large and small apertures and all having the same effective length. The distribution of these two types around the ring is determined by the azimuthal variation in momentum compaction.

TABLE 3.1

Dipole Parameters

Type	"H"	Window Frame	
No.	4	8	
Field	1.6 T	1.8 T	
Gap	157.5 mm	140 mm	
Effective length	4.97 m	2.89 m	
Steel length	4.79 m	2.73 m	
Overall length	∿ 5.3 m	∿3.4 m	
Width overall	∿ 1.8 m	∿2.5 m	
Good field ½ width	120 mm	282 mm	
Turns/pole	54	54 (12 in gap coil;42 in main coil)	
Conductor	24 x 24 mm²	32 x 17.3 mm²	25.2 x 24.5 mm²
Hole for cooling water	12.5 mm	7.8 mm	8.5 mm
No. of cooling circuits/pole	3	1	3
Current	1950 A	1950 A	1950 A
Power/magnet	202.8 kW	27.8 kW	93.6 kW
Δp	20 kp/cm²	20 kp/cm²	20 kp/cm²
ΔT	19.6°C	18.6°C	18.7°C
Mean length of one turn	11.2 m	7.7 m	8.2 m
Water flow/magnet	2.5 ℓ/s	0.4 ℓ/s	1.2 ℓ/s
Volts/magnet	104 V	14.2 V	48 V

In order that all F quadrupoles can be powered in one circuit and all D's in another, the focusing strengths of large and small types must be equal at equal currents. Thus the inscribed apertures are chose in the ratio $\sqrt{2}$: 1 and the excitation coils designed with a turns ratio of 2 : 1.

As in the case of the dipoles, the number of turns has been chosen to give an excitation current below 2,000 amps. The resulting quadrupole cross sections are shown in figures 3.3 and 3.4 and the main parameters are given in table 3.2.

The small quadrupole having a fairly low total flux has been designed with a parallel sided pole so as to allow the use of simple, flat, rectangular cross-section coils.

Also, a reduced aperture version of the small quadrupole will be produced for use in the injection beam line. This will have the same excitation coil and external dimensions, but a modified pole profile.

The large aperture quadrupole must have a tapered pole to avoid excessive saturation and in addition it is estimated that due to its length being almost equal to the inscribed diameter, the steel length will need to be equal to the required effective length.

It is proposed to shape the quadrupole profiles to provide the sextupole component which will make the chromaticity zero in both planes (see Section 2.5).

The magnet system will be powered in three separate circuits, one for the dipoles and one each for the F and D quadrupoles. Table 3.3 gives the overall characteristics of these three circuits.

TABLE 3.2

Quadrupole Parameters

	Large		Small		Injection
No.	16		8		8
Strength	1.85 T (F) 1.37 T (D)		1.85 T (F) 1.37 T (D)		4 T
Inscribed radius	208 mm		147.08 mm		75 mm
Effective length	0.54		0.54		0.54
Steel length	∿ 0.54		∿ 0.49		∿ 0.49
Overall length	∿ 0.86		∿ 0.77		∿ 0.77
Width overall	∿ 2.2		∿ 0.96		∿ 0.96
Turns/pole	40		20		20
Good Field ½ width	340		160		80
Conductor dimensions	21.5x18.0 mm²		14.5x18.2 mm²		
Hole for cooling water, diameter	8 mm		4.8 mm		
No. of cooling circuits/pole	1		1		
Mean length of one turn	2.6		1.7		
Flow/magnet	0.72 ℓ/sec		0.34 ℓ/sec		
Δp	20 kp/cm²		20 kp/cm²		
ΔT	20°C(F)	11°C(D)	18.8°C(F)	10.3°C(D)	5.4°C
Nominal gradient	3.429 T/m (F)	2.542 T/m (D)	3.429 T/m (D)	2.542 T/m (F)	7.41 T/m
Current	1550 A	1150 A	1550 A	1150 A	830 A
Power/magnet	59.2 kW	32.6 kW	26.4 kW	14.5 kW	7.6 kW
Volts/magnet	38.2 V	28.3 V	17.0 V	12.6 V	9.1 V

TABLE 3.3

Power Supply Parameters

1. Dipole Circuit

Magnet Current	=	1950 Amps
Magnet Voltage	=	914 Volts
Magnet Power	=	1.78 MWatts
DC Cables Voltage Drop	=	8.8 Volts
Reserve (including connections)	=	77 Volts
Power Supply	=	2000 Amps 1000 Volts (2.0 MVA)

2. F Quadrupole Circuit

Magnet Current	=	1550 Amps
Magnet Voltage	=	380 Volts
Magnet Power	=	0.6 MWatts
DC Cables Voltage Drop	=	7.0 Volts
Reserve (including connections)	=	63 Volts
Power Supply	=	1750 Amps 450 Volts (0.9 MVA)

3. D Quadrupole Circuit

Magnet Current	=	1150 Amps
Magnet Voltage	=	280 Volts
Magnet Power	=	0.32 MWatts
DC Cables Voltage Drop	=	6.9 Volts
Reserve (including connections)	=	43 Volts
Power Supply	=	1300 Amps 330 Volts (0.5 MVA)

3.2 Magnet fabrication

The fabrication techniques which will be employed for the magnetic circuits must be consistent with the high-precision pole profiles required and the very large magnet cross-sections. Since the total core length of any one type of magnet is rather small, it is unlikely that a large, precision punching die will prove to be an economical solution. Initial studies and discussions indicate that in all cases the most promising technique will be to clamp short stacks (1 to 2 m) of plates or laminations and machine them together. These would then be de-burred as necessary and, in the case of the dipoles, stacked against a curved reference surface before being bolted or welded into cores. With this procedure it is possible and preferable to distribute plates from each machining operation uniformly among the required number of magnet cores, to eliminate systematic differences due to the machining.

The excitation coils have all been designed to be as simple as possible. Wherever the requirements allow, the coils are flat and have rectangular cross-sections. Nevertheless, the small quantities required will probably not justify the development and fabrication of vacuum impregnation moulds. Since however very low radiation levels are expected and with the exception of the H type dipole, the coils are fairly short, it will be possible to insulate the coils by using a double half-lapped layer of B-staged glass-mica tape on the individual turns. The coil will then be clamped and heated to partially cure the turn insulation and fix the mechanical dimensions. After this the ground wrap of glass tape is applied and the assembly can be vacuum potted in an open "Y-th" type of mould. This technique, already widely used, combines the advantages of the higher voltage holding capabilities of mica tapes with the superior mechanical strength of a pure glass/resin insulation.

3.3 Correction elements

Since the ring will always be operated at the same field level, closed orbit corrections and adjustment of coupling may be achieved by displacing or tilting individual quadrupoles. Similarly, field imperfections may be cured by adding end shims to magnets where required.

Little space would be available in the lattice for chromaticity sextupoles. Since it is believed that the fixed correction to the quadrupole profile described in Section 2.5 will be sufficient for all purposes, we do not propose to incorporate any correction elements.

In the event that small corrections do prove necessary, it will be possible to obtain them by shimming. To this end it is foreseen to include a study of the effects of a range of shims as part of the magnetic measurements programme.

4. ANTIPROTON PRODUCTION AND BEAM TRANSFERS

4.1 General description

The position of the Cooling Ring and a schematic layout of the transfer lines is shown in Fig. 4.1. Protons at 26 GeV/c are extracted from the CPS and pass along the existing beam line in TT2. About 140 m downstream of the extraction point they are deflected to the right and traverse a 20 m long tube leading to the building which houses the Cooling Ring. Here the protons are focused onto a target to produce the antiprotons. In the injection transfer line the 3.5 GeV/c antiprotons are matched to the acceptance of the Cooling Ring. One injection takes place every 2.6 seconds. When enough antiprotons have been accumulated and cooled to a small emittance they are extracted and transferred to the SPS via the existing tunnel TT2a and after a bend of 152°, down TT60. A short tunnel has to be built for the connection from TT2a to TT60. In TT60 the antiprotons travel along the beam line which normally transports high energy protons from the SPS to the West Hall. The antiprotons are injected into the SPS through the extraction channel in LSS6.

The antiprotons can be directed to ring 1 of the ISR by energizing a bending magnet at the crossing point of the antiproton beam with the beam line in TT2.

4.2 Branch-off from TT2 and transfer to the antiproton production target

The layout of the branch-off from TT2 is shown in Fig. 4.2. Immediately downstream of quadrupole QF 215 two C-type bending magnets are installed which deflect the beam horizontally by 4.5^0 to clear the quadrupole QD 216. Two more bending magnets increase the total horizontal angle to 8.5^0 before the beam traverses the tunnel wall. A small extension to TT2 houses a safety beam stopper, two more quadrupoles and two steering dipoles. The beam level in the cooling ring is 1.9 m above that in TT2 so a vertical deflection is also required. This is achieved by a 15^0 tilt of the four bending magnets which provide the horizontal deflection.

From the extension a 20 m long tube leads to the target tunnel which forms part of the building housing the cooling ring. Details of the layout in this tunnel are shown in Fig. 1.2. Here the rising beam is first made horizontal by a vertical bending magnet and then focused by a quadrupole triplet onto the antiproton production target.

The two C-type bending magnets for the branch-off and the 4 quadrupoles situated in TT2 and its extension are of a standard CERN type. The triplet upstream of the target will use quadrupoles from the neutrino area of the CPS. The other two bending magnets in TT2 and the vertical bending magnet in the target tunnel are of the same type as those for the transfer from the cooling ring to the SPS (see Fig. 4.11).

4.3 Antiproton production

The target in which the antiprotons are produced should be made of a material with a short absorption length so that the source size is kept small and the phase space density is not diluted more than necessary. This is true even though it leads to the choice of a heavy material that may have a lower conversion efficiency.

The target should be a thin cylindrical rod or wire so as to minimize reabsorption of the antiprotons, many of which will escape sideways.

Although it would be possible to focus the primary beam down to a few tenths of a millimetre (and therefore to use a correspondingly thin target), this would lead to excessive heating in the target; it would be quickly destroyed by thermal stresses. From this point of view, it is advantageous to use a material with a high value of $\sigma_B/\alpha E$, where

σ_B = tensile strength

α = coefficient of thermal expansion

E = Young's modulus.

Tungsten appears to be the best choice; its absorption length is also sufficiently small. Calculations[7] show that it will probably be necessary to adopt a target diameter of at least 3 mm. This will reduce the efficiency by a factor 2 compared with a target of 0.5 mm diameter. The latter would, however, probably explode when hit by 10^{13} protons of 26 GeV/c.

It would nevertheless be possible to replace the target every pulse. This would not require an excessive amount of material, but the machinery needed to replace and stretch the tungsten wires would be complicated. This is a possibility for future improvement; the present proposal, however, does not include it.

The antiproton production in Lead has been measured by Dekkers et al.[8] for an incident proton momentum of 23.1 GeV/c and a $\bar{p}$ momentum of 4 GeV/c. At a production angle of 0^0, they found :

$$\frac{\partial^2\sigma}{\partial\Omega\partial p} = 28.7 \pm 4.9 \text{ mb ster}^{-1} \text{ (GeV/c)}^{-1} \text{ per nucleus.}$$

To obtain $\partial^2N/\partial\Omega\partial p$ per interacting proton, excluding elastic interactions, we divide this by the total absorption cross-section $\sigma_{abs} = 1750$ mb, as measured by Bellettini et al.[9]. Since the antiproton production increases rapidly with the proton momentum in this region (by a factor two between 19.1 GeV/c and 23.1 GeV/c) [8] we apply a gain factor of 1.5 for 26 GeV/c protons.

The difference in cross-section between 3.5 GeV/c and 4 GeV/c is expected to be small, because of the broad production maximum around 4 GeV/c. Similarly, the dependence on the target material is small[8] and the possible difference between the figures for tungsten and lead is therefore neglected.

For estimating the $\bar{p}$ production, we have therefore used the value

$$\frac{\partial^2 N}{\partial \Omega \partial p} = 0.0246 \text{ ster}^{-1} \text{ (GeV/c)}^{-1} \text{ per interacting proton.}$$

The angular dependence was approximated by a parabolic correction, giving a reduction by a factor two at 100 mr [8]. Since the largest production angle of interest is 50 mr, this is a small effect.

4.4 Target matching

Typical antiproton production angles are much larger than the angular acceptance of the cooling ring; on the other hand, the target diameter can be much smaller than the ring aperture. The optics of the transfer channel must provide the matching.

It was found that for the first part of the matching system, near to the target, the use of steel-core quadrupoles would somewhat restrict the acceptance that could be obtained, because of the limitation on their gradient-aperture product.

It is, therefore, proposed to do most of the matching by means of a small magnetic horn. Detailed calculations have shown that a factor of 1.5 can indeed be gained despite some scattering and absorption in the material of the horn.

Fig. 4.3 shows a cross-section of the horn. It will consist of an aluminium inner conductor with a thickness of 0.5 mm, shaped so as to give the required focusing effect, and surrounded by a cylindrical outer conductor. The current will be pulsed, with a peak value of 145 kA and a pulse duration of 20 μs (capacitor discharge).

The shape of the horn and the target length and position have been adjusted for optimum antiproton collection at 3.5 GeV/c.

For calculating the number of antiprotons per pulse, it is assumed that 10^{13} protons hit the target. The number of $\bar{p}$ accepted has been found by means of a Monte Carlo calculation, taking into account the following effects :

a) protons hitting the target with a Gaussian radial distribution; standard deviation 0.75 mm;
b) angular dependence of production as described in paragraph 4.3;
c) reabsorption of $\bar{p}$ in the target;
d) scattering and absorption of $\bar{p}$ in the horn material.

As a result, it is found that 2.5×10^7 antiprotons per pulse will be accepted in a horizontal and vertical acceptance of 100π mm.mrad each and within a momentum spread of $\pm$ 0.75%.

4.5 The injection transfer line

The antiprotons produced in the target and prematched by the magnetic horn must be transported and matched to the cooling ring. The layout of this beam line is shown in Fig. 1.2. It consists of 8 individually powered quadrupoles arranged in doublets and a horizontal bending magnet to compensate the dispersion of the injection septum magnet. The bending magnet also separates the antiprotons from the primary protons. A proton dump which consists of a water cooled steel cylinder 2 m long and about 300 mm diameter is installed just inside the target tunnel to allow an effective shielding. Collimation of particles outside the acceptance of the transfer channel is provided in the same region.

The 8 quadrupoles for the injection transfer line are a modified version of the small type for the cooling ring (Table 3.2). The two between the target and the dump will be equipped with radiation hard coils. The bending magnet (Bl = 1 Tm) must have a clear aperture of 80 mm and might also require radiation hard coils.

A small number of correcting dipoles is required to steer the beam onto the injection trajectory.

4.6 Injection into the cooling ring

An injection scheme must be designed that does not disturb the stack of antiprotons and allows the injected beam to be driven into the stack. The solution adopted consists of a C-shaped kicker magnet at a position where the momentum compaction function α_p is large so that with a slightly higher momentum, the injected beam is separated from the stack. Since the field of a C-shaped magnet falls off slowly, an efficient screen is required which during the pulse of the kicker protects the stack but which thereafter is removed to give a free passage for the injected beam to be driven into the stack. This scheme is similar to that used for injection into the ISR.

The lattice of the cooling ring is of the FODO type. The bending magnets are positioned so as to leave empty two consecutive half periods with a large α_p where the kicker can be installed and upstream of that at a phase distance of 90^0 two more empty half periods where the septum magnets can be placed. In the upstream empty periods the α_p was forced to be zero in order to keep the strength of the kicker magnet within a reasonable limit.

The layout of the injection elements can be seen in Fig. 1.2. Two kicker magnets each about 2 m-long are positioned in periods 3 and 4 close to the central F quadrupole and two septum magnets in periods 1 and 24 around the central D quadrupole. This arrangement allows the same septum magnets to be used for extraction (Section 4.7). The D quadrupole between the septum magnets is of the large type to give sufficient aperture for the injected and extracted beams.

A cross-section of one of the two kicker magnets together with the injected beam and the stack is shown in Fig. 4.4. Because of the changing β-function and α_p the distance between the two beams varies. At the upstream end of kicker magnet 1, it is only 32.8 mm. At the exit of kicker 2 it is more than 60 mm.

Five bunches of antiprotons are injected into the cooling ring over 1 turn (the primary protons occupy one quarter of the CPS circumference). The equidistant bunches have a length of 15-20 nanoseconds and the descent of the kicker pulse must therefore be less than 105 - 20 = 85 nanosec. The flat top must last for at least 440 nanosec. The aperture of the kicker magnets is 240 mm (horizontal) and 100 mm (vertical) and the nominal kick strength 0.04 Tm per magnet. Details of their construction are discussed in Section 4.8.

The trajectory of the injected beam in the straight sections where the septum magnets are situated is shown in Fig. 4.5. The beam approaches the central orbit at an angle of 6.5°. Taking into account the deflection by the D quadrupole in between the two septum magnets, they must provide 3° of bending. D.C. magnets are proposed, with their septa outside the ultra-high vacuum.

4.7 Extraction from the cooling ring

The stack of antiprotons will be extracted in 6 batches which have to be equally spaced around the SPS. As explained in Chapter 5 each bunch has a length of about half the circumference of the cooling ring (250 nanosec). The part of the beam to be extracted is driven into the gap of a C-shaped kicker magnet positioned at large α_p and is then kicked out of the machine. The capture of part of the stack into one bunch and its subsequent acceleration to the extraction orbit is described in Section 5.

The same type of kicker magnet as for injection could be used but would be an expensive solution. It is proposed to build a kicker with an aperture just sufficient for the cooled beam and to move it into place prior to extraction. The movement can be slow since extraction will take place at most a few times per day. An aperture of 40 mm (horizontal) by 20 mm (vertical) is foreseen, which compared to the

large aperture of the injection kicker (240 mm by 100 mm) makes its construction much easier. The extraction kicker must provide a nominal kick strength of 0.04 Tm. The rise time will be 200 nanoseconds and the flat top about 300 nanoseconds. The minimum time between two successive extractions of 30 ms is given by the time required for recharging the power supply for this kicker magnet and the corresponding one in the SPS for injection.

4.8 Kicker magnets for injection and extraction

The kicker magnets must be fast and relatively powerful and therefore must operate at high voltage. Satisfactory experience in the construction of a high voltage kicker has already been gained in the PS with the so-called Full Aperture Kicker (FAK) system; it is proposed that the injection and extraction kicker systems should draw heavily on FAK experience and use identical equipment wherever possible.

The kicker magnets must operate in ultra high vacuum and have strictly limited stray fields so as not to disturb the stack.

4.8.1 Injection kicker

The injection kicker is a static device located in two 2 m vacuum tanks up and downstream of quadrupole QFW4. Each tank contains six identical magnet modules of 0.008 Tm kick strength and 75 ns fall time (95-5%). Thus the total required kick strength of 0.08 Tm can be met with some margin to satisfy operational needs or equipment outage.

The magnet module is of the delay line type, has ten discrete cells and a characteristic impedance of 15 ohms. It is judged that 15 ohms is the lowest impedance which can be considered for reasons of cut-off frequency and pulse distorsion; the adoption of this impedance also allows many FAK designs to be used for the pulse generators.

The magnetic circuit of the magnet is a ferrite C-core which is profiled to improve the field uniformity in the aperture. The high voltage and earth conductors are placed around the back-leg so as to have free access between the aperture and the stack. The magnet capacitance is provided by interleaved high voltage and earth plates attached to their respective conductors. A capacitor plate spacing of 7 mm is proposed, identical to that which has given trouble free operation in the FAK.

The stray field from the injection kicker must not be allowed to disturb the stack. For reasonably acceptable stack blow-up it is desirable that the fast stray field at the stack centre be less than 2×10^{-3} of the kicker field. This requires an efficient moveable eddy current shutter between the kicker aperture and the stack.

A schematic cross-section of the magnet module with its shutter installed in the vacuum tank, is shown in Fig. 4.6. In this arrangement, assuming a stack/injected beam separation of 30 mm, it is still possible to kick the fringe of the injected beam closest to the shutter with 95% of the nominal kick.

Bake out at a temperature of 300°C is foreseen for which titanium or inconel are suitable plate materials.

Twelve 80 kV pulse generators are needed for excitation of the injection kicker modules. These can be identical to those already built for FAK. Because the injection kicker pulse length is much shorter than that of the FAK the PFN cable lengths can be shorter and the pulsed resonant power supply transformers reduced in size.

The main parameters of the proposed injection kicker system are given in Table 4.1.

4.8.2 Extraction kicker

The extraction kicker is a plunging device located in a 0.9 m tank downstream of quadrupole QFW22. Two options exist according to whether the difficulties are to be found in the magnet or pulse generator. The first option is to build the magnet as a 15 Ω delay line, in which case the magnet is large and heavy but the pulse generator is simple (identical to those of the injection kicker). The second option is to build the magnet as a lumped inductance with shunt capacitive compensation external to the vacuum tank. In this case the magnet is light and simple but one of the thyratrons of the pulse generator must be bidirectional because of the substantial reflection at the magnet.

On balance the second option is favoured because it leads to a smaller, lighter plunging assembly, allows better pumping of the ferrite, reduces the vacuum tank size and yet still gives an acceptable kick field rise time of less than 180 ns (2-98%). Further a high voltage bidirectional switch is already under development for the PS/SPS Multibatch Filling Project.

The lumped inductance magnet is a single turn ferrite C-cored device with the earth conductor located above and below the aperture to allow transfer of the stack for ejection. The stray field disturbance on the stack is of less concern than for the injection kicker because pulsing takes place only 5 times in the presence of stack. Horizontal screening plates, attached to the earth conductors, are proposed to reduce the stray field to an acceptable level. A schematic cross-section is given in Fig. 4.7.

As far as possible the pulse generator is the same as used for the inflection kicker. The thyratron at the remote end of the PFN must be bidirectional. Provided that the transmission cable length from the PFN to the magnet is less than about 24 m there is no requirement for

the thyratron at the front end of the PFN to be bidirectional because the magnet reflection can pass whilst the tube is still conducting the main pulse.

The parameters of the ejection kicker system are given in Table 4.2.

TABLE 4.1

Injection Kicker Parameters

Type of module	Delay line
Number of modules	12
Minimum aperture height (mm)	100
Useful aperture width - 95% kick (mm)	225
Module length (mm)	275
Inter-module spacing (mm)	40
Characteristic impedance (ohms)	15
Kick rise/fall time 5-95% (ns)	75
Module kick strength for 80 kV PFN voltage (Tm)	0.008
Remanent field (T)	5.10^{-4}
Module weight (kg)	> 300
Module ferrite weight (kg)	52
Ferrite type	8C11
Capacitor plate spacing (mm)	7
Capacitor plate material	Inconel or titanium
High voltage insulation	97-98% Al_2O_3
PFN voltage for nominal kick strength of 0.08 Tm (kV)	66.7
Kick pulse jitter, absolute (ns)	< 2
Pulse repetition rate (pulses/s)	< 1
PFN charging time (ms)	3

TABLE 4.2

Ejection Kicker Parameters

Type of module	Lumped inductance
Number of modules	1
Minimum aperture height (mm)	20
Useful aperture width - 98% kick (mm)	43
Module length (mm)	750
System characteristic impedance (ohms)	15
Kick rise time 2-98% (ns)	178
Kick variation on flat-top (%)	< 2
Maximum PFN charging voltage (kV)	70
Corresponding kick strength (Tm)	0.08
PFN voltage for nominal kick strength of 0.06 Tm (kV)	52.5
Corresponding peak magnet voltage (kV)	33.4
Half height duration (ns)	< 120
Ferrite weight (kg)	39
Ferrite type	8C11
High voltage insulation	97-98% Al_2O_3
Kick pulse jitter, absolute (ns)	< 6
Pulse repetition interval (ms)	30
PFN charging time (ms)	3
Number of consecutive pulses	6
Maximum transmission cable length (m)	24

4.9 Transfer of antiprotons to the SPS

The extracted antiprotons are transferred to the SPS along the existing tunnel TT2a and after a bend of 152° down the existing beam line in TT60 (see Fig. 4.1). Injection into the SPS uses the elements of the extraction channel in LSS6.

The proposed scheme does not use any part of a beam line that is required for injecting protons into the SPS. This allows the whole channel to be tuned prior to the transfer of antiprotons by using 3.5 GeV/c protons travelling in the opposite direction

The extracted antiprotons leave the cooling ring building through a tube of small diameter in the wall and re-enter TT2 immediately upstream of the branch-off to TT10. The layout of this region is shown in Fig. 4.8. A pair of tilted bending magnets one on each side of the wall brings the beam down to the level of TT2 and makes the two beam lines cross at an angle of 7.5° between the quadrupoles QD 332 and QF 333. Here a bending magnet can direct the antiprotons along TT2 towards ring 1 of the ISR or be turned off allowing the beam to go via TT2a to the SPS.

The transfer along TT2a requires 4 horizontal and one vertical bending magnet and a number of small quadrupoles installed at 20 m intervals.

The connection tunnel to TT60 is built where TT2a and TT3 join. (Fig. 4.9). The horizontal deflection of 152° uses two groups of five bending magnets with an F quadrupole in between to compensate the dispersion. The beam enters TT60 through a small hole in the tunnel wall. The last of the 10 bending magnets is installed just below the TT60 beam line and a vertical bending magnet several metres downstream brings the beam on axis. The vertical deflection required is achieved by tilting part of the ten bending magnets.

The cross-section and main parameters of these magnets are given in Fig. 4.11. The same type will be used both for the deflections in TT2a and for the 26 GeV/c protons downstream of the TT2 branch-off.

A provisional cross-section and parameters of the quadrupole needed up to TT60 is shown in Fig. 4.10.

The apertures in the existing TT60 line are adequate for a beam of 1 to 1.4 π mm.mrad.The beam line was designed for 200 GeV/c and in the upstream part for 400 GeV/c. When used for 3.5 GeV/c antiprotons, the magnets will be operated at about 1% of their normal strength. The power supplies for these magnets will be modified to achieve the required precision and stability at these low current levels.

4.10 Injection of antiprotons into the SPS

For injection of antiprotons into the SPS the extraction channel in LSS6 will be used. A possible trajectory has been calculated which uses the extraction kicker MKE, the electrostatic septum ZS and the thick septum magnet MSE. The ZS provides sufficient deflection so that the thin septum magnet MST need not be pulsed. No closed orbit bump will be applied in order not to run the MKE at too low a voltage.

The aperture of the SPS extraction channel is tightest in the MSE (gap 20 mm) corresponding to a beam of 1π mm mrad vertical emittance.

The pulse form of the MKE is adequate for injecting the 6 bunches of antiprotons. The risetime can be as long as 3.6 microseconds. The nominal deflection is about 1 mrad and only one of the two magnets will be pulsed, in order to avoid too low an operating voltage for the switch tubes. However, the multipulsing at intervals of about 30 ms requires an additional resonant charging supply with six primary capacitor banks.

The ZS deflects about 1 mrad which corresponds to a field strength of 3 kV/cm. For injection of antiprotons its polarity is reversed, by means of a remote switch.

The MSE current of 200 A (0.8% of its maximum) will be provided by a separate small power supply.

4.11 Injection of protons into the SPS

The protons which will collide with the antiprotons are injected into the SPS in the usual way. At the moment of injection the 6 bunches of antiprotons are already circulating in the SPS and would be kicked out of the machine when the inflector is pulsed. This is avoided by displacing the phase of the antiproton bunches with respect to the protons. The amount of the displacement is given by the rise time of the inflector.

The new inflector of the SPS for multibatch injection has a repetition time of not less than 0.5 second. Each proton bunch must, therefore, come from a different CPS pulse and the total time for the transfer is 5 x 0.65 = 3.25 seconds.

5. RF SYSTEMS FOR THE CPS AND THE COOLING RING

In this chapter we present a consistent series of RF manipulations designed to meet the needs of the proton-antiproton proposal, up to the point that antiprotons reach the SPS. Further manipulations in the SPS are described in Section 10. One can think of alternatives to many of these procedures. Some of these we can dismiss as incompatible with other links in the chain and others, while offering greater beam stability, have been eliminated because of their cost or complexity.

5.1 Filling one quadrant of the CPS with protons

The circumference of the antiproton cooling ring is one quarter that of the CPS. If the antiprotons produced by the impact of the CPS beam are to fit neatly into the circumference of the antiproton ring, one must find a scheme which crowds as many parent protons as possible into one quarter of the CPS circumference.

The CPS is fed by a four-ring booster. The circumference of each ring is just one quarter of the CPS and equal to that of the cooling ring. Clearly, one must endeavour to superimpose the four beams from the booster in the same quadrant of the CPS. This can be done by a combination of transverse and longitudinal stacking.

First, the beams from each pair of booster rings will be stacked in vertical phase space. In this way, two double strength beams may be formed, each one quarter of a CPS ring long. To cause these two beams to coalesce one must inject them sequentially into the CPS, but at slightly different momenta, onto two different mean orbits and their revolution frequencies will be different. Each beam is then trapped separately with reduced voltage. For this only a few of the PS cavities are needed. The harmonic number will be the same (i.e. 20) for both beams, but one string of five bunches will tend to overtake the other one. At the moment that the two bunch trains fall into register, the RF voltages are switched off and then on again at an increased voltage and at the centre frequency to form buckets which embrace both beams. Detailed calculations show that subsequent filamentation dilutes the combined bunch area by a factor between 1.5 and 1.7, leading to a total bunch area of 30 mrad.

The time constant of the CPS cavities (2 μs) is short enough to perform the proposed voltage gymnastics.

5.2 Acceleration in the CPS

At the cost of an extension of the CPS cycle by a few milliseconds, $\dot{B}$ can be reduced in the parabola and sufficient bucket area made available for this large bunch. The bunch area, twice as big as normally accelerated, should ensure that the beam is stable against longitudinal instabilities in spite of its unusually high intensity.

The five CPS bunches within one quadrant are fast ejected to impinge upon the target where they create antiprotons.

5.3 Debunching and stacking the antiprotons in the cooling ring

The antiproton beam of $\pm$ 7.5 $^{o}/_{oo}$ momentum spread from the production target, is allowed to debunch and then precooled to a momentum spread of $\pm$ 1 $^{o}/_{oo}$ in the antiproton ring. It must then be carried across the vacuum chamber from the injection orbit to be stacked with previous batches, which are in the process of being cooled. All this must be over before the CPS is ready, one cycle later, to create another burst of antiprotons.

In moving the beam its momentum is decreased by about 3% in 100 ms. The voltage required is small, but the bucket area needed to hold $\pm$ 1 $^{o}/_{oo}$ is large. We propose to use a single standard PS cavity with some additional capacitive loading to lower its tuning range to 1.8 MHz. This provides 8 kV, enough to contain the momentum spread. The harmonic number in the antiproton ring will be 1.

5.4 Bunching antiprotons for extraction from the cooling ring

We shall see in Section 10 that the antiproton bunches injected in the SPS must be rather long if space charge ΔQ due to the high line density is to be tolerable. An acceptable bunch length corresponds to half a turn of the cooling ring. Bunches must be formed at a harmonic number of 1 within the stack, and moved to an orbit where they may be extracted towards the SPS. To form and extract the six long bunches needed for the SPS, this must be repeated six times, although in initial tests at low luminosity only one such operation is needed.

The single PS cavity installed in the cooling ring to displace the antiprotons after precooling will be used. To keep the bucket area small enough to contain only one sixth of the beam, the voltage must be very low (92 V for a bunch area of 12 mrad). A larger bunch area would exceed the capacity of the SPS 200 MHz buckets, since 12 mrad in the cooling ring scaled as h/R becomes 1260 mrad in the SPS even before any blow-up has taken place.

The cooled antiproton beam must have a momentum spread of $\pm$ 1.5 x 10^{-3} to remove the beam in six passes with a bucket of 12 mrad. Careful control of the longitudinal acceptance must be exercised to keep the bunches of equal intensity. This can be facilitated by using the stochastic cooling loop to flatten the momentum distribution. Fortunately, such precise voltage control will not be required in early single-bunch transfers.

TABLE 5.1

RF PARAMETERS FOR THE COOLING RING

1) Stacking

γ_{tr}		2.43	
$\Delta p/p$ after initial cooling		1	$^{o}/_{oo}$
Corresponding bunch area at 3.5 GeV/c		45	mrad
Deceleration rate for $\sim$ 3% within 0.1 s		1	GeV/c/s
Energy loss per turn		524	eV
Accelerating voltage	without blow-up during adiabatic trapping	3	kV
Stable phase angle	without blow-up during adiabatic trapping	10	deg

2) Ejection

Total bunch area (6 bunches)	72	mrad
Total $\Delta p/p$ of coasting beam at 3.5 GeV/c	± 1.536	10^{-3}
RF frequency (h = 1, R = 25 m)	1.84	MHz
RF voltage for stat. bucket 12 mrad	92	V
RF voltage for bunch length $\pm 90^{o}$	514	V
$\Delta p/p$ of 12 mrad bunch ($\pm 90^{o}$)	± 6.74	10^{-4}
Length of 12 mrad bunch	$25\pi = 78.54$	m
Longitudinal stability $(Z/n)_{max}$ (12 mrad coasting)	$\sim$ 840	Ω
Longitudinal stability " (12 mrad bunched 180^{o})	~ 2560	Ω

6. STOCHASTIC COOLING

6.1 General description of momentum cooling

Fig. 6.1 illustrates the general principle of stochastic momentum cooling. A pick-up electrode is connected through a linear high-gain, wide-band amplifier to a wide-band accelerating gap (kicker). A particle that passes the pick-up induces a short pulse in it. The electrical delay in the system is such that this pulse arrives at the kicker together with the particle. The latter is therefore accelerated by the peak value of the pulse. This is called the coherent effect.

At the same time, other particles also create pulses. These are not infinitely narrow, due to the finite system band-width, so that some of them will also influence the particle under consideration. The mean effect of this noise (called Schottky noise) will be zero if the system does not transmit the d.c. component. It will, however, lead to an increase of the energy spread (incoherent effect).

Since the duration of the pulses is quite short compared to the revolution time, and since different particles have different revolution times, each particle will be influenced by a small and continuously changing fraction of the other particles. This quasi-random effect has been analyzed quantitatively[10], and it was found that the blow-up is similar to that which would result from purely random kicks. That is, the mean square energy change is proportional to the time and to the square of the electronic gain. The proportionality factor depends on the amount by which the particles overtake each other on each turn.

Two extreme regimes may be distinguished :

a) "good mixing". On each successive turn, the particle is influenced by different particles, i.e. the typical differences in revolution time between the particles are large compared to the pulse length;

b) "bad mixing". The population of particles seen by a specific particle on successive turns, changes only slowly. This situation exists in the present ring for all cooling systems.

It appears from the theory that a particle is only influenced by those frequency components in the noise spectrum that are nearly coincident with one of the harmonics of its own revolution frequency. In case a), the frequency bands belonging to different harmonic numbers overlap due to the large frequency spread between the particles. Each particle can therefore be influenced by many groups of other particles, each around a different revolution frequency. As a result, it is found that the blow-up effect is the same as that caused by purely random kicks. In case b), the Schottky bands do not overlap, and each particle is only influenced by particles with nearly the same revolution frequency. The blow-up is larger than in case a) and it is proportional to the local density of particles in frequency (or energy) space.

Additional blow-up is caused by the amplifier noise. In contrast with the Schottky noise, which is concentrated in narrow bands around the revolution harmonics, that from the amplifier has nearly equal density at all frequencies. With the present design, its density is well below the Schottky noise density at the frequencies that influence the particles (i.e. the Schottky bands) and so it does not affect the cooling appreciably. However, it is responsible for most of the total output power at the kicker terminals.

Since the coherent effect is proportional to the system gain, but the blow-up to the square, the gain has to be chosen so as to obtain an optimum balance between these two effects[11]. With bad mixing, the blow-up is proportional to the particle density in energy space, so the optimum gain will be inversely proportional to this density.

If the gain were the same for all particles, there would be no

cooling effect; only a general acceleration or deceleration. A concentration of particles (i.e. cooling) results only if the coherent effect pushes the particles in the direction of decreasing gain. This dependence of the gain on energy can be obtained either by shaping the pick-up electrode so that its gain depends on the closed orbit position (e.g. by using a linear transverse pick-up)[12] or by using a sum pick-up and including a filter in the electronics chain, using the fact that the revolution frequency depends on energy. The filter should act in a similar way on all harmonics of the revolution frequency and it should have a constant group delay[13].

6.2 Reasons for using two separate systems

The filter method is preferable for low-density beams (e.g. in the precooling system) where the amplifier noise is relatively important, since a sum pick-up produces as large a signal as can be obtained across the whole aperture. Moreover, a wide-band sum pick-up can be much shorter in the beam direction than a difference pick-up, because the use of a ferrite ring around the beam gives sufficient impedance even with a very short pick-up. (The length of a pick-up with variable gain across the aperture must be of the order of a quarter wavelength in the centre of the passband.) As a result, many more sum pick-ups can be placed in a given space, thus increasing the available signal. For the precooling system, the design includes 100 pick-ups in a straight section of 5 m length. A linear filter will be used so that the gain is linearly dependent on energy, as for a linear transverse pick-up. This is adequate for compressing the energy spread of each injected pulse by a factor 7.5 in two seconds.

For cooling the stack, on the other hand, such a system is not suitable. As discussed above the gain must be inversely proportional to the local particle density in the stack. Since theory shows[11] that a minimum aperture is required for the stack if the density profile versus energy has an exponential shape, we would need a filter with an

approximately exponential response. The ratio of density between the centre of the stack and its edge must be about 20000 for the required performance and this must also be the ratio by which the gain changes over a region in which the revolution frequency changes by 0.25%.

Although such filters can be designed, there is another reason why they cannot be used. This is connected with the feedback from the kicker towards the pick-up, via the beam. The total gain of the loop formed by pick-up-amplifier-kicker-beam-pick-up might exceed unity. This implies either a risk of instabilities or, if gain and phase shift versus frequency are such that the system is stable, a loop gain larger than one would lead to a decrease of the Schottky signals and, therefore, spoil the stochastic cooling. Theory shows[11] that both without a filter (for any pick-up shape), or with a linear filter, the condition for unit loop gain is about equal to the condition for zero cooling effect (i.e. blow-up cancelling the coherent effect). Thus to get useful cooling, the gain must be reduced so that the feedback effect will be small.

With higher-order filters, however, the loop gain would be higher at some frequencies. Such filters are therefore precluded. However, pick-ups with a gain strongly dependent on particle position can now be used, since the precooling has already increased the density enough to make the amplifier noise relatively harmless even with only 30 pick-ups.

6.3 Precooling system

The pick-ups for the precooling system should not see the particles in the stack to avoid overloading the output amplifier with their Schottky noise. Similarly, the precooling kickers should not kick the stack thereby causing blow up. The Schottky noise of the precooling system cannot blow up the stack because it does not overlap with the Schottky bands of the stack. The amplifier noise is present at all frequencies and it is much higher on the precooling kickers than

on the stack kickers because of the higher gain needed at lower density.

For this reason, the precooling pick-ups and kickers (which will be of similar construction) must surround the newly injected beam with their ferrite rings; the stack must pass outside. When the precooled beam is displaced by the RF system towards the top of the stack, part of the ferrite must be temporarily removed. A possible way of doing this is suggested in Fig. 6.2.

Obviously, these devices should be located at a point in the lattice where α_p is high, so that the injected beam and the stack are well separated. This, however, means that the kickers will not only change the particle energy, but also excite the horizontal betatron oscillations through components of the amplifier noise that coincide with the betatron Schottky bands. In order to reduce this effect sufficiently, these kickers will be grouped into two equal sub-assemblies, in straight sections that are half a betatron wavelength apart, as shown in fig. 1.2.

At present it is assumed that the pick-ups and kickers will have an impedance of 50 ohms, like those already used in the ISR experiments. The possibility of increasing this impedance will be investigated. This would improve the signal-to-noise ratio and reduce the amplifier output power required.

The linear filter (fig. 6.3) will be made by using a delay line D1 that is shorted at its end, fed by a current source. If the length of the line is such that its delay is half the revolution time at the centre of the particle distribution, it will have zero impedance at all harmonics of the corresponding revolution frequency. In a small region around each harmonic, the impedance will change linearly[19].

The delay line D1 is shunted by some lumped components (R, L, C) and by a combination of two further lines of the same length, D2 and D3.

The end of D2 is shorted, that of D3 is open. These components serve to reduce the gain between the Schottky bands, in order to decrease the output power due to amplifier noise. The combination D2-D3 behaves like a series tuned circuit, having zero impedance at two intermediate points between each two adjoining Schottky bands. The resistance R causes damping at those frequencies where the total impedance would otherwise become too high. L and C are added in order to make the degree of damping dependent on the harmonic number; this is desirable because the Schottky bands are wider at the high frequency end. The whole is optimized for minimum r.m.s. gain over the entire passband (150-400 MHz), while keeping the phase shift inside the Schottky bands to less than 30°. The resulting r.m.s. gain is 0.92 times the average gain at the edge of the Schottky bands.

Losses in the delay lines modify the characteristics slightly; in particular, around the zero-gain points the gain remains finite. This effect can be minimized by choosing a line of sufficiently large cross-section for D1, and then reduced to a negligible level by a compensating device, not shown in fig. 6.3. For D2 and D3, the losses are not important.

The main parameters of the precooling system are :

Number of pick-ups	100
Number of kickers	2 x 50
Impedance of pick-ups and kickers	50 Ω
System bandwidth	250 MHz
Lower frequency	150 MHz
Upper frequency	400 MHz
Noise figure of input amplifiers (one for each pick-up)	3 dB
Number of particles per pulse	2.5×10^{7}
Momentum spread	± 0.75%
Output power due to Schottky noise	1.8 kW
Output power due to amplifier noise	3.2 kW
Amplifier rating	25 kW

Fig. 6.4 illustrates the cooling expected from numerical computation. In two seconds, about 80% of the particles would be collected inside a momentum spread of ± 0.1%, i.e. 7.5 times smaller than the original one.

6.4 Momentum cooling of the stack

The radiofrequency system will deposit each new precooled pulse at the top of the stack. Allowing for a blow-up during RF stacking by a factor 1.5, the particle density in momentum space will be 5 times as high as the injected density. The ratio of Schottky noise to amplifier noise will therefore be more favourable, so that the number of pick-ups needed is smaller than for the precooling system. Moreover, the system gain at the top of the stack may be about 5 times lower than at the edge of the injected momentum distribution; this results in an output power much smaller than for the precooling system.

The gain of the stack system will decrease strongly towards the bottom of the stack. The gain profile has been determined in such a way that it results in a density profile with maximum slope, while still ensuring a constant particle flux in momentum space towards the stack bottom (i.e. climbing against the density gradient) equal to the average injected flux. Fig. 6.5 shows this density profile, together with some curves that demonstrate the build-up of the stack with time.

The cooling system will use pick-ups with a sensitivity that depends strongly on the horizontal position of the particles (Fig. 6.6). A linear filter similar to the one described for the precooling system, with zero gain at the stack bottom, will be used in addition.

Nevertheless, the gain needed around the stack bottom is so low that the amplifier noise would again be too high in that region if the only means of reducing the gain there would be the pick-up of fig. 6.6, together with the linear filter. In order to improve this, the system is

split up into three sections, with pick-ups displaced horizontally relative to each other. (A fourth section with a linear pick-up for cooling the densest part of the stack is added to these.)

The pick-ups that are most sensitive at the stack bottom are followed by less electronic gain, so that the overall gain profile is still as required. A block diagram is shown in fig. 6.7; the gain of the four sections vs energy in fig. 6.8.

Additional noise filters reduce the gain of sections 1 and 2 below the cross-over point where the next section takes over. In this way, the amplifier noise of these sections is reduced sufficiently in the bottom region of the stack where it would be most harmful. With the density distribution of fig. 6.5, the amplifier noise power density inside the Schottky bands will be at least three times lower than the Schottky noise density anywhere in the stack. The filters used for this purpose do not influence the cooling process much below the cross-over point; their phase shift is therefore irrelevant in that region. These filters will again use delay lines in order to obtain a filter characteristic that repeats itself around each harmonic.

The output power of section No. 3 will be much lower than that of sections 1 and 2, because of its low gain. Therefore it is possible to use a higher bandwidth (1-2 GHz) for this section. This improves the cooling near the stack bottom and keeps the number of particles remaining in the tail of the stack low (see the increased density gradient in this region in fig. 6.5).

Particles of different energy have different times of flight between the pick-ups and the kicker. For the high bandwidth section 3, these differences become comparable with the response time of the system. This explains the peculiar shape of the gain profile of section 3, as shown in fig. 6.8. The effect is small enough not to be troublesome.

The final momentum spread of the stack ($\pm$ 1.5 x 10^{-3}) is so small that it would be difficult to meet the requirements on selectivity of the linear filter, due to the losses in the delay line. For this reason, Section 4 will not use a filter, but it will be equipped with a linear transverse pick-up. The amplifier noise is quite negligible for this section, because of the high particle density and the low system gain. Techniques similar to those already used in the ISR experiments [14] may be applied. The cooling time at the final stack density would be 0.3 h, i.e. small enough to overcome the blow-up due to the intra-beam scattering.

The pick-ups for the stack cooling will be placed in straight sections 17, 18, 19 and 20 where α_p is large. This is needed for obtaining the required pick-up response. The kickers will be in straight section 13 where α_p is zero. The kickers will be in straight section 13 where α_p is zero. They will therefore not excite the horizontal betatron oscillations.

The main parameters of the stack cooling system will be as follows :

Maximum total stack width	$\Delta p/p = 2.5 \times 10^{-2}$
Final half width	$\Delta p/p = 1.5 \times 10^{-3}$

Section	1	2	3	4
Number of pick-ups	14	14	2	1
Number of kickers	50		20	4
Impedance of pick-ups, kickers	50		50	50 Ω
System bandwidth	250		1000	1000 MHz
Lower frequency	250		1000	1000 MHz
Upper frequency	500		2000	2000 MHz
Output power from Schottky noise	850		12	7.5 W
Output power from amplifier noise	725		3	0.5 W
Power amplifier rating	5000		50	20 W

6.5 Betatron cooling

It would be difficult to reduce the betatron amplitudes to an appreciable extent during the precooling of each injected pulse, because the amplifier noise would be too high in comparison with the betatron signal from a transverse pick-up. Moreover, it is preferable to do betatron cooling on the stack, because this relaxes the vacuum requirements (multiple scattering) and counteracts the blow-up by intra-beam scattering.

Reduction of the initial oscillation amplitudes by a factor 8.5 horizontally and 10 vertically is required. The cooling time should not be too long, in order to allow the collection of small stacks with the final emittance in a few hours, if required.

It appears that these requirements are not too difficult to satisfy and that we could even consider to cool only the bottom part of the stack. A stack of 6×10^{11} particles within the final momentum spread would have a cooling time constant of 0.5 h with an optimum gain system working between 1 and 2.5 GHz.

We could, however, greatly improve this by additional cooling during the stacking process. At lower densities than the final one, the cooling is correspondingly faster if we adjust the gain accordingly. For the horizontal cooling, this is achieved if more or less automatically, if we use the same pick-ups as for the momentum cooling; for the vertical cooling, similar pick-ups may be used where the upper and lower loop signals are subtracted before amplification.

No detailed design work has yet been done on these systems : it seems clear, however, that it will not be difficult to reach the required performance with simple means, comparable to those used in the ISR experiments. The output power required will be quite low and filters will not be needed.

In fact, it may be necessary to limit the reduction of the amplitudes in order not to increase the incoherent tune shift in the SPS beyond what can be tolerated (see Section 10).

7. VACUUM FOR THE COOLING RING

7.1 Influence of the rest gas

The rest gas will have the following effects on the circulating antiprotons :

i) Multiple Coulomb scattering will counteract the cooling of the horizontal and vertical emittance.

ii) Particles will be lost by single Coulomb scattering and nuclear interactions.

iii) The beam will lose energy due to ionisation.

iv) The positive ions created and attracted by the beam (neutralization) will increase effects i) and ii). Their density may under certain circumstances exceed the initial rest gas density.

v) The neutralization will influence the betatron tunes.

vi) Coupled ion - antiproton oscillations may cause a slow blow-up of the stack.

Analysis shows that effects i), iv) and vi) are the most important and that they determine both the pressure and the neutralization factor required. None of these effects can be calculated with high precision. The nominal design figures

$$p < 10^{-10} \text{ Torr (nitrogen equivalent)}$$
$$\eta < 0.03$$

were therefore chosen with a certain safety margin, also taking into account that no great saving would be made by increasing them even by an order of magnitude.

With these values, we expect that all effects mentioned will be sufficiently small :

i) The heating rate for the final stack with $E = \pi \times 10^{-6}$ rad.m will be 5×10^{-6} s^{-1}, i.e. 60 times less than the cooling rate. A gas composition of 90% H_2, 10% N_2 or CO is assumed.

ii) The single scattering lifetime will be about 1620 h, the nuclear interaction lifetime, 6000 hours.

iii) The relative energy loss will be 10^{-4} during 24 hours.

iv) The ion density inside the final stack with $\eta \approx 0.03$ will be roughly equal to six times the original gas density, thus increasing effects i) and ii) by a factor 7.

v) The neutralization will reduce the vertical tune shift by about 10^{-3}.

vi) This effect was calculated using the theory existing for electron-proton oscillations [15,16]. The high mass of the ions (assumed to be H_2) compared to electrons reduces their oscillation frequency in the potential well to a value less than the betatron frequency. Taking into account Landau damping due to the tune spread present in the stack, we should be below the instability threshold with $\eta = 0.03$. Moreover, even if this were not true (the theory being approximative), the growth rate would be considerably below the cooling rate.

7.2 Vacuum system layout and characteristics

The pressure requirement is such that a combination of titanium sublimation (PS) and sputter ion pumps (PI) are required. Furthermore vacuum annealed austenitic high tensile stainless steel will be required for the chambers so that specific degassing rates of 2×10^{-13} Torr $\ell\ s^{-1}\ cm^{-2}$ can be attained. This combination along with in-situ bakeouts should ensure the sort of performance which has become normal at the ISR. The bakeout temperature needs not exceed 300°C.

Figure 7.1 shows the vacuum system layout over one quadrant of the cooling ring. The injection region is illustrated in Fig. 7.2. It should present no major difficulty because the septum magnet is designed such that it is placed outside the vacuum system. The sputter ion pumps should have a speed of 200 to 500 $\ell\ s^{-1}$ and the sublimation pumps around 2000 $\ell\ s^{-1}$. There will be four sector valves (VS) placed at the regions where the beam sizes are a minimum. The beam stay-clear apertures in these

regions are somewhat smaller than the apertures of the enlarged ISR sector valves. Simple gate valves (GV) (in the form of shutters) may need to be added in the larger aperture regions of the vacuum sectors.

Pump-down during bakeout will be carried out by means of 100 ℓs^{-1} turbo-molecular pumps (PT); a minimum of two per quadrant is necessary and maybe a third if laboratory tests indicate that during the 24 hours of a bakeout the minimum pressure at 300°C is inadequate.

Vacuum gauges are distributed throughout the ring to facilitate leak detection. Two residual gas analysers per quadrant will be installed near to the potential sources of heavy gas species. It is important that the final gas composition contains at least 90% H_2 with the minimum possible of heavier molecules.

The maximum distance between pumps is 5 metres in the short bending magnets where the vacuum chamber conductance is around 1300 $m\ell s^{-1}$. The distance between pumps in the long bending magnets is 8 m where the conductance is only 610 $m\ell s^{-1}$. The highest pressure occurring in the bending magnets is expected to be well below 10^{-10} Torr.

These estimates are based on a specific degassing rate of 2×10^{-13} $T\ell s^{-1}$ cm^{-2}. .This will necessitate prebaking all parts of the stainless steel chambers at 950°C for up to ten hours in a vacuum furnace at a pressure of 10^{-6} Torr.

No details of the large tanks in the straight-sections are given because little is yet known of their vacuum characteristics. They will be supplied with enough pumping capability to maintain the average pressure at less than 10^{-10} Torr. Special precautions will be needed in those places containing ferrite or other porous materials.

All such tanks will be subjected to a low pressure limit test to ensure that they meet the vacuum requirements.

7.3 Clearing

The low value of η implies the use of ion clearing fields throughout the vacuum chamber. A similar arrangement to that used in the ISR with a pair of clearing electrodes at the exit of each bending magnet is expected to reduce the value of η to below 0.03 for a cool beam at a pressure of $< 10^{-10}$ Torr. The ions drift out of the magnet due to forces exerted by the "crossed" electric fields of the beam and the magnetic bending field. During the early stages of cooling and stacking with relatively feeble antiproton beam densities, the electric fields in the beam are not high enough to produce adequate drift velocities. In these early stages the η values are expected to approach unity in the bending magnets without affecting the heating rate due to Coulomb scattering on the ions. This, because, at that stage both the emittance E and the number of antiprotons N are such that the ion density is a factor of many hundreds less than that encountered by a cool beam.

The straight sections between magnets will also be equipped with clearing electrodes to avoid trapping ions in the cool beam potential of around 15 Volts with respect to the vacuum chamber walls. The voltage on all the clearing electrodes will need to be somewhat in excess of the cool beam potential.

8. INSTRUMENTATION AND CONTROLS

8.1 Introduction

During normal operation, the beam-derived signals driving the stochastic cooling systems contain information on several important beam parameters (see Section 6). Most of the additional diagnostic equipment is needed to facilitate the initial running-in and subsequent setting-up for operation.

The low intensity of an injected $\bar{p}$ pulse (2×10^7 $\bar{p}$pp) renders observation difficult. It is therefore assumed that most of the setting-up is done with p beams of an intensity permitting easy observation. After polarity reversal of the magnetic elements, the $\bar{p}$ should then behave in the same way. However, whenever possible, the $\bar{p}$ beams will be observed directly.

The proposed diagnostic systems are described below, and their locations shown in Figure 8.1.

8.1.1 Scintillator screens + TV

Scintillator screens will be used to detect the beam in the injection and ejection channels. This requires screens at the following locations :

- entrance to septum
- exit from septum
- entrance to injection kicker.

To observe the first-turn trajectory, a combined screen and beam stopper to prevent multiple traversals will be located

- after nearly 1 turn.

The scintillator screens are 1 mm thick doped alumina plates. The cameras are a radiation resistant version, developed at the PS. The sensitivity, as tested on the PS Booster, is 2×10^9 p/cm^2, and with a

special Vidicon tube, as used for ICE, it should be possible to see about 10^8 p/cm^2. The p test beam will then be easily visible and possibly also the pions accompanying the antiprotons. The ejection of a small $\bar{p}$ stack (10^9 $\bar{p}$) could be observed at the entrance and exit of the septum.

8.1.2 Beam transformers

The beam transformers will be similar to those used on the ISR and the SPS, with three ferromagnetic toroids : one is used in a magnetic amplifier circuit to extend the measurements down to d.c., a second feeds an integration circuit to extend the bandwidth upwards to a few MHz, and a third forms an independent passive transformer with a bandwidth of $\sim$ 100 MHz.

A version of the SPS beam transformer, improved for use on ICE, has reached a resolution of 5 μA at frequencies below 1 Hz and about 50 μA at the high frequency end. This just permits observation of the injected $\bar{p}$ beam and is adequate to observe the slow increase in stack intensity.

For operational reliability, 2 beam transformers will be installed at places where the required aperture is small.

8.1.3 Schottky signals

Schottky signals caused by statistical fluctuations in the proton beam current are not only the basis for stochastic cooling but also offer a convenient means of beam observation [17]. Spectrum analysis of a harmonic band of the current fluctuation gives the square root of the particle density versus revolution frequency, i.e. the particle density versus momentum. Furthermore, spectrum analysis of betatron sidebands will yield the vertical and radial Q values of narrow $\Delta p/p$ beams in the machine. By placing beams at various radial positions, complete working lines (Q_V, Q_H versus $\Delta p/p$) can be measured. This can be done with a single injected proton beam, positioned by phase displacement acceleration.

Perturbation and phase sensitive detection techniques, recently tried out in the ISR, will be used. It will also be possible to measure the Q values versus momentum in the antiproton stack.

Measurements of RMS betatron oscillation amplitudes versus momentum inside the stack are possible from betatron sidebands, once the working lines (Q_V, Q_H versus $\Delta p/p$) and the particle density versus $\Delta p/p$ are known.

Computer treatment of Schottky profiles is required to extract the beam parameters mentioned.

Pick-ups of the coupling loop type will be provided for these measurements in one of the straight sections where $\alpha_p = 0$.

8.1.4 Position pick-up electrodes

A total of 12 pick-up stations, each containing horizontal and vertical electrodes, will be mounted in somewhat enlarged pump connections, distributed regularly around the ring.

Conventional diagonally divided electrodes are proposed. They have good linearity and allow single turn observation. However, only bunched beams are seen.

Even with high input impedance head amplifiers mounted directly on the feed-throughs (as done for ICE) one probably cannot obtain sufficient sensitivity to measure a single injected $\bar{p}$ beam. Thus the exploration of the closed orbits as a function of momentum will have to be done with p beams. In this case, the signals are large enough to be transported over coaxial cables before amplification and the active electronics can be in a radiation free environment. The total bandwidth will be 100 kHz to 30 MHz.

The procedure by which the final stack is ejected in 6 batches can be clearly observed.

8.1.5 Measurement targets

Measurement targets similar to the ones installed on the PS Booster are foreseen. Where the target is flipped into the beam, all particles with an amplitude greater than the distance from the target edge to the closed orbit are intercepted. In this way, one can measure the integral of the amplitude distribution.

The vertical target will be placed at high α_p, so that the vertical amplitude distribution as a function of momentum can be studied by adjusting the horizontal position before flipping the target vertically.

In the horizontal plane a similar measurement is not possible. The target will be located at $\alpha_p \approx 0$ and average over all momenta will be measured.

8.1.6 Non-destructive profile monitors

At present, two non-destructive profile detectors are being developed and built for ICE, the Rubbia type and the Vosicki type. Both extract the electrons, liberated by the beam particles from the residual gas, by means of a transverse electric field with a magnetic field in the same direction to obtain good spatial resolution.

In the Rubbia detector, the electrons are post-accelerated to about 50 keV and penetrate through a thin foil into a wire chamber, operated in counting mode. The wires are spaced at 1 mm intervals so that a profile can be obtained with good resolution.

In the Vosicki detector, the electrons impinge with about 40 keV on a thin layer of scintillator. The light is observed with a wide-aperture lens, an image intensifier and a TV camera.

The decision whether to build one of these two devices will depend on the experience in ICE. A space of 2 x 1 m will be reserved.

8.1.7 Q measurement

It is important for the understanding and control of beam behaviour to measure the horizontal and vertical tunes to an accuracy of ± 0.001.

A kicker with a rectangular pulse lasting a fraction of a revolution will excite coherent oscillations with an amplitude of a few mm. The signal derived from a position PU will contain the frequencies

$$f_m = |m \pm Q|\ f_{rev}$$

where m is the mode number. Selecting two modes by filtering, and measuring the frequency gives the fractional part of Q. Alternatively, one can measure one mode and f_{rev}, but this is possible only with bunched beams.

Pulsing the kicker only in one plane and observing the oscillations in both planes allows the coupling between the planes to be determined. The Q kicker will occupy about 1 m.

8.1.8 Beam loss monitors

During the running-in period, it is useful to know where and at what time the beam is lost. Later on, the same information may be used to minimize the losses.

A simple beam loss detector (developed at FNAL and also used on the PS Booster) consists of a can of liquid scintillator in which a small photomultiplier is immersed. The loss of 10^7 p or $\bar{p}$ can be detected with a bandwidth near 100 MHz.

In total, 24 of these detectors are foreseen.

8.2 Controls

The control system of the cooling ring will be similar to the systems in use at the SPS and in construction for the PS. It will essentially consist of a control computer, interface equipment, a simple terminal for local control and a data link to the PS message handling computer. In this way the ring can be operated from the PS Control Centre after the initial running-in period.

Although a detailed list of the possible commands and data acquisitions does not yet exist, it seems probable that a single computer will be sufficient, both because of the concentration of all equipment in the same area and because of the d.c. operation of most components. Data acquisition from cycle to cycle will only be required for some purposes such as beam diagnostics where the rate is limited by the operator's capacity for interpretation.

The tight construction schedule will not permit the development of any appreciable amount of software in assembly language. Existing software (operating system, data modules) will therefore be adopted except for the specific application programs that will be written in the interpreter language NODAL.

The local control terminal will include disk storage for control programmes and a simple video unit for graphic displays. Analogue waveform displays will be provided in the standard way, with switching controlled by software. Transmission of these signals to the PS Control Room will also be provided.

The access to the ring building will initially be controlled from the local control room. After running-in, this will be transferred to the PS Control Centre.

9. BUILDINGS

9.1 Introduction

The building for the antiproton ring is determined by a few basic requirements. The general area must be such as to allow the 26 GeV/c protons from the PS to be led to the production target, and the cooled antiprotons at 3.5 GeV/c to be conveyed both to the SPS and to the ISR. This fixes the location alongside the transfer line TT2 (Fig. 1.1), which allows the cooled antiprotons to be injected in the reverse direction in the SPS via TT2a and TT60 or into ring 1 of the ISR. In addition, it keeps open the possibility of injecting antiprotons in the normal direction in the SPS, should the need arise.

The choice of location on the North side of TT2 was determined both by the lower ground level, requiring less excavation, and to avoid blocking the passage along TT2 with the switching magnets.

9.2 Main Halls

The basic layout of the building has been determined by a variety of boundary conditions. Firstly the majority of the civil engineering work, the subsequent installation and maintenance of the machine must be able to procede independently of the operation of TT2, since both the SPS and ISR are filled via this line. This requirement leads to the need for a minimum of 4 m of concrete and rock between TT2 itself and the excavation.

The production target area should be well separated and shielded from the machine, so as to avoid radiation damage of the machine components and so that the building housing the machine needs little or no shielding.

There must be good access to the building for large and very heavy components and direct communications across the ring for the stochastic cooling signals. For these reasons the building consists of a rectangular

hall of 65 x 58 m partially submerged in the molasse rock, with a road access at one end (Fig. 9.1). This contains the ring itself, the area inside the ring will serve for most of the large power supplies, etc. as well as for the direct connections required by the stochastic cooling. To reduce the amount of excavation required, and avoid an excessively long or steep access road, the building has a floor level 1.9 m above that of TT2. This corresponds to a floor level about 7 m below the surface of the molasse, so that lateral shielding will not be required, although it will be necessary to close the access road during machine operation.

9.3 Target tunnel

The antiproton production target is located about mid-way along a 30 m long tunnel, 3 m high and 6 m wide which leads into the semi-underground hall housing the cooling ring.

The beam pipe enters this area through a 80 cm diameter hole bored in the molasse which connects with a small gallery constructed alongside TT2 (Fig. 4.2).

This effectively separates the access and operation of the machines from that of TT2.

The proton beam entering the target tunnel is inclined upwards by about 2^{o} to allow for the 1.9 m higher floor level of the building. The beam is deflected into the horizontal plane, then accurately steered and focused by a quadrupole triplet onto a tungsten target 10 cm long and less than 3 mm in diameter. The antiprotons produced are then collected by a small magnetic focusing horn of about 45 cm length and matched into the 3.5 GeV/c line for transfer to the cooling ring. The antiprotons are deflected 4.5^{o} to the left and the non-interacted protons continue almost straight on ($\sim \frac{1}{2}^{o}$ right) into a beam dump.

Since the target and beam dump area and components will become highly activated, considerable attention has been devoted to the conceptual layout.

The antiproton production system can be divided into three parts having quite different characters :

i) a conventional proton beam transport system with little or no beam loss and consisting of conventional elements;

ii) the target zone itself, with very high radiation levels and potentially fragile components such as the target and magnetic focusing horn;

iii) the collimator and beam dump area, again with high radiation levels but containing large mainly passive elements which are expected to have very high reliability.

The design philosophy is to minimize both the number and complexity of components in the high radiation areas, isolate them from adjacent areas and arrange for easy access to components. Thus the arrangement foreseen consists of a curtain of 80 cm thick shielding blocks suspended from the roof, separating the beam line from the rest of the tunnel, and a 30 cm thick wall just upstream of the target, to separate the first two areas.

All cables, cooling water pipes, etc. will be situated on the East wall and connections made by crossing the tunnel in transverse ducts.

In area i) normal access for maintenance will be possible due to the shielding alongside areas ii) and iii) and just upstream of the target.

In area ii) components will be pre-aligned on marble bases, and enclosed in marble whenever possible. These assemblies could for instance be moved into position on a removable trolley and lowered onto precision supports.

The electrical and cooling supplies pass via the marble base as indicated in Fig. 9.2 , so that all connections and disconnections, except for the vacuum pipe, can be made with the shielding curtain in place. It should be noted, however, that the target + horn assembly will be in air and so need no vacuum pipe connections. Thus, as presently envisaged, area i) ends with a piece of beam pipe through the 30 cm shielding wall, containing a vacuum window.

Wherever vacuum disconnects are necessary, it is foreseen to use quick disconnect flanges which can be operated with special tools.

In area ii), the beam dump and collimator are foreseen as installations fixed once and for all which would not be touched afterwards. If however some repair or modification should be needed, the shielding followed by the equipment would then be moved into the hall.

The shielding layout is shown in Fig. 9.3. This gives access to the tunnel via a labyrinth for personnel. For equipment and vehicle access, a removable plug is planned.

Initial calculations based on 5×10^{18} protons per year show that with this layout, the maximum dose received by the cables, etc. on the East wall of the tunnel is about 1 Mrad per year, and the maximum level in the passageway 24 hours after shutting off the beam is 20 mrad/hour (Fig. 9.4).

After stacking and cooling, the beam re-enters TT2 via a pipe through the molasse. For injection counterclockwise in the SPS, a connection will be made between TT2A and TT60 (Fig. 4.9).

9.4 Services

To house the cooling plant, electrical sub-station and local control room, a surface building is located along the East side of the hall. This is of conventional construction with a double floor which connects to an existing technical gallery. The total installed power will be about 5 MW and the machine components will be cooled by a conventional demineralized water circuit with a supply pressure of 25 bars and a total flow rate of about 4 m^3/minute. This will be cooled via heat exchangers and primary water from cooling towers.

The ventilation system foreseen will operate closed circuit during machine operation with the addition of a small supply of fresh air to maintain a slight overpressure in the building and to compensate for leaks. To avoid excessive heat loss, the walls and roof of the building will have additional thermal installation.

As presently envisaged, the building will be equipped with two 5 ton cranes, each with a span of 32 m covering a half of the hall, but the metallic structure is designed to support their possible replacement by 50 ton cranes.

10. SPS ASPECTS

This chapter delas with the modifications and additions necessary to the SPS. Extra hardware for the low beta insertion, the RF systems and for diagnostic purposes are described and intensity, lifetime and stability limits discussed. As a foreword we describe the status of the SPS machine development studies related to the proposal.

10.1 Results of SPS machine development studies

Studies relevant to the $p\bar{p}$ proposal have been carried out in machine development sessions on the SPS throughout 1977. Results to date are encouraging.

i) A normal circulating beam at 200 GeV has been stored for periods of more than an hour. The decay time during storage is in excess of 15 hours, consistent with a measured average pressure of 5×10^{-9} Torr. At the design energy of 270 GeV the decay time should be double this figure. The key to obtaining long-lived beams is careful control of chromaticity to keep the Q spread small, and careful tuning to avoid fifth order stop bands.

ii) A single bunch 5 ns long containing more than 10^{11} protons has been injected. The space-charge Q spread caused beam to be lost to betatron resonances as predicted by theory. At the start of acceleration, 300 ms after injection, 6×10^{10} protons are left and of these, 3×10^{10} pass transition to reach high energy. This reproduces the space charge conditions for the design luminosity of 10^{30} cm^2 s^{-1}.

iii) No transverse instabilities causing beam loss have so far been encountered, although we are within a factor three of the bunch population needed to reach design luminosity.

iv) Single bunches have been stored at 200 GeV, though in these preliminary experiments only 10^{10} protons were accelerated; an intensity per bunch midway between that normally accelerated in the SPS and that required by the new scheme. No adverse effects were seen.

v) Preliminary measurements of beam growth during storage are within the theoretical estimates quoted below.

vi) The CPS has injected 3.5 GeV/c protons into the SPS and injection parameters adjusted to obtain a centered closed orbit with only one or two millimeters of distortion, an optimum Q value and zero chromaticity. In spite of the rather large transverse and longitudinal emittances of the proton beam, roughly twice that to be expected when antiprotons are injected, beam decay times of almost one second were obtained. It is expected that this decay, thought to be due to non linear resonances, will be considerably extended when smaller emittances are injected and when measures are applied to compensate the stop bands.

Further experimental investigation will be needed to develop the 3.5 GeV/c injection scheme and study the effects of the low beta insertion. These early experiments must also be translated into an operationally reliable procedure.

10.2 Intensity limitations

10.2.1 Single particle phenomena

The antiprotons, injected at 3.5 GeV/c, are three times more sensitive to remanent field imperfections in the SPS guide field than the protons, injected at 10 GeV/c. Careful correction of closed orbit and betatron resonances will be required and facilities installed in the SPS but rarely used because of its good magnetic purity will no doubt have to be brought into operation. The SPS at 3.5 GeV behaves rather like the FNAL main ring. One can therefore hope, with some confidence, that an acceptance of :

$$A_V/\pi = 1 \text{ mm mrad}$$
$$A_H/\pi = 1.4 \text{ mm mrad}$$

can be made available even at 3.5 GeV/c.

The invariant emittances of the antiproton beam assumed at injection and used as a basis for calculation of space charge Q shift correspond both to the physical acceptance of the transfer channel and the SPS physical acceptance assumed. They are :

$$E_V \beta\gamma/\pi = 3.73 \text{ mm.mrad}$$

$$E_H \beta\gamma/\pi = 5.22 \text{ mm.mrad}$$

One must expect some dilution of these emittances during acceleration and for the calculation of luminosity, beam-beam Q shift and gas scattering dilution at 270 GeV/c, larger antiproton invarient emittances are assumed. They are :

$$E_V \beta\gamma/\pi = 5.5 \text{ mm.mrad}$$

$$E_H \beta\gamma/\pi = 11.0 \text{ mm.mrad}$$

Because the proton beam undergoes fewer manipulations and is injected at a higher energy we assume a value based upon experience with the SPS which at all energies has an invarient value of :

$$E_V \beta\gamma/\pi = 10.0 \text{ mm.mrad}$$

$$E_H \beta\gamma/\pi = 20.0 \text{ mm.mrad}$$

10.2.2 Transverse collective phenomena

Possible limitations on beam intensity due to transverse collective phenomena were thoroughly studied during the design of the SPS. Reference 18 contains a complete review of possible instabilities. Experience with large accelerators leads us to believe this review to be valid, both qualitatively and, apart from minor reservations, quantitatively.

In its $p\bar{p}$ storage mode the SPS will be loaded with six antiproton bunches and six proton bunches, each containing 10^{11} particles. The mean current in each beam averaged over the circumference is low by SPS standards and collective effects which depend on mean current or are driven

by impedances whose time constants are comparable to, or longer than a revolution period, are not expected to be troublesome. One can therefore discount :

i) *The low frequency transverse instability* or "*resistive wall effect*" which appears in the SPS at 15 mA mean current (2×10^{12} particles) at a frequency below 1 MHz.

ii) The high frequency transverse instability at 460 MHz, which appears with over 5×10^{12} particles circulating, and which is driven by parasitic deflecting modes in the rf cavities whose bandwidth, 15 kHz, indicates a time constant of more than one revolution.

Since there is ample time between the passage of bunches for ions and electrons to diffuse away, the effects mentioned in Reference 18 due to neutralization may also be discounted.

Although the mean $p\bar{p}$ current is low, the local current or bunch population is high, 10^{11} compared with 2×10^{9} per bunch in normal SPS operation. The two remaining collective phenomena, which Reference 18 warns us to be beware of, are single bunch instability and space charge Q spread.

10.2.3 Single bunch transverse instabilities

Reference 18 contains a prediction by Sacherer for this effect. At 2×10^{9} protons per bunch, the rise time should be 80 ms falling to just over 1 msec for bunches of 10^{11} particles. We would expect this "head tail" effect to just overcome the Landau damping present in the beam and appear at a threshold 10^{11} protons per 200 MHz bunch. Sacherer's calculation assumes that the only transverse impedance driving the effect is that of the vacuum tube itself.

Having succeeded in injecting 10^{11} protons into the SPS in a single bunch and in accelerating 60% of this to transition, we feel reasonably confident that the single bunch limit is close to Sacherer's 1972 estimate.

Gareyte has shown that the sensitivity of the CPS to single bunch instabilities is much larger than that calculated from the impedance of the pipe itself and high frequency impedances presented by major discontinuities in vacuum chamber geometry have been invoked to explain this. We can only conclude from SPS experiments that such additional impedances should not be scaled up with the machine radius and that in the SPS they no more than double the effect of the pipe itself.

However, it would be too optimistic to hope that we will reach the design luminosity without having to deal with the lowest mode of the instability. Our single bunch experiments already show an unexplained loss at transition which may be due to single bunch instability. Careful chromaticity control should deal with any such difficulty.

10.2.4 Laslett Q shift

The effect of the Laslett Q shift is negligible in normal operation with 10^{13} protons spread around the 7 km of SPS circumference. But because it depends on local current density it becomes a force to be reckoned with in the proton-antiproton application. Although only 6×10^{11} particles circulate in each beam they are eventually compressed into a total beam length of only 30 m. At 10 GeV/c, this would produce an unacceptable Q shift of 0.15 and at 3.5 GeV/c, because the effect is proportional to $1/\gamma^2$ for a given invariant emittance, the Q shift would be ten times larger.

In a bunched beam there is a change in ΔQ as particles pass from the intense centre of the bunch to the rarefied ends. A particle with maximum synchrotron amplitudes will pass twice per synchrotron period from a Q value which is depressed by ΔQ, back to the unperturbed Q of the lattice. Even if one retunes the lattice by some fraction of ΔQ to restore the centre of probability of the Q distribution, a Q spread remains whose full width equals ΔQ which must fit between neighbouring stop-bands. The problem is similar to that of the Q spread due to SPS chromaticity combined with momentum spread. Experiments have shown that, in a machine of this size, significant fraccions of injected beam begin to be lost if the chromatic Q spread exceeds 0.05 full width.

It is principally for these reasons that we propose to inject the antiprotons into the long buckets of a 2.6 MHz low frequency RF system at 3.5 GeV/c. Protons are also injected into these long buckets at 10 GeV/c and only at 18 GeV/c are the bunches squeezed into the short 200 MHz buckets in which they are accelerated and stored at 27^{0} GeV/c. The details of these RF manipulations are described in Section 10.5. At each stage the bunches are compressed only when their γ has risen sufficiently for the Q shift to be acceptable at a higher line density. Table 10.1 shows the Q shift expected at each stage. The most serious Q shift is encountered by antiprotons at 3.5 GeV/c but it is still somewhat smaller than the Q shift calculated for the single bunch simulation performed recently in the PS.

TABLE 10.1

Q shift due to space charge

	p (GeV/c)	Total beam (units of 10^{11})	Bunch length (m)	Number of bunches	ΔQ	
					$\bar{p}$	p
at injection	3.5	6	80	6	0.06	-
for h = 60	18	6	11.5	6	0.016	0.006
after compression	18	6	1.4	24	0.032	0.012
after merging 4 bunches into 1	270	6	1.4	4	0.0006	
SPS simulation experiment	10	0.6	1.4	1		0.08

(Emittances are the low energy values defined in Section 10.2.1).

10.3 Scattering and SPS vacuum

10.3.1 The SPS vacuum

The SPS vacuum is considerably better than its design value. During the last six months, careful surveys of the pressure measured at ion pumps around the ring and at pressure gauges between the pumps show an average of 7×10^{-7} Torr dropping to 5×10^{-9} Torr as pressure bumps due to small leaks have been progressively eliminated. Eventually we expect the average pressure to be no higher than that of the best sextant (i.e. 2×10^{-9} Torr).

Approximately half the pumping ports in the SPS were deliberately left without ion pumps when the present system was installed, and by mounting extra pumps on these ports one might drop the pressure even further to 10^{-9} Torr. Further improvements, particularly in rate of pump down, are to be expected if heating elements are attached to vacuum tubes to allow a mild bake-out. The benefits of baking are under study.

10.3.2 Beam loss lifetime

Estimates of nuclear scattering beam loss depend upon gas composition and further losses due to Coulomb diffusion to the walls dep[illegible] n assumed aperture stop radius for the machine, but one can estimate [illegible] effects and scale them from measurements at higher pressure made a[illegible]. Both methods agree and predict lifetimes at 5×10^{-9} Torr (N_2 equivalent) of 40 hours at 200 GeV and 50 hours at 270 GeV. At 2×10^{-9} Torr lifetimes should be several days. With careful chromaticity compensation and Q tuning, SPS experiments have achieved decay rates of only 2% in the first hour at 5×10^{-9} Torr and at 200 GeV. The natural 1/e life time corresponding to this decay is 25 hours; we seem within striking distance of the theoretical lifetime.

10.3.3 Emittance growth and degradation of luminosity due to scattering

The Coulomb scattering due to the residual gas may be calculated exactly using Molières solution of the diffusion equation :

$$\theta_e(t) = \sqrt{\theta_0^2 + \frac{0.27\ Pt}{p_0^2}}$$

where : θ_e is the rms divergence after time, t.
θ_2 is the initial value of θ.
P is the gas pressure in Torr assuming N_2.
p_0 is the momentum of the stored particles in GeV/c.

Suppose a small scattering angle $\delta\theta$, is produced at a point in the machine where the betatron function is $\beta(s)$, and observed as a displacement, $\delta\sigma$, at a reference point where $\beta=\hat{\beta}$ which is distant in phase from the scattering event by $\Delta\psi$. Then, from a well known expression in Courant and Snyder :

$$\delta\sigma^2 = \delta\theta^2\hat{\beta}\beta(s) \sin\Delta\psi$$

To calculate the mean square displacement due to all such events wherever they occur in β or ψ we must take the mean of the above expression

$$\overline{\delta\sigma^2} = \frac{\delta\theta^2_{rms}\ \hat{\beta}\ \overline{\beta}}{2}$$

This, combined with the first expression gives a formula for the increase in the standard deviation, or half width at half height, of a Gaussian shaped beam profile observed at $\hat{\beta}$ (at other points in the ring the dilation, like the beam itself, scales as $\beta^{\frac{1}{2}}$)

$$\sigma(t) = \sqrt{\tau_o^2 + \frac{0.27\ \hat{\beta}\ \overline{\beta}\ Pt}{2p_o^2}}$$

We notice that σ^2 grows linearly with time

$$\frac{d(\sigma^2)}{dt} = \frac{0.27\ \hat{\beta}\ \bar{\beta}\ P}{2p_o^2}$$

Extensive measurements of scattering dilation have been made at FNAL [19] at elevated vacuum pressures above 10^{-7} Torr where this effect predominates. The results clearly demonstrate the expected pressure and energy dependence and curves of σ^2 versus time exhibit the expected linear slope. Putting their measured value for the slope in the above equation gives a pressure of 3.10^{-7} Torr for the FNAL main ring vacuum. This value is consistent with other estimates and measurements of their vacuum pressure. There exists of course the usual uncertainty of a factor 2 in such estimates in the absence of a gas analysis.

We can therefore with some confidence predict the growth rate for the SPS. Taking :

$\bar{\beta}$ = 55 m P = 2.10^{-9} Torr (N_2 equivalent)

$\hat{\beta}$ = 110 m p_o = 270 GeV

one predicts :

$$d(\sigma^2)/dt = 2.2\ 10^{-11}\ m^2/s$$

In 24 hours the growth is $(1.39\ mm)^2$ and taking normalised emittances of 20 π mm.mrad horizontally and 10 π mm.mrad vertically corresponding to σ's of 1.4 and 1.0 mm respectively, the luminosity, inversely proportional to the product of the two σ's, drops by a factor 2.4.

Bearing in mind that we have assumed pessimistically that at these low pressure the gas is nitrogen while gas analysis suggests at least half is a partial pressure of lighter and much less dangerous elements, we conclude that the emittance growth of the beam will be tolerable at 2.10^{-9} Torr.

Remembering that the antiproton beam may have a smaller emittance initially and that one may find that optimum luminosity is achieved in practice with fewer protons within a smaller emittance, we still feel that a further reduction of residual pressure obtained by adding pumps may well be a valuable investment.

10.3.4 Beam-beam interaction

The design luminosity is ultimately limited by the electromagnetic forces on a particle as it passes through the colliding bunch of the other beam. The forces are of a non-linear nature and can drive destructive non-linear stopbands just like imperfections in the guide field. Solution of the non-linear problem is complex and depends on particle distributions in all three phase planes of both beams. A calculable measure of their strength, however, is the linear Q shift. Experience with the ISR shows that if decay rates due to related non-linear driving forces are to be smaller than 10 hours, this Q shift must be less than 0.01.

Assuming elliptical beam cross sections, Gaussian distributions, frontal collisions and $v = c$, the tune shift is

$$\Delta Q = \frac{r_p N}{\pi \gamma} \left[\frac{\beta_v}{(a+b)b} \right]_{\text{average}}$$

where r_p is the proton radius
N is the number of particles
a is the RMS beam half width
b is the RMS beam half height

Examination of this expression shows that it is independent of momentum for an invarient emittance and of the azimuthal structure of the beams.

The formula assumes that the n bunches of each beam collide in 2 n points around the ring. The quantitiy in brackets is averaged over

all these meeting points and since both numerator and denominator scale as beta, contribution from the low beta interaction point will be no more important than those from each of the 11 other meeting points. Small differences arise only from the aspect ratio of the beams at the different points.

The worst beam-beam Q shift is that experienced by protons in the vertical plane as they traverse the antiproton beam whose normalised emittances are 5 and 10 mm.mrad. The calculated value at full luminosity is a Q shift of 0.064 and much larger than may be tolerated. We must aim to prevent collisions at the unwanted meeting points by displacing the beams tranversely. ISR calculations[20] suggest a separation of 7.5 rms beam half widths is sufficient to reduce the non-linear forces by an order of magnitude. At 270 GeV this corresponds to 8 mm at maximum beta.

The orbit separation must be produced by electrostatic deflectors which, unlike magnetic deflectors, produce orbit deformations of opposite sign for the two beams. One such deflector 5 m long and operating at a field of 60 kV/cm will produce a deformation in each orbit of 6 mm amplitude which has the form of a sine wave of azimuthal frequency Q = 26.6. Since this frequency is unrelated to the 12 fold symmetry of the meeting points, one expects the average separation at meeting points to be the necessary 8 mm.

For quite independent reasons, namely to scan the beams across each other at the low beta points vertically and radially in order to determine luminosity and measure backgrounds, four such electrostatic deflectors will be installed in each plane close to the low beta section. Each quartet can be used to steer the beam at the low beta location and at the same time produce the necessary orbit distortion elsewhere in the ring.

With the beams separated at all but the low beta section, the Q shift is reduced to a tolerable 0.009.

10.4 The low beta insertion

10.4.1 The long straight sections

The lattice of the SPS has six long straight sections formed by simply omitting 20 dipole magnets without perturbing the regular focusing pattern. Of the six, one, LSS5, is almost unused and can be modified by adding quadrupoles to produce a low beta in both horizontal and vertical phase planes. A similar modification may also be made in LSS4 if the beam dump system, which occupies some of the space, is displaced to another long straight section.

10.4.2 The low beta insertion

Fig. 10.1 and Table 10.2 show the modifications to the focusing structure and beam dynamics at the insertion. The programme AGS[21] has been used to arrive at this solution. The low beta values are : 4.7 m horizontally and 1.0 m vertically, and the momentum compaction function, α_p, is essentially zero over the whole of the long straight section. The normal lattice quadrupoles in the neighbourhood of the insertion are left in place, but are modified in strength to form an integral part of the insertion design. The entire half cell between quadrupoles Q517 and Q518 is left free of obstruction for experimental equipment at the interaction region. This total free space is 29 m. The asymmetry of the design stems from the fact that one is producing minima in the beta functions at points where such extrema do not exist in the unperturbed lattice. To produce a symmetric solution, a normal SPS quadrupole would have to be removed.

10.4.3 Effect on SPS dynamics

The insertion inevitably perturbs the dynamics of the SPS. To obtain a low value at the intersection point, beta must be allowed to rise to five or six times the normal maximum of 100 m on either side of the insersection. If the insertion were to be switched on throughout the acceleration cycle of the SPS, quadrupoles and bending magnets about the insertion would need to be enlarged in aperture to allow the passage of the large emittance beam at 10 GeV/c or 3.5 GeV/c.

Furthermore, the modifications to beta functions make the phase advance over the long straight section very different from that at other straight sections. A superperiodicity of one is introduced and systematic sextupole and decapole errors, principally in the remanent fields of the dipole magnets, become capable of driving all third and fifth integer betatron resonances. The dislocation also breaks the regular pattern of 72 chromaticity correcting sextupoles which could then excite all third integer resonances.

It is expected that at 270 GeV the effect of remanent fields will be weak enough and the emittance small enough for these effects to be tolerable, given some modification to the pattern of correcting sextupoles. The problem has yet to be studied with computer simulation. But at 10 GeV/c, where the SPS is known to already be sensitive, even to non-systematic betatron resonances, one can be sure that such a dislocation to the optics is intolerable. Injection at 3.5 GeV/c and space charge Q-shift would only make things worse.

10.4.4 The "in-flight" insertion

We propose to circumvent this problem of aperture and stopbands at low energy as follows. The SPS will accelerate to 270 GeV with the seven extra quadrupoles of the insertion switched off, and with its full complement of normal quadrupoles in series. Once the beam is stored at 270 GeV, individual supplies, powering the extra quadrupoles, and active shunts by-passing nine SPS quadrupoles whose strengths are to be modified, are ramped to slowly transform the unperturbed machine into the configuration shown in Fig. 10.1. That a continuity of solutions exists between unperturbed and perturbed configurations, must be checked, but such "in-flight" transformations have been applied to SPEAR and ISR with success. Some further modification and additions to the proposed quadrupole locations may prove necessary to ensure this continuity.

Altogether nine SPS quadrupoles must be equipped with active shunts. Five of them are only trimmed by a small amount. The others must be

altered considerably and in the case of 516 and 518 reversed in polarity. This will require stout cables from the active shunts. The seven extra quadrupoles (Q1 through 7) must also be powered individually through cables from the surface.

The lengths and apertures of all quadrupoles are standard values for the SPS and all strengths are velow the saturation limit. Nevertheless, several of the quadrupoles must run DC at full field and new coils with larger cooling holes may have to be constructed and installed. An alternative solution is to install more quadrupoles at the risk of obstructing space otherwise left free for experimental equipment.

TABLE 10.2

Quadrupole modifications

$$k = \frac{(dBy/dx)}{B\rho}$$

Normal SPS locations

Number	$k\ (m^{-2})$	
513	0.0123	weak active shunts (3) + main bus
514	-0.0141	
516*	0.0108	
517	0.025	strong active shunts + main bus (3)
518*		
519	0.0118	
520	-0.007	
522	-0.0142	weak active shunts + main bus (2)
533	0.0123	

Extra quadrupoles

Q1	0.006	individual power supplies (5)
2	-0.0196	
3		
4	0.0215	
5	0.0229	
6	-0.0198	
7		

($k = 0.015\ m^{-2}$ is a standard SPS strength)

* Reversed

10.4.5 Insertion design procedure

The first step in calculating a system to produce the required values of β_H, β_B and α_p and their derivatives at the centre of the insertion is to slightly modify the strength of quadrupoles 513, 514, 522 and 523. These are within the bending structure on each side of the insertion and may be adjusted to make α_p zero throughout the long straight section [22].

The second step is to place three quadrupoles next to Q517 and three next to Q518 to form, together with these quadrupoles, strong doublet lenses which pinch beta to a minimum in both planes. To achieve sufficient perturbation, each member of the doublet is really two quadrupoles.

With modifications to the strength of 519 and 520 downstream and 516 plus an extra quadrupole, Q1, upstream, eight variables are available, sufficient to match β_H, β_V plus their derivatives into each side of the lattice. All the quadrupoles varied in this second phase are within the bending free region and so the initial α_p match is not perturbed. Note that normal quadrupoles 516 and 518 have opposite polarity from their normal configuration. Their active shunts must provide about twice the normal quadrupole current.

Finally, one adjusts the strength of all the other lattice quadrupoles to restore Q, perturbed by the additional phase advance introduced by the insertion. After a second iteration of this procedure, AGS gives a consistent solution.

10.4.6 Errors and tolerances

We have studied the effects of errors in the focusing strength of the insertion quadrupoles. An error of 3×10^{-4} in a quadrupole at a high beta point causes a 2% modulation of the beta function around the ring and doubles the half-integer stopband width due to gradient errors in the unperturbed machine. To be safe, bearing in mind that there are several such quadrupoles with errors weighted according to β, it would seem reasonable to ask for a gradient precision of 10^{-4} or better.

It seems one can make quite large changes to the Q of the machine of the order of unity by means of the normal SPS quadrupoles, without disturbing the low β, low α_p condition.

A large number of solutions exist and one may shift the location of the intersection point by several metres or provide larger betas or different aspect ratios without moving quadrupoles. However, to produce a significantly lower beta, more quadrupole strength and better precision would be required.

10.5 RF systems for the SPS

The present SPS RF system has a nominal frequency of 200 MHz and, when augmented as is planned in the present SPS improvement programme, will supply a peak voltage per turn of 8.8 MV. One half of this is available for p and $\bar{p}$ each. A single bunch riding in a stationary bucket formed by the RF system will have a length less than 5 ns. This is consistent with the experimenters need for a short interaction region and a high luminosity. Each stored beam will consist of six such bunches equally distributed in azimuth and each containing a nominal 10^{11} particles.

One may calculate the phase space area of these bunches from the momentum spread obtained in the cooling ring. In Section 2.7, we show that the momentum spread has a minimum value mainly determined by the necessity of limiting the intra-beam scattering. Although the bunch area thus calculated is small enough to fit in at 270 GeV stationary bucket, it is too large to be accelerated in a single 200 MHz bucket in the critical region just above transition where the bucket area for a given voltage is considerably reduced.

We propose to overcome this difficulty by sharing the longitudinal phase space area of the bunch among four consecutive 200 MHz buckets during the acceleration process and then merging them into a single bunch at high energy. A special 16.9 MHz RF system is required for this manipulation.

A second special RF system tunable to 2.6 and 9.1 MHz is required to cover the low energy part of the acceleration cycle from 3.5 to 18 GeV/c. In Section 10.2.4 we show how serious the Laslett space charge Q shift can be in this energy region if one attemps to keep 10^{11} particles in short bunches. Even when 80 m long bunches of antiprotons are injected into the buckets of the proposed 2.6 MHz low energy RF system, the line density is high enough to produce a Q spread of 0.055.

The parameters of these two new RF systems and the conditions prevailing at critical points in the acceleration process are to be found in Table 10.3. Details of the manipulations are described below.

10.5.1 Acceleration from 3.5 to 18 GeV/c

Six long bunches of antiprotons, each with an area of 12 mrad, a length of 80 m and a momentum spread of $\pm$ 6.7 x 10^{-4} are extracted in turn from the cooling ring and deposited in 2.6 MHz buckets in the SPS. The 2.6 MHz RF system proposed consists of four CPS type ferrite tuned cavities giving a maximum total voltage of 80 kV and operating at a harmonic number of 60.

Initially the space charge Q spread is 0.055 but as acceleration proceeds this falls as $1/\gamma^2$ and one can afford to increase the acceleration rate, thus shortening the bunches. Nevertheless acceleration to 18 GeV/c will take more than 10 s and considerable improvements will have to be made in 3.5 GeV/c beam lifetime if a large fraction of the antiprotons are to survive.

10.5.2 Injection of protons

Protons will be injected at a momentum in the range 10 to 14 GeV/c and the acceleration of the antiprotons will be arrested for 3.25 s to allow the SPS kicker to fire and recover six times, transferring six CPS bunches into equally spaced slots around the SPS circumference. The proton bunches will be matched to the buckets of the low frequency RF system by voltage manipulations in the CPS. Care must be taken not

to kick out antiprotons and the collision point of the two opposing beams must be some distance from the long straight sections, at this time.

10.5.3 Manipulations at 18 GeV/c

Following injection of protons the low frequency RF system accelerates both beams to 18 GeV/c where the Laslett Q spread has fallen to the level where one may compress the low frequency bunches into the four 200 MHz buckets which will take them to high energy.

During acceleration from 3.5 to 18 GeV/c the low frequency bunches have shrunk to a length of 11.5 m. Their momentum spread is $\pm 10^{-3}$ and they are rather prone to longitudinal instability ($Z/n = 48\ \Omega$). To fit into four 200 MHz buckets each bunch must be compressed to less than 6 m length. This may be done by suddenly increasing the RF voltage so that the long shallow bunch rotates in a much taller bucket until after one quarter of a synchrotron revolution it becomes short and tall. This process of bunch compression has worked successfully in the CPS.

Unfortunately the four CPS cavities do not provide sufficient voltage for this manoeuver at a harmonic number of 60. However, the bunches are short enough at 18 GeV/c to fit in a bucket produced by retuning the cavities to harmonic number 210. The details of this change in harmonic number are as follows. The beam is held at harmonic number 60 with three of the four cavities giving their full voltage of 60 kV. The fourth cavity is tuned to h = 210 and powered to 20 kV, a voltage which matches the bunch at this higher harmonic number. The first three cavities may then be switched off and retuned to h = 210, leaving the beam under the control of the fourth cavity. By then rapidly raising the additional three cavities to their peak Volts, an 80 kV bucket is formed in which the bunch rotates. All cavities are then switched off and the 5.7 m long bunch adiabatically captured in four adjacent 200 MHz buckets in which it is accelerated to full energy.

10.5.4 Acceleration to 270 GeV/c

The SPS 200 MHz travelling wave cavities accelerate only in one direction. Particles passing in the opposite direction see only a small resultant perturbation.

By the time the $\bar{p}$-p scheme is implemented, the SPS will have been equipped with four cavities as part of the programme to increase intensity and repetition rate. Each pair of cavities will provide almost as much voltage per turn as those presently installed. One has only to connect one pair in the opposite sense to the other for antiprotons. In this way, the two beams may be treated separately. They may be given slightly different frequencies so that the interaction point where bunches clash can be made to migrate to a different point in the ring. With six bunches, there will be twelve such interaction points. At injection these should be remote from the long straight sections to avoid kicking out antiprotons as protons are fed in. As acceleration proceeds they will be made to migrate to be coincident with the experiments in the long straight section(s).

An alternative method of using the cavities is to pump RF power from one end as the protons pass, and from the other end as antiprotons pass. This is possible because the filling time of the cavity is only one thirtieth of a turn. In this way the full voltage of the four cavities may be applied to each beam providing large bucket areas. This mode of operation however would require there to be five rather than six bunches in each beam. With six bunches the two beams would arrive simultaneously at the cavities which like the low beta point are located in a long straight section and therefore at an interaction point.

10.5.5 Compressing four bunches into one

At high energy the high frequency RF system has sufficient bucket area to contain each train of four bunches in a single bucket. The transformation is made by a bunch rotation similar to that made at 18 GeV/c. The 200 MHz is momentarily switched off and large buckets formed by a 16.9 MHz system in which the four bunches rotate (Fig. 10.2) from being a string along the phase axis until they extend along the momentum axis

of longitudinal phase space. The voltage required is 1 MV and the RF system to produce it at this frequency is expensive. Nevertheless this final manipulation is necessary to achieve the design luminosity.

Once rotated the four bunches, superimposed in time, may be captured in a single 200 MHz bucket by switching back to the normal RF system.

10.5.6 Longitudinal instability

Intense bunches are inevitably prone to longitudinal instabilities and care must be taken to ensure that the RF systems not active at any given time are "shorted" to present a minimum impedance to the beam. The danger points are just before the two bunch rotations where Z/n of 20 to 50 Ohms can produce an instability.

10.6 Diagnostics

10.6.1 Present equipment in SPS

The SPS is equipped with instrumentation designed to monitor a continuous beam with 200 MHz structure at intensities in the range of 10^{11} to 10^{13} protons (800 μA to 80 mA). Detectors and instrumentation include :

i) Beam current transformers (BCT) with a noise and long term drift of 240 μA (3 x 10^{10} protons).

ii) Closed orbit measurement systems using 216 electrostatic pick-ups looking at the 200 MHz structure of the beam and capable of 1 mm accuracy at 10^{11} ppp (800 μA).

iii) Q measurement systems which operate by kicking the beam and processing the signals from broad-band electrostatic pick-ups. The signal is sampled at the revolution frequency through a gate which is presently long compared with a single bunch. Fourier analysis determines the fractional part of Q and indicates the Q spread.

TABLE 10.3

RF parameters for the SPS

Particles per bunch	10^{11}
γ_{tr}	24
$E_V^{\beta\gamma} = E_H^{\beta\gamma}/2$	$3.73\pi.10^{-6}$ rad m

a) SPS low frequency - low energy 3.5 GeV/c → 18 GeV/c

RF frequency (h = 60)	2.6	MHz
Area of 12 mrad cooling ring bunch in SPS	16.4	mrad
Length of bunch	±122.7	deg
Length of trapping bucket	±130	deg
Blown-up bunch area	17.6	mrad
RF voltage for trapping	12.68	kV
Longitudinal stability $(Z/n)_{max}$	∿2200	Ω
Incoherent Q spread	-0.055	
Initial ϕ_s (const.bunch length)	12	deg
Initial RF voltage for acceleration	17.1	kV

b) Injection of p bunches from PS

Momentum	10-14	GeV/c
Bunch area in PS (h = 20) corresp. to 17.6 mrad in SPS (h = 60)	65	mrad

c) Change of h = 60 to h = 120 in the SPS (typical)

Momentum	18	GeV/c
Voltage on h = 60	60	kV
Bunch length	±18	deg
Voltage on h = 210	21	kV
RF frequency at h = 210	9.1	MH·
Blown-up bunch area (h = 210)	65	mrad
Bunch length in m	11.5	m
Bunch height in Δp/p before filamentation	$\pm 9.4 . 10^{-4}$	
Z/n before change of h } = worst case	48	Ω
ΔQ before change of h } = worst case	-0.014	

d) First bunch compression in the SPS

Momentum	18	GeV/c
Maximum V_{RF} on h = 210	80	kV
Time of ¼ rotation	15	ms
Bunch length after rotation	5.67	m
ΔQ after rotation	-0.028	

e) Adiabatic trapping on h = 4620

Momentum	18	GeV/c
Number of filled buckets	4	
Number of particles in each of two inner buckets	34	%
Number of particles in each of two outer buckets (for parabolic distrib.)	16	%
Bunch area of each of the inner bunches on h = 4620	∿500	mrad
V_{RF} on h = 4620 for 500 mrad	1350	V
ΔQ after trapping	-.035	

f) Acceleration in the SPS

		*)	
Number of accelerating tanks	2	4	
Maximum bucket area at 18 GeV/c (ϕ_s = 0)	900	1250	mrad
Maximum stable phase angle ϕ_s for 500 mrad	16.5	25.5	deg
Acceleration rate for ϕ_s max. at 18 GeV/c	50	160	GeV/c/s
Maximum stab. phase angle at $\sqrt{3}.\gamma_{tr}$ (39 GeV/c)	25	33	deg
Accel. rate for $\phi_s = 25/33^0$ at 39 GeV/c	80	200	GeV/c/s
Bunch length for ϕ_s max. at 18 GeV/c	1	0.85	m
$\Delta\hat{Q}$ (1/0.85 m, 18 GeV/c)	-0.053	-0.062	
Max. bucket area at 270 GeV/c (h = 4620)	2.63	3.72	rad

g) Bunch compression in the SPS

Momentum		270	GeV/c
Harmonic number		390	
Frequency		16.9	MHz
RF voltage		1000	kV
Time of ¼ rotation		9.6	ms
Longitudinal stability for inner bunches	before rotation	26	Ω
" " " outer "	before rotation	∿18	Ω
Blown-up bunch area after rotation		2.6/3.7	rad
Longitudinal stability after rotation		240/490	Ω

* not possible with 6 bunches

iv) Wide-band transverse and longitudinal pick-ups with a response which is flat into the GHz range, give either continuous or sampled pictures of bunch configuration revealing longitudinal and transverse high frequency instabilities. These signals can also be used for spectrum analysis to determine $\Delta p/p$ in an unmodulated beam.

v) Precision Ionization Beam Scanners (IBS) which measure horizontal and vertical beam profiles with a resolution of better than 1 mm above 5×10^{12} ppp.

vi) Beam scrapers and fast ejection profile detectors capable of measuring beam distributions destructively as a check on IBS profiles.

Before single bunches of protons and antiprotons are injected, the SPS will be tuned for 3.5 GeV/c and 10 or 14 GeV/c injection and acceleration with continuous beams of protons. All these devices will then be employed since one must rely heavily on this preliminary tuning when the machine is switched first to single bunch mode and finally to accelerate and store the antiprotons.

This kind of mode switching without disturbing injection and SPS acceleration conditions, presents a major operational challenge to the SPS and has yet to be developed as a technique.

10.6.2 Special requirements for observation of single-bunch and coasting beams

Even if one relies heavily on mode switching, some improvements to the SPS diagnostics will be required for machine studies leading up to $p\bar{p}$ operation, to check mode switching and to monitor the $p\bar{p}$ beams once injected. Some improvements include :

i) Beam current transformers

Considerable improvements have been made to the SPS type beam current transformers with a view to installation in ICE and the APR. Improvements to the magnetic amplifier and integrating current transformer have reduced the noise/long-term drift level to 5 μA. These improvements will be incorporated in some of the existing BCT's to meet the need to monitor the acceleration and coasting lifetime of single proton and antiproton bunches.

ii) Closed orbit monitoring and correction

At present, it is customary to use closed orbit dipoles to correct both remanent field errors and misalignment errors at injection. The admixture of these two components will be different at the two injection energies, 3.5 GeV/c and 10 GeV/c. While in principle one can provide exact correction at both energies by correcting only the remanent field errors with dipoles and adjusting lattice alignment, this has yet to be proved practicable. Meanwhile, one should keep open the possibility of adding time-dependent reference generators to the closed orbit dipole supplies.

Once one has corrected the orbit at the two energies in continuous beam mode, it is unlikely to change during mode switching. Nevertheless, a few more sensitive position monitors may be needed to check that the injection orbit is still the same in the single-bunch mode. The increase in sensitivity required is not a large one; closed orbits have already been measured at the 10^{11} level. Sensitivity may be increased by driving a high impedance rather than a matched load at the expense of placing electronics close to the beam.

iii) Q measurement

While we have already managed to measure Q_z with single bunches of 10^{11} protons the signal to noise ratio may be considerably improved by shortening the gate length. By locating the detectors correctly, one

may hope to distinguish between the signals from the passage of the protons and antiprotons.

The technique, being detrimental to the beam if not destructive, is not suitable for repeated monitoring of coasting conditions or for checking the transition from an unperturbed machine as the low-β insertion is powered. Continuously active, non-destructive techniques, similar to those used at the ISR, should be studied for this application.

iv) Wide-band observations

Single densely populated bunches will give more signal strength above 200 MHz than is available at present. We have already demonstrated that with sampling scope techniques, the development of the length of a single bunch can be monitored during coasting. It would be useful to reject noise with a gate compatible with spectrum analysis techniques.

v) Profile detectors

The Ionization Beam Scanner is limited by noise to intensities above a few 10^{12} ppp. Moreover, even the high precision version of this device requires a local vacuum bump of a few x 10^{-6} Torr.m, comparable to the total residual gas in the whole ring. We shall certainly require at least three of these precise IBS's to study beam growth with continuous beams, but to monitor bunched beams we must look to devices being developed for ICE (Section 8.1.6). These integrate over an extended time (50 ms) and can operate at gas pressures of 10^{-9} Torr and beam intensities as low as 10^{10} particles per APR circumference, and seem to meet the SPS requirements. One version of this device, in which electrons from beam-gas collisions are imaged in a wire chamber, seems particularly promising from the point of view of computer acquisition.

Such devices should be installed at locations where the p and $\bar{p}$ beams are separated : they may thus distinguish the profiles of the two beams, an essential requirement if one is to understand the causes of poor luminosity.

10.6.3 Beam separation

One needs to be able to separate the beams at the low beta point to measure luminosity. About 5 m of electrostatic field of 60 kV/cm is needed to separate the beams by twice their full width at 270 GeV. Two such electrostatic devices are required in each plane on either side of the low beta point, but in high beta locations. Their phase advance to the centre of the insertion should be an odd multiple of $\pi/4$. There must be another high beta location where one can locate profile mode monitors between each pair of deflectors at an odd multiple of $\pi/2$ in phase from the deflectors. The medium straight sections, where two magnets are missing on either side of the long straight section, are obvious possible locations for the deflectors but some modification to the insertion may be necessary to obtain the right phase advance.

Distribution (open)

Distribution (of abstracts)
PS, ISR and SPS Scientific Staff

/ed

11. REFERENCES

1. C. Rubbia, unpublished.
   See also K. Hübner, D. Möhl, L. Thorndahl, P. Strolin, Estimates of ISR luminosities with cooled beams, ISR Workshop Oct. 1976, PS/DL/Note 76-27.

2. J.I. Budker et al., Experimental study of electron cooling, Institute for Nuclear Physics, Novosibirsk, Preprint 76-33. Translation : Brookhaven, BNL-TR-635.

   J.I. Budker et al., New experimental results of electron cooling, Institute for Nuclear Physics, Novosibirsk, Preprint 76-32. Translation : CERN, PS/DL/Note 76-25.

3. F. Bonaudi et al., Antiprotons in the SPS, CERN/DG-2. Preliminary descriptio of the pp facility, SPS/DI/PP/Int.Note 77-9-

4. B. Autin, Dispersion suppression in the antiproton ring (in preparation).

5. A. Piwinski, Intra-beam scattering, Proc. IXth Conf. on High Energy Acc. (1974) 405.

6. E. Keil, W. Schnell, Concerning longitudinal instability in the ISR, CERN ISR-TH-RF/69-48 (1969).

7. P. Sievers, private communication.

8. D. Dekkers et al., Experimental study of particle production at small angles in nucleon-nucleon collisions at 19 and 23 GeV/c, Phys. Rev. 137, B962 (1965).

9. G. Bellettini et al., Proton-nuclei cross-sections at 20 GeV, Nucl. Phys. 79 (1966) 609.

10. S. Van der Meer, Influence of bad mixing on stochastic acceleration, SPS/DI/PPInt.Note 77-8 (CERN).

11. F. Sacherer, L. Thorndahl, S. Van der Meer, Some contributions to the theory of momentum cooling (in preparation).

12. R.B. Palmer, BNL, private communication (1975).

13. G. Carron, L. Thorndahl, Stochastic cooling of momentum spread by filter techniques in the cooling ring, ISR-RF/LT/ps (Ttechnical Note, Jan. 1977).

14. G. Carron, L. Faltin, W. Schnell, L. Thorndahl, Experiments with stochastic cooling in the ISR (1977 Particle Accelerator Conference, Chicago).

15. H.G. Hereward, Coherent instability due to electrons in a coasting proton beam, CERN 71-15.

16. E. Keil, Intersecting storage rings, CERN 72-14.

17. H.G. Hereward, Statistical phenomena - Theory
W. Schnell, Statistical phenomena - Experimental results
Proc. of the 1st Course of the Internat. School of

18. Spring study on accelerator theory (1972), AMC-1 (available from SPS Division Secretariat).

19. C.M. Ankenbrandt et al., Proc. National Conf. on High Energy Accelerators, Chicago (1977).

20. K. Hübner, private communication.

21. E. Keil et al., AGS - The ISR computer program for synchrotron design, orbit analysis and insertion matching, CERN 75-13.

22. P. Bryant, A. Hutton, private communication.

APPENDIX A

Participants in Design Study

B. Autin
B. Bianchi
R. Billinge
D. Blechschmidt
J. Brunet
B. Couchman
L. Evans
D. Fiander
G. Gravez
M. Höfert
E. Jones
H. Koziol
D. Möhl
A. Poncet
J. Rouel
C. Rubbia
F. Sacherer
G. Schröder
N. Siegel
H. Stucki
L. Thorndahl
S. van der Meer
E. Weisse
T. Wikberg
E. Wilson
C. Zettler

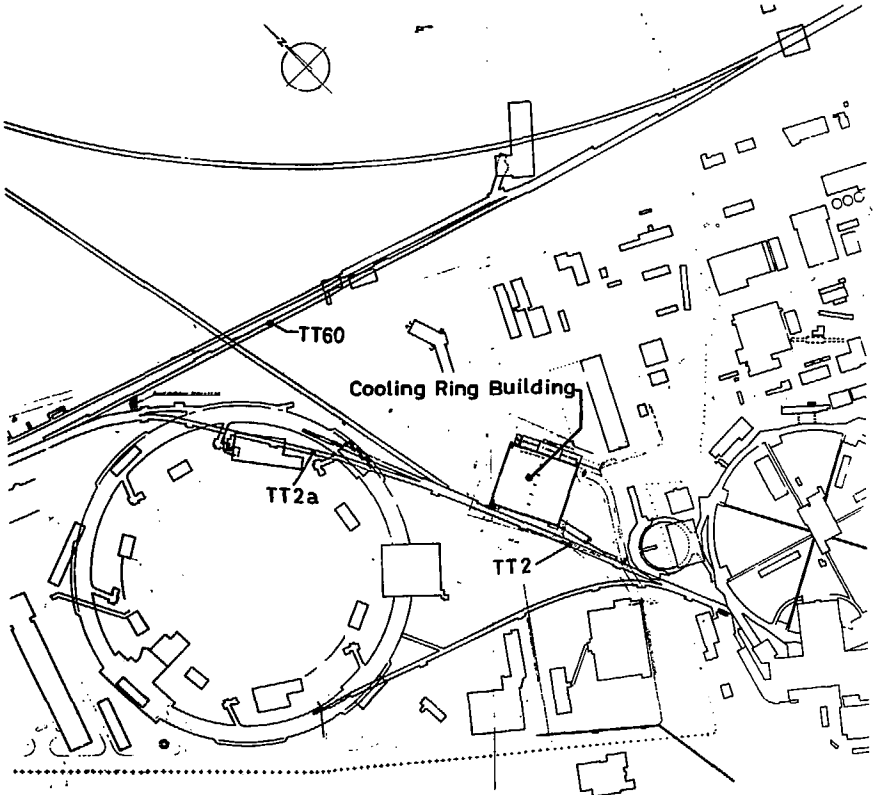

Fig. 1.1 Overall Site Layout

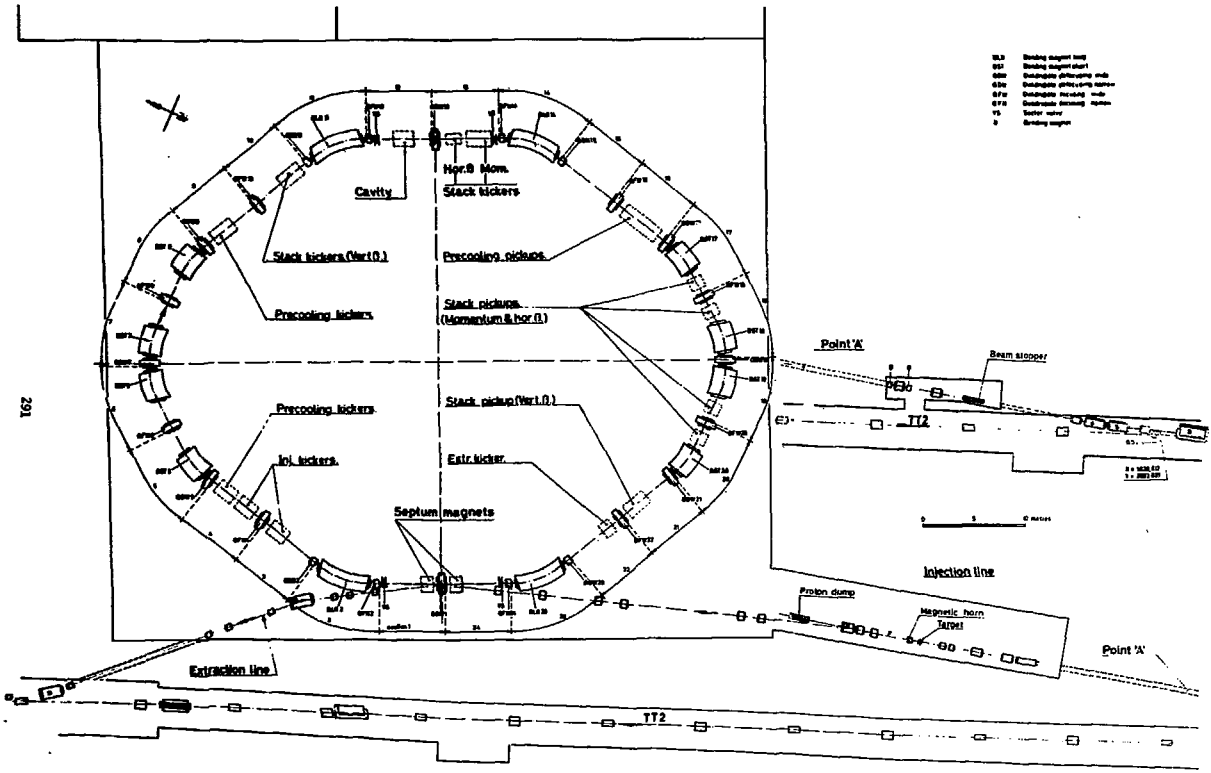

Fig. 1.2 General Layout Of The Antiproton Accumulator

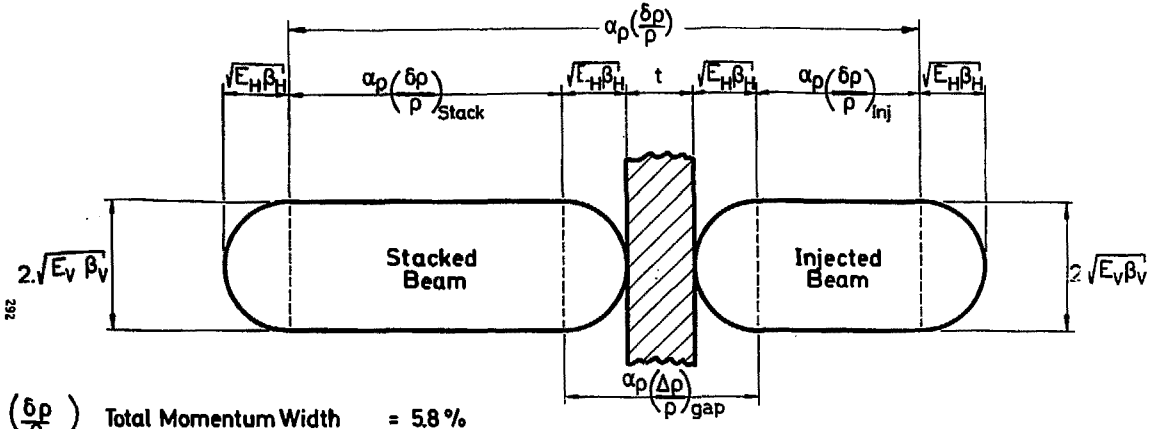

$\left(\frac{\delta p}{p}\right)$	Total Momentum Width	= 5.8 %
(πE_V)	Vertical Emittance	= 100 π μ-θm
(πE_H)	Horizontal Emittance	= 100 π μ-θm
$\left(\frac{\delta p}{p}\right)_{St}$	Stack Momentum Width	= 2.5 %
$\left(\frac{\delta p}{p}\right)_{Inj}$	Injected Momentum Width	= 1.5 %

Fig. 2.1 Machine Acceptance

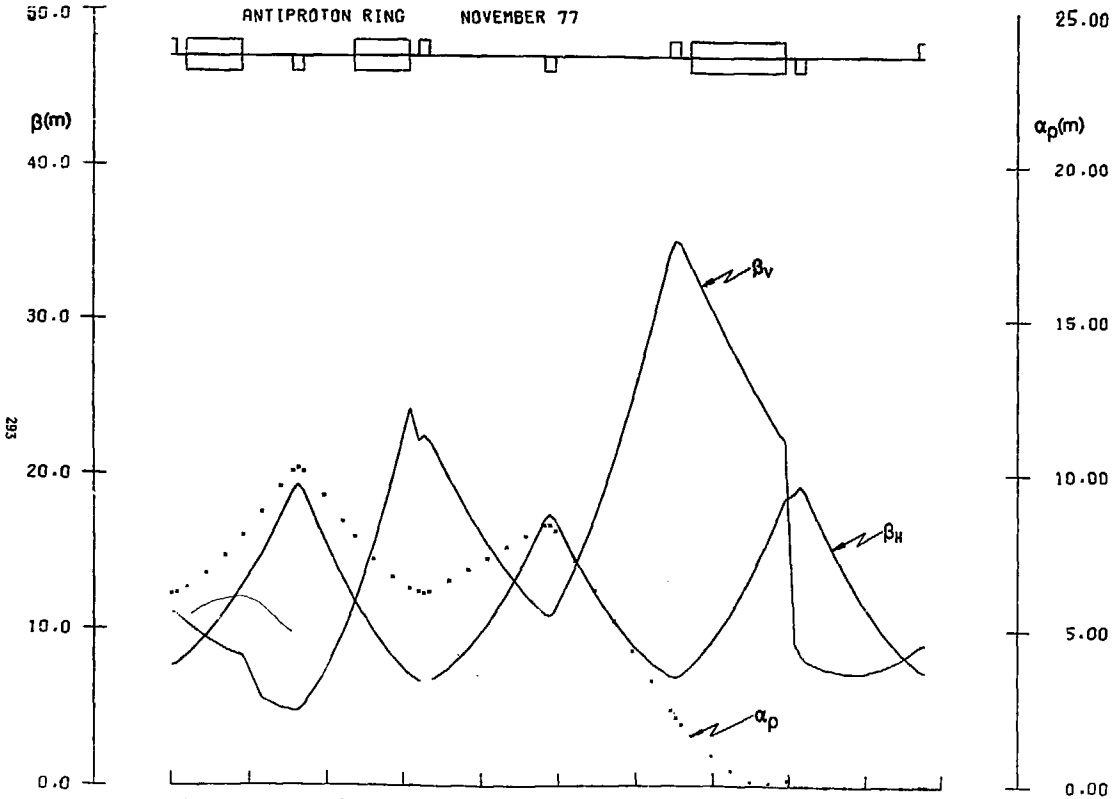

Fig. 2.2 Lattice Functions

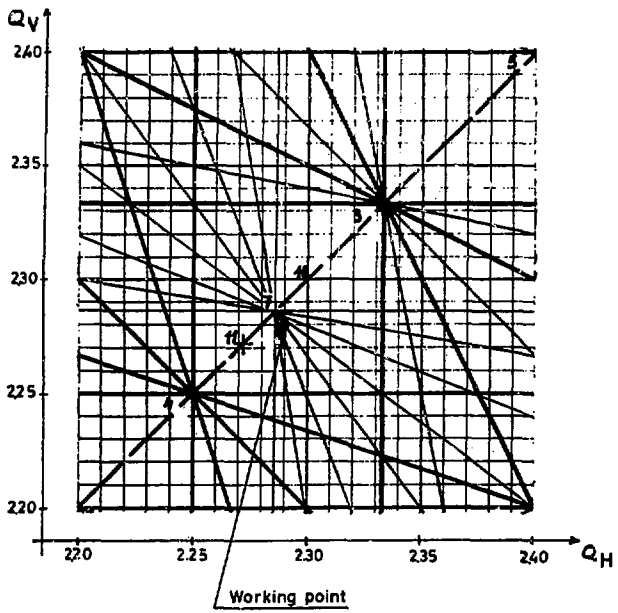

Fig. 2.3 Working Diagram

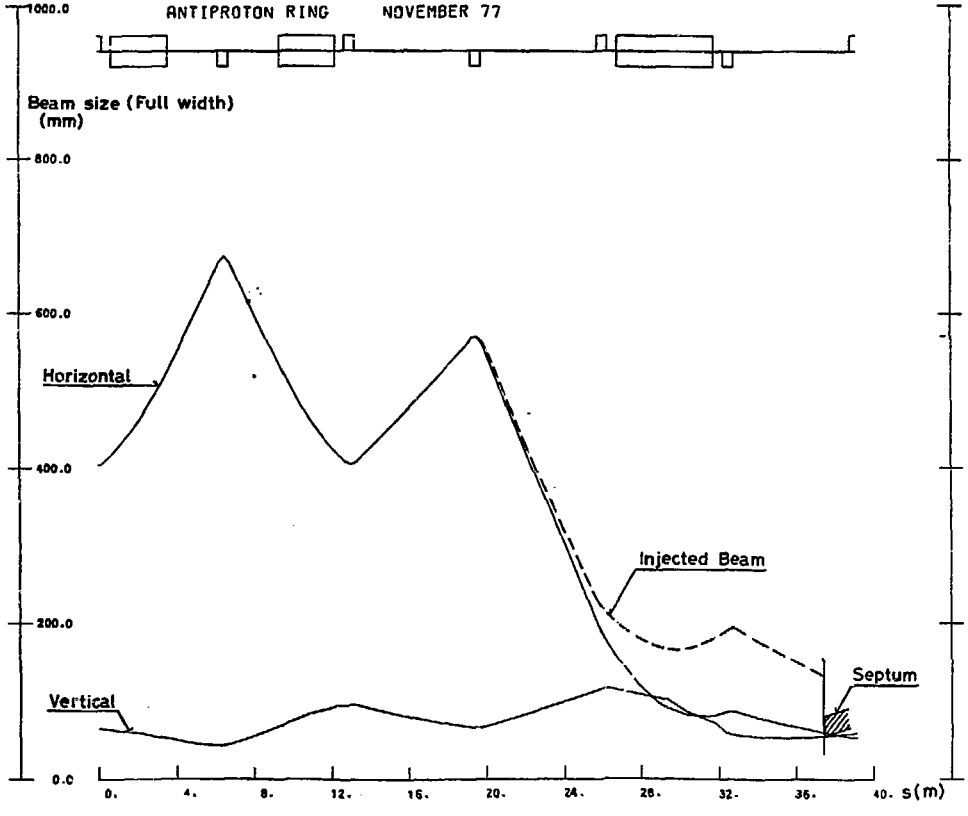

Fig. 2.4 Beam Sizes In A Quadrant

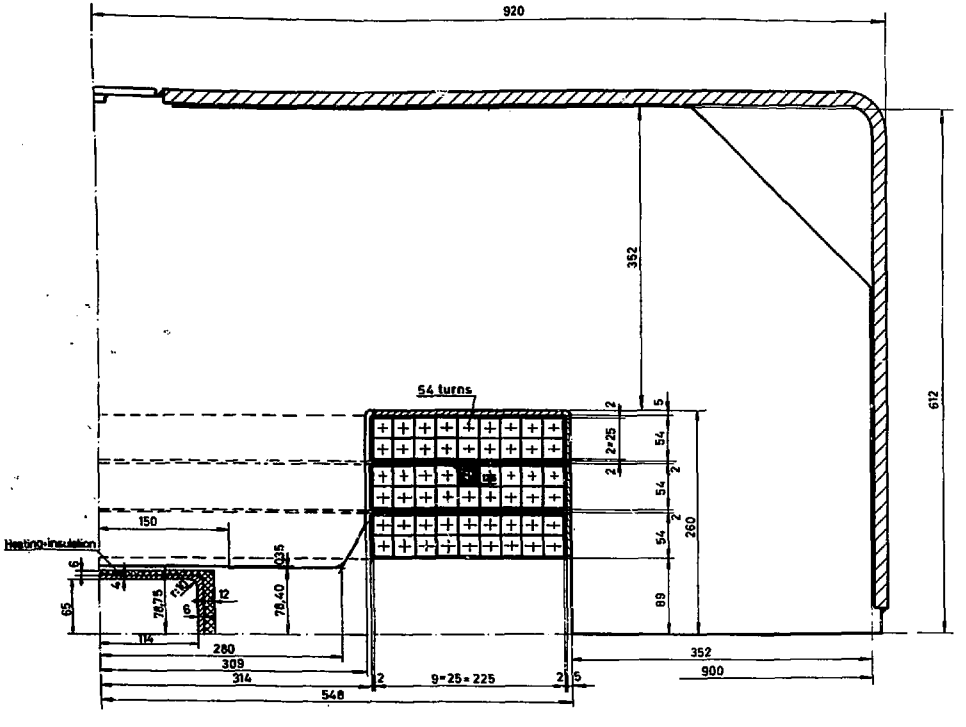

Fig. 3.1 'H' Magnet Cross Section

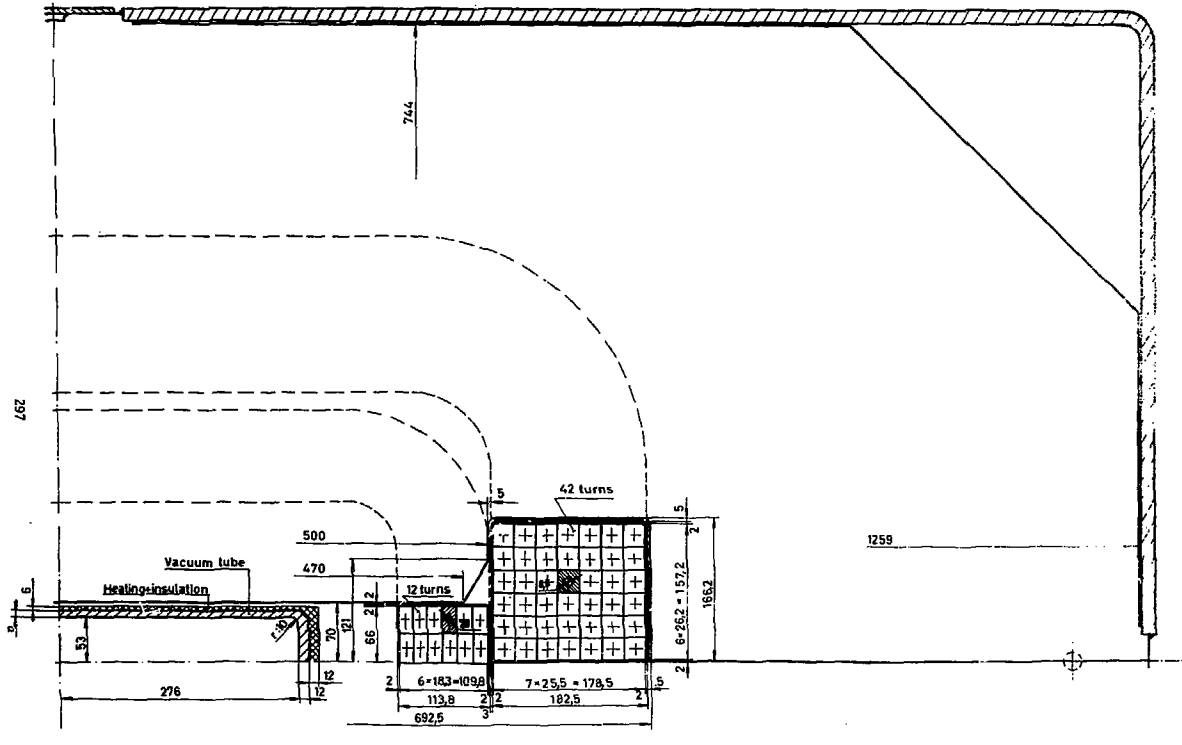

Fig. 3.2 Window-Frame Magnet. Cross Section

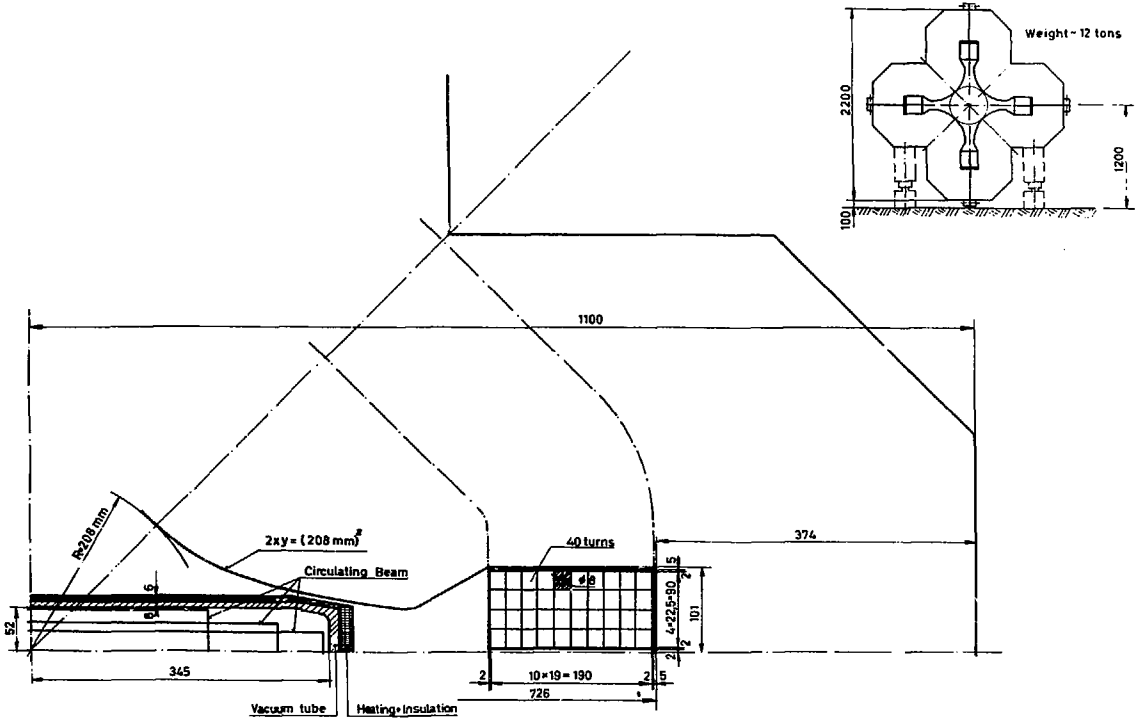

Fig. 3.3 Wide Quadrupole. Cross Section

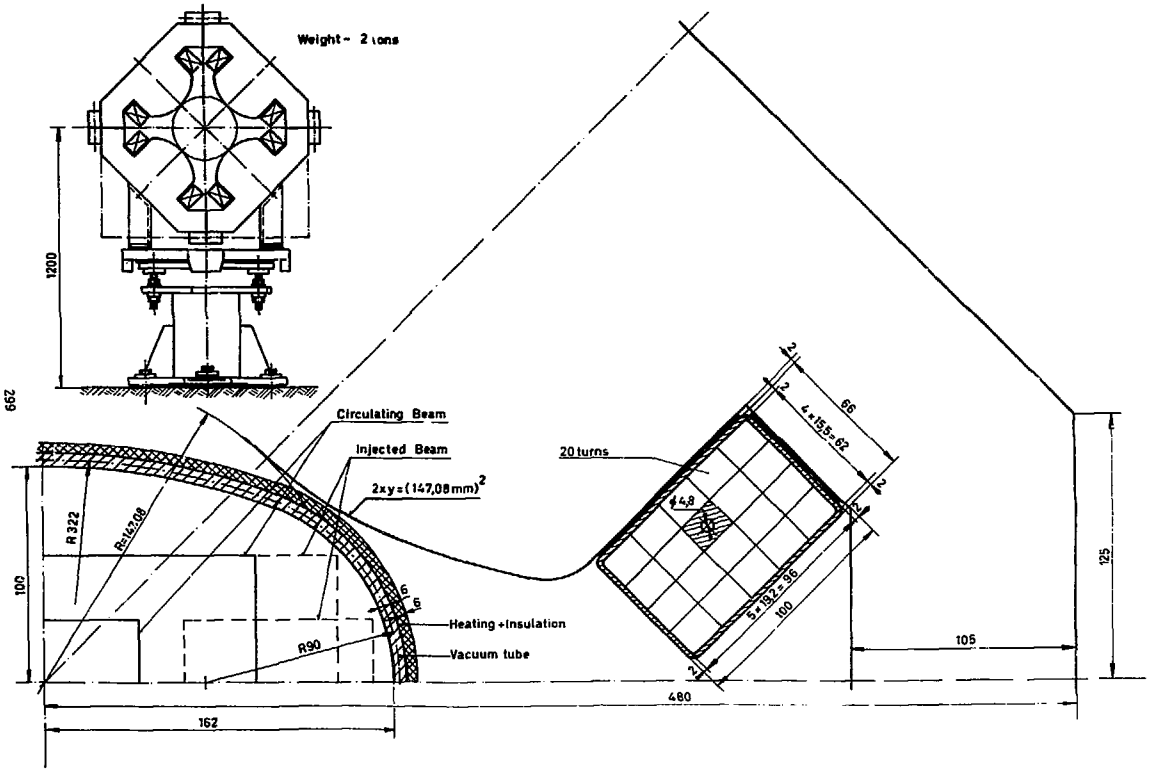

Fig. 3.4 Narrow Quadrupole. Cross Section

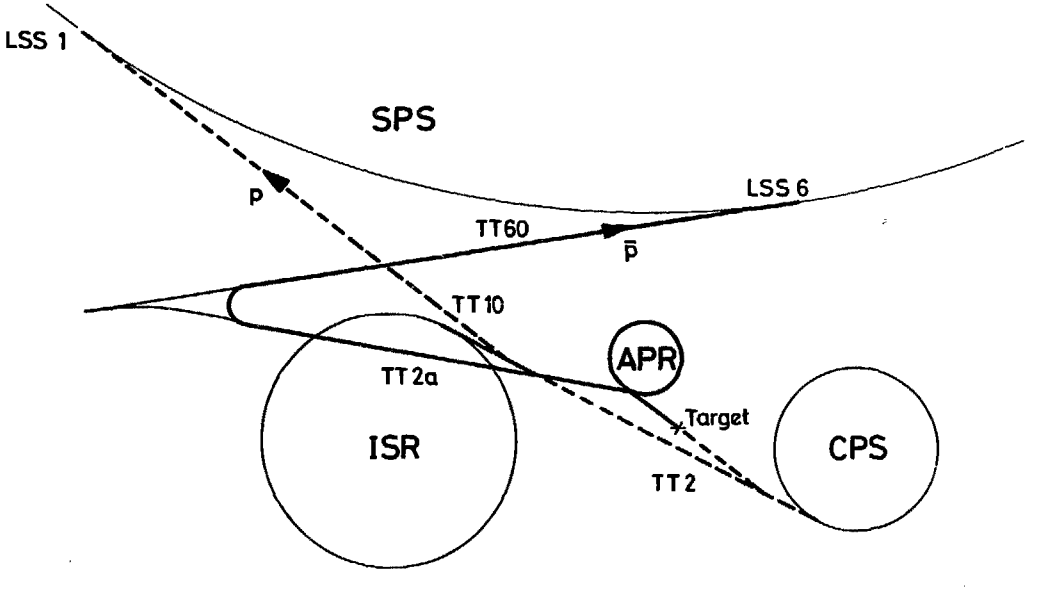

Fig. 4.1. Schematic layout of beam transfers.

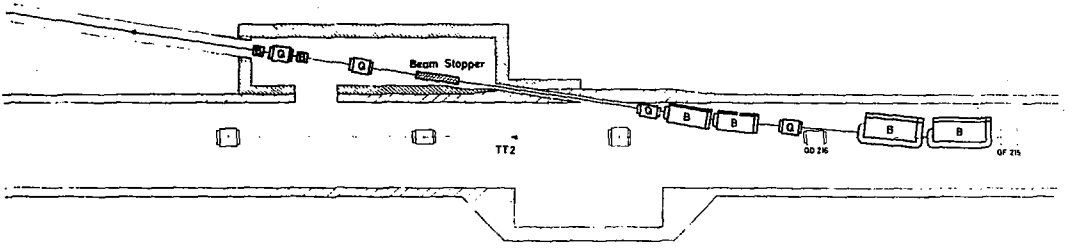

Fig. 4.2. Layout of Branch-off TT2

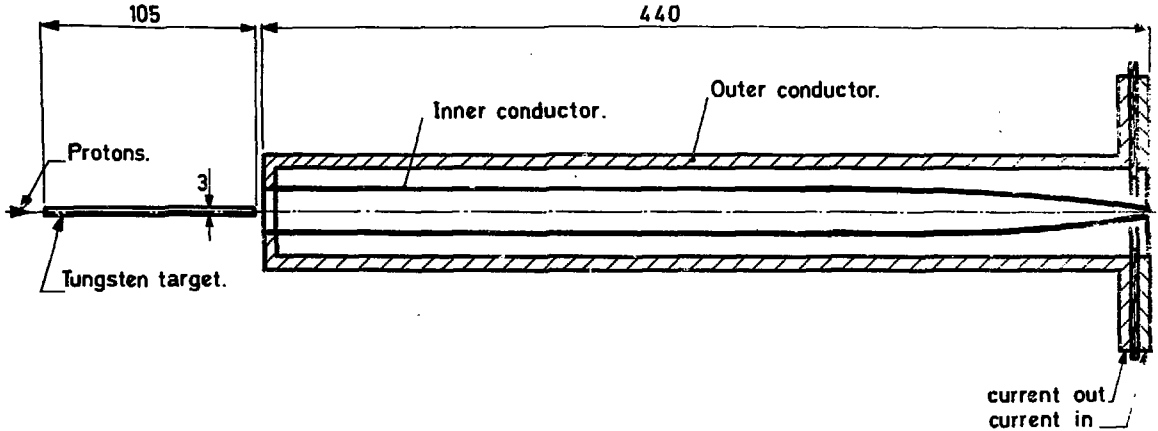

Scale 1:2

Fig. 4.3 Cross section of focusing horn.

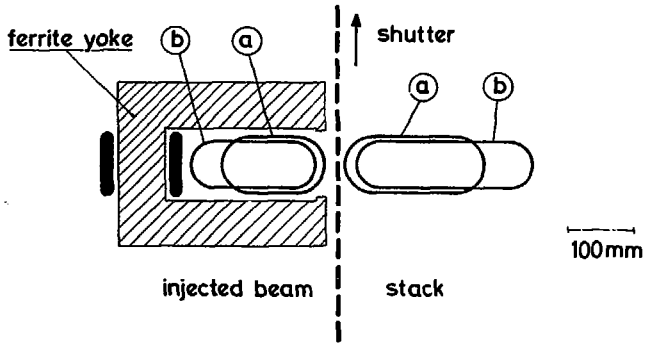

Fig. 4.4. Schematic cross section of the injection kicker; beams (a) at entrance and (b) at exit of kicker 1.

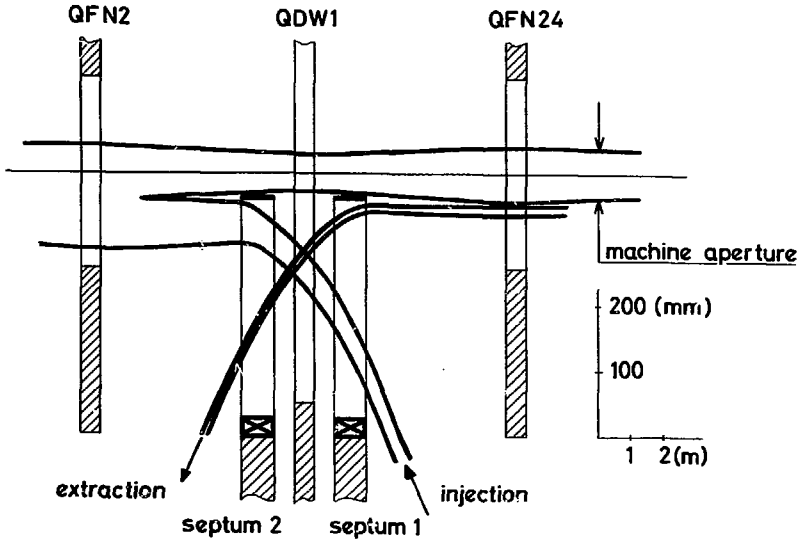

Fig.4.5. Layout of septum magnets for injection and extraction

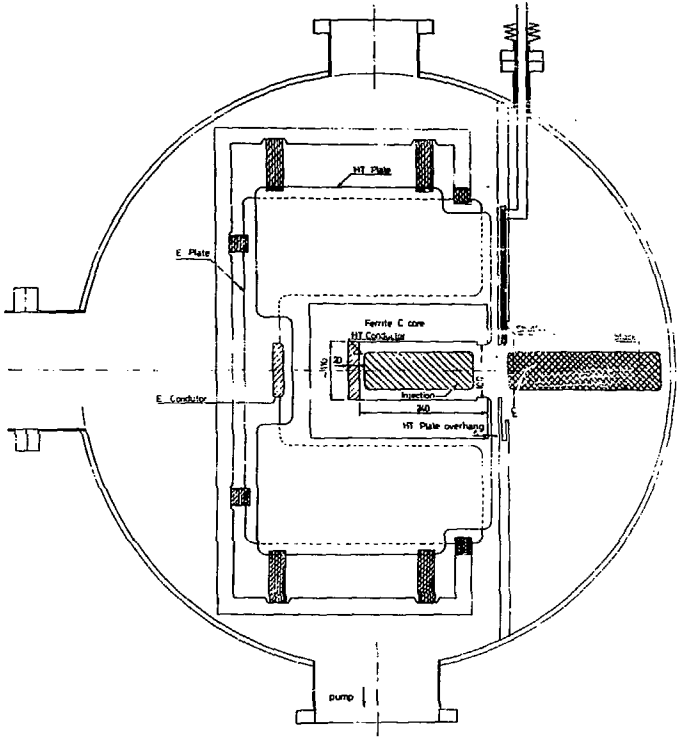

Fig. 4.6 Injection Kicker. Cross Section

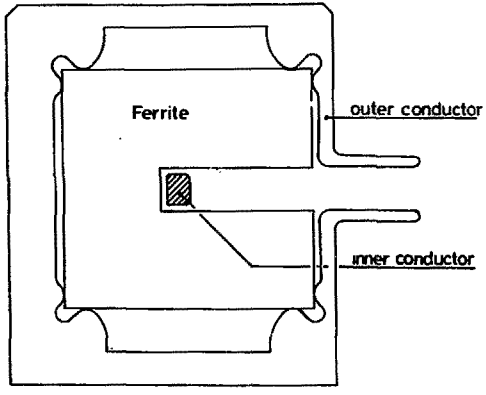

Fig.4.7 Extraction Kicker. Cross Section

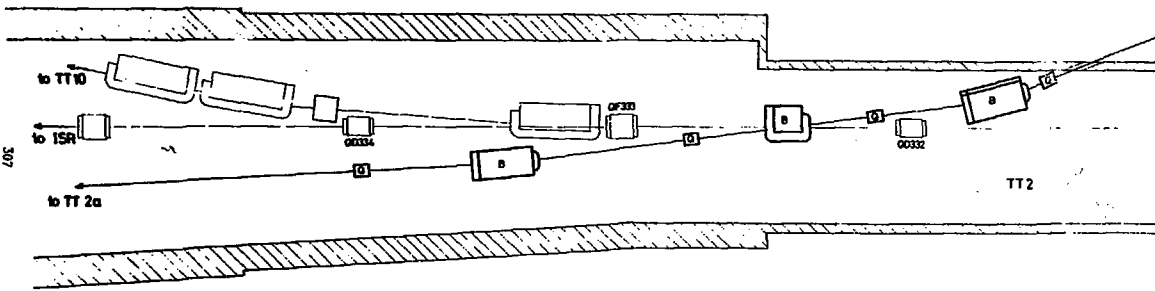

Fig. 4.8. Transfer of Antiprotons to the SPS ; Crossing TT2

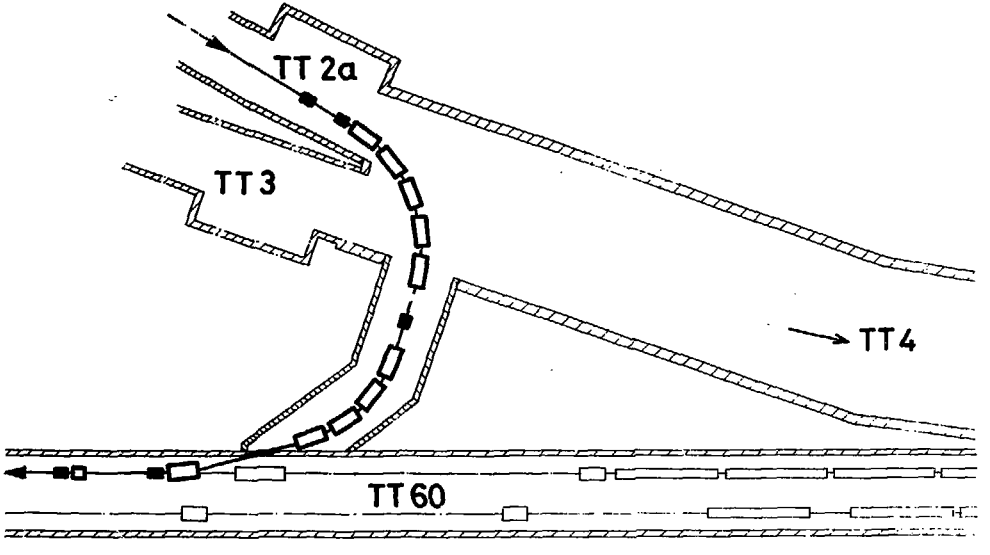

Fig. 4. 9 . Transfer of Antiprotons to the SPS ; junction TT60 - TT 2a.

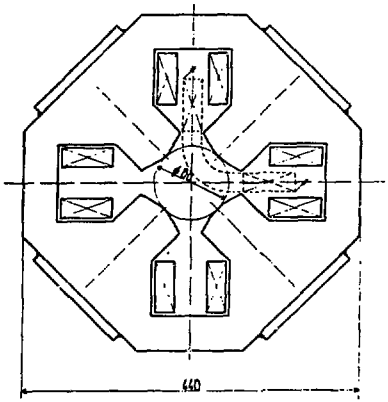

Nominal gradient	: 5 T/m
Inscribed diameter	: 80 mm
Core length	: 500 mm
Core width	: 440 mm
Number of turns per pole	: 27
Conductor	: 5 x 7.5 mm
Cooling hole diameter	: 3 mm
Nominal current	: 120 A
Power dissipation at I_{nom}	: 1440 Watt
Steel weight	: 370 kg
Copper weight	: 43 kg

Fig. 4.10 Cross-section of beam transfer quadrupole

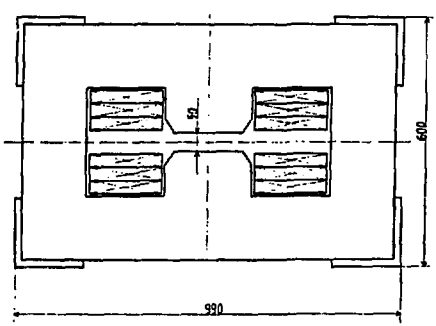

Nominal field	: 1.7 T
Gap height	: 50 mm
Core width	: 990 mm
Core height	: 600 mm
Steel length	: 1.9 m
Number of turns	: 192
Conductor	: 11 x 11 mm
Cooling hole diameter	: 6 mm
Nominal current	: 390 A
Power dissipation at I_{nom}	: 28.3 kW
Steel weight	: 6800 kg
Copper weight	: 775 kg

Fig. 4.11 Cross-section of beam transfer bending magnet

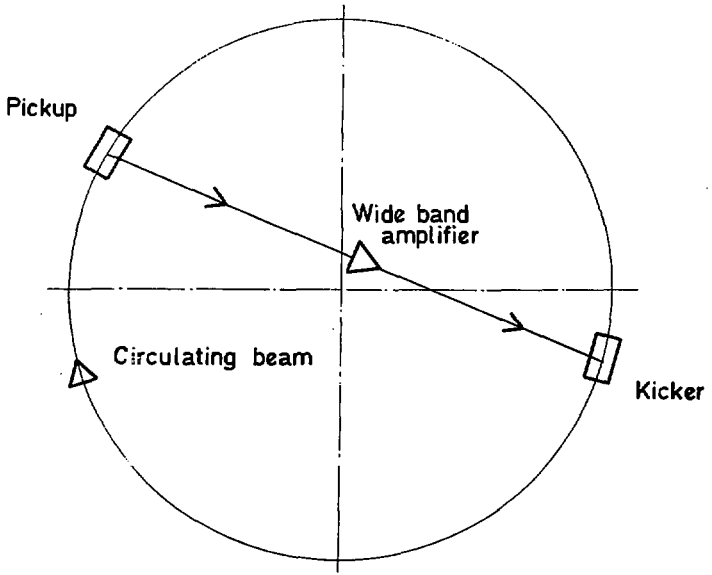

Fig. 6.1 Schematic representation of a storage ring with momentum cooling.

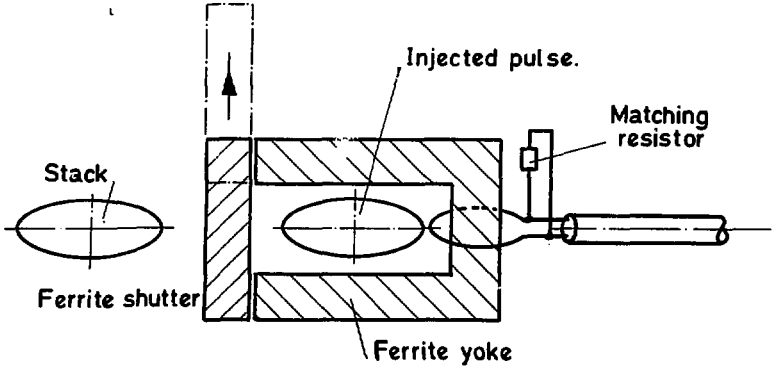

Fig. 6.2 Schematic cross section of precooling pickup or kicker.

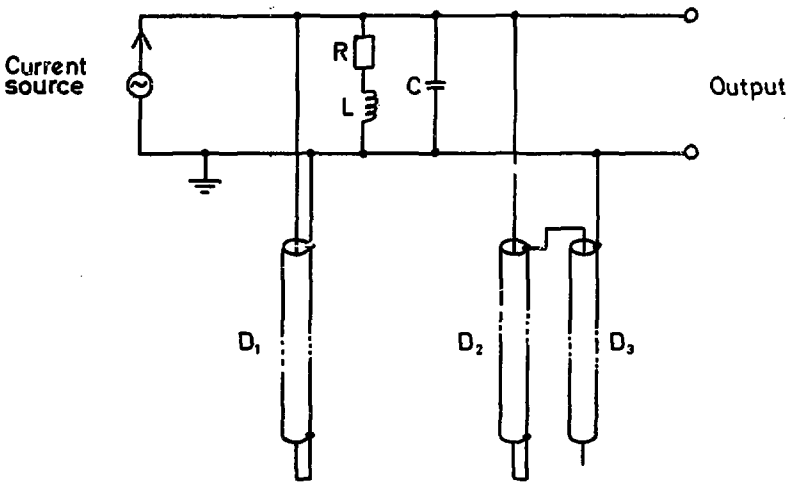

Fig. 6.3 Precooling filter

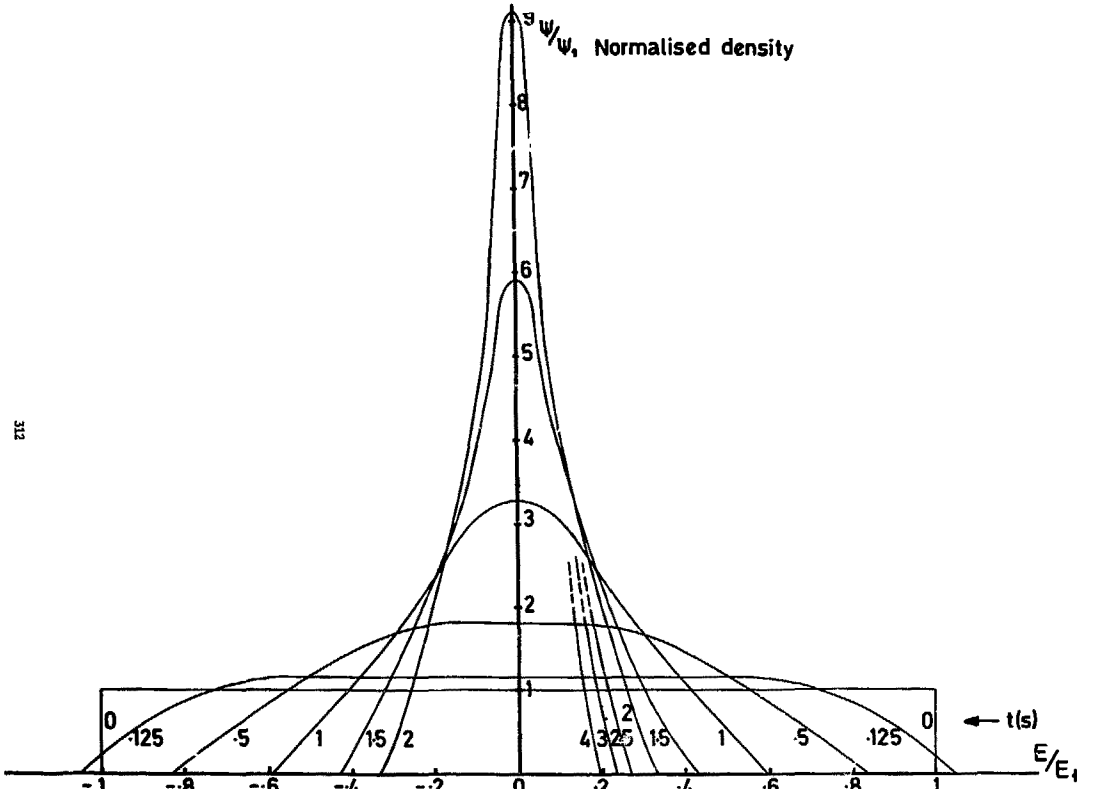

Fig.6.4 Precooling curves.

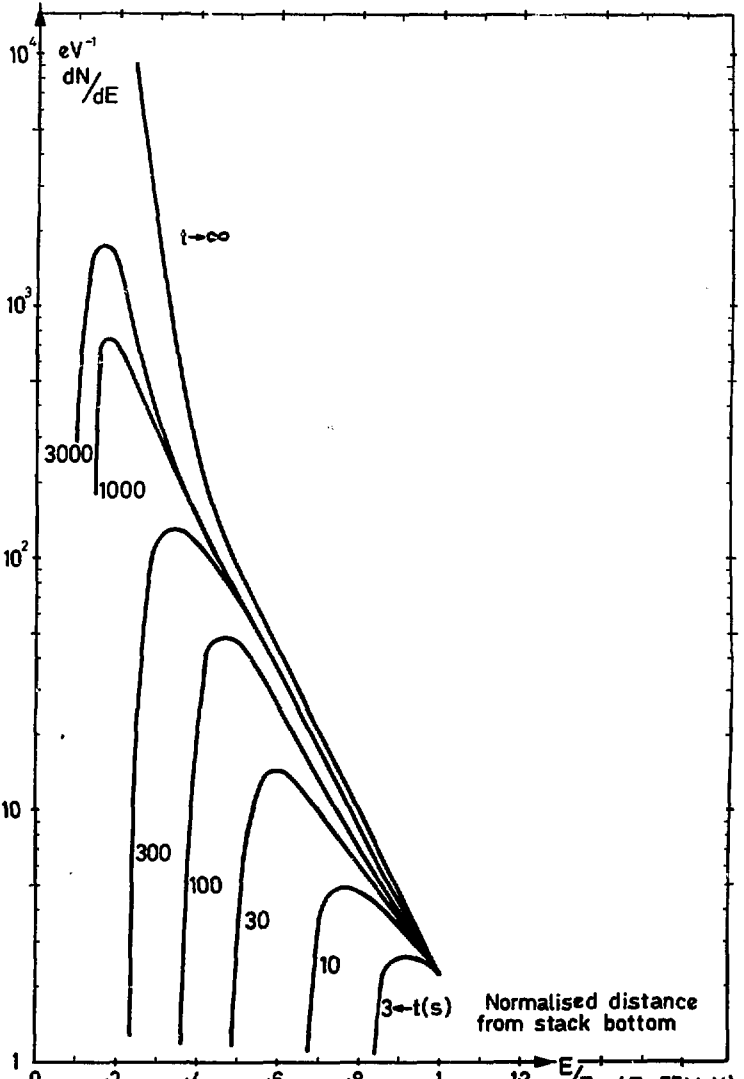

Fig. 6.5. Density profile of the stack for a constant particle flux towards the stack bottom.

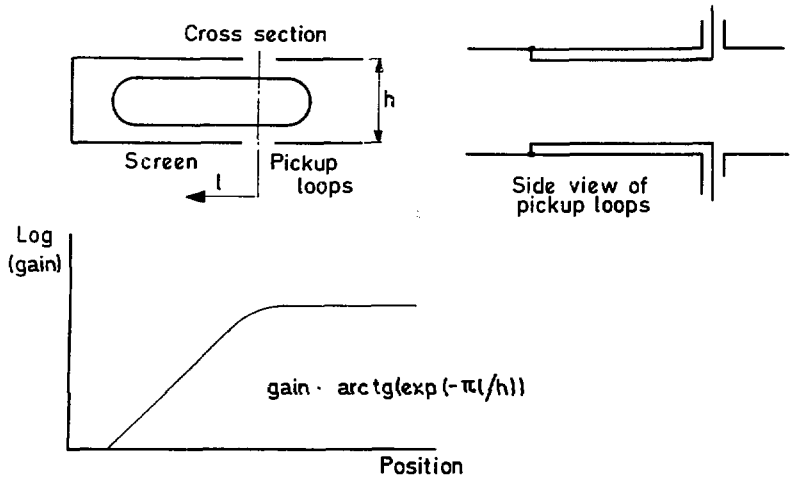

Fig.6.6 Schematic cross section and gain profile of the stack pickups.

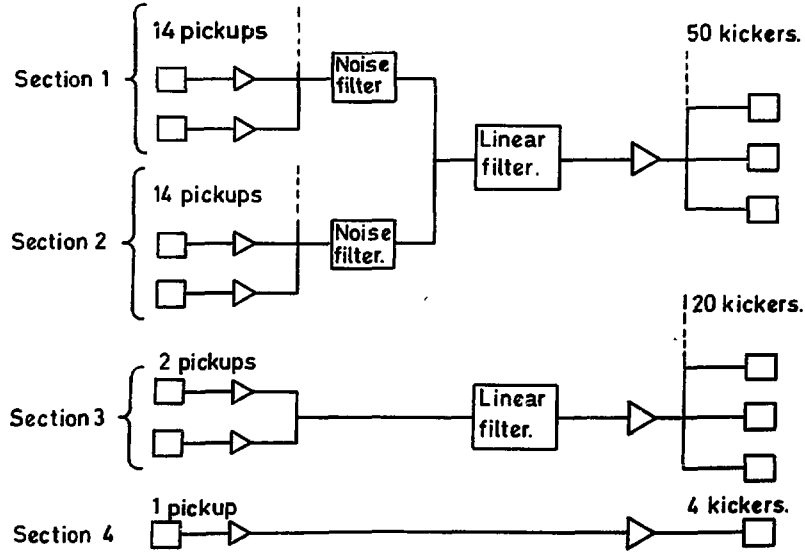

Fig.6.7 Block diagram of the stack cooling system.

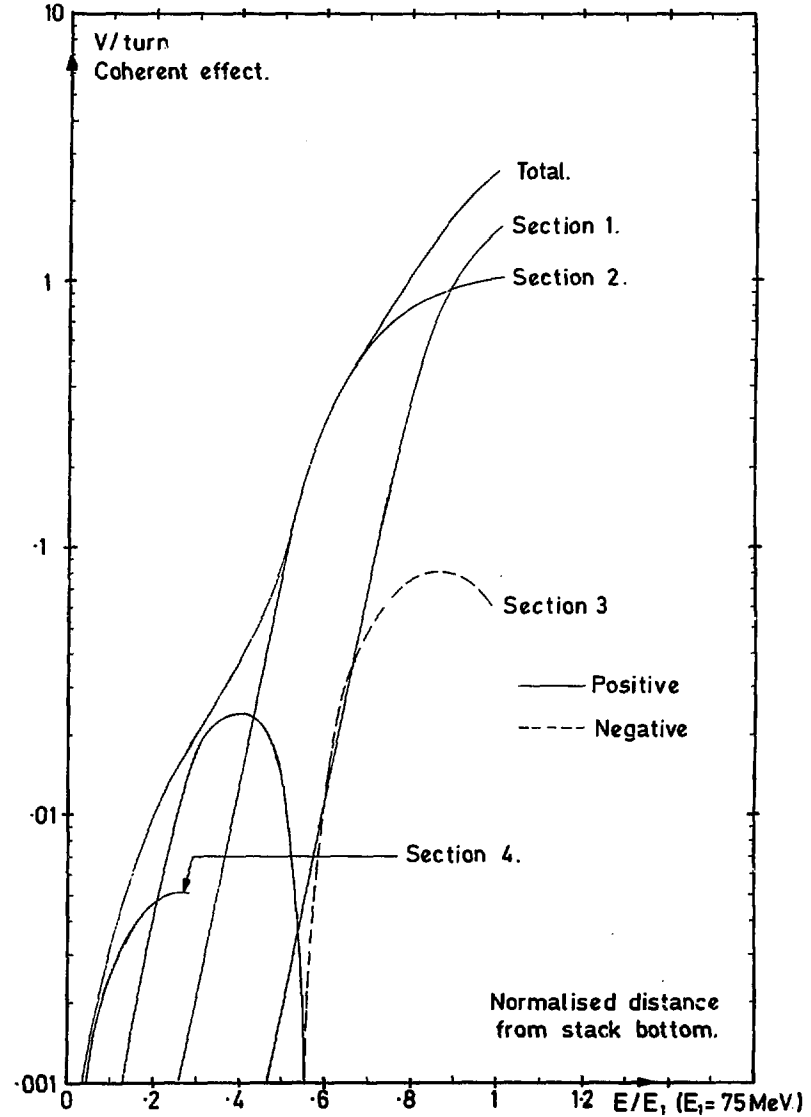

Fig. 6.8. Gain curves for stack cooling system.

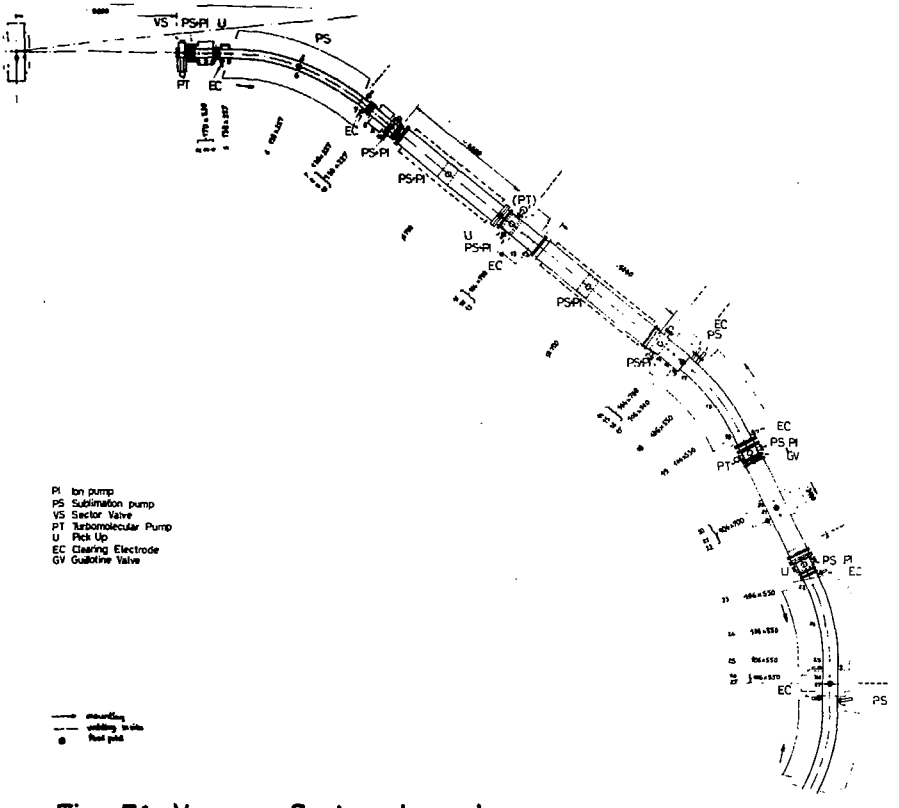

Fig. 7.1 Vacuum System Layout

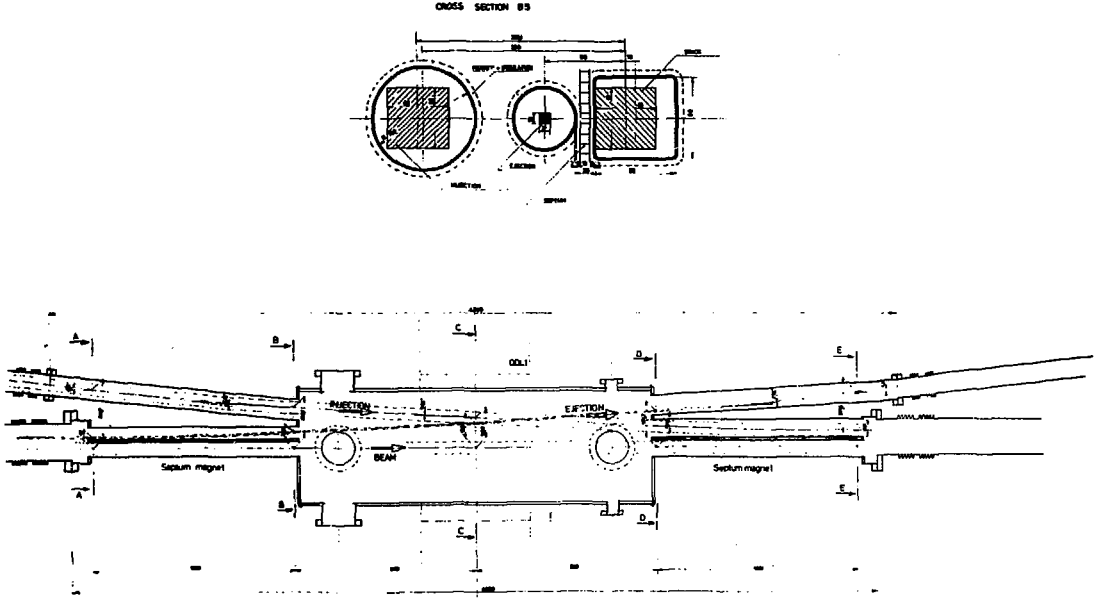

Fig. 7.2 Vacuum chamber. Injection/Extraction region

Fig. 8.1 Beam Diagnostics

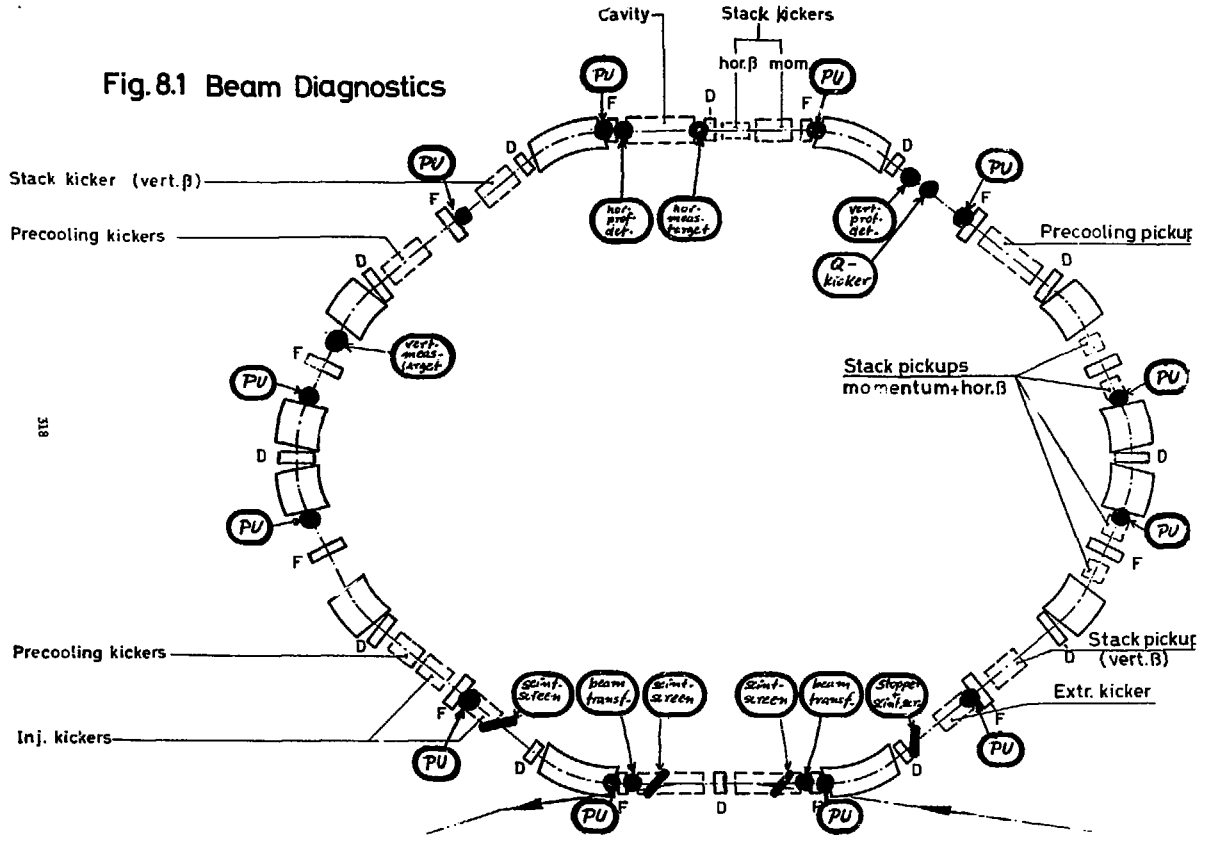

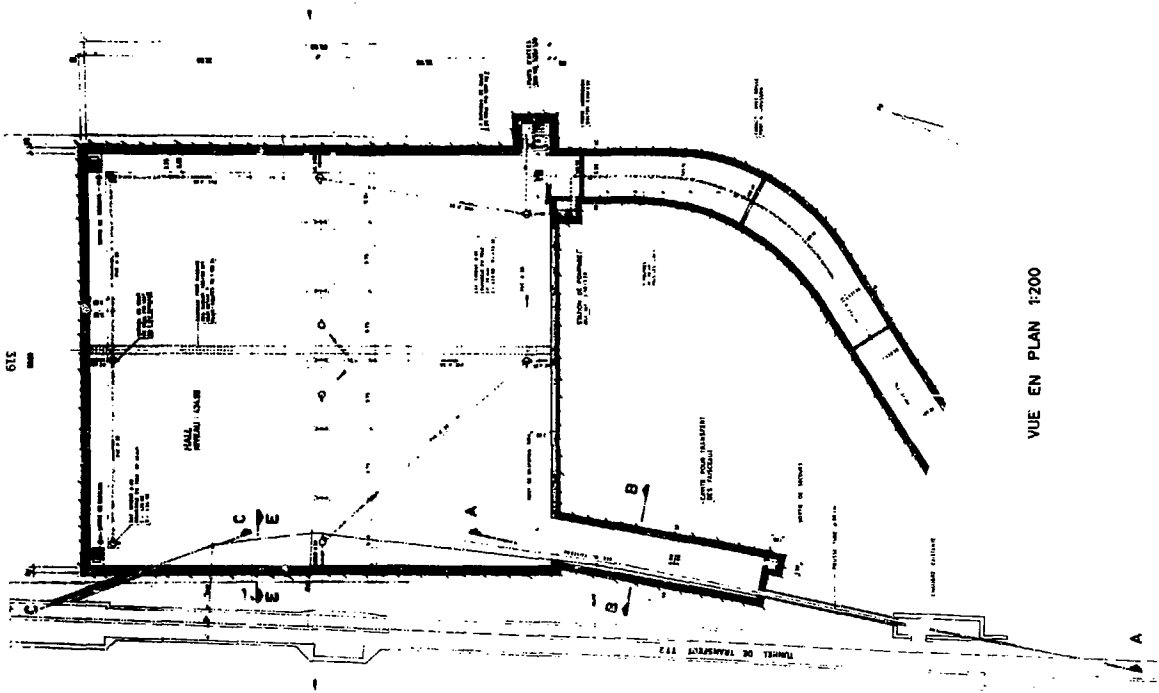

Fig. 9.1 Building Overall View

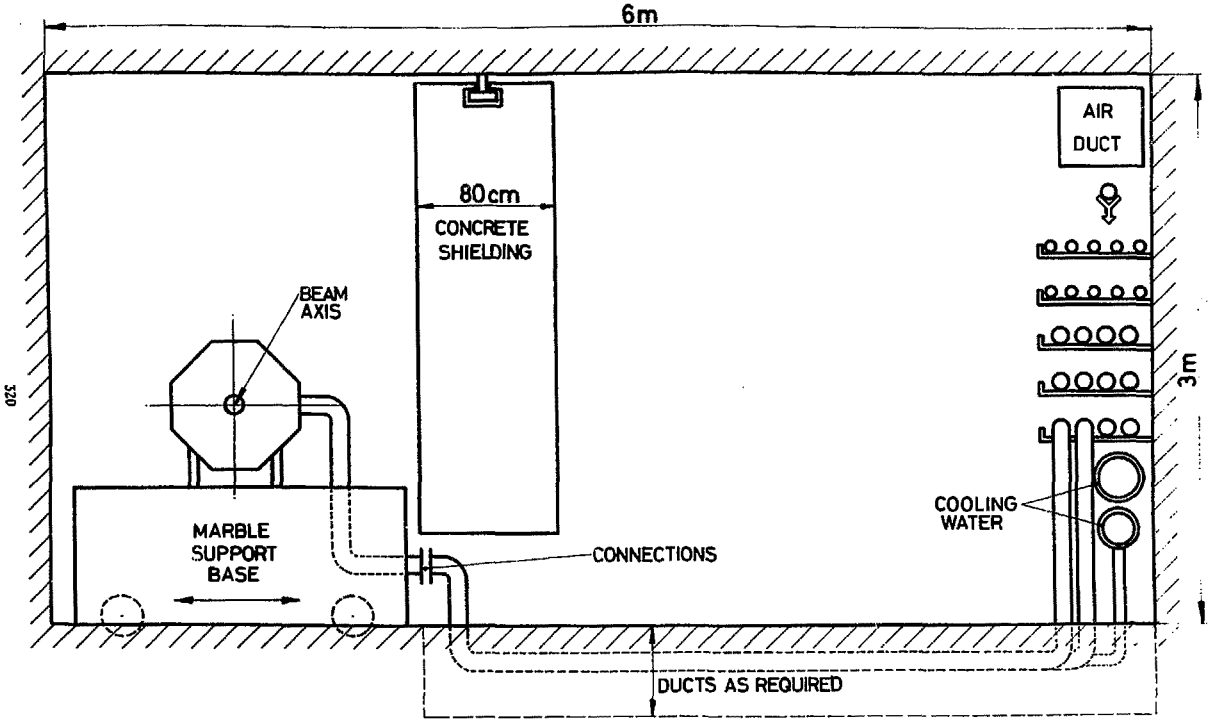

Fig. 9.2 Target area Schematic cross section

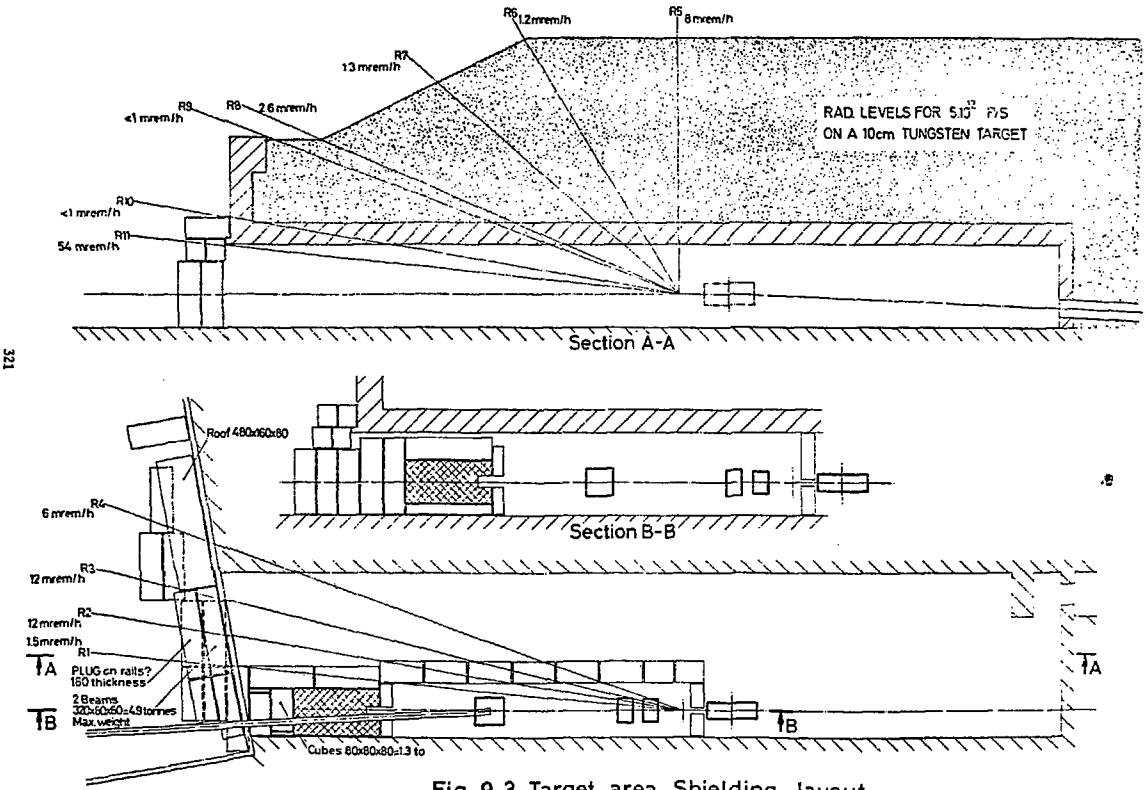

Fig. 9.3 Target area Shielding layout

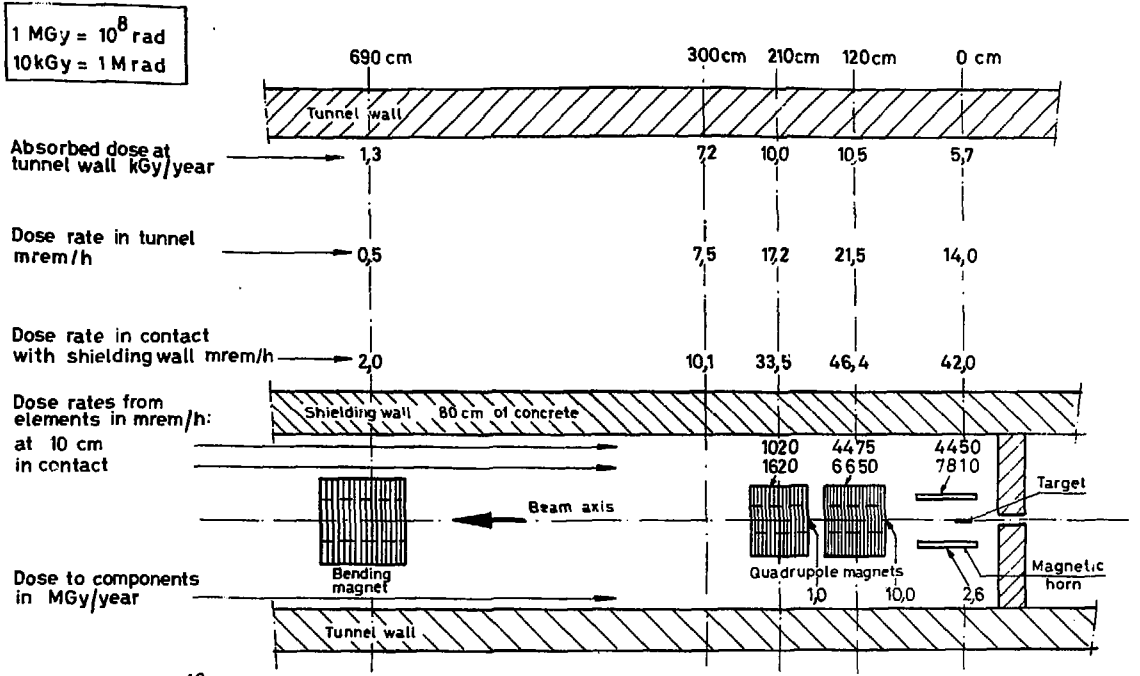

Assumption: $5 \cdot 10^{18}$ p/annum and 24h cooling! ; for 2h cooling multiply dose rate figures by 3 ; for 15 min cooling multiply by 4,5.

Fig. 9.4 Target area Calculated radiation levels

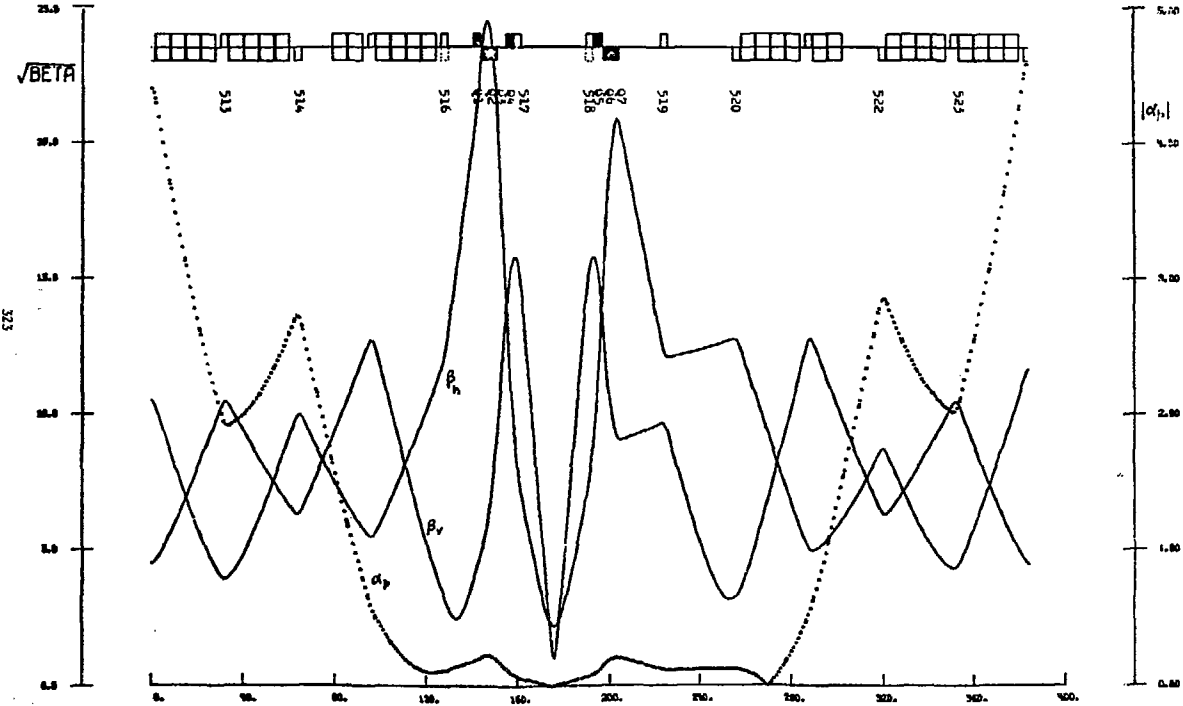

Fig. 10.1 SPS Insertion for low beta at proton-antiproton interaction point

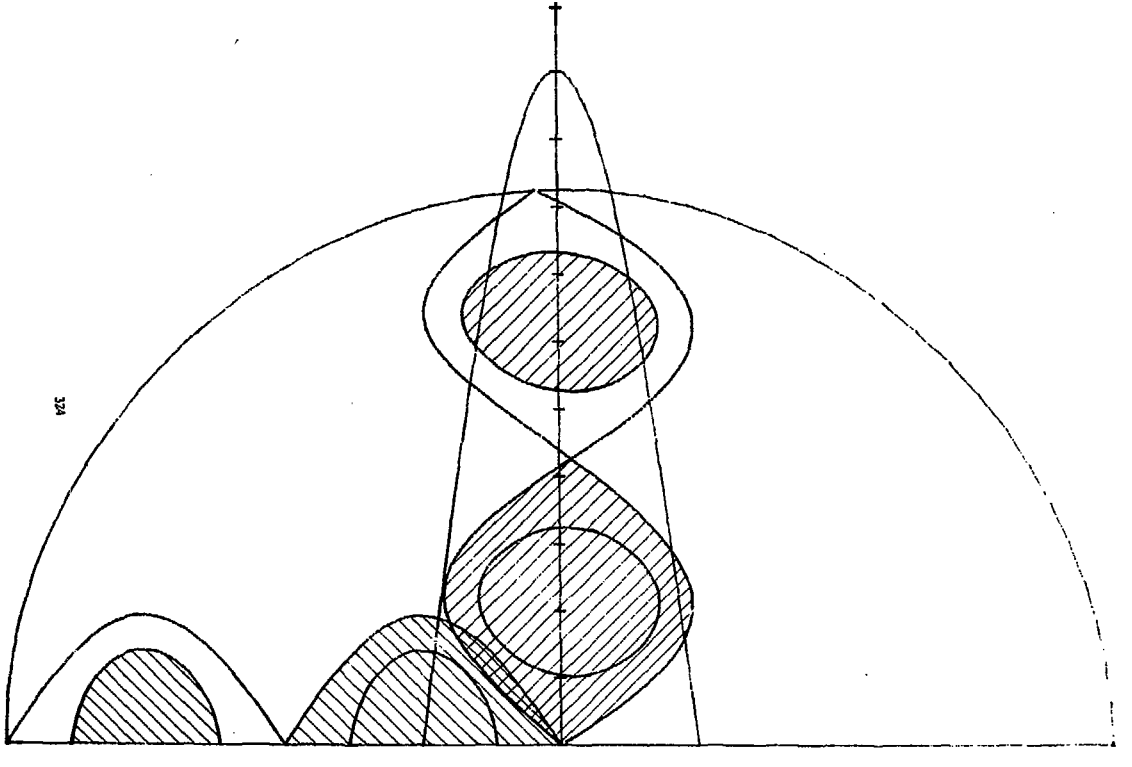

Fig. 10.2 Bunch rotation at 270 GeV.

Collecting Antiprotons in the Fermilab Booster and Very High Energy Proton-Antiproton Interactions

D. Cline, P. McIntyre, F. Mills and C. Rubbia*

Fermilab
P.O. Box 500
Batavia, Illinois 60510

Department of Physics
Harvard University
Cambridge, Massachusetts 02138

Department of Physics
University of Wisconsin
Madison, Wisconsin 53706

ABSTRACT

We describe a technique for producing an intense beam of antiprotons to be used for very high energy $\bar{p}$-p colliding beams. The Fermilab Booster is to be used as a collector for antiprotons produced on an external target. The antiprotons are decelerated and transferred to a 200 MeV storage ring (Freezer Ring) and then collapsed in phase space by electron cooling. Repetitive accumulation over 10^4-10^5 Booster pulses, acceleration to 8 GeV and injection into the main ring lead to the possibility of $\bar{p}p$ collisions at several hundred GeV with luminosity in excess of 10^{29} $cm^{-2}sec^{-1}$.

*Presently at CERN, Geneva, Switzerland.

Contents

I. INTRODUCTION

It is an old dream of particle physicists to construct a proton-antiproton colliding beam machine. High energy accelerator beams produce copious numbers of antiprotons. Recently we[1] have pointed out that the existing high energy rings at CERN and Fermilab can be transformed into $\bar{p}p$ storage rings of about 800 GeV in the center of mass. Furthermore the forthcoming Energy Doubler/Saver at Fermilab could give access to the fantastic energy of 2 TeV in the center of mass and would be quite suitable for a high performance storage ring.[2] In order to transform existing machines into $\bar{p}p$ colliding beams a method must be devised to collect and cool the antiproton phase space followed by reinjection of the $\bar{p}$ beam into the storage ring. Several methods have been devised to carry out this repetitive accumulation and cooling.[3,4,5]

A fundamental progress in this direction has been accomplished by the Novosibirsk group, which has recently demonstrated the possibility of damping betatron motions and momentum spread of 80 MeV protons with the help of collinear electrons travelling at the same speed[3] (electron cooling). In these beautiful experiments the proton beam size collapses to sub millimetric dimensions and $\Delta p/p \sim 10^{-5}$ in about 80 milliseconds.[6]

In order to adapt this technique to antiproton cooling, one faces the problem that phase space compression with electrons works efficiently only at non-relativistic energies ($\tau \sim \beta^4\gamma^5$), while the greatest majority of $\bar{p}$'s are produced fast in the laboratory system, i.e. $\langle\gamma_{\vec{p}}\rangle \sim \sqrt{E_p/2m}$. For instance for $E_p = 100$ GeV $\langle\gamma_{\vec{p}}\rangle = 7$ and the cooling time will then increase

by the factor $2^4 \cdot 7^5 = 260{,}000$!! Furthermore the technological problems associated with an electron cooler operating at $\gamma = 7$ are formidable[6], (e.g. the electron accelerating voltage must be 3.5 million volts) and they have not been satisfactorily solved to date.

It has occurred to us that one could bridge the gap between optimum production and cooling energies for antiprotons by introducing an additional stage of deceleration between the production of $\bar{p}$'s and the subsequent electron cooling[7]. We elaborate a realistic scheme making use of the rapid cycles of the Fermilab booster to decelerate $\bar{p}$'s to 200 MeV where we could perform Budker-type cooling and stacking in a modest ring (Freezer) housed in the same tunnel.

We believe this scheme has several attractive features among which are the availability of the major components, their inherent reliability, and the modest nature of the required 200 MeV storage ring. It could be carried out at modest cost and with very little need for new technological innovations. Thus within a few years the Fermilab accelerator can be transformed into a high energy $\bar{p}p$ storage ring device.

The scheme consists of three separate phases:

1. Antiproton production, deceleration and accumulation. Secondary particles at about 6.5 GeV/c are produced by 100 GeV/c protons from the main ring impinging on a small tungsten target. Particles are injected into the booster ring and decelerated to 200 MeV. Only $\bar{p}$'s survive at the end of the process.

The beam is transferred to the storage ring where it is cooled and added to the stack of previous accumulations.
One expects to accumulate 4 x 10^7 $\bar{p}$/pulse leading to $\sim 10^{11}$ particles in 2 x 10^3 pulses (3 hours).

ii. Injection of p and $\bar{p}$ in the main ring, and experimentation in $p\bar{p}$ collisions. The $\bar{p}$ beam is transferred from the Freezer to the Booster, accelerated to 8 GeV, and reverse injected in the main ring (MR). A standard proton Booster pulse is then injected in the main ring, with appropriate phasing in order to give collisions at the desired point of the main ring. There are then 84 proton and 84 antiproton bunches counter-rotating. With 10^{11} $\bar{p}$'s and 4 x 10^{12} p's with standard emittances, we expect a luminosity of $\sim 10^{29}$ $sec^{-1}cm^{-2}$ in the low-beta section designed by T. Collins. The scheme is shown in Fig. 1.

iii. Antiproton beam regeneration. After some time, beam-gas scattering, R.F. noise and higher order resonances could lead to an appreciable blow-up of the beams with consequent loss of luminosity. In order to restore beam quality, we propose to dump the proton beam, decelerate $\bar{p}$'s first in the MR to 8 GeV then in the Booster to 200 MeV, then cool again in the Freezer. The cooling process should take only seconds. After this, $\bar{p}$'s are accelerated again by the Booster, injected in the MR with a new companion proton beam and accelerated to high energies.

The main open question is how well electron cooling works. The recent results of Budker's group at Novosibirsk have shown that it is possible to cool a modest proton beam of 50-80 MeV in less than 100 msec. This impressive result allows one to attempt extrapolations to our conditions. However it is clearly imperative to perform additional experimentation at Fermilab on cooling techniques (see Appendix I, III).

II. MAIN PHYSICS MOTIVATIONS

The past ten years have seen remarkable progress in the understanding of elementary particles. First there is the experimental discovery of $\Delta S = 0$ weak neutral currents,[8] which when contrasted with the previous limits on $\Delta S = 1$ neutral current decay processes[9] leads to the suggestion of additional hadronic quantum numbers in nature.[10] Evidence now exists for new hadronic quantum numbers that are manifested either directly[11,12] or indirectly.[13] The experimental discoveries are complemented by the theoretical progress of unified gauge theories.[14] These developments lead to the expectation that very massive intermediate vector bosons (50 - 100 GeV/c^2) may exist in nature.[14] The search for these massive bosons and other new phenomena require three separate elements to be successful: a reliable physical mechanism for production, very high center of mass energies, and an unambiguous experimental signature to observe them. In addition to the high center-of-mass energy available in $\bar{p}$-p collisions, several considerations suggest that they may present a much better opportunity of discovering new phenomena than p-p collisions.[15]

First we consider production process. There is now very strong support for the notion of pointlike constituents in the hadron obtained from lepton-hadron scattering and very high energy neutrino experiments. The experimental detection of weak interaction processes in hadronic collisions almost certainly involve quark-antiquark (or proton-antiproton) annihi-

lation processes very much like $e^+ e^-$ collisions. (For example, the processes $u + \bar{u} \to \mu^+ + \bar{\mu}$ or $u + \bar{d} \to \mu + \nu$.) There are clearly more antiquarks in an antiproton, then in a proton, and furthermore the antiquarks in an antiproton, being valence quarks, carry a much larger fraction of the total energy than do the (sea) antiquarks in a proton. The exact size of these effects at high energy are uncertain, but qualitatively cross sections probably differ by a factor up to 10 - 100 in favor of the $\bar{p}p$ system.

The $\bar{p}p$ system is an eigenstate of charge conjugation (C) invariance whereas the pp system is not. Thus there are many simple experimental tests of C violation in the $\bar{p}p$ system. The observation of C violation may be an important technique to observe the effects of weak interactions in very high energy collisions. In the case of the pp system the "equivalent" way to observe weak interaction effects is through parity violation. This very likely involves polarization measurements which are considerably more difficult than tests of C violation. Thus proton-antiproton collisions at the highest energy offer distinct advantages in the search for new phenomena in nature, especially those associated with the weak interaction.

We now turn to the specific case of the production and detection of the weakly interacting intermediate vector bosons. Present neutrino data indicate a mass limit of >20 GeV for the charged intermediate vector boson.[16] The center-of-mass energy available in a proton-antiproton storage ring is .4-2.0 TeV, sufficient to produce very large mass intermediate vector

bosons. In the Weinberg-Salam model the W^0 the W^+ 1,14,16 masses are now estimated to be 80 ± 6 GeV and 64 ± 11 GeV, respectively. This mass is outside the reach of the presently planned new generation of e^+e^- storage rings.

The derivation of the W^0 cross section exposes the basic simplicity of the assumptions for the case of $\bar{p}p$ collisions.[1,15] By analogy the $\bar{q}q$ annihilation behaves like e^+e^- scattering. In the e^+e^- case a sharp resonance peak would be expected in the cross section for the process

$$e^+ + e^- \to W^0 \to e^+ + e^-$$

$$\to \mu^+ + \mu^-$$

$$\to \begin{matrix} u + \bar{u} \\ d + \bar{d} \end{matrix} \left(\begin{matrix}\text{hadron} \\ \text{jet}\end{matrix}\right) + \left(\begin{matrix}\text{antihadrons} \\ \text{jet}\end{matrix}\right)$$

In order to estimate the cross section for $\bar{p}p$ collisions the structure functions of partons must be known. Neutrino and charged lepton scattering experiments provide the necessary structure functions and have set limits (>20 GeV) on any non-locality in the parton form factor.[17] The main difference with respect to e^+e^- is that now the kinematics is largely smeared out by the internal motion of the q's and $\bar{q}$'s. The average center of mass energy squared of the q-$\bar{q}$ collision is roughly

$$\langle S_{q\bar{q}} \rangle \sim S \langle x_q \rangle_p \langle x_{\bar{q}} \rangle_{\bar{p}}$$

S is the center of mass energy squared of the $\bar{p}p$ system and $\langle x_q \rangle_p = \langle x_{\bar{q}} \rangle_{\bar{p}}$ we find $\langle S_{q\bar{q}} \rangle \sim 0.04\ S$. For $M = 100\ \text{GeV}/c^2$

this suggests $S > 2 \times 10^5$ GeV^2 or $\sqrt{S} \geq 450$ GeV. In the case of pp scattering the $\langle x_{\bar{q}} \rangle_p$ is expected to be much less and the x distribution probably falls very rapidly.

Detailed estimates have been given by several authors[2,15] and give

$$\sigma(p\bar{p} \rightarrow W^\circ + \text{hadrons} \rightarrow e^+ + e^- + \text{hadrons}) \approx 10^{-32} \text{cm}^2$$

More optimistic cross section estimates also exist in the literature.[18]

The cross section estimated above leads to 3.6 events/hour given a luminosity of 10^{29} cm^{-2}sec^{-1} and 100% detection efficiency. The $\mu^+\mu^-$ is expected to be very small compared to the W° signal. Furthermore if the W° decay into hadronic states is detected the corresponding event rate will increase. We note that since the q and $\bar{q}$ have comparable x distributions in $\bar{p}p$ collisions, a large fraction of the W's produced will have low x_W and hence decay symmetrically in the lab. In pp collisions, the widely different q and $\bar{q}$ x distribution can produce sizeable x_W. Finally the charged vector bosons may well have lower mass and thus larger cross sections, with a somewhat weaker experimental signature.

Another challenging possibility is a search for fractionally charged quarks. Overwhelming evidence favors the existance of light, fractionally charged constituents inside the hadrons. Absence of direct production of free quarks suggests the existence of confinement mechanisms (bag). It is not known, but it appears likely that at very high energies the "bag" could be broken, thus liberating the elementary constituents. A search for quarks in very high energy hadron-hadron collisions is mandatory.

Finally there is one additional possibility for interesting and unique physics with the low energy antiproton storage ring itself. It appears that the present universe has a net positive baryon number for unknown reasons. A simple, but seemingly unlikely possibility is that the antiproton is unstable and has a lifetime much shorter than 10^{10} years. The present limit on the antiproton lifetime is likely no better than milliseconds. Using a small antiproton storage ring with 10^{10} - 10^{12} antiprotons stored for periods of days it appears possible to detect an unstable antiproton if the lifetime is less than ~ 10^{7} years. This must be considered a long shot but we know of no other way to discover antiproton disintegration.

The observation of an unstable antiproton, coupled with the observed stability of the proton (>10^{29} years); would violate the PCT theorem.

III. ANTIPROTON PRODUCTION AND DECELERATION

III-1. Introduction

In this phase, the Booster is alternately accelerating 12 proton pulses and decelerating 12 antiproton pulses (see Fig. 2). The settings of the magnetic cycles are unchanged. However, the rf is turned on alternately on the rising and falling sides of the magnet ramp and the phase sequence among cavities is inverted. Since the p and $\bar{p}$ currents are vastly different (4×10^{12} p vs 3×10^{7} $\bar{p}$pp) two separate beam control systems will be necessary. In order to ease the extraction of the 100 GeV primary protons, 12 Booster pulses are injected in the Main Ring, leaving a time gap between pulses to allow for the rise and fall times of the kicker magnet. We propose to eject the beam from the medium straight section F17 and to transport it along the newly-planned line from there to the Booster (Fig. 1 and Fig. 3). Targeting and the beam dump occur along this line, and $\bar{p}$'s can be reverse injected in the Booster through the new 8-GeV proton extraction channel. We have taken the "good field" Booster ring acceptances[19] at 200 MeV and adiabatic extrapolation to other energies. We understand that these goals have not been reached as yet and that more work is necessary.[20]

III-2. Gymnastics on Proton Beam, Ejection and Targeting.

The largest possible beam current is accelerated to 100 GeV/c, then the main ring is flat-topped with rf at maximum voltage. With $V_{rf} = 3.4 \times 10^6$ Volt, h = 1113, f = 53.4 kHz and $\eta = 3.3 \times 10^{-3}$ we calculate

$$\nu_s = [h\eta \ eV/2\pi E]^{1/2} = 3.65 \times 10^{-3}$$

The bunching factor B (bunch length/bunch separation) is then

$$B = (\frac{h}{2\pi}) \ (8f\eta/p \ \nu_s)^{1/2} \ A_b^{1/2} = 0.27 \ A_b^{1/2}$$

where A_b is the invariant bunch area, expressed in eV - sec. Taking A_b = 0.1 eV sec, which is about four times the injection area in the booster, we get

$$B = 0.085$$

$$\frac{\Delta p}{p}_{full} = \frac{1}{\beta} \ [8A_b \ f \ \nu_s/p\eta]^{1/2} = 1.67 \times 10^{-3}$$

We eject 84 bunches of the main ring at a time and focus the beam on a very small tungsten target. The extraction of 100-GeV protons is shown in Fig. 3. At position E48 in the Main Ring, there is a missing magnet position giving a straight section of 7m available length. A pulsed magnetic kicker S_1 at that position produces a horizontal bump of 3cm at the medium straight section F17 ($\Delta\nu$ = 0.81). There exists there an available length of 14m. Two Lambertson septa S_2 will deflect the beam vertically by 25 mrad, producing a deflection of 18 cm at the face of the next dipole.

Taking an invariant transverse beam emittance of $E.\beta\gamma = 30\pi\ 10^{-6}$ rad m and $\beta_v = \beta_H = 2.5$m at the target which can still be realized with standard gradient quadrupoles, we calculate a spot of 0.30 mm radius (two standard deviations in the guassian approximation). The focus has to be made a chromatic in order to avoid additional contributions from the relatively large momentum spread.

It has been calculated that $5 \times 10^{13}/12 = 4.16 \times 10^{12}$ particles is about the maximum beam intensity which can be concentrated on a tungsten target of special construction. substantially higher beam intensities would lead to destruction. Heat propagates in tungsten with a speed about 1 m/sec. Since successive pulses are ejected at 66 ms in time, we can cool the target between pulses by simple conduction.

After the target, the residual proton beam must be separated from the low-energy particles by bending and absorbed in a suitable beam dump.

III-3. Bunch Synchronization

The antiproton bunches have the same time structure as the protons in the Main Ring and they must also fit precisely within the buckets of the Booster. This is not an entirely trivial operation. Frequencies are quantized by the requirement of integer harmonic numbers in the Main Ring and the Booster. The two frequencies are automatically

matched for particles of equal energies. However, antiprotons have an energy which is substantially lower than that of the parent protons while retaining the same time structure, and frequency shift cannot be neglected.

We propose to overcome this difficulty by increasing by one unit the harmonic number in the Booster for antiproton capture and deceleration, i.e., instead of h = 84 which is the nominal value for protons, we propose to operate at h = 85. In order to make this possible, the proton and antiproton relativistic factors γ_p and $\gamma_{\bar{p}}$ have to satisfy the relation:

$$\frac{1}{2\gamma_{\bar{p}}^2} - \frac{1}{2\gamma_p^2} = \frac{1}{85}$$

giving $\gamma_{\bar{p}} = 6{,}518$, corresponding to $T_{\bar{p}} = 5.177$ GeV. This is sufficiently away from the transition energy $\gamma_t = 5.446$ to present no complications. The area of the antiproton bunches is determined by the bucket area at 200 MeV, which is 0.0352 eV sec. At the magic energy $T_{\bar{p}} = 5.177$ GeV, we have $\eta = \frac{1}{\gamma_t^2} - \frac{1}{\gamma^2} = 6.43 \times 10^{-3}$, $f = 0.637 \times 10^6$ Hz. For the maximum rf voltage eV = 700 KeV/turn and cos $\phi_s = 1/2$ we calculate

$$\nu_s = [h\eta eV \cos \phi_s / 2\pi E]^{1/2} = 2.16 \times 10^{-3}$$

$$B = (h/2\pi)[8Af\eta/p\nu_s]^{1/2} = 0.122$$

$$\Delta p/p_{full} = \frac{1}{\beta}[8Af\nu_s/p\eta]^{1/2} = 3.0 \times 10^{-3}$$

In order to match bunches, we must increase the proton bunching factor from 0.085 to 0.122. This can be easily done by reducing the MR voltage from 3.4×10^6V to 8.0×10^5V during extraction.

III-4. Production and Collection of Antiprotons

The booster acceptances, after allowance for alignment errors, are taken to be

$$A_V^{(200\ \mathrm{MeV})} = 40\pi\ 10^{-6}\mathrm{m\ rad}$$

$$A_H^{(200\ \mathrm{MeV})} = 40\pi\ 10^{-6}\mathrm{m\ rad}$$

Acceptances must match the beam emittances at 200 MeV. Assuming adiabatic damping during deceleration the emittances scaled to 5.2 GeV injection energy are

$$A_V^{(inj)} = A_H^{(inj)} = 4.0\pi\ 10^{-6}\mathrm{m\ rad}$$

The value of the β function for the antiprotons at the production target is taken to be $\beta_V = \beta_H = .025$m. The $\bar{p}$ angular divergence is then $\theta_V = \theta_H = 13$ mrad, and the solid angle accepted is $\Omega = \pi\ \theta_V \theta_H = 5.3 \times 10^{-4}$ steradian.

Inclusive $\bar{p}$ and π^- production has been parametrized for the existing data in Ref. 21:

$$E\frac{d^3\sigma}{dp^3}(\bar{p}) = 0.26N\ [p_\perp^2+1.04]^{-4.5}(1-x_R)^7$$

$$E\frac{d^3\sigma}{dp^3}(\pi^-) = N\ [p_\perp^2+0.86]^{-4.5}(1-x_R)^4$$

We establish the normalization N from the data of Ref. 22 in the region $s>1000$ GeV^2 where scaling holds: N=10.2 mb GeV^{-2}

Also in Ref. 22 is a plot of the production ratio $f(s) \equiv \bar{p}/\pi^-[x=0.35, p_\perp=0.5\ \text{GeV/c}]$ in the range $25<s<2830\ \text{GeV}^2$. Using the cross section parametrizations we extrapolate to obtain $f_o(s) = \bar{p}/\pi^-[x=0, p_\perp=0]$. By normalizing to the saturation value $f_o(\infty)$ in the region of scaling, we obtain the scaling parameter $\alpha(s) \equiv f_o(s)/f_o(\infty)$ which is plotted in Fig.4. We then have

$$E\frac{d^3\sigma}{dp^3}(\bar{p}) = 2.65\ \alpha(s)\ [p_t^2+1.04]^{-4.5}(1-x_R)^7\ [\text{mb GeV}^{-2}]$$

This invariant cross section, expressed in convenient lab frame variables, is just $(1/p^2)\frac{d^2\sigma}{d\Omega(\Delta p/p)}$. This cross section is plotted in Fig. 5 as a function of $\bar{p}$ momentum, for various primary proton energies. For $p_{\bar{p}}=6.5$ GeV/c, the optimum primary proton energy is 100 GeV, and the cross section is 57 mb/sterad. The 5 cm tungsten target has an efficiency of $\varepsilon=1/3$. The momentum acceptance of the Booster from Sect.III-3 is $\Delta p/p = 3.0 \times 10^{-3}$. The $\bar{p}$ yield is then

$$Y = \frac{N_{\bar{p}}}{N_p} = \varepsilon\frac{d^2\sigma}{d\Omega(\Delta p/p)}\frac{\Omega\ \Delta p/p}{\sigma_{tot}} = 7.5 \times 10^{-7}$$

This result agrees within 30% with the Monte Carlo cascade calculation of Ref.23. With 4.6×10^{13} protons in 12 Booster pulses in the MR, this corresponds to $N_{\bar{p}} = 3.5 \times 10^7$.

We have designed with some detail the critical parts of the $\bar{p}$ collection channel. It consists of three distinct parts:

i) The collecting lens system.

It is a 6-quadrupole system consisting of an intial doublet (Q_1,Q_2), two field-lenses (Q_3,Q_4) and a final matching doublet. The quadrupole dimensions and gradients are listed in Table II. We show in Fig. 6 trajectories of off-momentum particles and several limiting rays.

ii) A momentum matching section. This section separates the antiprotons from the main proton beam and matches dispersion of the beam to the requirements of the Booster.

iii) Injection into the Booster. Here we can use the new extraction system to be installed in straight section 3 (see Fig. 7). Although the detailed design is only now in progress, it is well within present technology and we anticipate no major problems.

IV. ANTIPROTON STORAGE AND COOLING

IV-1. Design Criteria.

Antiprotons are transferred to a 200 MeV storage ring (Freezer Ring) where cooling and repetitive accummulation takes place.

We suggest a very simple lattice and reduced periodicity. The central requirement of the lattice is a good acceptance and adequate long straight sections for electron cooling. The major goal is to design a lattice with a minimum number of dipoles and quadrupoles that gives the longest good quality straight sections. We present here one example of a lattice which approximately satisfies these criteria. The basic lattice has 12 cells, 24 dipoles, and 36 quadrupoles. Figure 8 shows a unit cell and the resulting betatron functions. The machine parameters and performance are given in Table III. A large acceptance is obtained that is well matched to the booster or to the Fermilab linac should the Freezer be used as a proton cooler or for multiturn linac injection (see Appendix III).

We would like to preserve the possibility of transferring synchronously to the Freezer. This places a constraint on the circumference of the Freezer, since in order to match harmonics with the Booster we have

$$\frac{h_F}{85} = \frac{C \times 13.25}{2\pi \times 10^3 m.}$$

The choice $h_F = 86$ yields $C = 479.78$ m, which fits comfortably in the Booster tunnel (see Figure 9 and 10).

When we return the cooled and stacked anti-protons to the

Booster for reacceleration and injection in the MR, it is necessary to do so with h = 84 in the Booster. This dictates $h_F = 85$. This corresponds to a circumference C = 479.85m, negligibly different from that for injection to the Freezer.

The transfer of the $\bar{p}$ beam from the Booster to the Freezer has to have sufficient aperture to accommodate the full Booster beam acceptance. This can be achieved using a fast kicker B_1 in long straight 7, followed by a pulsed current septum B_2 in long straight 6. These elements are described in Table II. A second, identical pair of elements are then used in reverse sequence in the Freezer ring for injection.

The transfer from the Freezer into the Booster is accomplished at straight 5 with a more modest version of B_1, B_2, since the aperture requirement is now minimal.

We find that because of the rise and decay times of the full aperture kickers which are necessary to extract and inject the relatively large beam, as many as 3 bunches corresponding to 100 nsec may be lost in the transfer process.

IV-2. Magnetic Structure

There are several possible designs for the bending and quadrupole magnets that form the building blocks of the Freezer lattice. The bend can be either a window-frame or H design; the quadrupole can be either a standard design with iron pole tips, or a Panofsky quad formed by a box of 4 alternating current sheets. We are presently evaluating each design in regard to the required field quality and cost.

For the bending magnet, we have examined a number of existing

designs (Fermilab 10' EPB dipole, SLAC 18D72, ANL BM105, 107, 109, 110, 114). It seems in general that the fraction ε of horizontal "good field" aperture to physical aperture is $\varepsilon \sim (1+2\alpha)^{-1}$ in a good design of either an H or window frame, where α is the ratio of vertical/horizontal aperture in the desired good field region. For the case discussed here $\varepsilon = 0.5$. The field quality in the window frame is, however, sensitive to coil placement, and places rather stringent demand on the fabrication process. This also potentially produces significant variations in multipole moments from one magnet to another. For the design case presented here, we use a scaled replica of the 10' EPB H dipole, shown in Fig. 11.

One question that arises in the context of the bending magnets is what guide field should be used. Three considerations arise in this connection. First, the field quality of a dipole below a few kG suffers from the variation of Fe magnetization at low field. Second, the sagitta for a magnet of given bending angle decreases as guide field increases. The sagitta δ [m] of particles of momentum p [GeV] in a magnet of field B [T], bend angle ϕ[rad] is

$$\delta = \frac{p\phi^2}{2.4B}$$

Thus for a fixed number of bends (fixed ϕ), sagitta is minimized for maximum B. Third, as will be discussed in the next section it seems desirable to locate a distributed ion pump system in the fringe field of the dipoles. An optimized design of such a system improves in pumping speed up to a field of ~4kG. We have tentatively chosen for this design a guide field of 5kG, corresponding to 24 1m dipoles.

For the quadrupoles, there exist 21 quadrupoles that previously

formed the muon channel of the Chicago synchrocyclotron. The design is shown in Fig. 12. We are examining their suitability for the Freezer ring. Several Panofsky quads have been built at Cornell.[25] The Panofsky design is problematic for a storage ring for the same reasons as a window frame dipole. Additionally, its power requirements are greater for a given gradient that for a standard quad.

The parameters of both magnets are given in Table IV.

IV-3. Long Straight Sections for Electron Cooling

In order to obtain rapid cooling of the beam it is desirable that the $\bar{p}$ beam have a small divergence in the straight section. This requirement can be met by having β_H, β_V large in the straight section. We have achieved one simple design of such a straight section using two quadrupole triplets that match well the basic cell described before. The horizontal acceptance remains ~100π m and 8" bore quadrupoles are adequate for the triplets. The β_V, β_H are in the range of 15-40 m leading to an angular divergence of ~(1-2)mr. The p function (off momentum function) goes to 1±2m in the same straight section. We suggest that the cooling straight sections be instrumented in this way whereas the other straight sections need fewer quads (~2 doublets, incorporating the D quads of the regular cells).

IV-4. Vacuum System

The Freezer ring must be capable of storing an antiproton beam for a time of the order of a day without serious losses due to beam-gas scattering. We will examine the vacuum requirements implied and discuss one attractive approach to meeting them.

Beam growth occurs by Coulomb scattering from gas molecules, and beam loss occurs each time an antiproton collides with a gas nucleus. The rate of increase in the mean square of the projected angle of Coulomb scattering is:[26]

$$\frac{d\langle\phi^2\rangle}{dt} = \frac{4\pi\, r_p^2 c}{\beta^3\gamma^2} \sum_i n_i Z_i^2 \ln 38360/\sqrt[3]{A_i Z_i}$$

where $r_p = 1.54 \times 10^{-16}$cm the proton radius, n_i is the density and Z_i and A_i are the atomic number and atomic weight of atoms of type i. Snowdon[27] has analyzed the residual gas composition in the MR at a pressure of 0.21μ Torr. We will assume the same composition in the Freezer, and follow here his calculation of beam growth. The angular growth is

$$\frac{1}{p}\frac{d\langle\phi^2\rangle}{dt} = 0.25 \text{ rad}^2\text{sec}^{-1}\text{Torr}^{-1}$$

The diffusion rate of the quantity $W = (dy/d\theta)^2+\nu^2y^2$ is $D = R^2 d\langle\phi^2\rangle/dt$ where y is the amplitude of betatron motion, $\nu \sim 4$ is the tune, and R = 75m is the average radius. The beam lifetime is[28]

$$\tau = \frac{1}{D}\left(\frac{2\nu a}{2.4}\right)^2$$

where a = 1 cm is the tolerable aperture growth. The lifetime against Coulomb scattering is then $\tau\ [\text{sec}] = 8.0\times10^{-7}/p\,[\text{Torr}]$
A lifetime of one hour requires a mean pressure of 2×10^{-10}Torr. Clearly we must rely on electron cooling to damp the growth of the stack.

The fraction f of beam removed by nuclear collisions with gas is

$$df/dt = \beta c \sigma_{p\bar{p}} \sum_i n_i A_i$$

where $\sigma_{p\bar{p}} = 170$ mb is the $p\bar{p}$ total cross-section at 650 MeV/c.

$$\frac{1}{p} \Sigma n_i A_i^{2/3} = 1.5 \times 10^{17} \text{cm}^{-3}\text{Torr}^{-1},$$

$$\tau \text{ [sec]} = 2.3 \times 10^{-3}/P\text{[Torr]}$$

A lifetime of one day requires a mean pressure of 2.5×10^{-8}Torr.

The vacuum in the Freezer should thus be $\lesssim 10^{-10}$ Torr. One appealing approach to achieving this in the bending lattice is to locate a distributed ion pump system in the fringe field of the dipoles.[24] Rowe and Winter[29] estimate a pumping speed of 1600 ℓ/sec from each 1m dipole so equipped. The cost is about 1/2 that of a standard ion pump of capacity 500 ℓ/sec. Standard ion pumps would still be required in the straight sections. The conductance of a 5m section of the Freezer vacuum pipe is approximately 22 ℓ/sec.

IV-5. Electron Cooling

The Novosibirsk group has demonstrated that low-momentum proton beams can be "cooled" to very small transverse dimensions and very small momentum spread.[3] The basic idea is that the transverse and longitudinal oscillations of the proton beam are transferred by Coulomb scattering to an electron beam that is injected in one of the straight sections of the storage ring. For maximum cooling efficiency the velocity of the $\bar{p}$ and of the e^- should be the same ($\beta_{\bar{p}} = \beta_e$), since the Coulomb scattering cross section will be a maximum. Their results will be used to extrapolate the cooling rates expected in our case.

We assume the entire Booster beam is transferred in one turn at 200 MeV into the Freezer Ring. The emittances of the beam

at this stage are $A_V = A_H = 40\pi\ 10^{-6}$m. $\Delta p = 1.3$ MeV/c. The beam is assumed to be adiabatically debunched either in the Booster or in the Freezer. In the cooling points ($\beta_V = \beta_H = 15$m) the half-beam sizes are as follows:

$$W_\beta = \sqrt{A_H \beta/\pi} = 2.5 \text{ cm} \qquad W_{\Delta p} = \chi_p \cdot \frac{\Delta p}{p} = 0.4 \text{ cm}$$

$$h = \sqrt{A_V \beta/\pi} = 2.5 \text{ cm}$$

The total area is then $A = \pi(W_\beta + W_{\Delta p}) \cdot h = 23$ cm^2. Angular divergencies are also of interest. They are

$$\theta_H = \sqrt{A_H/\beta\pi} = 1.6 \text{ mrad}$$

$$\theta_V = \sqrt{A_V/\beta\pi} = 1.6 \text{ mrad}$$

which are, as we shall see, quite comparable to the angles of the electron beam.

An approximate formula for the cooling time for a parallel e^- and p (or $\bar{p}$) beam is given by ($\theta_e << \theta_{\bar{p}}$)

$$\tau = .05 \left(\frac{m_{\bar{p}}}{m_{e^-}}\right) \frac{\gamma_{\bar{p}}^5 \beta_{\bar{p}}^3 \theta_{\bar{p}}^3}{n_e r_e^2 c L \eta \ln(\theta_{\bar{p}}/\theta_e)}$$

This formula reduces to

$$\tau = \frac{1.2 \times 10^7 \gamma^5 \beta^4 \theta_{\bar{p}}^3}{j_e \eta \ln(\theta_p/\theta_e)} = \frac{2.5 \times 10^6 \theta_{\bar{p}}^3}{j_e \eta}$$

where τ = end-point cooling time [sec]

j_e = electron beam current density [A/cm^2]

r_e = classical electron radius [cm]

n_e = electron beam density [cm^{-3}]

$\theta_{\bar{p}}$ = $\bar{p}$ beam divergence [rad]

$\gamma = E_{\bar{p}}/m_{\bar{p}}$, $\beta_{\bar{p}} = (P_{\bar{p}}/E_{\bar{p}})$

η = cooling length/total circumference of cooling ring

L = Coulomb logarithm $\approx$ 15

In the approximation $\theta_e >> \theta_p$, the formula will contain the factor θ_e^3 instead of θ_p^3.

The latest experimental results from Novosibirsk are as follows:

Proton energy	65 MeV
Electron energy	35 keV
Cathode diameter of the electron gun	20 mm
Electron current I_e	0.1 - 0.8 A
Proton current I_p	20 - 100 μA
Average vacuum	5×10^{-10} Torr
Equilibrium size (diameter) of the proton beam in the middle of the section	0.47 mm
Cooling Time (I_e = 0.8A) τ_e	83 msec
Proton life time in the cooling regime	more than 8 hours
Angular divergence of electrons	$\theta_e \cong$ 3 mrad
Specific flux of neutral hydrogen atoms $(\frac{dN}{dt}/I_e\ I_p)$	$80\ A^{-1}\mu A^{-1}sec^{-1}$

In order to extrapolate to our situation, we must take into account the following factors:

(i) The kinetic energy is higher, 200 MeV instead of 65 MeV. According to the $\gamma^5\beta^4$ scaling law, this increases the cooling time by a factor 10.8.

(ii) The angular divergence of the electron beam which dominates with respect to that of the (anti) proton in both cases is given by the formula discussed in Appendix II:

$$\Gamma = \frac{V_r}{\dot{z}} = 0.102 \frac{I}{BVr_o}$$

For our case, r_o = 2.5 cm, V=1.1 x 10^5V , B = 0.2T, and and I = 23A. Comparing it with Budker's case, we can see that electron temperatures are expected to be comparable. Hence, the factor is the same for both cases.

(iii) The fraction of circumference with electron beams was $\eta = 0.016$ for Budker and it is $\eta = 0.063$ for us. This decreases the cooling time by a factor 4.

A detailed comparison between the Novosibirsk and Fermilab situations is summarized in the following table:

		Novosibirsk	Fermilab
Proton energy	T	65	200 MeV
Electron energy	T_e	35	110 keV
Electron current	I_e	0.8	23A
Proton current	I_p	100	3 μA
Electron beam radius	r_e	1	2.5 cm
Fraction of circumference cooled	η	0.016	0.06
Angular electron spread	θ_e	3.0	3.0 mrad
Proton angular spread	θ_p	-	1.6 mrad
Cooling time	sec	0.086	0.0466 (*)

(*) Extrapolated using the dependence

$$\tau \sim \gamma^5\beta^4\theta^3/\eta j_e, \text{ where } j_e = I_e/\pi r_e^2$$

We remark that the cooling time is expected to be appreciably shorter than necessary.

In the above table, the space charge of the electron beams lead to a tune shift of about .25 in both transverse dimensions. Although this may seem large, it should be noted that the electron density must, in any case, be very uniform so the tune spread will be small and correction, if necessary, can be straightforward. The half integral stopbands caused by the electron beam can be cancelled by proper periodicity of the cooling regions in the cooling ring.

IV-6. Electron Beam and Electron Gun

We propose that a total of at least 30m of cooling length be incorporated into the machine. The electron beam must be maintained parallel over 10m length. Space charge effects will blow up the electron beam unless a solenoidal magnetic field is maintained over the entire length of cooling. Furthermore, as discussed in Appendix II, the magnetic field lines must be shaped and carried all the way back into the electron gun cathode. The electrons, after exiting the cooling section, are to be decelerated to regain the large energy in the beam. The system is shown schematically in Fig. 13.

The accelerating voltage must be 110 kV, equivalent to a beam power of 2.5 MW. Assuming a 98% efficiency of recovery, we have a dissipation of 50kW/beam or a total of 200kW, which is acceptable.

The electron current requirement is about 1 A/cm^2 over approximately 10 cm^2 at 110 KeV energy. CW electron guns have been constructed that give this performance. For example, one such gun is shown in Fig. 14, that is to be used in PEP. This gun gives ∿ 23A of current for a voltage of 110 keV over an area of approximately 18 cm^2.

IV-7. Stacking in the Freezer

Two techniques are used for stacking in the Freezer. Electron cooling can be used to move the beam and therefore to remove the antiprotons from the injection area after the previous Booster capture has been cooled. This motion is slow, and a more efficient technique will be needed to move each booster capture into a preliminary stack that will contain all 12 captures. For this purpose rf stacking is to be used. During the time that the Booster is being filled with protons and the protons accelerated in the Main Ring, a modest rf will be used to adiabatically capture the newly-cooled beam. This can be done without disturbing the cool beam already present at the inner edge of the aperture. The new beam is then moved over to the stack and stacked next to it. This procedure is shown schematically in Fig. 15.

V $\bar{P}P$ COLLISIONS IN THE MAIN RING

The accumulation cycle for collecting antiprotons from a full MR pulse requires a time of ∿3 sec. We estimate a yield of 3.7×10^7 antiprotons per cycle, based on a MR filling of 5×10^{13} protons. The cooled $\bar{p}$ stack then has 4.5×10^{10} $\bar{p}$'s after one hour of accumulation.

Extraction at 8 GeV is done in booster straight section 8, following a pulse of the fast kicker B_1 in long straight 9. Again, aperture requirement is minimal, and the existing spare extraction septum can be used. The 8 GeV $\bar{p}$'s then are bent through an arc and enter the transfer line for 8-GeV reverse injection to the main ring.

We assume that these antiprotons are now injected into the MR together with 4×10^{12} protons, so that the MR now contains two counter-circulating beams of 84 RF buckets (one Booster pulse) each. The beams are accelerated synchronously to 150 GeV/c.

The luminosity at a collision site is then

$$\mathcal{L} = \frac{N_1 N_2 f}{2\pi \sqrt{\sigma_{x_1}^2 + \sigma_{x_2}^2}\ \sqrt{\sigma_{y_1}^2 + \sigma_{y_2}^2}\ N_B}$$

where N_1 and N_2 are the number of protons and antiprotons, N_B=84 is the number of buckets in each beam, and f=47 kHz is the MR revolution frequency. The (Gaussian) beam sizes are obtained under the assumptions:

$$\sigma_{x_2} \ll \sigma_{x_1}, \qquad \sigma_{y_2} \ll \sigma_{y_1}, \qquad \sigma_{x_1} = \sigma_{y_1} = \sigma$$

The emittance of a Main Ring proton beam is $\varepsilon = 6\pi\sigma^2/\beta^* = \varepsilon_o/\gamma$ where $\varepsilon_0 \simeq 20\pi\ 10^{-6}$m is the invariant emittance of the present Main Ring beam, and $\beta^* = 2.5$ m is the local β in the intersect.[30]

$$\mathcal{L} = \frac{3N_1N_2f\gamma}{\varepsilon_0\beta N_B} = 3.0 \times 10^{28}\ \text{cm}^{-2}\text{sec}^{-1}$$

Thus a luminosity of 10^{29} $\text{cm}^{-2}\text{sec}^{-1}$ can be obtained in $\sim$ 3 hours of $\bar{p}$ accumulation.

VI $\bar{P}$ BEAM REGENERATION

We can estimate the $\bar{p}$ beam lifetime in the Main Ring as in Section IV-6. The mean Main Ring vacuum is $\sim 5 \times 10^{-7}$ Torr. The beam loss due to nuclear collisions gives a lifetime of 2.7 hours. After this time, we must begin again the $\bar{p}$ accumulation process.

We also estimate the beam growth due to Coulomb collisions. The proton beam size is $\sigma = \sqrt{\beta_{av}\varepsilon_o/6\pi\gamma} = 1.2$mm for $\beta_{av} = 70$m. Thus, luminosity will decrease by a factor ~ 2 for a beam growth of 1mm, and quickly thereafter. The Coulomb lifetime for 1mm growth is then 190 sec.

Clearly a major concern for implementing $\bar{p}p$ colliding beams will be the possibility of improving the present Main Ring vacuum. We are advised that it may be possible to reduce the vacuum by a factor $5 \div 10$ before being limited by conductance or basic design.

In any case, it will be desirable to regenerate the $\bar{p}$ beam using electron cooling to compensate for the growth from Coulomb scattering. The most straightforward way of accomplishing this is to dump the p beam and decelerate the $\bar{p}$'s to 8 GeV/c, then transfer them to the Booster through the existing injection system and transfer tunnel. After deceleration in the Booster, they would be re-cooled in the Freezer and the cycle repeated.

VII. CONCLUSIONS

We believe that the possibility of implementing, at modest cost, $\bar{p}p$ colliding beams at Fermilab in the near future is established. The direct study of electron cooling at Fermilab is a high initial priority. The physics of high energy $\bar{p}p$ colliding beams has definite advantages for the observation of many conceivable new phenomena. This is especially true for processes that involve parton-antiparton collisions, where the rates will be maximal and the background due to parton-parton collisions minimal. $\bar{p}p$ colliding beams of luminosity $10^{29}cm^{-2}sec^{-1}$ can be obtained and are adequate to observe exciting phenomena such as W production. Finally, the construction of a realistic electon cooling device at Fermilab is likely to have a large impact on accelerator development in the United States for years to come. Each of these reasons is sufficient motivation for this project; in total we believe they provide a compelling necessity.

ACKNOWLEDGEMENTS

We gratefully acknowledge the contributions of A. Ruggiero to the evolution of this project. We also thank M. Barton, T. Collins, E. Courant, C. Curtis, D. Edwards, H. Edwards, R. Huson, D. Johnson, R. Johnson, J. Laslett, M. Lebacque, P. Livdahl, J. LoSecco, S. Snowdon, L. Teng, R.R. Wilson, D. Winn, and W. Winter for helpful discussion. Special thanks are due to E. Rowe and W. Trzeciak for lattice design.

References

1. C. Rubbia, P. McIntyre and D. Cline, Producing the Massive Intermediate Vector Meson with Existing Accelerators, submitted to Phys. Rev. Letters, March 1976.

2. D. Cline and C. Rubbia,"Energy Doubler at FNAL as a High Luminosity pp Storage Ring Facility"." Report in preparation.

3. G. I. Budker, Atomic Energy 22,346 (1967); G. I. Budker, et al: "Experimental Facility for Electron Cooling," BNL-TR-588 (1974); "Preliminary Experiments on Electron Cooling," BNL-TR-593 (1974); "Experimental Study of Electron Cooling," BNL-TR-635 (1976).

4. S. Van der Meer, CERN-ISR-PS/72-31 August, 1972 (unpublished).

5. D. Cline, P. McIntyre, and C. Rubbia, "Proposal to Construct an Antiproton Source for the Fermilab Accelerator," Fermilab Proposal Number 492 (1976).

6. G. I. Budker, et al.,"New Results of Electron Cooling Studies," preprint submitted to Nat. USSR Conf. on High Energy Accelerators (Dubna) Oct. 2, 1976.

7. The possibility of using the Booster accelerator for phase-space cooling has been remarked at informal meeting by ourselves, D. Berley, and R. Johnson.

8. F. J. Hasert, et al.,and A. Benvenuti et al., papers submitted to the Sixth International Symposium, Bonn (1973); F. J. Hasert et al., Phys. Letters 46B, 138 (1973; A. Benvenuti et al., Phys. Rev. Letters 32, 800 (1974).

9. U. Camerini, D. Cline, W. Fry and W. Powell, Phys. Rev. Letters 13, 318 (1964); M. Bott-Bodenhausen et al., Phys. Letters 24B, 194 (1967).

10. S. L. Glashow, J. Iliopoulos and L. Maiani, Phys. Rev. D2,1285, 1970.

11. B. Aubert et al., "Experimental Observation of $\mu^+\mu^-$ Pairs Produced by Very High Energy Neutrinos," in Proceedings of the Seventeenth International Conference on High Energy Physics, London, 1974 and in Neutrinos - 1974, AIP Conference Proceedings No. 22, edited by C. Baltay (American Institute of Physics, New York, 1974), p. 201. A. Benvenuit et al., Phys. Rev. Letters 34, 419 (1975), ibid. 34, 597 (1975), J. J. Aubert et al., Phys. Rev. Letters 23, 1404 (1974), and J. E. Augustin et al., Phys. Rev. Letters 23, 1406 (1974).

12. J. von Krogh et al., Phys. Rev. Letters 36, 710 (1976); J. Blietschau et al., Phys Letters 60B, 207 (1976).

13. J. J. Aubert et al., Phys. Rev. Letters 33, 1404 (1974); J. E. Augustin et al., Phys. Rev. Letters 33, 1406 (1974).

References (Continued)

14. S. Weinberg, Phys. Rev. Letters 19, 1264 (1967), and A. Salam in Elementary Particle Physics (edited by N. Svortholm. Almquist and Wiksells, Stockholm, 1968), p. 367.

15. L. Okun and M. Voloshin,"Production of Intermediate Bosons in pp and $p\bar{p}$ Collisions," Preprint ITEP-III, 1976. Many informal calculations have been made by several authors.

16. J. D. Bjorken, Report at the 1976 SLAC Summer School.

17. A. Benevenuti et al., "Test of Locality of the Weak Interaction in High Energy Neutrino Collisions," submitted to Phys. Rev. Letters (March, 1976).

18. T. K. Gaisser, F. Halzen and E. A. Paschos, "Hadronic Production of Narrow Vector Mesons," BNL preprint 21489.

19. Booster Synchrotron, Fermilab TM-405, edited by E.L. Hubbard (1973).

20. F. Mills, private communication.

21. D. Carey et al., "Unified Description of Single-Particle Production in p-p Collisions," NAL-Pub-74/49-THY/EXP.

22. M. G. Albrow et al.,"Negative Particle Production in the Fragmentation Region at the CERN ISR," Nucl. Phys. (1973).

23. B. Chirikov, V. Tayursky, H. Mohring, J. Ranft and V. Schirrmeister, "Optimization of Antiproton Fluxes from Targets Using Hadron Cascade Calculations," KMU-HEP 7606 (preprint), March 1976.

24. Cummings et al., "Vacuum Systems for SPEAR," SLAC-Pub-797.

25. M. Tigner, private communication.

26. B. Rossi, "High Energy Particles," Prentice-Hall, New Jersey, 1952.

27. S. Snowdon, "Residual Gas Analysis in Main Ring to Obtain Mean-Square Scattering Angle and Beam Lifetime," Fermilab TM-341.

28. L. C. Teng, Accelerator Experiment Note (1/11/72) Fermilab.

29. E. Rowe and W. Winter, private communication.

30. T. Collins, "Easy Low β for the Main Ring," TM-649, March 11, 1976.

Appendices

Appendix I Initial Experimental Test of Electron Cooling - Racetrack Ring Set Up On the Surface

While electron cooling has been experimentally demonstrated, it is far from well established for the high current-large divergence antiproton beam proposed here. While the simple theoretical estimates give rapid cooling times as discussed in 6b, it is of great importance to have detailed measurements of the cooling phenomena. Setting up the Freezer ring in the booster tunnel would limit the experimental measurements since the booster is constantly in use. It is therefore proposed that the same magnetic structure, but with only two long straight sections (Racetrack), be initially assembled on the surface at Fermilab near the linac so that a 200 MeV proton beam is available for cooling studies.

The 12 period lattice described in 5a can be abbreviated using the same elements, as shown in Fig. 17. The overall size then becomes 25 x 40 m^2. There is of course a saving in the number of quadrupoles needed for the ring as well as the length of vacuum pipe needed. One or both of the long straight sections should be instrumented for electron cooling as described in 6c. These cooling studies and studies of the performance of the storage ring will be invaluable for the operation of the Freezer in the booster tunnel.

Appendix II Theory of Electron Confinements in a Magnetic Field

In order to damp betatron oscillations and momentum spread of a proton or antiproton beam in a storage ring, Budker has proposed to make it interact with a strong current of almost parallel electrons travelling with the same average speed as the beam. In the practical realization of such larger currents, space charge effects must be taken into account. A simple way of compensating for the divergence due to space charge forces consists of sending electrons along the axis of a uniform solenoidal magnetic field.[2]

Brillouin[3] has investigated the conditions in which stable cylindrical electron beams could be produced. His work has been extended by other authors.[4,5] Unfortunately, as we shall see, the Brillouin solution cannot be applied to our case, since it implies a too large difference in velocity between peripheral electrons and paraxial electrons. Instead of magnetically focussed flow, we must operate in the limiting condition of magnetically confined flow. The main effect of increasing the field is the one of producing periodic scallops on the beam. These scallops are very small and affect only very slightly the beam shape.

We shall start with a review of the theory of confined electron beam.[6]

2. Bush's theorem.

Let us define a frame of polar coordinates, r, θ and z as shown in Figure 16. The Bush theorem gives the angular velocity of an electron in which neither the electric nor the magnetic field has component in the θ direction. This is obviously the most general case for an axially symmetric set-up.

The Lorentz force equation can be written as:

$$\ddot{r} - r\dot{\theta}^2 = -\eta(E_r + B_z r\dot{\theta}) \tag{1}$$

$$\frac{1}{r}\frac{d}{dt}(r^2\dot{\theta}) = -\eta(-B_z\dot{r} + B_r\dot{z}) \tag{2}$$

$$\ddot{z} = -\eta(E_z - B_z r\dot{\theta}). \tag{3}$$

where $\eta = e/m = 1.76$ coulombs/kG.

From the expression $\nabla \cdot B = 0$, we get $B_r = (-r/2)\frac{\partial B_z}{\partial z}$ and remembering that $\frac{d}{dt} = \dot{r}\frac{\partial}{\partial r} + \dot{z}\frac{\partial}{\partial z}$ we can interprete Eq.(2) to give

$$r^2\dot{\theta} = \eta\int(B_z r\dot{r} + \frac{r^2\dot{z}}{2}\frac{\partial B_z}{\partial z})dt = \eta\frac{B_z r^2}{2} + c.$$

The initial constant can be related to the cathode conditions $r = r_o$, $\dot{\theta} = o$ and $B_z = B_o$. Then:

$$r^2\dot{\theta} = \frac{\eta}{2}(B_z r^2 - B_o r_o^2). \tag{4}$$

Using the Larmor angular frequency $\omega_L = \eta\frac{B_z}{2}$ and putting $\omega_o = \eta\frac{B_o}{2}$ we can rewrite the (4) as

$$\dot{\theta} = \omega_L - \omega_o^2(\frac{r_o}{r})^2. \tag{5}$$

Equation (5) is known as Bush's theorem.

3. Brillouin flow.

Inserting the Equation (5) in Equation (1) we obtain:

$$\ddot{r} = -\eta E_r + r(\omega_o^2\frac{r_o^4}{r^4} - \omega_L^2). \tag{6}$$

From the Gauss's theorem for a uniform cylindrical beam of current I_o, $B_r = -I_o/2\pi\varepsilon_o u_o r$, and therefore:

$$\ddot{r} = \frac{\eta I_o}{2\pi\varepsilon_o u_o r} + r\left(\frac{\omega_o^2 r_o^4}{r^4} - \omega_L^2\right). \tag{7}$$

From Eq.(7) one can see that the magnetic field is most effective when $\omega_o = 0$, i.e., the cathode is outside the field. For a cylindrical beam, obviously $\ddot{r} = 0$, which gives

$$B_B^2 = \frac{2I_o}{\pi\eta\varepsilon_o u_o r^2} = \frac{2\omega_p^2}{\eta^2} = \frac{\sqrt{2}\, I_o}{\pi\eta^{3/2}\varepsilon_o r^2 V_a^{1/2}}$$

$$= 7.0 \times 10^{-7}\, I_o/V_a^{1/2} r^2. \qquad (8)$$

where B_B is the Brillouin field value. From Eq.(5) we see that $\dot{\theta}_B = \omega_L$, when $\omega_o = o$. Electrons then pivot about the z axis with Larmor's angular frequency. One can easily show that the Brillouin's condition is equivalent to balancing the centrifugal force and the electrostatic force with the magnetic force.[6]

From Eq.(7) we can derive the result

$$-\eta E_r = r\dot{\theta}_B^2 = \frac{\partial V}{\partial r}\eta$$

or, by integration, since $\dot{\theta}_B^2 = \text{const}$:

$$V = V_a + \frac{r^2\dot{\theta}_B^2}{2\eta}B$$

The electrons at the periphery then have a larger energy than the one at the center of the beam. By equating kinetic and potential energies we get

$$(\dot{z})^2 + (r\dot{\theta})^2 = 2\eta V = 2\eta V_a + r^2\dot{\theta}_B^2.$$

from which we get

$$\dot{z} = u_o = \sqrt{2\eta V_a}$$

which means that all electrons have the same <u>longitudinal</u> velocity, corresponding to the potential along the axis.

The transverse velocity at the periphery is

$$r\dot{\theta}_B = r\omega_L$$

Let us consider a practical example. Assume $\frac{I_o}{\pi r^2} = 10^4 A/m^2$ and $V_a = 5 \times 10^4$ volt. From Eq.(8) we get $B_B = 55.95 \times 10^{-4}$ Tesla. The Larmor frequency is $\omega_L = 432$ Mc/s, giving a radial velocity $r\omega_L = 4.92 \times 10^6$ m/sec already at r = 1 cm, to be compared to $\dot{z} = 1.237 \times 10^8$ m/s. This corresponds to about 40 mrad max angular spread of the electron beam of 1 cm radius, and it is much too large to be acceptable. Therefore, the Brillouin flow is not useful to our application.

4. "Brute force" confinement

We try next to make the magnetic field strong enough to restrict the transverse motion to an acceptable amount.

Suppose we have a disk cathode of radius r_o normal to a strong magnetic field B in the z direction. We shall assume that the cathode is the same as at any plane along the beam. This solution is very attractive for its simplicity as long as the cathode has sufficiently large emission density. Those sophisticated forms of confined flow will be considered at the end. Equation (7) becomes:

$$\ddot{r} = \eta \frac{\partial V}{\partial r} + r\eta^2 \frac{B_z^2}{4} \left(\frac{r_o^4}{r^4} - 1 \right).$$

The paths of the peripheral electrons are helices and the beam assumes a scallopped form. At the equilibrium radius r_m, $\ddot{r} = 0$. inserting $\frac{\partial V}{\partial r}$ from Gauss's law we get:

$$1-\left(\frac{r_o}{r_m}\right)^4 = \frac{\sqrt{2}\, I_o}{\pi\varepsilon_o \eta^{3/2} B_z^2 V^{1/2} r_m^2} \tag{9}$$

Therefore, increasing B, gives $r_m \to r_o$. According to Pierce[6] we can define

$$K = \frac{I_o}{\sqrt{2}\,\pi\varepsilon_o \eta^{3/2} B_z^2\, V^{1/2} r_o^2} = 3.5 \times 10^{-7} \frac{I_o}{B_z^2\, V^{1/2} r_o^2} \tag{10}$$

and Eq.(9) becomes

$$\left(\frac{r_m}{r_o}\right)^4 - 2K \left(\frac{r_m}{r_o}\right)^2 - 1 = 0$$

or

$$r_m = r_o \left[\sqrt{(K^2+1)} + K\right]^{1/2} \tag{11}$$

It is interesting at this point to evaluate K for the typical case $B_z = 0.1$ Tesla, $I_o/\pi r^2 = 10^4 A/m^2$ and $V = 5 \times 10^3 V$. Inserting numerical values, we get $K = 3.9 \times 10^{-4}$. Hence, the approximation $K \ll 1$ is solid since one can approximately write:

$$r_m \cong r_o \left(1 + \frac{K}{2}\right) \tag{12}$$

We proceed next to the investigation of the ripple on the beam i.e. the motion around r_m. To do this we use the method of Kleen and Pösche[7]. We put

$$r(t) = r_m\,[1 + \delta(t)] \tag{13}$$

Since δ is small, we expand r^{-1} and r^{-3} by the binomial theorem. With these substitutions in Eq.(7) we get

$$\frac{d^2\delta}{dt^2} + 2\left(1 + \frac{r_o^4}{r_m^4}\right) \omega_L^2\, \delta = 0 \tag{14}$$

which is the classic harmonic oscillator solution for an angular frequency.

for an angular frequency $\tilde{\omega} = \sqrt{2\left(1 + \left(\frac{r_o}{r_m}\right)^4\right)}\,\omega_L \approx 2\omega_L$:

$$\delta = c_1 \cos(\tilde{\omega}t) + c_2 \sin(\tilde{\omega}t)$$

At the cathode t=0 and $r=r_o$ or $r_o=r_m(1-\delta)$;

$$\delta = \left(1 - \frac{r_o}{r_m}\right) \cos(\tilde{\omega}t) \qquad (15)$$

The maximum ring diameter is then z or,

$$r_m\left(2 - \frac{r_o}{r_m}\right) = r_m\left(1 + \frac{K}{2}\right) = r_o\left(1 + \frac{K}{2}\right)^2$$

Since the minimum is r_o, the ratio of maximum to minimum is $(1 + K/2)^2$. This is an extremely small variation since for our numerical case $K = 3.3 \times 10^{-4}$.

The anuglar speed $\dot{\theta}$ can be easily described from the Bush's theorem:

$$\dot{\theta} = \omega_L\left(1 - \frac{r_o^2}{r^2}\right) \qquad (16)$$

The radial sp~ed r is in turn calculated confirming Eq.(13) and Eq.(15).

$$\dot{r} = \tilde{\omega}\, r_o \sin\tilde{\omega}t$$

The total radial velocity V_r can be composed from the two orthogonal components $\dot{\theta}r$ and $\dot{r}$. One can easily find, again in the approximation K<<1 that it corresponds to an helical motion with speed given by

$$V_r = \frac{\dot{I}}{\sqrt{2}\,\pi e n^{1/2} B\, V^{1/2} r_o}$$

$$= 6.06 \times 10^4 \frac{I}{B\, V^{1/2} r_o}$$

The parameter which is relevant to our application is the ratio between the longitudinal and transverse speeds:

$$\Gamma = \frac{v_r}{\dot{z}} = \frac{I}{2\pi\epsilon\eta BVr_o} = 0.102\ \frac{I}{BVr_o}$$

where $\dot{z} = \sqrt{2\eta V}$. Thus, as the magnetic field is made stronger and stronger, more and more electrons tend to travel in nearly straight lines from the cathode parallel to the beam axis and along the field lines. This method is more effective than the Brillouin solution. For the numerical case r = 1 cm, $\frac{I}{\pi r^2} = 10^4 A/m^2$, V = 5 x 10^4 volt, we get now $\Gamma = 6.41 \times 10^{-3}$ rad, which is considerably smaller than the Brillouin case. Note also that Budker et al.[2] have chosen I = 1A, r = 0.5 cm B = 0.1 Tesla and V = 5 x 10^4 volt giving with our formula at the beam periphery $\Gamma = 4 \times 10^{-3}$ rad to be compared with the measured rms value ~3 x 10^{-3}rad.

5. General case of confined flow.

A more sophisticated form of confined flow is that in which the electron paths of the given region are designed to be along the lines of the field, which is no longer constant. The treatment presented here is due to Kleen and Pöschl.[7] The set-up is the one shown in Fig.13. The magnetic shield is adjusted until the electron trajectories near the cathode surface lie along the magnetic field lines. The Equation (6) can be rewritten after some manipulations in the form:

$$\frac{B_o^2}{B_z^2}\frac{r_o^4}{r_m^4} + \frac{2\sigma}{r_m^2} \pm 1 = 0$$

where $\sigma = Kr_o^2 = \frac{3.5\times10^{-7}I_o}{B_z^2 V^{1/2}}$

Then:

$$r_m = \sigma^{1/2}\left(1 + \sqrt{1 + \frac{B_o^2 r_o^4}{B_z^2 \sigma^2}}\right)^{1/2}$$

As before we put $r = r_m(1+\delta)$, and use expansion approximations to obtain:

$$\frac{d^2\delta}{dt^2} + 2(A+1)\omega_L^2\delta = 0$$

where

$$A = \left(\frac{B_o r_o^2}{B_z r_m^2}\right)^2, \quad 0 \le A \le 1$$

Then $\delta = C_1 \cos \sqrt{2(A+1)}\ \omega_L t + C_2 \sin \sqrt{2(1+A)}\ \omega_L t$.

The origin is taken at the aperture separating region 1 from region 2 (see Fig.14). Let $r = r_a$ at the origin and let the beam be converging to the axis by an angle α_o. Then,

$$C_1 = \frac{r_a - r_m}{r_m} \qquad C_2 = \frac{u_o \tan\alpha_o}{\sqrt{2(1+A)}\omega_L r_m}$$

The maximum radius is then given by:

$$\frac{r_{max}}{r_{min}} = 1 + \frac{r_a}{r_m}\sqrt{\left(\frac{r_m}{r_a} - 1\right)^2 + \frac{1}{2(A+1)}\left(\frac{u_o \tan\alpha_o}{\omega_L r_A}\right)^2}$$

The value of $\frac{r_{max}}{r_{min}} \to 1$ only if $\frac{r_m}{r_o} \to 1$ and also the second term under the radical goes to zero, i.e. $\alpha_o \to 0$. If this is achieved then the beam at high field will be smooth and uniform.

Finally, in order to compare various experimental situations, we shall derive a useful relation between the magnetic flux enclosed by the mean diameter $2r_m$ and the flux through the cathode surface, at optimum adjustment settings. We define the flux ratio α as

$$\pi r_o^2 B_o = \alpha \pi r_m^2 B_z$$

i.e.

$$\alpha = \frac{r_o^2 B_o}{r_m^2 B_z} = A^{1/2}$$

Then for $\ddot{r} = 0$, i.e., $r = r_m$, we can rewrite Eq.(6) as follows:

$$\frac{\omega_p^2}{2} = \omega_L^2 (1-\alpha^2)$$

or alternatively

$$\alpha^2 = 1 - \frac{\omega_p^2}{2\omega_L^2}$$

In the Brillouin case $\omega_p^2 = 2\omega_L^2$, therefore $\alpha^2 = 0$ and no flux hits the cathode. In the uniform field case $\omega_p^2/2\omega_L \to 0$ and $\alpha^2 \to 1$ and all the flux goes through the cathode. For instance, at twice the Brillouin field $\alpha \sim 0.86$. The percentage of flux cutting the cathode grows very rapidly once $2\omega_L^2 > \omega_p^2$. Using the Bush theorem we get

$$\dot{\theta} = \omega_L (1-\alpha).$$

Which shows that the minimum angular divergence of the beam can be achieved with $\alpha = 1$, i.e., the flux must thread the cathode for maximum cooling efficiency.

5. Discussion.

There are several questions which deserve further consideration:

(a) Is flow stable? The answer to this question is in general , yes. We refer to the book of Pierce for details.

(b) All the theory is based on laminar flow, i.e., the trajectories do not crosseach other. This assumption is not completely correct.[8] Some experimental work is needed to clear up the implication of such a simplifying assumption.

(c) Effects of thermal velocities. Again the effect are expected to be small.

(d) Matching around the accelerating region near the cathode and e.s. lens effects around the cathode. Some jump of radial velocity are expected and they must be investigated.

(e) Positive ions effects. Positive ions can easily neutralize the space charge of the beam and modify the present discussion

It is expected however that the present treatment elucidates the most salient features of the device, and constitutes a valid guide to the construction of an experimental prototype.

References

1. G. I. Budker; Report on International Conference, Orsay 1966.
2. V.V. Anashin, et al. Set up for electron cooling experiments, Report IYaF74-86, USSR Academy of Sciences Siberian Division (in Russian).
3. Brillouin, Phys. Rev. 67, 260 (1945).
4. Samuel, Proc. IRE, 37, 1252 (1949).
5. Wang, Proc. IRE 38, 135 (1950).
6. J. R. Pierce, Theory and Design of Electron Beams, D. Van Nortrand Co., New York (1954).
7. Kleen and Pöschl; AEU 9, 295 (1955).
8. Harker, Jour. Apl. Phys. 28, 645 (1957).

Appendix III Freezer Ring as an Accumulator and Proton Cooler to Increase Luminosity

It appears that the Freezer ring might be useful to decrease the emittance of the booster proton beam in normal operation and possibly increase the luminosity for $\bar{p}p$ colliding beams.

One problem with the Fermilab booster system presently comes from the horizontal aperture limitation which is ~30π rather than the theoretical 90π. This aperture prohibits the originally planned radial 4-turn injection from the linac; the emittance from the linac is ~10-15π for currents of 250 mA. Furthermore, the linac is running idle most of the time, being used only ~3μsec for every booster cycle (66 msec). Increasing the linac current increases the emittance and does not lead to large gains in the current stored in the booster.

There is one obvious and simple solution - decrease the emittance of the linac beam and store the linac beam during the "idle" times. The Freezer ring is potentially extremely useful for this purpose provided electron cooling of the beam takes place in times comparible to the booster repetition rate.

The basic scheme would be to inject the linac beam into the Freezer ring during the idle time of ~66 msec. Multi-turn injection could be accomplished if the electron cooling time can be decreased to ~20-30 msec. The cooled proton beam is then injected into the booster after the normal injection cycle. The current in this reduced emittance beam will be limited by space charge in the booster. Several kinds of

problems related to tune shift, resistive wall instability, nonlinear resonances, etc., depend strongly on emittance, and should become much more controllable than at present. Additionally, synchronous transfer from the Freezer to the Booster should improve the rf capture efficiency. This would result ultimately in improved luminosity.

Table I. Parameters of $\bar{p}$ injection and deceleration in the Booster.

Antiproton injection energy (kinetic)	$T_{\bar{p}}$	5.717 GeV
Target length and material	ℓ_t	5cm, tungsten
Target efficiency		0.3
Proton beam size at target		$\equiv$ 0.5 mm
Betatron function of $\bar{p}$'s at target center		
- vertical betatron	β_V^*	0.025 m
- horizontal betatron	β_H^*	0.025 m
- momentum dispersion	χ_p^*	$\approx$ 0
Acceptances of the Booster ring at 200 MeV		
- vertical	A_V	$40\pi\ 10^{-6}$ r.m.
- horizontal	A_H	$40\pi\ 10^{-6}$ r.m.
- longitudinal	A_o	3 eV sec
Acceptances from the target		
- production angle	θ_{pwi}	0^o
- solid angle	$\Delta\Omega$	5.3×10^{-4} sterad
- momentum acceptance (B = -.12)	Δp	2.0 MeV/c
Antiproton yield for incident proton	$\bar{p}/p$	0.83×10^{-6}

Table II. Major Beam Transfer Elements

Element	Description	Length	Field	Deflection Angle
S1	Fast Magnetic Kicker	7m	0.05 T	1.0 mrad
S2	Lambertson Septum(2)	7m	0.9T	20 mrad
B1	Fast Magnetic Kicker(2)	2.5m	0.06T	7 mrad
B2	Pulsed Current Sheet Septum	5m	0.3T	70 mrad

Quadrupole	Length(m)	Half Aperture(cm)	Gradient(Tm^{-1})
Q1	1.0	7.0	+1.560
Q2	1.0	9.0	-1.365
Q3	1.0	3.0	-1.950
Q4	1.0	2.0	-2.925
Q5	1.0	2.0	+0.780
Q6	1.0	2.0	-0.975

Table III Tentative parameters of the Freezer Ring

Nominal momentum	p_0	644 MeV/c
Guide field	B_0	0.5T
Magnetic radius	ρ	4.3 m
Orbit radius	R	75 m
Focussing Type		*separated function*
Number of cells		12
Length of each cell		39.3 m
Rotation functions:		
- *maximum value*	β_{max}	27 m
- of the cooling sections	$\beta_{straight}$	15 m
Momentum compaction	$x_{p\ max}$	6 m
Transition - energy	$x_{p\ straight}$	ν_z m $\gamma_t = 9$
Length of cooling straight sections		7.5 m
Betatron acceptance	E_H	$96\pi\ 10^{-6}$m
	E_V	$75\pi\ 10^{-6}$m
Momentum acceptance	$\Delta p/p$	$\pm 5 \times 10^{-3}$
Phase advance per cell	ϕ_x	0.27
	ϕ_y	0.26

Table IVa. Freezer Ring Dipole

Field Strength	0.5T
Magnet Length	1.0m
Magnet Gap	3"
Pole Aperture	12"
Field Aperture	6"
Field Quality	±0.1%
Coil Turns(Top + Bottom)	140
Copper Conductor Cross Section	.325" x .325"
Water Cooling Hole Diameter	.181"
Conductor Corner Radius	.063"
Conductor Current	220 A
Magnet Inductance	.006 H
Coil Resistance	.12 Ω
Voltage Drop	26 V
Power	5.7 kW
Cooling Water Pressure	150 psi
Number of Water Paths	4
Water Flow	1.4 GPM
Temperature Rise	20°C
Outside Dimensions	25" x 15"
Iron Weight	3000 Lb.
Copper Weight	3001b.

Table IVb. Frqezer Ring Quadrupole

Field Gradient	10 T/m
Magnet Length	10"
Aperture	8" dia.
Width of Good Field Gradient	±5"
Gradient Quality (ΔB/B at 1.5" Rad.)	±.1%
Coil Turns per Pole	30
Copper Conductor Cross Section	.325" x .650"
Water Cooling Hole Diameter	.128"
Conductor Corner Radius	.981"
Conductor Current	300A
Magnet Inductance	.010H
Coil Resistance	.011Ω
Voltage Drop	3.3 V
Power	1.0kW
Cooling Water Pressure	150 psi
Number of Water Paths	1
Water Flow	0.6 GPM
Temperature Rise	8 ^{o}C
Outside Dimensions	27" dia.
Iron Weight	1300 lb.
Copper Weight	200 lb.

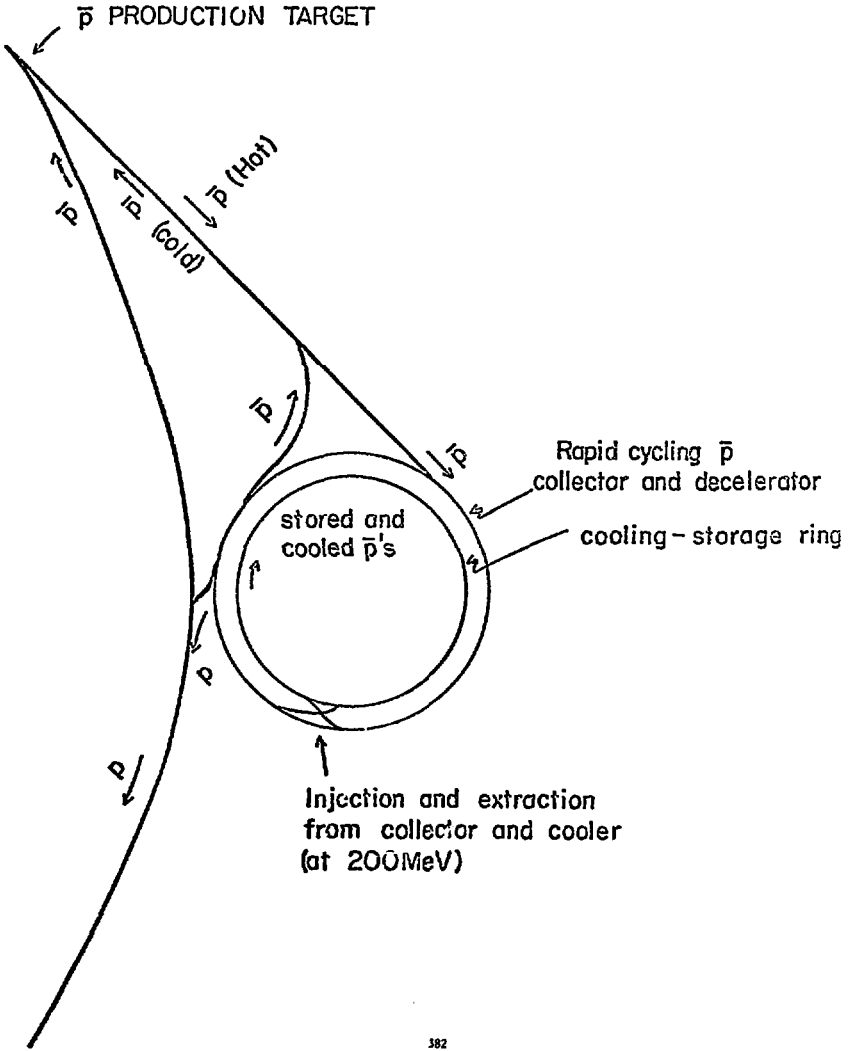
p̄ PRODUCTION TARGET
p
p̄ (cold)
p̄ (Hot)
p̄
p̄
Rapid cycling p̄
collector and decelerator
stored and
cooled p̄'s
cooling – storage ring
p
p
Injection and extraction
from collector and cooler
(at 200MeV)

FIG - 1

MAIN RING CYCLE DURING $\bar{P}$ PRODUCTION

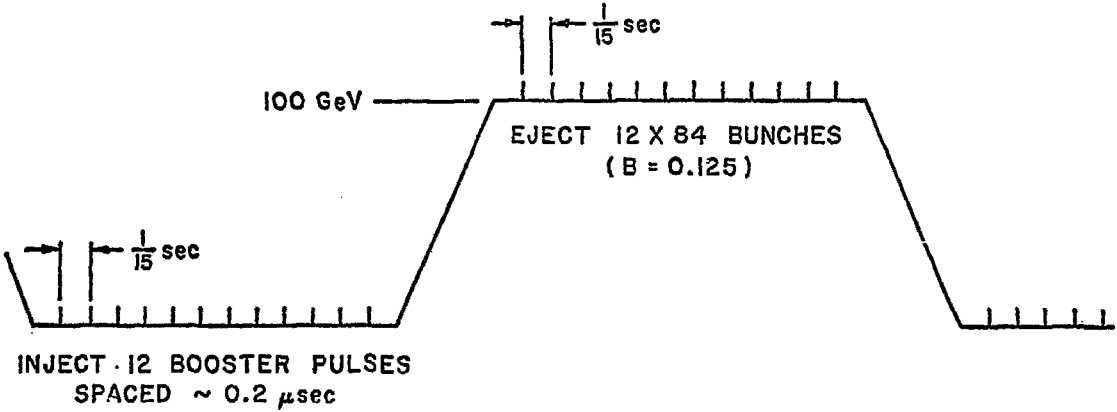

FIG - 2

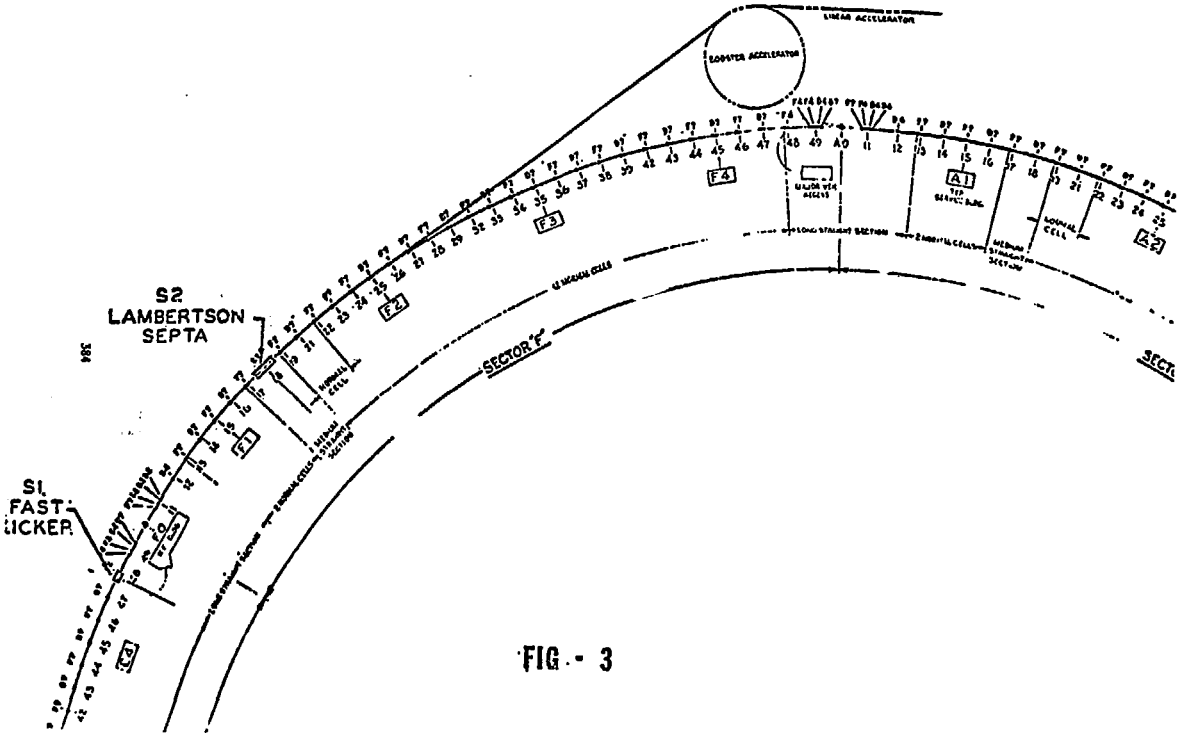
S2
LAMBERTSON
SEPTA
S1
FAST-
TICKER
SECTOR "E"
LINEAR ACCELERATOR
BOOSTER ACCELERATOR
F1
F2
F3
F4
A1
A2

FIG - 3

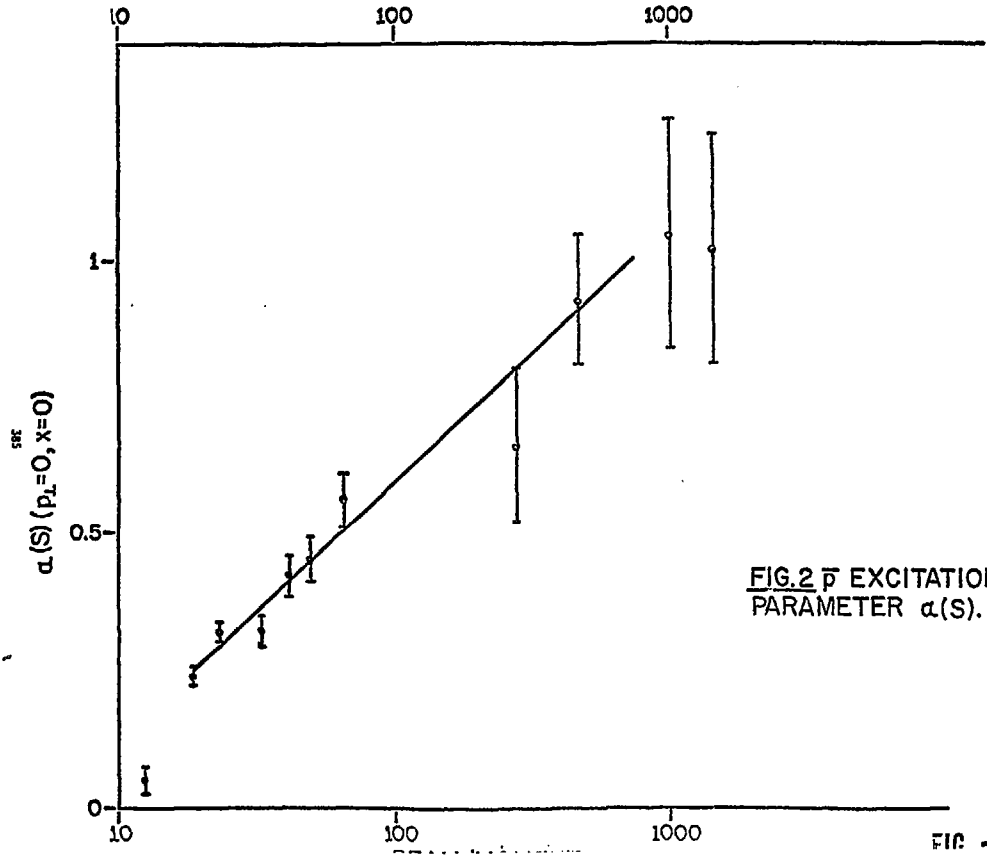

FIG. 2 $\bar{p}$ EXCITATION PARAMETER $\alpha(S)$.

FIG. 4

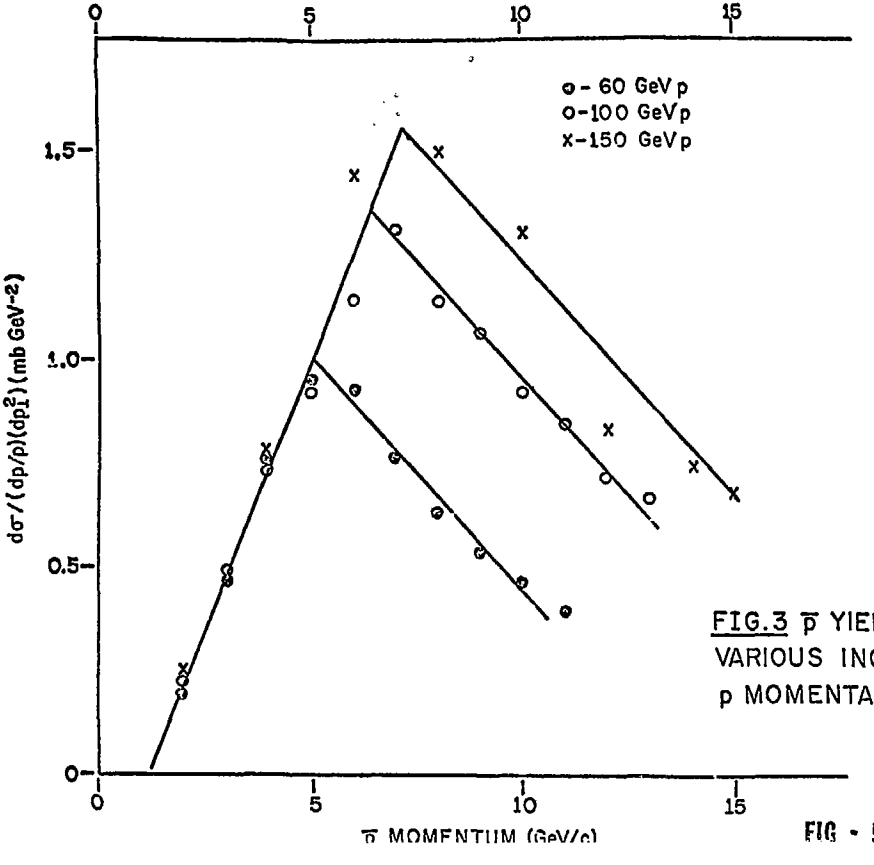

FIG.3 $\bar{p}$ YIELD FOR VARIOUS INCIDENT p MOMENTA.

FIG - 5

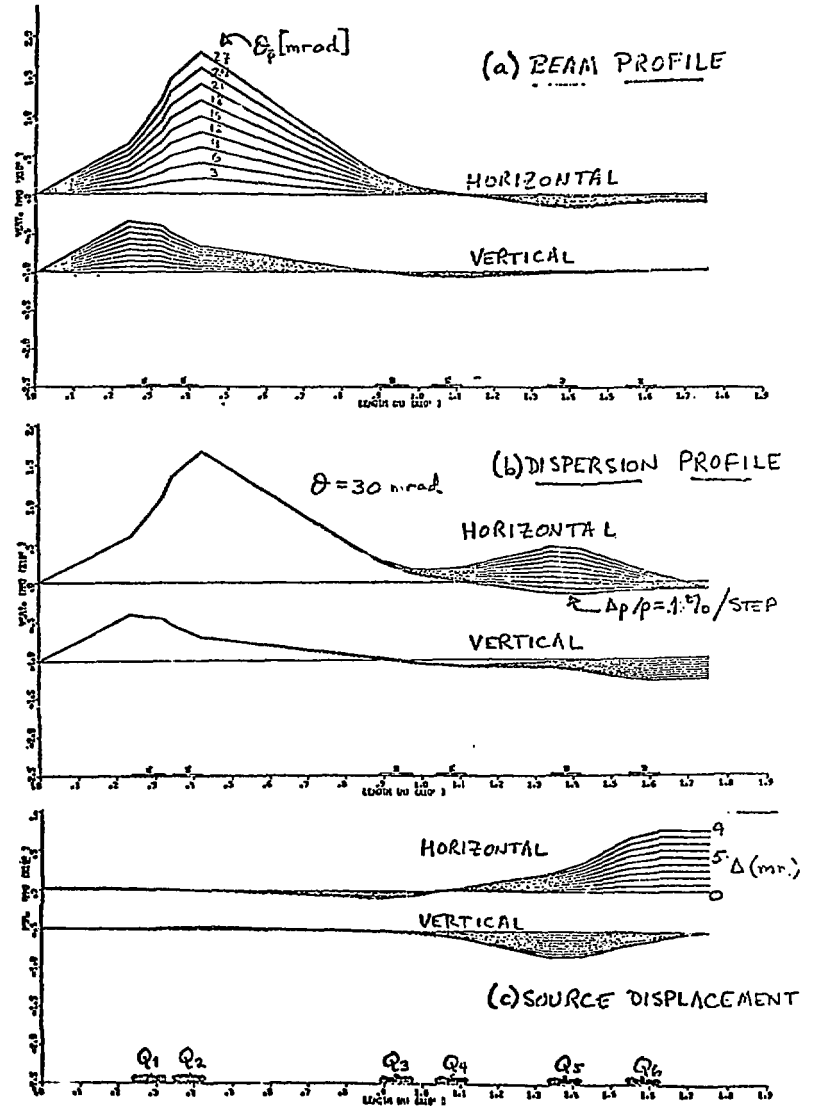
(a) BEAM PROFILE
HORIZONTAL
VERTICAL
(b) DISPERSION PROFILE
θ = 30 mrad
HORIZONTAL
Δp/p = 1.5% / STEP
VERTICAL
HORIZONTAL
VERTICAL
(c) SOURCE DISPLACEMENT
Q1 Q2 Q3 Q4 Q5 Q6

FIG - 6

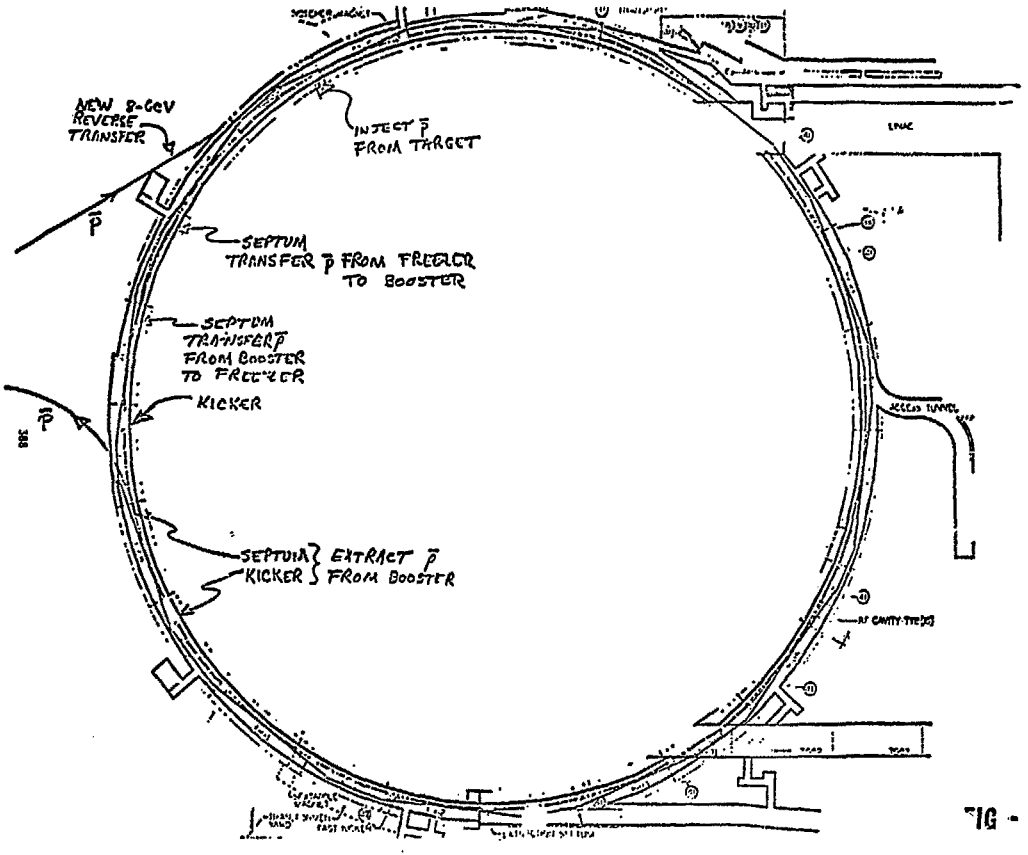
NEW 8-GeV
REVERSE
TRANSFER
$\bar{p}$
INJECT $\bar{p}$
FROM TARGET
SEPTUM
TRANSFER $\bar{p}$ FROM FREEZER
TO BOOSTER
SEPTUM
TRANSFER $\bar{p}$
FROM BOOSTER
TO FREEZER
KICKER
$\bar{p}$
SEPTUM } EXTRACT $\bar{p}$
KICKER } FROM BOOSTER
LINAC
ACCESS TUNNEL
RF CAVITY TYPICAL

FIG - 7

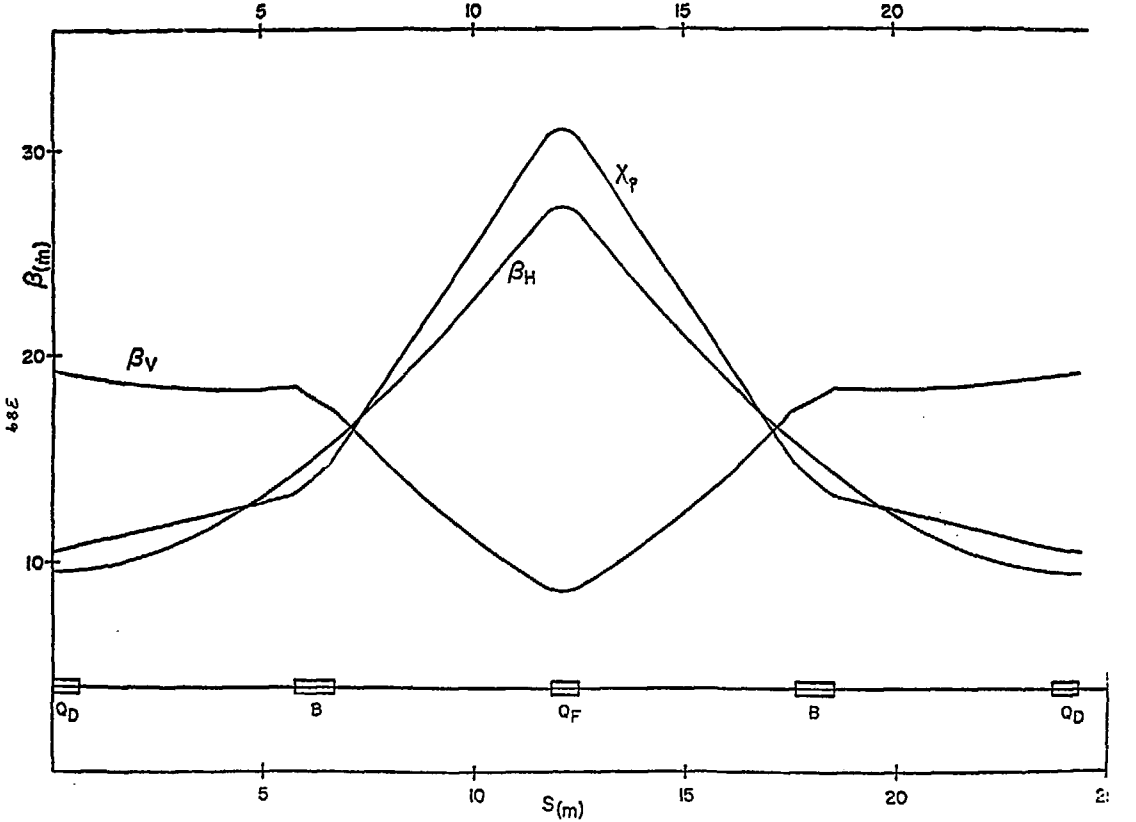
5
10
15
20
30
20
10
$\beta_{(m)}$
χ_p
β_H
β_V
3884
Q_D
B
Q_F
B
Q_D
5
10
15
20
S(m)

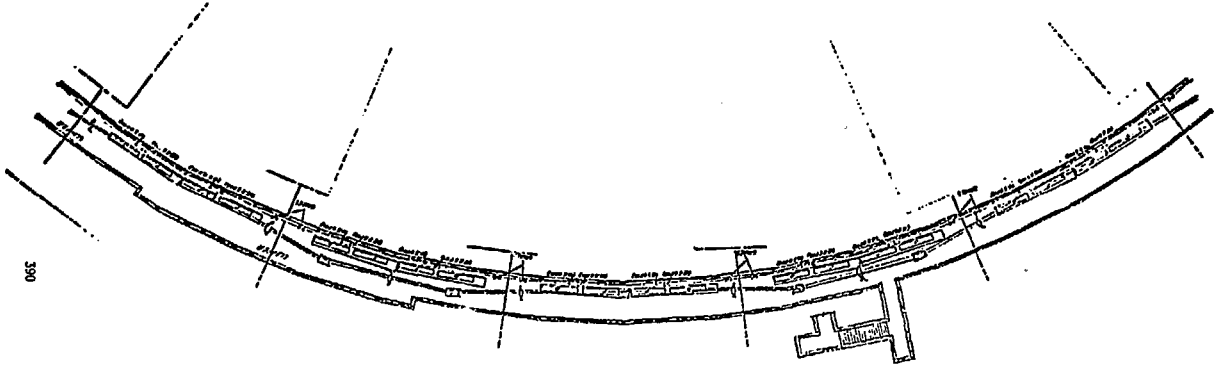

FIG - 9

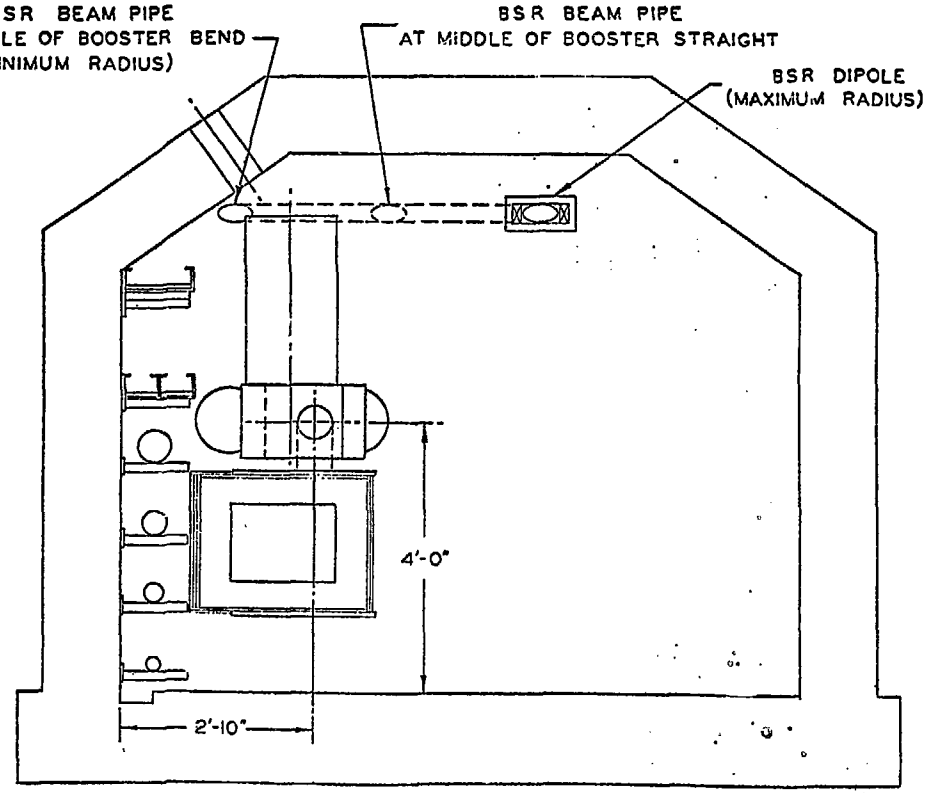
BSR BEAM PIPE
AT MIDDLE OF BOOSTER BEND
(MINIMUM RADIUS)
BSR BEAM PIPE
AT MIDDLE OF BOOSTER STRAIGHT
BSR DIPOLE
(MAXIMUM RADIUS)
4'-0"
2'-10"

FIG - 10

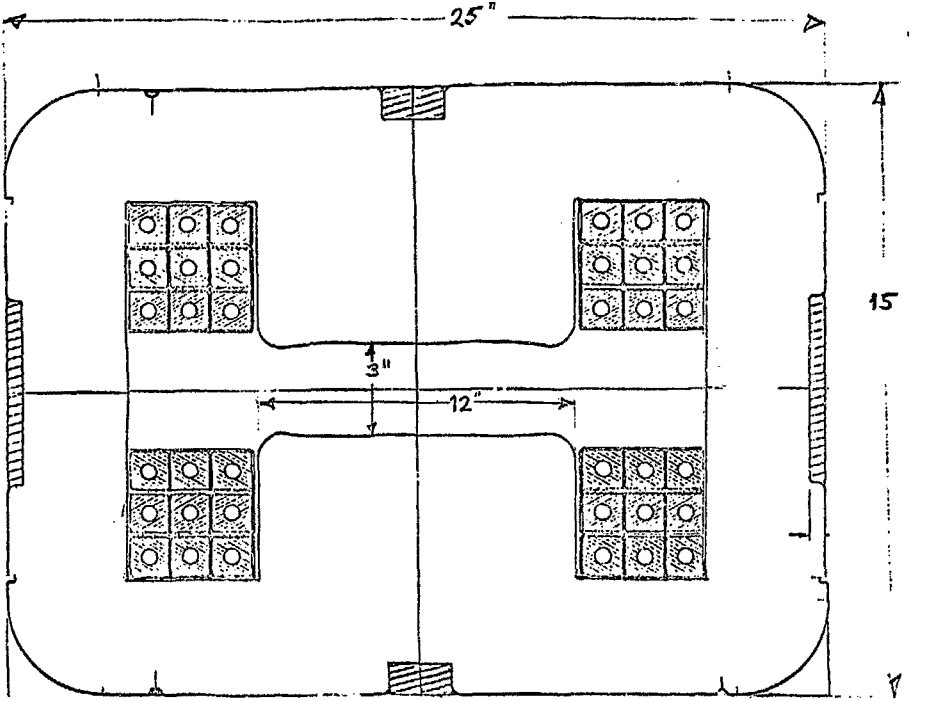

FIG

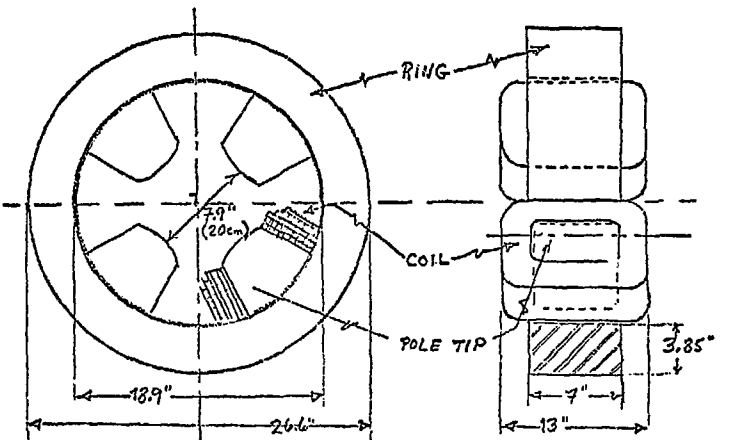

FIG - 12

Cooling Straight Section
(Schematic)

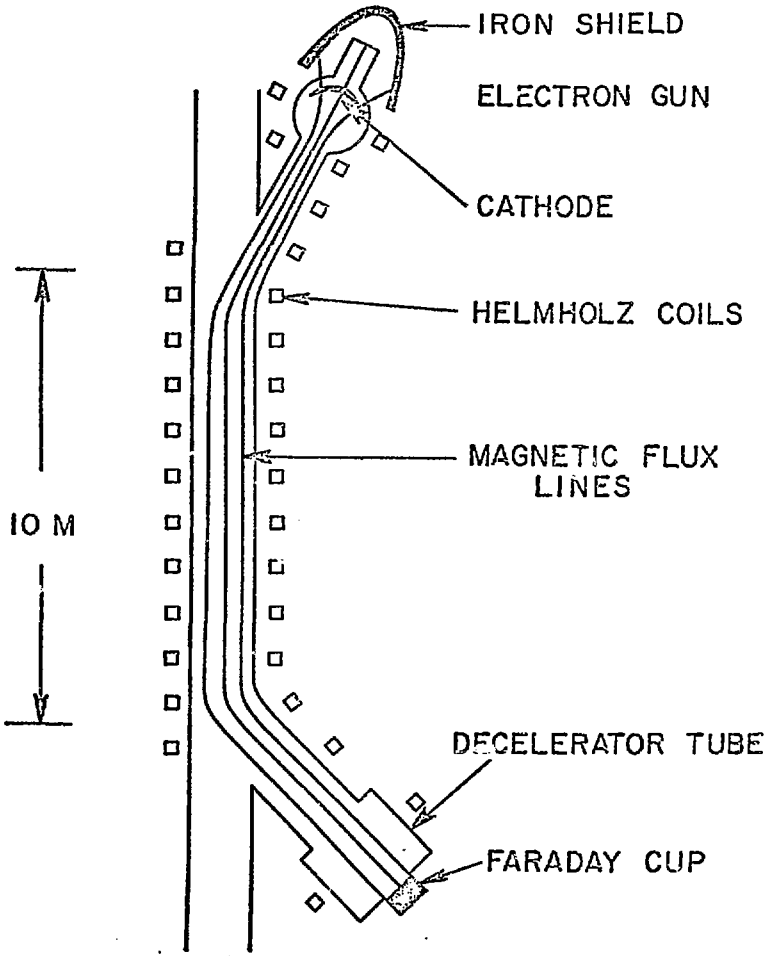

FIG - 13

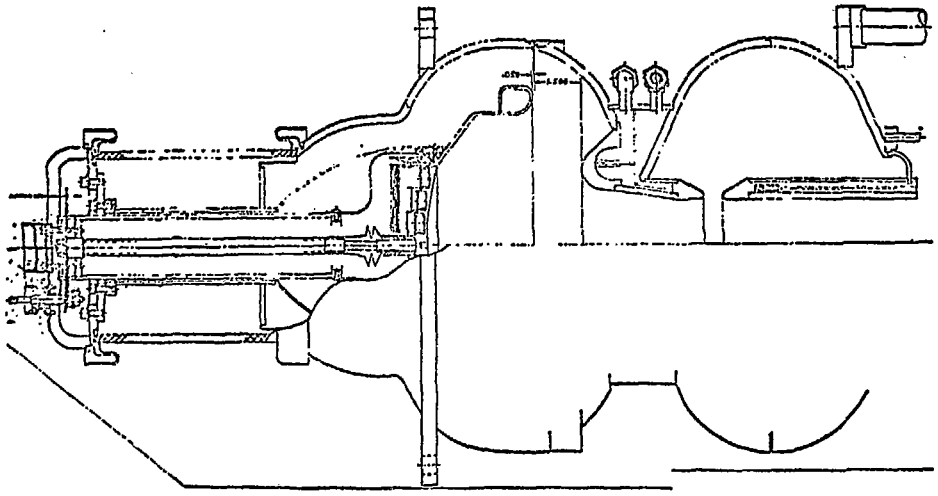

FIG. - 14

Schematic of Stacks in the Freezer

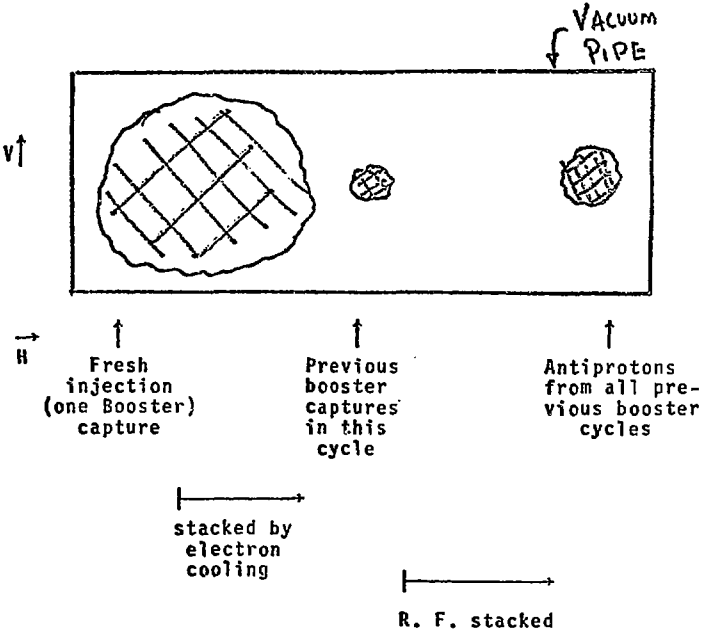

FIG - 15

Motion of Antiprotons in the Electron Rest System

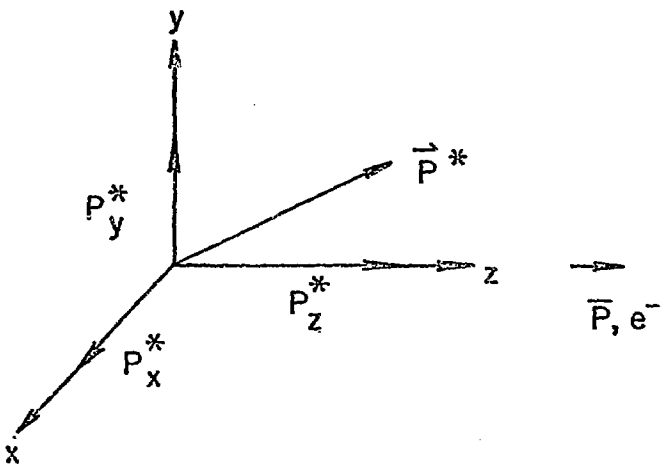

P_x^* and P_y^* α f (t)

P_z^x ~ const.

FIG - 16

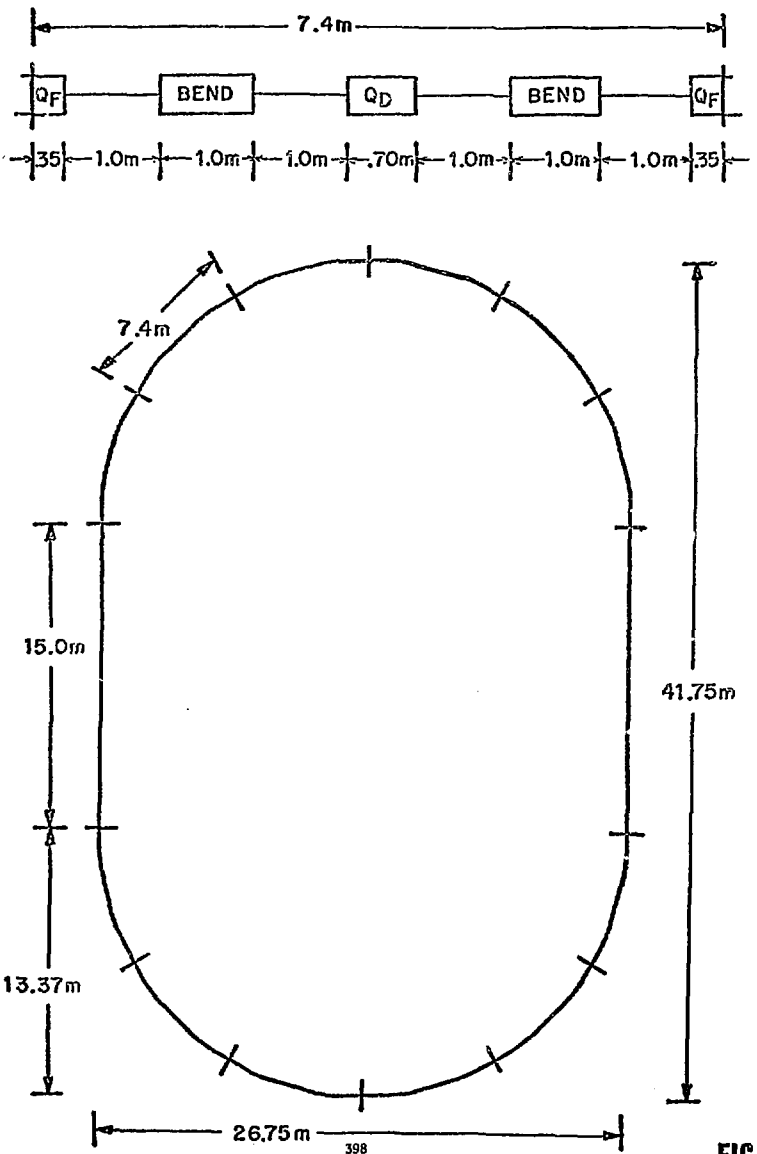
UNIT CELL (DOFOD)
7.4m
Q_F
BEND
Q_D
BEND
Q_F
.35
1.0m
1.0m
1.0m
.70m
1.0m
1.0m
1.0m
.35
7.4m
15.0m
13.37m
41.75m
26.75m

FIG - 17